

# FIESTA

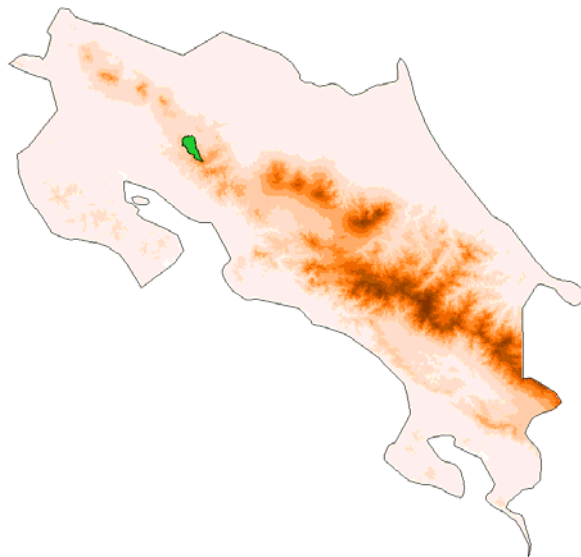
## Fog Interception for the Enhancement of Streamflow in Tropical Areas

Final Technical Report

Dr. Mark Mulligan  
King's College London  
[www.kcl.ac.uk/geography](http://www.kcl.ac.uk/geography)

Dr. Sophia Burke  
AMBIOTEK

[www.ambiotek.com/fiesta](http://www.ambiotek.com/fiesta)



**citation : Mulligan, M and Burke, S.M. (2005). FIESTA Fog Interception for the Enhancement of Streamflow in Tropical Areas Final Technical Report for KCL/AMBIOTEK contribution to DfID-FRP project R7991.**

## TABLE OF CONTENTS

<b>1</b>	<b>EXECUTIVE SUMMARY</b>	<b>6</b>
1.1	This Document	6
1.2	Policy outcomes	6
1.3	Acknowledgements	11
<b>1.</b>	<b>PART I TECHNICAL REPORT</b>	<b>12</b>
<b>1.4</b>	<b>OBJECTIVES of the sub-contract</b>	<b>13</b>
1.4.1	Small (San Gerardo scale) scale model (3-10ha)	14
1.4.2	Chiquito scale model (10Kha)	14
1.4.3	‘Delivery’ model (6Mha+)	14
1.5	The modelling platform	15
1.6	Modelling approach	16
<b>2</b>	<b>THE SAN GERARDO SCALE</b>	<b>18</b>
2.1.1	Advanced Rainfall Interpolation	18
2.1.1.1	Objectives	18
2.1.1.2	Methodology	18
2.1.1.3	Results	21
2.1.2	Vegetation	23
<b>3</b>	<b>THE CHIQUITO SCALE</b>	<b>26</b>
3.1.1	Land cover	28
3.1.2	Forest edges	31
3.1.3	Meteorology	32
3.1.3.1	Temperature	32
3.1.3.2	Monthly Rainfall	34
3.1.3.3	Annual and COV Rainfall	38
3.1.3.4	Wind speed	39
3.1.3.5	Wind direction	42
3.1.3.6	Ground cloud (fog) frequency	44
3.1.4	Topographic	45
3.1.4.1	Topographic exposure (TOPEX)	46
3.1.5	Human	47
3.1.5.1	Roads	47
3.1.6	Sampling	48
3.1.7	Vegetation	48
3.1.7.1	Isolated trees	48
3.1.7.2	Vegetation properties sampling strategy	49
3.1.8	Development of land use change scenaria	55

<b>4</b>	<b>THE (INTER)NATIONAL SCALE</b>	<b>57</b>
4.1.1	Topography and derivatives	57
4.1.2	The regional context	57
<b>4.2</b>	<b>Climate</b>	<b>58</b>
4.2.1.1	Cloud cover	58
4.2.1.2	Potential solar radiation	60
4.2.1.3	An analysis of the exposure of national climate network.	60
4.2.1.4	Temperature and daily temperature range	61
4.2.1.5	Precipitation	62
4.2.1.6	Humidity	64
4.2.1.7	Mean sea level pressure	64
4.2.1.8	Wind speed	64
4.2.1.9	Wind direction	65
4.2.1.10	Wind exposure	66
<b>4.3</b>	<b>Vegetation</b>	<b>68</b>
<b>4.4</b>	<b>Development of land use change scenaria</b>	<b>71</b>
<b>4.5</b>	<b>Forest cover and forest protection in Costa Rica : by altitude</b>	<b>72</b>
<b>4.6</b>	<b>Climate Change Scenaria</b>	<b>73</b>
<b>4.7</b>	<b>Software development : PCRASTER</b>	<b>74</b>
<b>4.8</b>	<b>Hydro-climatic Model development</b>	<b>75</b>
4.8.1	Introduction	75
4.8.2	Policy application	76
4.8.3	Model Summary	76
4.8.3.1	Temporal	76
4.8.3.2	Spatial	77
4.8.3.3	Simulated Processes	77
<b>4.9</b>	<b>Detailed outline of the FIESTA_delivery model</b>	<b>78</b>
4.9.1	Intention	80
4.9.2	Timestep	80
4.9.3	Spatial scale	80
4.9.4	Processes simulated	81
4.9.4.1	Surface area	81
4.9.4.2	Vegetation cover	81
4.9.4.3	Fog settling	81
4.9.4.4	Forest edges	81
4.9.4.5	Sedimentation surface area	82
4.9.4.6	Intercepted energy fractions	82
4.9.4.7	Input climate data	83
4.9.4.8	Input cloud cover data for time of day and season	83
4.9.4.9	Temperature, dewpoint and liquid water content	83
4.9.4.10	Lifting condensation level	84
4.9.4.11	Ground level cloud (fog) occurrence	84
4.9.4.12	Radiation receipt and correction for cloud and fog	84

4.9.4.13	Net radiation	85
4.9.4.14	Wind speeds modified for exposure	86
4.9.4.15	Impaction fluxes	86
4.9.4.16	Vegetation areas for fog interception	88
4.9.4.17	Ratio of impaction to sedimentation	89
4.9.4.18	Evapo-transpiration	89
4.9.4.19	Water balance calculation	90
4.9.4.20	Runoff calculation and summary	90
<b>4.10</b>	<b>Model verification</b>	<b>90</b>
<b>4.11</b>	<b>Model sensitivity</b>	<b>91</b>
<b>4.12</b>	<b>Model Validation</b>	<b>91</b>
4.12.1	Evapotranspiration validation	92
4.12.2	Validation versus FIESTA Rio Chiquito flow data	94
4.12.3	Validation versus Penas Blancas flow data	95
4.12.4	Runoff Validation vs National runoff station database	99
<b>4.13</b>	<b>Model simulations : General outcomes</b>	<b>106</b>
4.13.1	Fog inputs.	106
4.13.2	Fog as a proportion of rainfall	107
4.13.3	Fog as a proportion of water balance	108
4.13.4	Wind driven rain	109
4.13.5	Evapotranspiration	111
4.13.6	Water balance	111
4.13.7	Analysis by catchment	112
4.13.8	Analysis by protected area	114
4.13.9	Analysis by province	116
4.13.10	Fog runoff as a percentage of runoff	117
4.13.11	Seasonal variation	118
<b>4.14</b>	<b>An examination of model processes</b>	<b>122</b>
4.14.1	Wind driven rain	124
<b>4.15</b>	<b>Results of scenario runs</b>	<b>126</b>
4.15.1	PES Scenario	126
4.15.2	NOPEs scenario	130
4.15.3	Cloud forest only removed scenario	131
4.15.4	Climate change	133
<b>4.16</b>	<b>Comparison with the work of Zadroga</b>	<b>138</b>
<b>4.17</b>	<b>Extending Zadroga’s analysis across Costa Rica</b>	<b>145</b>
<b>4.18</b>	<b>International patterns</b>	<b>149</b>
4.18.1	Seasonal patterns	153
<b>4.19</b>	<b>International historic land use change scenario</b>	<b>161</b>
4.19.1	Summary of Central American simulation results	165
<b>4.20</b>	<b>Economic Implications</b>	<b>166</b>

<b>4.21</b>	<b>References</b>	<b>168</b>
<b>5</b>	<b>PART II MODEL DOCUMENTATION</b>	<b>169</b>
<b>5.1</b>	<b>Installing the PCRASTER software</b>	<b>170</b>
5.1.1	Main product	170
5.1.2	PCRaster Manual	171
5.1.3	Percalc update download	171
5.1.4	Aguila update download	172
5.1.5	Nutshell and Mapedit downloads	172
<b>5.2</b>	<b>The FIESTA delivery model policy exercises</b>	<b>173</b>

# 1 EXECUTIVE SUMMARY

## 1.1 This Document

This final technical report (FTR) describes work done by King's College London and AMBIOTEK towards the development and application of simulation models for hydrological processes to understand the impacts of forest conversion in tropical montane cloud forests (TMCFs) of Costa Rica within the context of the DfID-FRP FIESTA project (R7991). The report is organised into a technical report which outlines the objectives, methods and results of the activity carried out followed by a documentation set which describes the models and datasets produced for use outside the project and outlines the kinds of analyses and policy options that can be investigated using these tools.

## 1.2 Policy outcomes

This work was carried out to provide an improved scientific basis for understanding the role of Payments for Environmental Services (PES) schemes in the management of water resources in tropical montane catchments with some TMCF cover. Approximately 12% of tropical forest cover may be defined as significantly cloud-affected to the extent that they are hydrologically cloud forests (Mulligan and Burke, 2005a). These forests usually occur in some of the wettest tropical montane areas (with high precipitation inputs and low evaporation outputs) and thus tend to have high water balances even without the fog inputs. The main policy-relevant outcomes of this work are:

### Fog inputs and cloud forest hydrology

- (1) Fog inputs tend to be relatively low (mostly <150 mm/yr) except at a few, highly exposed sites (up to 400 mm/yr) which usually have high rainfall inputs too.
- (2) In most of Central America these inputs are a small (<5%) contribution to the overall water balance because of high rainfall and low evapotranspiration. Fog inputs are much more significant to water balances in northern Central America (e.g. Honduras) and Mexico, where rainfall inputs are lower.
- (3) Fog contributes significantly to some stream flows within cloud forest areas but rarely represents more than 1-2% of the flow of major downstream (lowland) rivers.
- (4) Fog contributions are seasonally significant even in Costa Rica in areas with pronounced dry seasons during which fog inputs are maintained.

Overall: cloud forests are of minor importance for water balances upstream of high rainfall areas but can be important (especially seasonally) upstream of dry areas.

### Land use change impacts :methods

- (5) Measuring runoff ratios or hydrological budgeting are not a good means of understanding fog contributions at large spatial scales because the uncertainties in rainfall measurement are so high in tropical mountains, even at small spatial scales.
- (6) There is little evidence to support Zadroga's suggestion that fog inputs to Atlantic catchments resulted in runoff ratios >100%. In fact, the observed

- ratios are more likely to result from underestimation of rainfall inputs on windward slopes because of the higher gauge densities required (but rarely available) to accurately estimate rainfall in these environments. Neither were his rainfall estimates corrected for wind losses around the gauges.
- (7) Process modelling provides insight into the magnitudes and spatial variability of fog contributions to catchments. The model developed here validates well where high quality validation data are available
  - (8) Providing accurate spatial rainfall data is still the greatest challenge to hydrological budgeting in windward tropical mountains (even at small scales) and as a result such budgets are likely to be rather inaccurate (even if they do close).
  - (9) Catchments budget closure can occur if all elements of a budget are accurate or if a number of elements are inaccurate (in opposing directions). Thus catchment budget closure is not always a reliable method of estimating particular hydrological fluxes, especially in highly spatially variable environments where the various fluxes are difficult to measure and scale up; or in tectonically active mountain zones (like Costa Rica) where there is no guarantee that the catchments are watertight.

Overall: There is still a good deal of work to do in understanding the hydrological budgets of (especially windward) tropical montane catchments and, as will be argued below, this creates difficulties in the implementation of PES schemes.

#### **Land use change impacts : results**

- (10) Land use change (conversion of forest to pasture) increases annual flow totals because of reduced evapotranspiration, albeit much less so for cloud forests). Any negative effects on flow totals after cloud forest conversion (through reduced fog interception) are usually restricted to highly exposed areas and count for little at larger spatial scales.
- (11) Expected climate change will have much greater impacts on flows than even severe land use change and these effects will tend to be negative in Costa Rica (because of the projected decrease in rainfall and higher temperatures).
- (12) Water balances are significantly greater throughout the region today as a result of historic human impacts on the original forests, which have led to widespread reductions in evapotranspiration and thus increased flows. Though fog inputs to cloud forests have generally reduced upon forest removal (by reducing the available leaf area for fog deposition), inputs have in places, increased because a fragmented forest captures more fog by impaction than a full (continuous) forest cover.
- (13) Impacts vary considerably in magnitude from catchment to catchment and there are no ready rules of thumb that can be applied to extrapolate from one catchment to another. This is because a catchment's response to land use change depends upon the pattern as well as the overall magnitude of land use change, and on the specific climatic, topographic and other physical characteristics of the catchment and the catchment size/scale of analysis. Detailed spatial modelling using appropriate data is a better approach to upscaling than simple extrapolation.
- (14) There are many other impacts of land use change than water quantity alone, including biodiversity, carbon sequestration, water quality, soil erosion,

and slope stability, and these too must be considered for a more holistic view of the benefits or dis-benefits of land use change.

Overall : Forest replacement by pasture overwhelmingly tends to increase water quantities, even from cloud forests though to a much lesser extent. Some cloud forest areas can show reduced flows as a result of forest loss but these tend to be highly localised and are small in most downstream contexts.

### **Implications for PES**

(1) Charges for forest conservation on the basis of water quantity benefits alone seem inappropriate, though possibly less so for the maintenance of dry season flows in areas with low or very seasonal rainfall. Charges based on other forest environmental services are probably more appropriate and should ideally be quantified and included.

(2) Catchments vary considerably in terms of the magnitude of land use impacts on water quantities because of differing catchment characteristics and land use patterns. It seems that simple rules of thumb are not apparent. This means that local schemes cannot be based on a generic assumption or rule of thumb concerning the water resource value of 'forest'. Each patch of each catchment will have a different value and in some catchments or at some scales in a catchment the effect of forest on water resources may be different in direction as well as magnitude to that assumed. So there are operational difficulties in the assignment of costs to downstream users since benefits to those same users cannot be guaranteed. Sophisticated spatial models are the best hope for systematically understanding the potential benefits but these require catchment specific data for each catchment in which a PES scheme is proposed. Or, better, PES schemes should be non-local and based on the cumulative benefits integrated across whole catchments or countries.

(3) Cloud forests do trap cloud water which would otherwise pass over catchments and remain in the atmospheric subsystem of the hydrological cycle. These inputs can be significant locally (in dry environments) and seasonally (in seasonally-dry environments). Moreover, cloud forests occur in environments with low energy for evapotranspiration. The net result of fog inputs and lower evapotranspiration in cloud forest environments is that cloud forest areas shows smaller increases in water flows on forest loss than do lowland forests (see Figure 161) because evaporation is limited by available energy (not forest cover) in the mountains. This means there is much less to be gained hydrologically from cutting cloud forests upstream of water scarce areas; in fact in the driest months such an approach could lead to significant reductions in flows. Where cloud forests are found in and upstream of very wet areas there is inherent danger in cutting forests since high rainfall inputs and low evaporation means that these areas are very water productive and this, combined with the steep slopes and concentration of flows that we find in upland environments makes the role of forests in protecting soil from erosion become all the more important than is the case for lowland forests.

In any case the utility of any water gains achieved from forest management will depend upon whether that water can be effectively used downstream. i.e. whether it comes at the appropriate time of year, with sufficient quality and at appropriate rates

of flows for the intended use. Many of these questions are also land cover dependent, but their quantification would be a project in itself.

### **Recommendations for the operational spatial scale of PES Schemes**

On the basis of this work, we (Mulligan and Burke) believe that if downstream "users" are to pay locally specific upstream "providers" (forest/land managers) for water-based environmental services then those users will expect to:

- (a) know how much water they can expect for their payments,
- (b) receive this water reliably year on year for as long as they are making payments.

On the other hand upstream "providers" will expect to:

- (c) have a reliable source of income from downstream users
- (d) be sure that the upfront investments of time, effort and money that they make will have long term payoffs.

We believe that these expectations cannot be met by local (operational scale) schemes for the following reasons:

(a) Whilst we will be able to give reasonable answers as to the water yields by different land uses we can never know how much of the water yielded by upstream providers will reach particular communities downstream. Subterranean mixing between catchments may be common in highly tectonic mountain environments and if downstream users are obtaining water from groundwater (on the Pacific plain of Costa Rica for example) then the water from those aquifers is likely to be a mixture of the waters from many of the surrounding mountain catchments. Thus it is possible to know how roughly much water is produced by upstream providers but not how much is received by downstream users (or indeed which 'providing' catchments provide to which 'using' catchments).

(b) Interannual and decadal climate variability is common in the tropics (especially in the lowlands) and regional climate change resulting from the greenhouse effect and from large-scale land use change are likely to make this variability greater and less predictable (for prediction on the basis of existing datasets). If climate variation means downstream users do not obtain the water that they had hoped from upstream providers in a year or a run of years (even though they may be receiving more than they would if the land upstream were managed differently) would the users still pay or would payments stop until the wet years returned?

(c) If as a result of climate variation providers do not have a reliable source of income from downstream users (or if globalisation or other market related effects, land degradation or alternatives in tourism move downstream users away from water-demanding agriculture and thus the downstream demand for water is reduced) how can upstream users be expected to take up this activity and what are their alternatives when the payments do not come?

(d) Can local schemes be designed to last long enough for farmers to recoup the investments of changing their land use or will they last only as long as the supporting local government bureaucracy.

In summary, the problem with tying payment to a specific resource from a specific set of providers to a specific set of users, is that the resource cannot be guaranteed over time. Furthermore, it is unknown who is exactly providing what resource to whom

whereas demands also change. These all mean that local schemes are, in our view, unsustainable.

A national scheme, on the other hand, recognises that :

- (a) a nation's water resources are important for people, industry, agriculture and environment,
- (b) once water hits a nation's surface it contributes to one or more of those functions somewhere in the nation (whereas passing over in the atmosphere it does not),
- (c) losses and gains of water in one area (catchment) will have knock-on effects in many others through associated trans-catchment flows of people (migration), agricultural or energy production and associated internal and export income, health, poverty and associated need. In this way all the nation are effectively "downstream" of the mountaintops providing the nation's water even though they are not in the same hydrological catchment.

A national scheme based on fuel tax or better a tax on domestic water is more likely to be politically sustainable in the long term, provides a better incentive to upstream providers to get involved, survives the vagaries of climate variation (since everyone pays), does not suffer from local changes in water demand and permits a more centralised, water-strategic mechanism than is possible through a series of uncoordinated catchment specific PES systems. Scientists can concentrate on determining which areas are receiving and releasing most water (rather than where that water goes, as in the delivery model approach) and base the distribution of the incentives on that information in the knowledge that once water is in the land part of the hydrological cycle it is available for environmental or human use somewhere in the nation.

Moreover, in the few cases where there is one single downstream user (e.g. a Hydro-Electric Power plant) then a local payment scheme is effectively a national one anyway since the electricity company will pass the costs of the payment on to their customers wherever the customers are in the nation. Concentrating on national incentive schemes provides the opportunity to provide payments for areas producing water (which we know well) without having to resort to identifying the precise users receiving that water (which we know less well) and guaranteeing these users specific water resource "rewards" for their payments.

Overall : Forest conservation is important in both dry and very wet environments but not necessarily for their water quantity benefits alone. Local (operational scale) PES schemes seem fraught with scientific and implementation difficulties whereas national scale systems which do not target specific users to specific producers of water (such as currently exist in Costa Rica) seem much more appropriate.

### **1.3 Acknowledgements**

Sampurno Bruijnzeel provided the opportunity and the collaboration needed to carry out this work together and his generosity, foresight, patience and insight are gratefully acknowledged.

This work would not have been possible without the financial support of the UK DfID Forestry Research Programme (FRP), the support and patience of John Palmer at FRP is gratefully acknowledged.

Individual data sources are acknowledged in the text but the bulk of the data and knowledge generated by the project was the result of years of hard work in the field and lab by the project team (particularly Arnoud Frumau and Conrado Tobon and their field assistants). Other data were provided by Julio Calvo or Jorge Fallas. All other members of the project contributed data, ideas, discussion, comments and friendship.

The model developed here originated as the Tambito hydrological model and all involved in our work there are gratefully acknowledged.

Specific support in this work was given by Sophia Burke, Gemma Dunjo-Denti and Robert Figueras.

# **1. PART I TECHNICAL REPORT**

#### 1.4 OBJECTIVES of the sub-contract

The AMBIOTEK subcontract incorporates the following objectives towards the overall aim of FIESTA which was to

*‘to quantify the impact of cloud forest conversion to pasture on streamflow in the Tiláran Range of northern Costa Rica using hydrological process research and modelling’*

This was achieved through a combination of intensive field measurement and monitoring at two scales (the San Gerardo forest and pasture sub-catchments, 10 ha and the ‘operational scale’ for the Rio Chiquito catchment, 90km<sup>2</sup>) by VUA. This was coupled with process-based, dynamic spatial modelling of land use effects on hydrology at three scales (San Gerardo, by KCL/AMBIOTEK), Chiquito (by VUA and KCL/AMBIOTEK) and the national scale, 61815 km<sup>2</sup> (by KCL/AMBIOTEK).

Field measurement alone could not have realised the aim since in order to quantify the impact of cloud forest conversion through field measurement one would need to monitor hydrological properties and fluxes over a sufficient long period of time to establish the ‘equilibrium’ hydrological conditions and then apply a cloud forest conversion to one of two very similar catchments in a paired catchment study. Such an activity is not possible within the context of a 3-4 year study. Moreover that approach assumes that all fluxes in and out of the paired catchments can be quantified by measurement with a high degree of certainty. In reality this is difficult even at the San Gerardo scale and much more so at an ‘operational’ scale such as for the Chiquito catchment, largely because of uncertainties introduced into the measurement process by two factors:

- (i) the high spatial variability of hydrological fluxes in montane landscapes which cannot be fully represented even with relatively dense measurement networks
- (ii) the impact of subterranean leakage between catchments and the implications for closing catchment-scale hydrological budgets.

Modelling offers the ability to integrate our understanding of processes and, with appropriate assumptions, to simulate the spatial variability of fluxes in more detail than can be taken from interpolation of field measurements and to test the likely impacts of various scenarios for land use change in this hydrologically variable environment.

The aim of the modelling activity was :

*‘To produce a process-based, spatially distributed catchment hydrological model and a user-friendly parsimonious parameter derivative which may be used to predict changes in streamflow following (cloud) forest conversion to other land uses, notably pasture’.*

This breaks down into three objectives which are realised by the different scale models and the field programme as indicated below:

1.4.1 *Small (San Gerardo scale) scale model (3-10ha)*

To better understand the detail of rates and processes of fog/WDR interception in the Costa Rican context, their controlling factors and spatial and temporal variability (*fieldwork, small scale model*) including :

- To integrate the various field data and calculate budgets.
- To better understand the processes.
- To identify the important parameters.
- (data demanding, complex, not easily scaleable therefore)

1.4.2 *Chiquito scale model (10Kha)*

To better understand the contribution of fog/WDR interception to the hydrological budget of forest and pasture areas and the likely impact of forest conversion to pasture upon catchment *streamflow (fieldwork, chiquito model)*

- Simplified and scaled up to policy relevant scale.
- To investigate the impacts of spatial variation and spatial pattern.
- To investigate the impacts of land use change on streamflow.
- (requires field campaign and modelling expertise therefore)

1.4.3 *'Delivery' model (6Mha+)*

To provide a replicable model, using only baseline data and providing estimates of fog interception and its likely impact on terrestrial water resources (*delivery model*). Simple and deliverable to end users.

- Based on the lessons from 1 and 2.
- Multiscale and scenario-based.
- Using only baseline data, thus replicable elsewhere.

The links between the different scales of model, data and knowledge are shown in Figure 1.

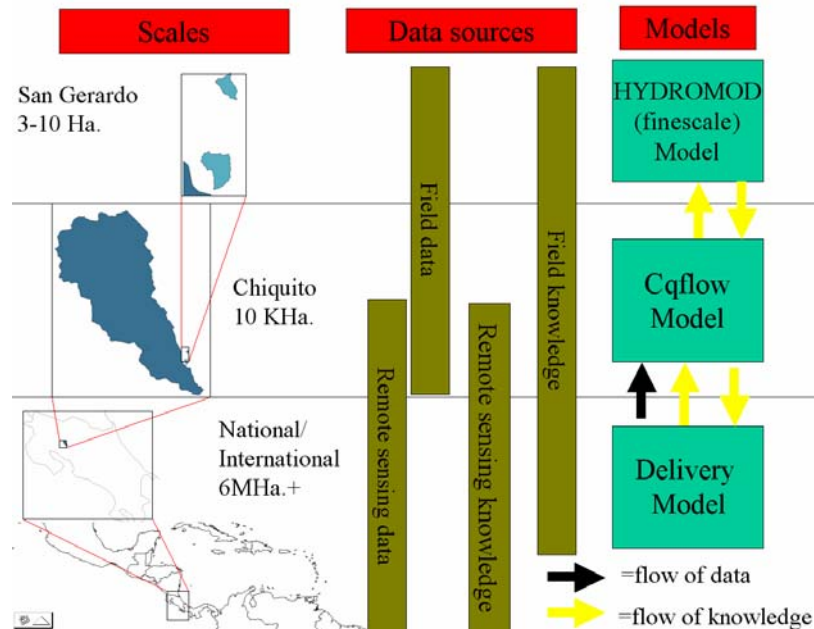


Figure 1 Connections between the different modelling scales and data sources

KCL/AMBIOTEK's work thus fell in two major areas:

- (a) the production of spatial data for modelling at the San Gerardo, Chiquito and National scales

(b) the development of detailed spatial models of hydrological processes and impact of land use and climate at the San Gerardo scale (the so-called FIESTA\_SG model) and the National scale (the so-called FIESTA delivery model and contributions towards modelling at the Chiquito scale (for the so-called FIESTA Cqflow model).

Formally the terms of reference for the work were stated :

1. Module 2.2: Assistance in the formulation of routines for the FIESTA model
2. Module 1.3: Collaboration on distributed canopy characterisation of the San Gerardo and Monte de Olivos areas via photography
3. Module 1.5: Collaboration on integration of existing and new spatial data on topography, vegetation type and distribution in Chiquito catchment
4. Module 2.4: Collaboration on completion and validation of FIESTA model at the small catchment scale
5. Module 2.5: Collaboration on model application to Chiquito basin
6. Module 3.3 Attending and reporting final workshop

### **1.5 The modelling platform**

A number of platforms and techniques are available for model development. One of the first decisions that need to be made in model development is which platform will be used. The prerequisites for choosing a platform here were as follows:

- (a) An interactive high level spatial modelling language for rapid model development,
- (b) A minimum of programming overheads and thus maximum focus on science rather than technology,
- (c) compatible with GIS data formats,
- (d) fast operation,
- (e) free or cheap to the end user and suitable for windows operating system
- (f) relatively easy to learn
- (g) graphical.

Of the available platforms the most suitable for this work is the PCRASTER<sup>1</sup> Environmental Modelling language which is a computer language for construction of iterative spatio-temporal environmental models. The advantages and disadvantages of PCRASTER can be stated as follows:

*Advantages:*

- handles complex spatial processes (eg lateral flow of water)
- script based or command line
- runs in PC windows environment, links with ARC/INFO
- includes some visualisation functionality
- low training overhead
- low coding overhead
- free of charge

---

<sup>1</sup> <http://pcraster.geog.uu.nl/>

- includes integrated geostatistical modelling program (GSTAT) and error propagation (ADAM)

*Disadvantages:*

- not as flexible as programming in code
- interpreted (not compiled), so slower than code
- interface too technical for use as a Decision Support System (DSS)

The components PCRASTER are shown in Figure 2. PCRASTER model scripts are developed in a text editor such as NOTEPAD. They are run from the command line in a DOS shell and model outputs are written to disk as time series files or maps which can be displayed as 2D or 2.5D (perspective) maps.

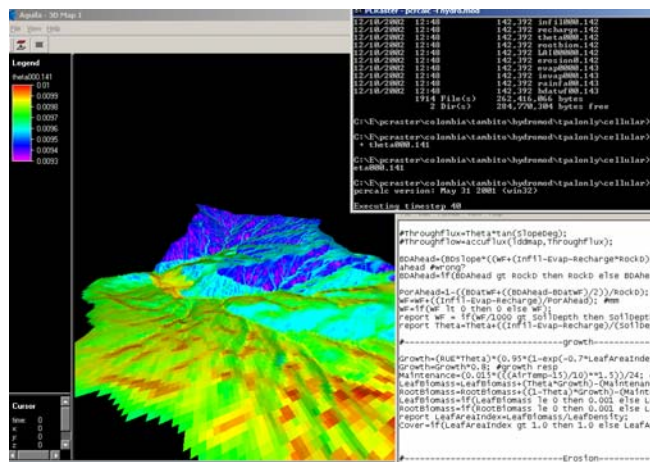


Figure 2 The PCRASTER interface

## 1.6 Modelling approach

Much of the modelling can be carried out with standard hydrological methods. However, because of the potential importance of fog inputs to cloud forest hydrological response to land use, innovation was necessary in the areas of:

- spatialisation of climate and land surface variables in this heterogeneous environment,
- vegetation parameterisation and spatialisation,
- modelling of wind driven rain and interception processes,
- modelling of fog and interception processes.

To model cloud interception one needs to know:

- where the ground level cloud is,
- where the cloud forests are
- the magnitude and variability of the fog flux,
- the fog interception efficiency of the vegetation present.

The fog interception process in simple terms is :

$$\text{Fog Interception} = \text{Air Flux} \times \text{LWC} \times \text{Interception efficiency} \times \text{Area exposed}$$

Equation 1

where

Air Flux = the flux of air past an intercepting surface

LWC = the liquid water content of the moving air

Interception efficiency = the capacity of the vegetation to trap water particles by deposition and impaction

Area exposed = the area of vegetation exposed to the depositing and impacting fluxes

To model air flux one must model wind flows and speeds in complex topography. To model LWC one must model the humidity of the air and the potential for condensation of that humidity into liquid water. Knowing interception efficiency means modelling the significant complexity of forest vegetation at multiple scales and knowing the area exposed means analysing the spatial complexity of forest/pasture mosaics when viewed from particular azimuthal wind directions and inclinations of fog water flux.

The forthcoming sections of this report outline how these models were constructed at a range of scales with a few specific examples, the spatial data generated to support them and a series of model experiments addressed towards understanding the magnitude and spatio-temporal variability of fog inputs to cloud forests in a range of contexts and the contribution of this fog water to downstream flows. Not all of the work carried out can be discussed here so at each scale a series of examples are given as case studies.

## 2 The San Gerardo scale

Two example applications are detailed for the San Gerardo scale work. First we describe some spatial climate modelling for the interpolation of spatial rainfall fields at this scale. Secondly, we describe detailed characterisation of the vegetation cover and type at this scale through a combination of aerial photography and high-resolution satellite image interpretation.

### 2.1.1 *Advanced Rainfall Interpolation*

#### 2.1.1.1 Objectives

- (a) To produce the most accurate representation of *areal total* rainfall inputs for catchment budget studies,
- (b) To produce the most accurate *spatial distribution* of rainfall inputs for process modelling,
- (c) To account for wind driven rain effects on measured rainfall catches,
- (d) To make the best use of data from a sparse rainfall network data.

#### 2.1.1.2 Methodology

Requires:

An automatic weather station (AWS) with hourly rainfall, wind speed and wind direction data,

A series of daily or monthly rainfall totalisers distributed across the area of interest (all raingauges must be of the same design),

A DEM.

The process is as follows:

- (a) correct gauge catches for wind losses based on DEM-extracted gauge-site topographic conditions,
- (b) produce a map of spatial correction factors relative to base station (AWS) and which describes the enhancement/diminution of gauge catches spatially because of wind funnelling, windward/leeward effects and, at larger scales, differences in vertical rainfall inputs,
- (c) apply process model to convert the local gauge catches of (b) to local vegetation catches according to height of vegetation within windfield, angle of incoming rainfall relative to slope gradient and bearing of incoming rainfall relative to slope aspect on which the vegetation occurs.

#### **2.1.1.2.1 Stage 1 *Simple wind-loss corrected spline interpolation (corrects for gauge losses and captures wind funnelling effects and windward/leeward effects)***

- (1) Prepare a file for the AWS site of columns : hourly rainfall totals, hourly average windspd, hourly wind direction
- (2) Prepare a series of maps of monthly total rainfall by performing a spline interpolation of points representing monthly gauge windloss-

corrected rainfall totals at the various raingauge positions (including the AWS). The windloss correction is achieved in an Excel spreadsheet by taking the hourly data from each of the gauges and applying the corrections according to Arazi et al (1996) using the coincident hourly wind speeds and directions modified for the DEM-derived topographic conditions at the gauge sites. The topographic modification is achieved using the methods discussed herein. This produces surfaces for the spatial distribution of gauge windloss-corrected rainfall totals by month.

- (3) These surfaces are converted to rainfall correction factors which express the deviation of wind gauge loss corrected rainfall at each cell relative to the wind gauge loss corrected value measured at the AWS. This is achieved by dividing the monthly total at each cell by the corresponding value at the AWS position. These spatial ‘rainfall correction factors’ can then be used to derive hourly rainfall receipts at all positions in the landscape given the an hourly rainfall total at the AWS. This is a simple but gauge wind loss corrected rainfall interpolation. The correction factors are produced on a monthly basis to take into account seasonal changes in exposure to prevailing winds and associated rainfall receipts.

A typical set of correction factors (for the FIESTA pasture site) are given in Figure 3 and indicate some areas with rainfall reductions (<1) relative to the station location and others with significant rainfall increases up to 5 times the value at the AWS site. At this scale of application the correction factors are likely to reflect wind funnelling of rainfall around the overall topography of the site. The values are highly variable seasonally depending on overall wind strength (which is greater than 5 m/s on average in Jan, Feb, Mar and Dec.). Thus at this scale, the spatial variability of rainfall is highly dependent upon wind speeds (and their effect on funnelling of rainfall). Thus spatial variability in rainfall receipt is much greater at wind speeds above 5 m/s.

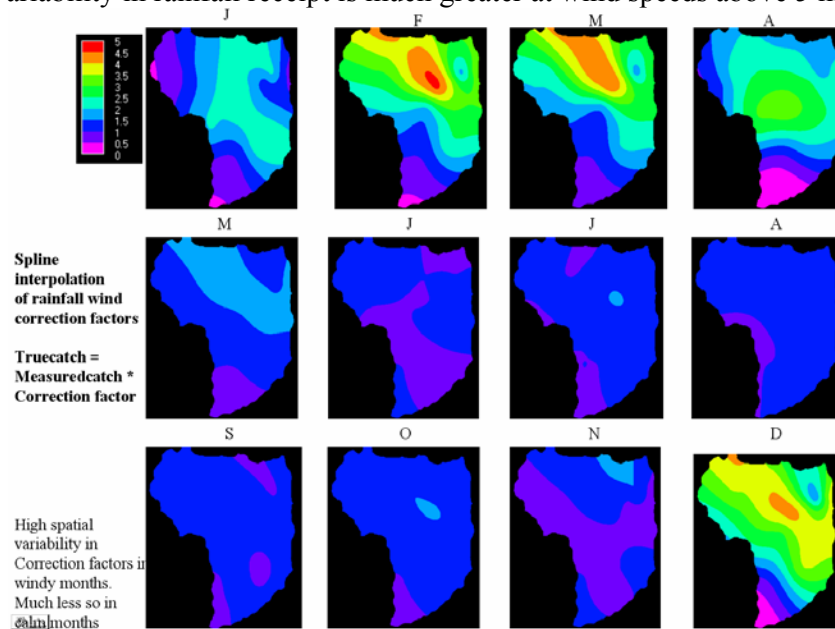


Figure 3 Monthly spatial rainfall correction factors for FIESTA pasture site (2002/3)

In summary this method can be used to remove the local effects of gauge wind losses and to generate spatial patterns of rainfall receipt around the catchment which are more representative of actual gauge rainfall catches.

**2.1.1.2.2 Stage 2 *Improved interpolation through process modelling of wind-driven rain (captures small scale terrain catch effects)***

Whilst the method outlined is useful for estimating the approximate spatial distribution of rainfall on the basis of measured values, correcting those for local gauge losses and capturing the spatial variation in planimetric rainfall receipts that results from wind funnelling and leeward/windward effects, it does little to take into account the effects of wind on the actual receipts of rainfall by the underlying spatially-variable topography. In order to do that some further steps are necessary.

- (4) If one is working at large spatial scales for which there is likely to be spatial variation in rainfall catches for reasons other than differential gauge wind losses (i.e. spatially variable rainfall inputs or wind funnelling) then one carries through the next stage using the spatially interpolated rainfall data described above. If one is working at small spatial scales where these wind effects are likely to be the only ones controlling spatial differences in rainfall and no wind funnelling is likely then one can apply the next stage directly to the single, best (most reliable, long term, average exposure) station. If wind funnelling is likely to be important then it is best to apply the following technique to the spatially interpolated rainfall data described above
- (5) Using this initial rainfall distribution and taking the hourly wind speed and wind direction data from the AWS the methods developed for the FIESTA fog delivery model (section 4) are used to convert the AWS measured wind speed and direction to a wind direction for each grid cell in the DEM using the TOPEX approach for wind speed and a topography-based approach for wind direction. In this way for each hour of the AWS rainfall, wind speed and wind direction input, maps of the corresponding wind speed and wind direction for all grid cells of the area of interest are developed. The wind direction map is used to calculate topographic exposure of each cell to winds coming from the mapped direction (which may not be the same as the AWS direction for that hour).
- (6) From this topographic exposure an ‘exposure wind speed ratio’ is calculated based on Ruel et al. (2002) and the hourly raw AWS wind speed is corrected for the exposure of the AWS monitoring site as :

$$W_c = W_m / EWSR_{AWS}$$

Where

$W_c$  – exposure corrected wind speed (m/s)

$W_m$  – measured windspeed (m/s)

$EWSR_{AWS}$  – exposure wind speed ratio at site of AWS

- (7) Now exposure-corrected wind speeds can be calculated for each grid cell as the product of the AWS-measured wind speed and the exposure wind speed ratio

- (8) Wind speeds are now corrected for the difference between the measurement height and the vegetation height (based on the vegetation map) and using wind profile measurements taken at forest and pasture sites, leading to the following relationships:

For pasture areas,  $F = 0.1428 \cdot \ln(\text{VegHt}) + 0.878$

For forest areas,  $F = 0.7898 \cdot \exp^{(0.1004 \cdot \text{VegHt})}$

The wind speed at the vegetation height is then

$$W_v = W_c \cdot F$$

- (9) Rainfall correction on the basis of topography is now simply a matter of applying the Arazi et al. (1996) equations to the wind speeds ( $W_v$ ) and interpolated, gauge-loss corrected, rainfalls of each cell, by calculating the relationship between slope gradient and the angle of falling rain at the calculated wind speeds ( $W_v$ ), and the relationship between the wind direction and compared with the direction in which the slope is facing. This process yields the results displayed in Figure 4.

### 2.1.1.3 Results

Using the (wind-loss uncorrected) AWS-measured value gives a rainfall total of **4198.7 mm** for day 183, 2003 to day 182 2004 at the pasture site. The windloss corrected and spline interpolated value is **6393.1 mm**. The windloss corrected and process model distributed total (i.e applying both techniques) is **7696.0 mm**. Applying the process modelling approach only (which does not account for wind funnelling effects) gives **4893.9 mm**. The most accurate and spatially realistic of these is likely to be the windloss corrected and process model distributed total (i.e applying both techniques) : 7696.0 mm for 2003/2004, since this calculates terrain-received rather than gauge received totals, corrects the original gauge data for wind losses and incorporates the spatial effects of wind funnelling of rainfall. Much of this extra is rainfall travelling near-horizontally at high wind speeds and caught by forest vegetation (see Figure 4). This rainfall would not form part of the input for this catchment if the- particularly tall – vegetation, which is thus subject to higher wind speeds, were absent.

*The spatial patterns in annual totals produced by the different techniques are shown in Figure 4.*

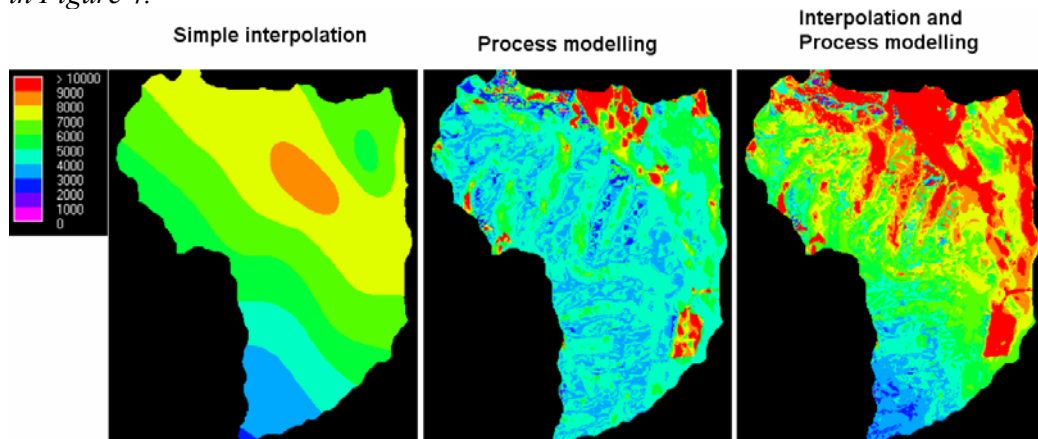


**Figure 4 Spatial patterns in annual total rainfall inputs according to the three interpolation techniques**

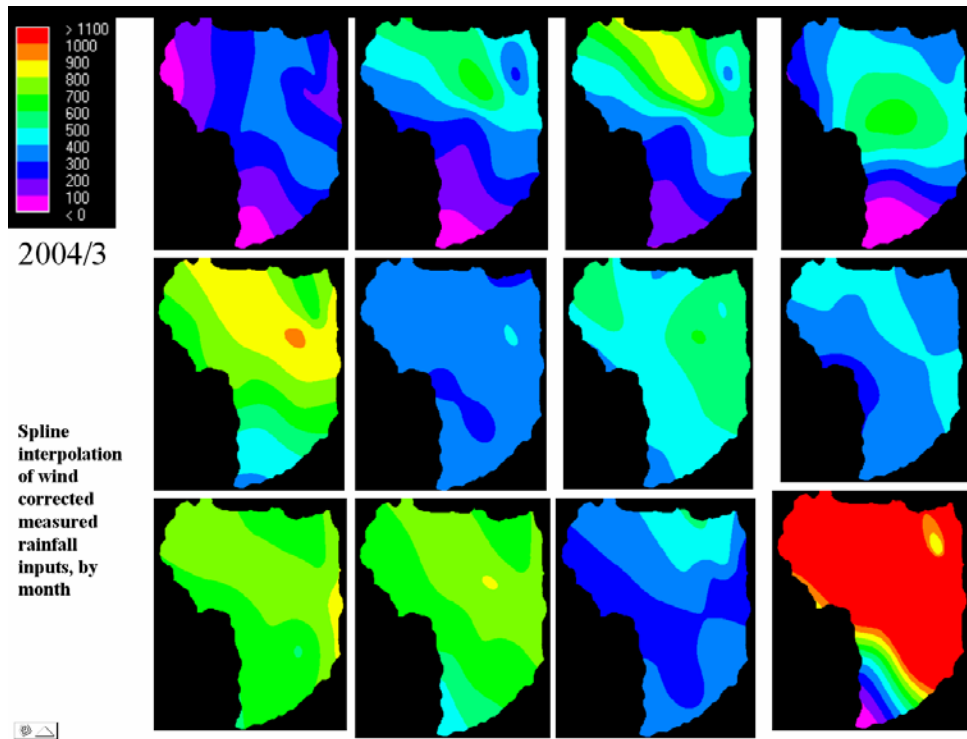


Figure 5 Monthly spatial rainfall receipts from spline interpolation of gauge loss corrected values for FIESTA pasture site (2004/3)

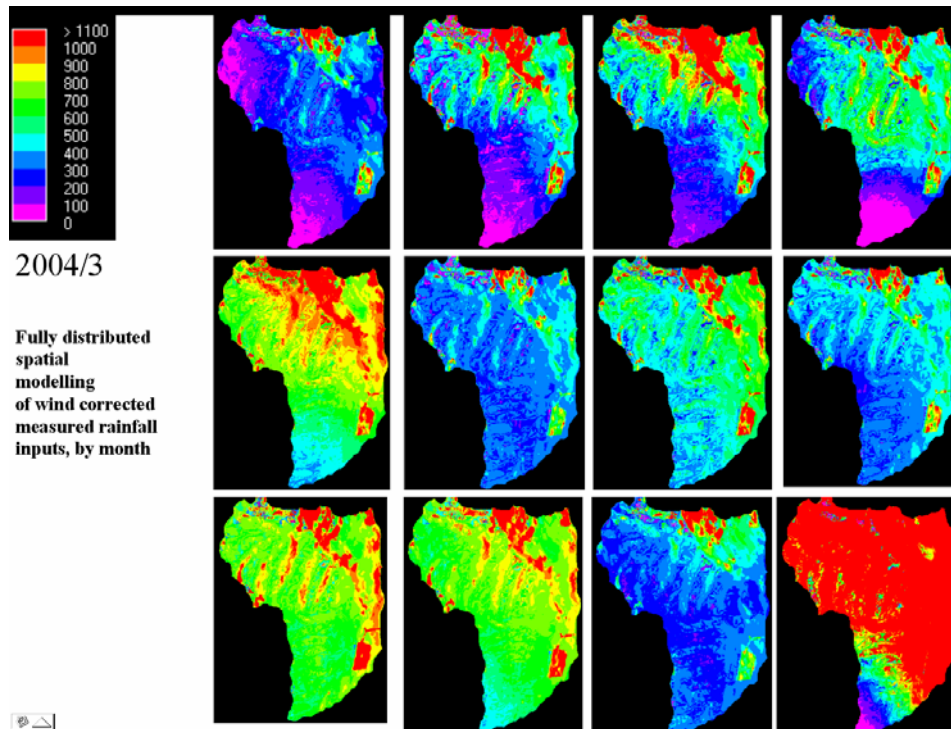


Figure 6 Monthly spatial rainfall receipts from process based modelling of gauge loss corrected spline interpolated values for FIESTA pasture site (2004/3)

Figure 5 and Figure 6 show the monthly progression of spatial rainfall using the two interpolation methods. The emerging rainfall patterns are a function of the

relationship between AWS measured rainfall and rainfall elsewhere (the spatial correction factors of Figure 3) and the combination of monthly total rainfall and wind speed. The wettest month at the AWS (September, see Figure 7) is not necessarily the wettest month over the catchment as a whole (December) because of the influence of the spatial correction factors, which have their greatest influence in Mar, Apr, May, September, October and December. In other words the wettest month as measured by a single gauge may be quite different to the actual wettest month for that gauge or for the whole catchment (that month with the highest rainfall but also high wind speeds which reduce the gauge catches but not the terrain or vegetation catches).

The process-modelled results indicate higher rainfall receipts on ridges exposed to the (dominant) NE winds, especially in the northern part of the site where topographic funnelling leads to higher measured catches. The most exposed parts yield very high inputs over small areas. Vegetation also clearly has an effect with the areas covered in forest and individual trees (@15m high) receiving high inputs of rainfall (where they are oriented favourably compared with the wind direction) than the surrounding grassland because of the higher wind speeds aloft.

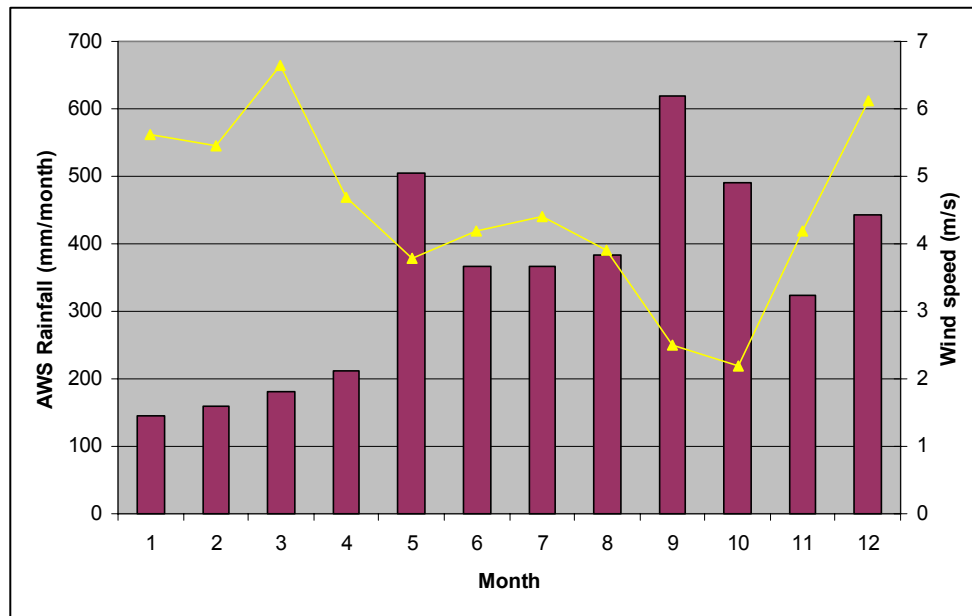
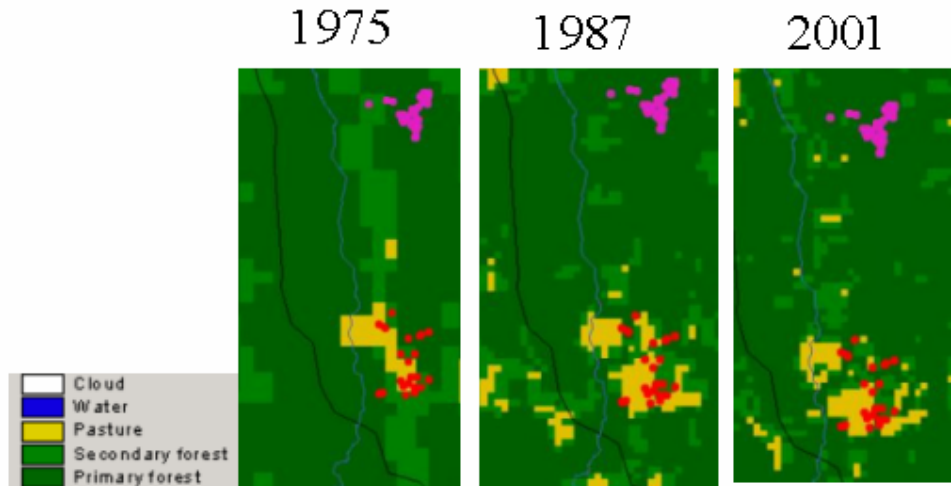


Figure 7 Raw wind speed and rainfall inputs to modelling at pasture AWS 2004/3

### 2.1.2 Vegetation

Small extent hydrological studies require much more detailed characterisation of the vegetation cover and characteristics than is usually necessary for larger extent (coarser scale) studies. A supervised classification of landsat imagery for the scenes, which cover the Chiquito catchment, also provided information on the land cover type of the San Gerardo catchments. As is clear from Figure 8, the pasture site has been pasture since at least 1975 though it has likely increased in size since then. The forest site has been forest since at least 1975 and likely much longer.



**Figure 8 Land use in the San Gerardo forest and pasture catchments. The red and pink dots mark the locations of instruments at the sites.**

In order to better understand and model aspects of hydrology at the SG sites, much more spatially detailed land cover information were required. This was achieved with a combination of georeferenced IKONOS imagery and ground based (tethered helium balloon) aerial photography. Georeferenced image mosaics were produced from both sources in order to map forest blocks and isolated trees for both sites which were used in the precipitation characterisation outlined above, amongst other things. Some of the very spatially detailed pasture site aerial imagery was used (by C. Tobon) for mapping cow trails.

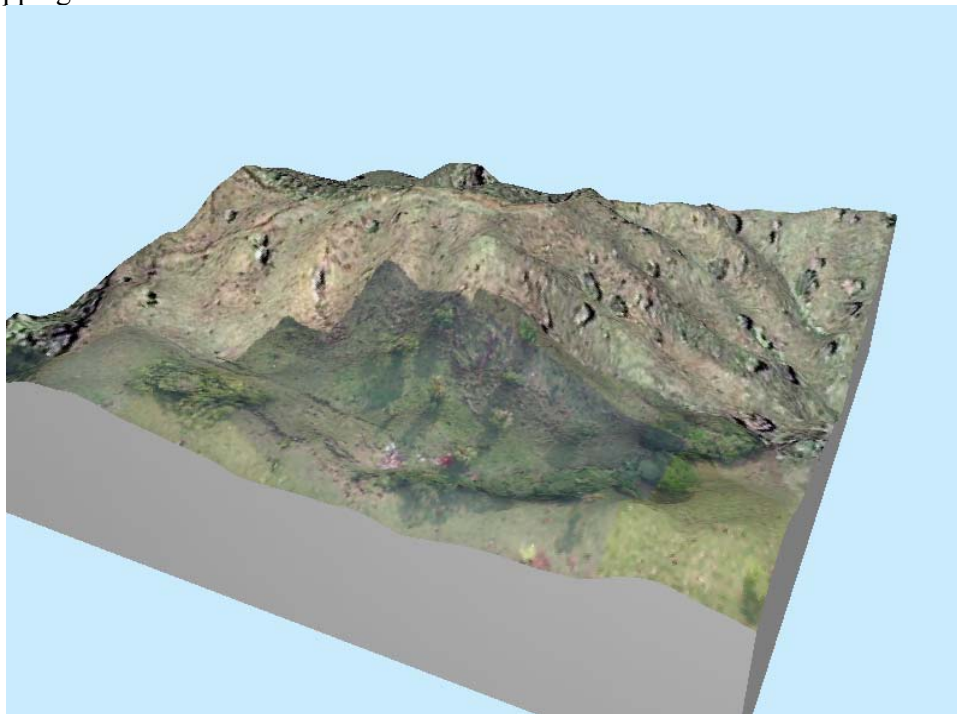


**Figure 9 Combined IKONOS and tethered aerial photographic mosaic of pasture site, overlaid on topography.**

Figure 9 shows an ortho-mosaic of the aerial photography and IKONOS data superimposed on the DEM for the pasture site. The resulting vegetation cover map which shows forest blocks and isolated trees at the SG site are shown in Figure 10. It is this map which is used in the earlier precipitation receipt analysis.

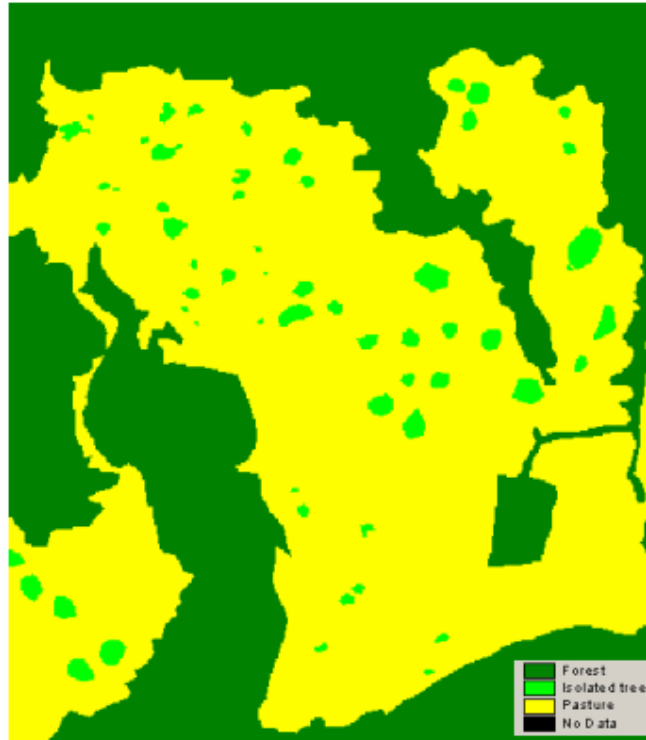


**Figure 10 Resulting vegetation cover map (1m grain)**

In addition to these maps a differential GPS and laser rangefinder survey was carried out in order to map the locations of all instruments at both sites (see Figure 8. for the resulting distributions). These locations were important to various of the SG site analyses.

### 3 The Chiquito Scale

KCL/AMBIOTEK's efforts at the Chiquito scale were focused on the spatialisation of climate and terrestrial data for the parameterisation of the Chiquito model on the basis of newly produced (two field campaigns) or existing (GIS and remote sensing) measurements. The data outlined in Table 1 were produced and all were supplied with 25m grid, cut to the whole of Chiquito catchment, and in a geographic coordinate system WGS84 DATUM. Not all were used in the final model but many were (see CqFlow chapter for further detail). Short explanations are given in the table, and some of the methods used are explained in section 4. Space precludes detailed explanation of the production methods of all maps used here.

Data	Explanation
<b>forest edges (forest pasture boundaries)</b>	
south_edge.asc	forest-pasture boundaries facing south
north_edge.asc	forest-pasture boundaries facing north
east_edge.asc	forest-pasture boundaries facing east
west_edge.asc	forest-pasture boundaries facing west
edge_dist.asc	distance from forest edge to interior (metres)
forest_edge_dir.asc	the direction of the forest edge, 1=north,2=east,3=south,4=west
forest_edge_length.asc	the length of the forest edge (metres)
forest_edges.asc	a map showing all forest edges (edge=1, nonedge=0)
dist_edge.asc	the distance from the forest interior to the nearest edge (metres)
<b>land cover</b>	
sp87_01.asc	land converted from secondary forest to pasture from 1987 to 2001
sp75_87.asc	land converted from secondary forest to pasture from 1975 to 1987
ps75_87.asc	land converted from pasture to secondary forest from 1975 to 1987
ps87_01.asc	land converted from pasture to secondary forest from 1987 to 2001
fp75_87.asc	land converted from forest to pasture from 1975 to 1987
fp_87_01.asc	land converted from forest to pasture from 1987 to 2001
for_age.asc	age of forest (years)
pasture_2001.asc	pasture in 2001
pastage.asc	age of pasture (years)
lu1975.asc	the land use classes in 1975
lu1987.asc	the land use classes in 1987
lu2001.asc	the land use classes in 2001
<b>meteorology</b>	
febrainfall.asc	Mean monthly rainfall for february, for six best ICE <sup>2</sup> stations average of daily data for 1991 to 2003
marrainfall.asc	Mean monthly rainfall for march for six best ICE stations average of daily data for 1991 to 2003
aprrainfall.asc	Mean monthly rainfall for april for six best ICE stations average of daily data for 1991 to 2003
mayrainfall.asc	Mean monthly rainfall for may for six best ICE stations average of daily data for 1991 to 2003
junrainfall.asc	Mean monthly rainfall for june for six best ICE stations average of daily data for 1991 to 2003
julrainfall.asc	Mean monthly rainfall for july for six best ICE stations average of daily data for 1991 to 2003

<sup>2</sup> Instituto Costarricense de Electricidad

---

augrainfall.asc	Mean monthly rainfall for august for six best ICE stations average of daily data for 1991 to 2003
seprainfall.asc	Mean monthly rainfall for september, for six best ICE stations average of daily data for 1991 to 2003
octrainfall.asc	Mean monthly rainfall for october, for six best ICE stations average of daily data for 1991 to 2003
novrainfall.asc	Mean monthly rainfall for november for six best ICE stations average of daily data for 1991 to 2003
decrainfall.asc	Mean monthly rainfall for december, for six best ICE stations average of daily data for 1991 to 2003
janrainfall.asc	Mean monthly rainfall for january for six best ICE stations average of daily data for 1991 to 2003
annrainfall.asc	Mean annual rainfall, for six best ICE stations average of daily data for 1991 to 2003
dry days_pc.asc	% of non rainfall days, for eight best ICE stations daily data 1991 to 2003
mean_monthly_rain.asc	Mean monthly rainfall for six best ICE stations 1991 to 2003
cov_month_rain.asc	Coefficient of variation of monthly rainfall (rainfall seasonality) from six best ICE stations 1991 to 2003, %
windir.asc	Average wind direction, 1=north,2=neast,3=east
av_windn.asc	Average wind speed (m/s)
windspratio.asc	Ratio of windspeed without topographic effect to windspeed with topographic effect, after Ruel (1996)
av_topo_wind.asc	Wind speeds (m/s) modified for topographic exposure of dominant wind directions (from NE)
av_ann_temperature.asc	Average annual temperature (C), three best FIESTA stations 2002-2004
av_temp_01.asc	Average temperature for January (C ), three best FIESTA stations 2002-2004
av_temp_02.asc	Average temperature for february (C ), three best FIESTA stations 2002-2004
av_temp_03.asc	Average temperature for march (C ), three best FIESTA stations 2002-2004
av_temp_04.asc	Average temperature for april (C ), three best FIESTA stations 2002-2004
av_temp_05.asc	Average temperature for may (C ), three best FIESTA stations 2002-2004
av_temp_06.asc	Average temperature for june (C ), three best FIESTA stations 2002-2004
av_temp_07.asc	Average temperature for july (C ), three best FIESTA stations 2002-2004
av_temp_08.asc	Average temperature for august (C ), three best FIESTA stations 2002-2004
av_temp_09.asc	Average temperature for september (C ), three best FIESTA stations 2002-2004
av_temp_10.asc	Average temperature for october (C ), three best FIESTA stations 2002-2004
av_temp_11.asc	Average temperature for november (C ), three best FIESTA stations 2002-2004
av_temp_12.asc	Average temperature for december (C ), three best FIESTA stations 2002-2004
windtopo_1dd.asc	Ignore this
windtopos_1dd.asc	Flow directions for winds from the south, mediated by topography according to section 4.2.1.9
windtopon_1dd.asc	Flow directions for winds from the north mediated by topography according to section 4.2.1.9
windtopow_1dd.asc	Flow directions for winds from the west mediated by topography according to section 4.2.1.9
windtopose_1dd.asc	Flow directions for winds from the south east mediated by topography according to section 4.2.1.9

---

---

windtopoe_1dd.asc	Flow directions for winds from the east mediated by topography according to section 4.2.1.9
windtopone_1dd.asc	Flow directions for winds from the northeast mediated by topography according to section 4.2.1.9
windtoponw_1dd.asc	Flow directions for winds from the northwest mediated by topography according to section 4.2.1.9
windtoposw_1dd.asc	Flow directions for winds from the southwest mediated by topography according to section 4.2.1.9
Ground cloud frequency	Frequency of ground level cloud by combining observed MODIS cloud frequency with ground level frequency of condensing conditions
<b>topography</b>	
ruggedness.asc	A measure of topographic roughness in a single cell window around the cell of interest
order.asc	Stream order, after Strahler
catch.asc	Catchments
aspect.asc	Aspect (deg N)
slopedeg.asc	Slope gradient (deg)
topexne.asc	Topographic exposure, 8 maps, one for each wind direction after Ruel (1996), used in the calculation of wind overspeed
<b>human</b>	
roadsn.asc	Digitized roads from area covered by IKONOS imagery, 1=major (tarmaced) road,2=minor road
mainroad.asc	Digitized roads from area covered by IKONOS imagery, 1=major (tarmaced) road
minorroad.asc	Digitized roads from area covered by IKONOS imagery, 1=minor (not tramaced) road
<b>sampling</b>	
all_sites.asc	Locations of the forest, pasture and secondary forest sites
ikonos.asc	Area for which IKONOS imagery is available
chiq_stnn.asc	Locations of the chiquito met stations
<b>vegetation</b>	
numtrees_filled.asc	Number of isolated trees in each grid cell
Bromeliads	Estimated number of bromeliads (individuals/hectare)
crown epiphytism	Estimated crown epiphytism (m <sup>3</sup> epiphytes/Ha.)
gap fraction	Gap fraction
LAI	Estimated Leaf area Index(m <sup>2</sup> leaves/m <sup>2</sup> ground)
stem density	Estimated stem density (stems/hectare)
whole tree epiphytism	Estimated whole tree epiphytism (m <sup>3</sup> epiphytes/Ha.)
tree height	Estimated tree height (m)

---

**Table 1 Maps provided for Chiquito scale modelling (not all used)**

### 3.1.1 Land cover

Information on recent land use change in the Chiquito is fundamental to understanding both the nature of land use change in the region and the likely future course of land use and thus the development of scenaria for change. Figure 11 to Figure 13 show land cover changes in the Chiquito from 1987 to 2001.

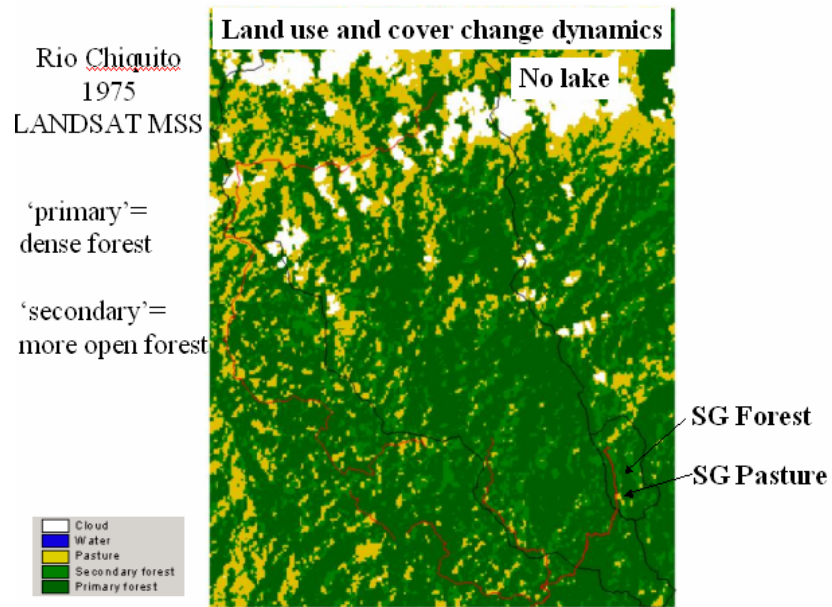


Figure 11 Land use 1975. SG= San Gerardo.

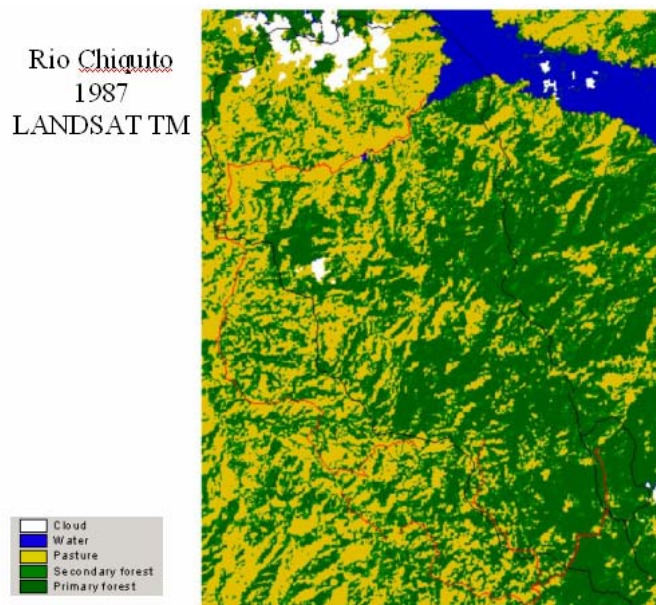
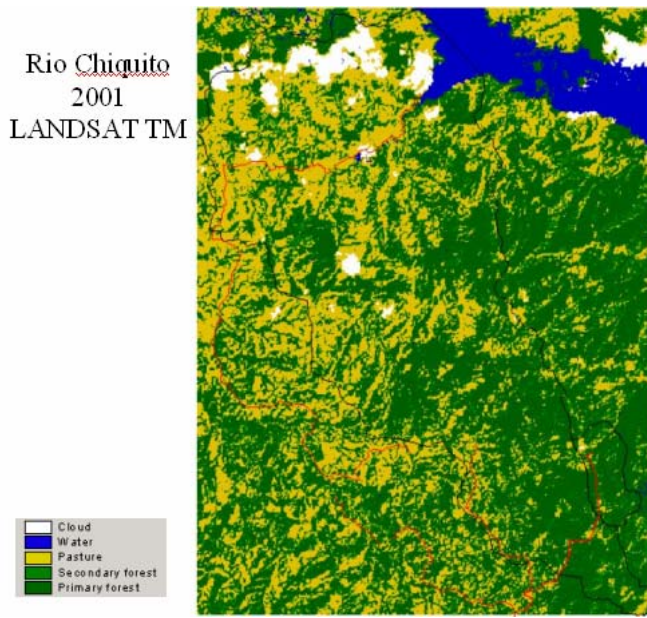


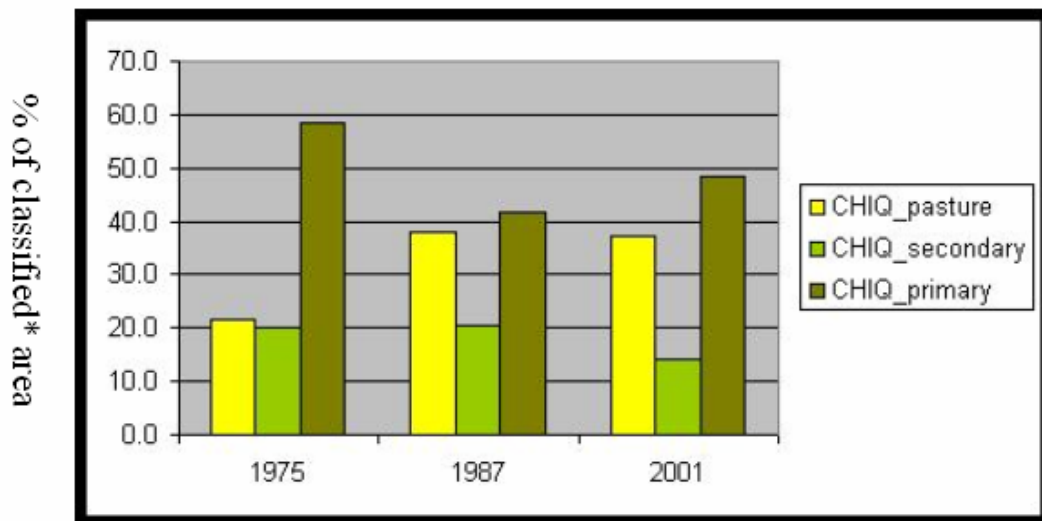
Figure 12 Land use 1987



**Figure 13 Land use 2001**

These were produced with a simple supervised classification of purchased landsat data. The distinction between ‘primary’ and ‘secondary forest’ is based on the NDVI (Normalised Difference Vegetation Index) and thus represents a difference in forest density. The analysis shows that primary forest cover in the Chiquito was already down to <60% by 1975 and is now less than 50%. Pasture-isation was greatest from 1975-1987 with the most significant change from 1987 to 2001 being a decrease in secondary forest (see Figure 14).

Land use in the Chiquito 1975-2001



\* i.e. excluding cloud and water

**Figure 14 Land use change in the Chiquito.**

A multitemporal analysis (Figure 15) indicates that forest loss and forest regeneration occurred simultaneously in different parts of the catchment. The analysis indicates that conversion rates of forest to pasture were greatest from 1975-1987 and were especially concentrated in the lower parts of the catchment. Rates were much lower by 1987-2001 and tended to be greatest in the middle altitudes. Forest regeneration occurred in both periods and was highest in the lowlands from 1975-1987 but with two peaks (at 650 and 1025m) by 1987-2001.

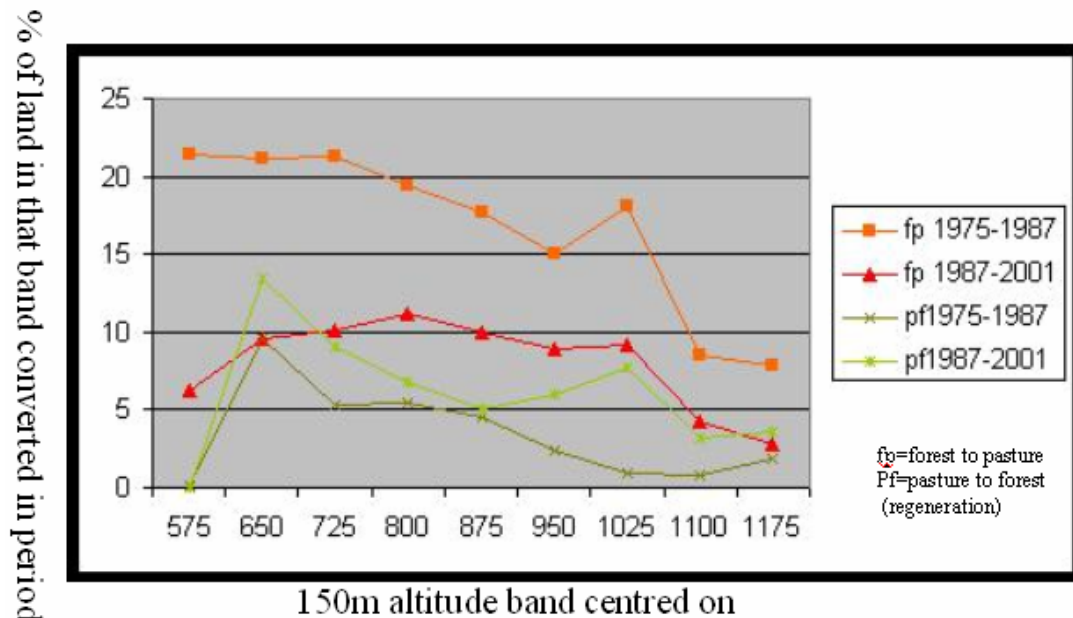


Figure 15 Land use change by altitude for the Chiquito catchments

### 3.1.2 Forest edges

Forest-pasture boundaries (or edges) are important because of their exposure to horizontal precipitation and fog and thus their potential to enhance these ‘occult’ inputs in fragmented landscapes (see section 4.3. for methodological detail). Forest edge calculations for the Chiquito catchment are shown in Figure 16 which indicates the location and direction of edges relative to wind directions and also the distance to the nearest edge (a measure of the intactness of remaining forest and of forest exposure). Clearly very few large intact areas of forest remain and these are all in the upper reaches of the catchment.

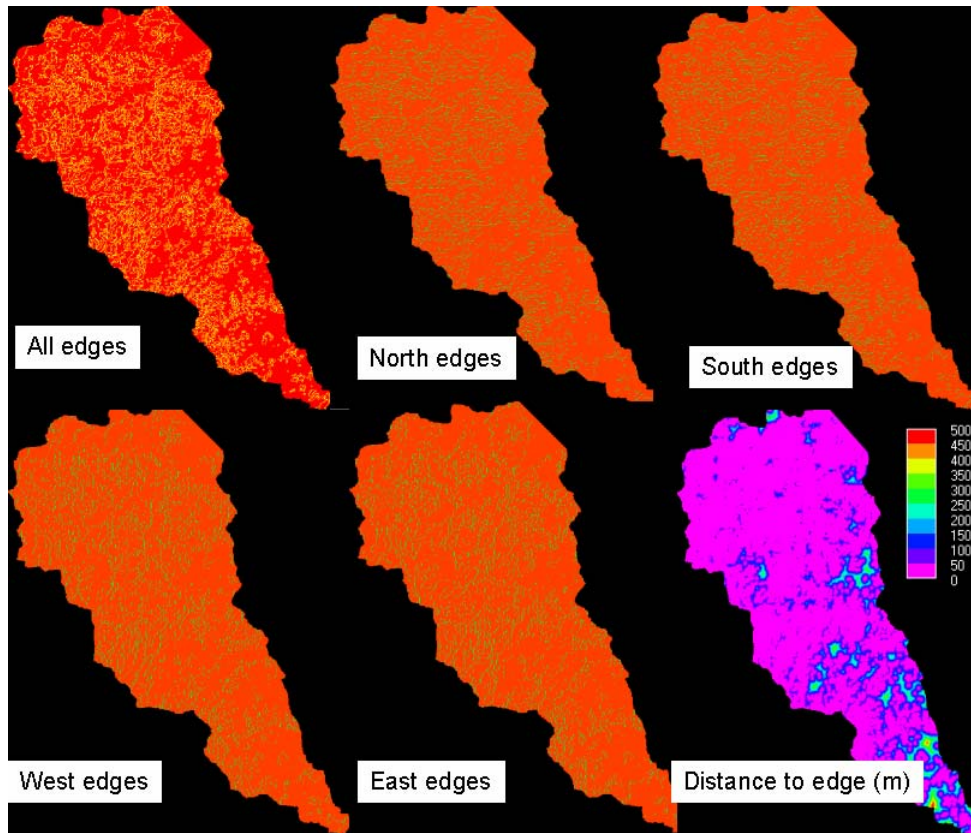


Figure 16 Forest-pasture edge metrics for the Chiquito

### 3.1.3 Meteorology

The various meteorological spatialisations were produced from a combination of existing (ICE) station data and project data at the Chiquito stations (see Table 1). In all cases data were quality controlled and derived for contiguous and comparable periods before being spatialised using a combination of altitude based relationships and spline-interpolations, as appropriate.

#### 3.1.3.1 Temperature

The monthly progression of temperature is shown in Figure 17 and indicates that May-September are the warmest months with temperatures varying from 16 to 25 °C depending on altitude. The coolest months are November through February, which still have temperatures of around 22 °C in the lowest parts of the catchment but down to 10°C in the highest parts. The maps were generated in a two stage process. In the first stage a linear relationship between mean comparable temperature for the stations incorporating all comparable data from 2002-2004 and altitude is produced. For the Chiquito stations at 620, 942, 1115 and 1193 masl the relationship for mean annual temperature is:  $y = -0.0087x + 27.423$ ,  $R^2 = 0.964$ . This process is used to produce an initial altitude-based interpolation on a monthly basis. For each station a monthly offset (residual) from the predicted temperature is then calculated as a measure of the regional (non-altitudinal) controls on temperature. These offsets are shown along with the regression relationships on a monthly basis in Table 2. With reference to Figure 17, clearly the range in temperature across the catchment is large and often 15°C between the upper and lower reaches: indicative of the importance of

spatialisation and distributed rather than lumped modelling in this kind of environment.

	Average of Temp 2m, [°C]chiq1	Average of Temp 2m, [ °C] chiq2	Average of Temp 2m, [ °C], chiq3	Average of Temp 2m, [ °C], chiq4	Regression relationship
Altitude	620	1193	942	1115	
<b>measured</b>					
Jan	21.0	16.2	18.0	15.0	
Feb	21.8	17.8	18.7	16.3	
Mar	22.2	17.5	19.0	17.2	
Apr	22.7	18.3	19.3	17.7	
May	22.9	19.8	19.1	17.9	
Jun	22.7	20.2	20.5	18.0	
Jul	22.5	19.7		17.4	
Aug	22.6	19.8		17.5	
Sep	22.7	20.3		18.0	
Oct	22.5	19.9	19.2	17.9	
Nov	21.9	17.8	19.1	16.3	
Dec	21.4	16.2	18.8	15.8	
<b>modelled</b>					
Jan	21.0	15.4	17.8		16.2 y = -0.0097x + 26.985
Feb	21.5	16.7	18.8		17.4 y = -0.0084x + 26.735
Mar	22.0	17.0	19.2		17.7 y = -0.0087x + 27.423
Apr	22.4	17.6	19.7		18.3 y = -0.0084x + 27.638
May	22.3	18.4	20.1		18.9 y = -0.0068x + 26.487
Jun	22.5	19.0	20.5		19.5 y = -0.0061x + 26.267
Jul	22.3	18.4	20.1		18.9 y = -0.0068x + 26.483
Aug	22.4	18.5	20.2		19.0 y = -0.0068x + 26.6
Sep	22.5	19.1	20.6		19.5 y = -0.006x + 26.225
Oct	22.0	18.5	20.0		19.0 y = -0.0061x + 25.753
Nov	21.8	16.8	19.0		17.5 y = -0.0088x + 27.264
Dec	21.5	15.8	18.3		16.6 y = -0.0099x + 27.643
<b>residuals</b>					
Jan	0.0	0.8	0.2	-1.2	
Feb	0.2	1.1	-0.1	-1.0	
Mar	0.1	0.5	-0.2	-0.5	
Apr	0.3	0.7	-0.4	-0.5	
May	0.6	1.5	-1.0	-1.0	
Jun	0.2	1.2	-0.1	-1.5	
Jul	0.2	1.3		-1.5	
Aug	0.2	1.3		-1.6	
Sep	0.2	1.2		-1.5	
Oct	0.5	1.4	-0.8	-1.1	
Nov	0.1	1.0	0.1	-1.1	
Dec	-0.1	0.4	0.4	-0.8	

Table 2 Temperature altitude relationships for the Chiquito and regional offsets

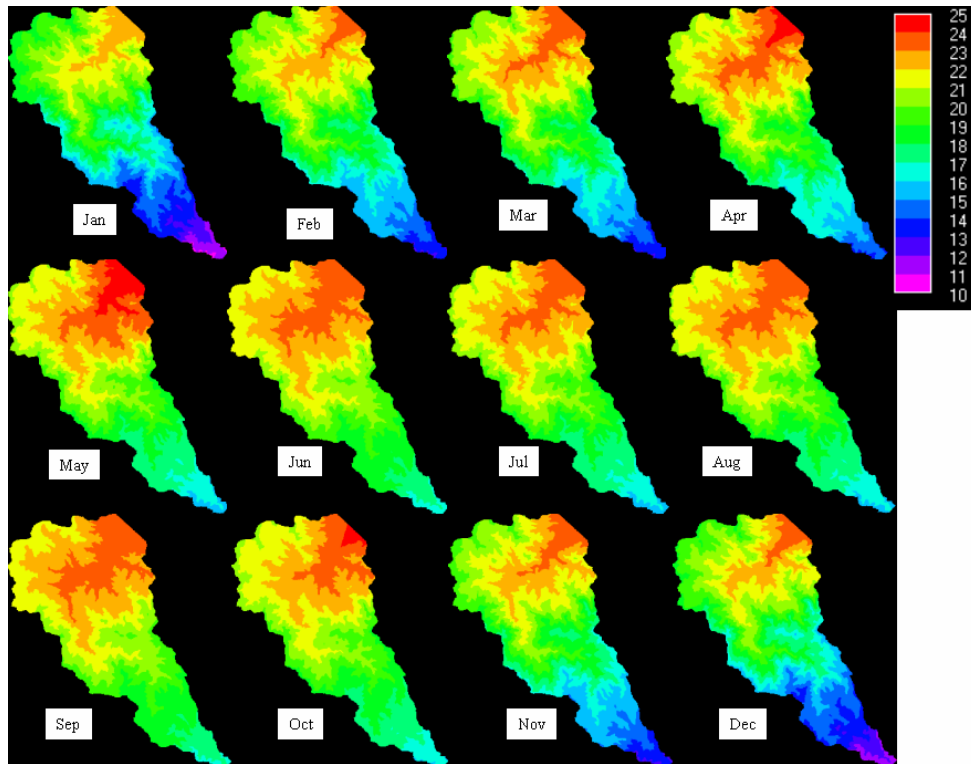


Figure 17 Annual progression of mean monthly temperature for Chiquito

### 3.1.3.2 Monthly Rainfall

Rainfall spatialisation was achieved from data for the six best ICE stations (Caño Negro, Cerro Chiripa, Guayabos, Las Nubes, San Bosco, San Gerardo) from an average of daily data for periods of comparable data quality for the six stations from 1991 to 2003. Rainfall shows a strong linear relationship with altitude for the catchment ( $y = 0.7559x + 2708$ ,  $R^2 = 0.8202$ ). The relationship between rainfall seasonality (measured as the coefficient of variation of monthly rainfall) and altitude is more exponential ( $y = 0.1659e^{0.0005x}$ ,  $R^2 = 0.9552$ ).

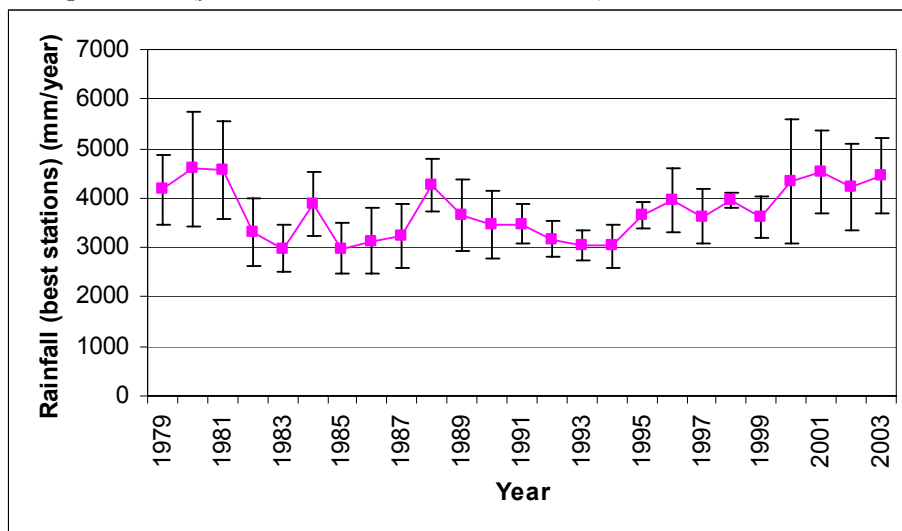
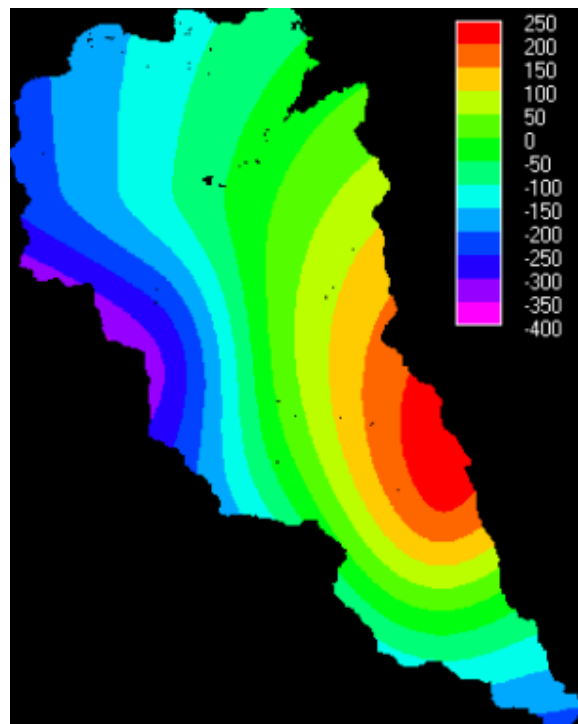


Figure 18 Time series of mean and standard deviation of annual rainfall for six best stations.

Figure 18 shows the rainfall series for these Chiquito stations and indicates a cyclic pattern of variation with peaks in the late 1970s and late 1980s and a gradual increase from the early 1990s to the present day. Station to station variability tends to be greater during periods of high average rainfall. It is clear from Figure 20 that the monthly variability in rainfall is greater than the spatial variation in rainfall across the catchment within a month. Lowest rainfalls are observed February-April. Rainfall is always significantly higher in the upper reaches of the catchment. Rainfall spatialisation was a two stage process. First the regression between altitude and rainfall discussed was used to present an altitudinal spatialisation of rainfall. Then for each station, an offset was calculated on a monthly basis to represent the regional deviation from the rainfall-altitude relationship and this was interpolated using a tension spline and used as a correction to represent non-altitudinal effects of rainfall. These spatial correction factors which represent exposure and other effects are highly variable from month to month, the annual total effect is a strong one as is clear from Figure 19 which indicates enhancements over the altitudinal effect of +250mm in the exposed south-east of the catchment and reductions of up to -400 in the drier western slopes. As is also the case with temperature, the correction factors are more important in some months than others since in some months the altitudinal relationships/controls are less strong. The final rainfall interpolations were the integral of the altitudinal effect and the regional effect on a monthly basis (see Figure 20) though the seasonality is clearer in Figure 21. These data are also given in tabular form (Table 3).



**Figure 19 Annual total rainfall offsets.**

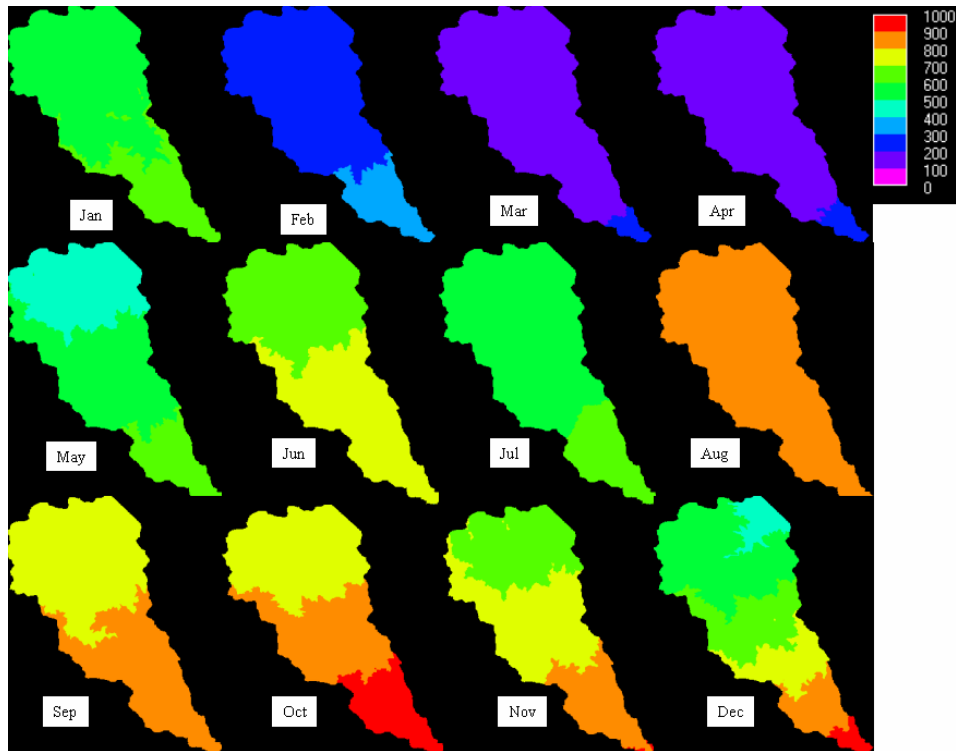


Figure 20 Annual progression of rainfall for the Chiquito catchment.

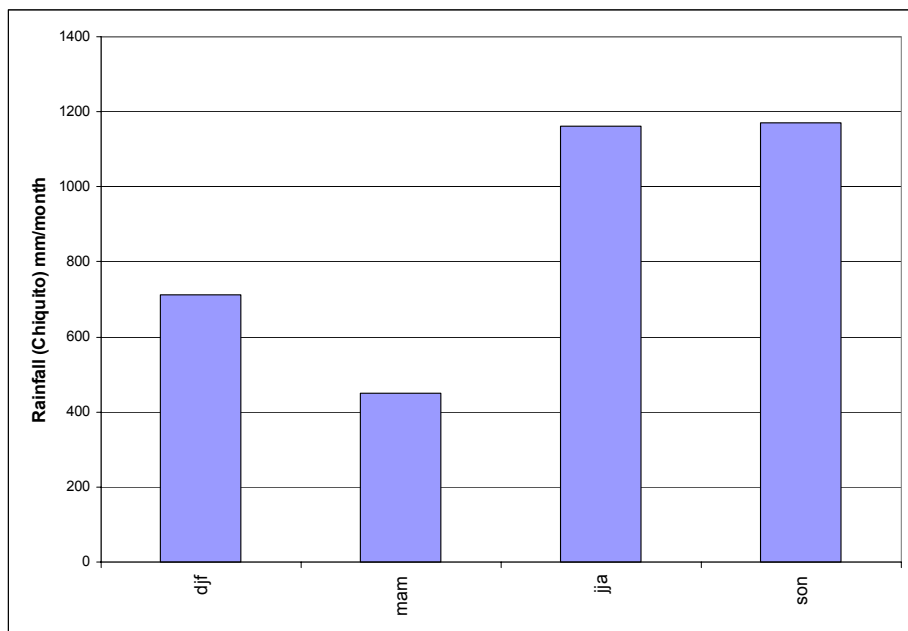


Figure 21 Pattern of rainfall seasonality for the 6 best Chiquito stations.

FIESTA Final Technical Report

	Place	Caño Negro Rainfall (mm)	Cerro Chiripa Rainfall (mm)	Guayabos Rainfall (mm)	Las Nubes Rainfall (mm)	San Bosco Rainfall (mm)	San Gerardo Rainfall (mm)	
	Altitude	730	1038	600	1300	1400	1620	
Annual	R	3259.8	3492.6	3161.5	3690.6	3766.2	3932.5	$y = 0.7559x + 2708$ $R^2 = 0.82$
Jan	O	1414.9	41.8	-4.4	-193.1	190.8	-35.0	
	R	1893.2	2172.9	1775.1	2410.8	2501.6	2701.4	$y = 0.9081x + 1230.3$ $R^2 = 0.94$
Feb	O	2290.2	22.8	-27.1	-51.4	140.3	-84.4	
	R	1455.7	1627.2	1383.3	1773.1	1828.8	1951.3	$y = 0.5568x + 1049.3$ $R^2 = 0.58$
Mar	O	1281.3	-201.5	66.4	-35.5	276.9	-106.4	
	R	810.5	944.6	754.0	1058.6	1102.1	1197.9	$y = 0.4352x + 492.84$ $R^2 = 0.71$
Apr	O	1064.8	17.6	42.8	-168.5	515.2	108.0	
	R	1010.9	1079.7	981.8	1138.3	1160.6	1209.8	$y = 0.2235x + 847.78$ $R^2 = 0.47$
May	O	792.8	77.8	0.9	-144.6	-100.7	65.8	
	R	2950.5	3266.2	2817.3	3534.8	3637.3	3862.8	$y = 1.025x + 2202.3$ $R^2 = 0.64$
June	O	1207.9	-358.2	198.7	-231.2	362.9	27.9	
	R	4086.7	4277.1	4006.3	4439.1	4501.0	4637.0	$y = 0.6183x + 3635.4$ $R^2 = 0.88$
July	O	992.5	65.8	-3.8	-147.7	58.1	27.5	
	R	4922.7	4864.8	4947.1	4815.6	4796.8	4755.5	$y = -0.1878x + 5059.8$ $R^2 = 0.03$
Aug	O	1935.1	-32.6	95.2	-592.7	507.3	23.0	
	R	5191.4	5092.4	5233.2	5008.2	4976.1	4905.4	$y = -0.3214x + 5426.1$ $R^2 = 0.16$
Sep	O	1464.3	-407.9	194.5	-94.8	315.4	-7.1	
	R	4592.1	4828.2	4492.4	5029.0	5105.7	5274.3	$y = 0.7666x + 4032.5$ $R^2 = 0.39$
Oct	O	553.1	502.8	-336.8	270.7	-162.6	-274.3	
	R	4642.5	5044.8	4472.8	5387	5517.6	5804.9	$y = 1.306x + 3689.2$ $R^2 = 0.76$
Nov	O	539.6	458.1	-242.6	-122.2	90.4	-183.9	
	R	4157.8	4536.8	3997.9	4859.2	4982.2	5252.9	$y = 1.2304x + 3259.7$ $R^2 = 0.8$
Dec	O	1741.8	63.5	20.8	-297.5	168.5	44.8	
	R	3238.2	3969.0	2929.8	4590.6	4827.9	5349.9	$y = 2.3726x + 1506.3$ $R^2 = 0.87$
	O	3150.5	365.1	-69.9	-569.5	186.5	87.7	

**Table 3** Altitudinal and regional relationships for Chiquito rainfall. **O**= regional offset (mm), **R**= rainfall from altitudinal regression (mm)

### 3.1.3.3 Annual and COV Rainfall

Thus the best rainfall interpolation produces annual totals ranging from 3000 mm in the lower reaches to 4100 mm in the upper reaches (but spatial differences are likely to be larger because of wind driven effects, see section 4.9.4. The pattern is one of least rainfall in the lower altitude northern and also the western parts of the catchment with higher rainfalls in the south and east. The coefficient of variation of monthly rainfall (COV,%), a measure of rainfall seasonality, indicates higher seasonality in the lower parts of the catchment (45%), though rainfall seasonality is still high (40%) even in the upper reaches. This was calculated from a regression relationship with altitude, with no local offsets.

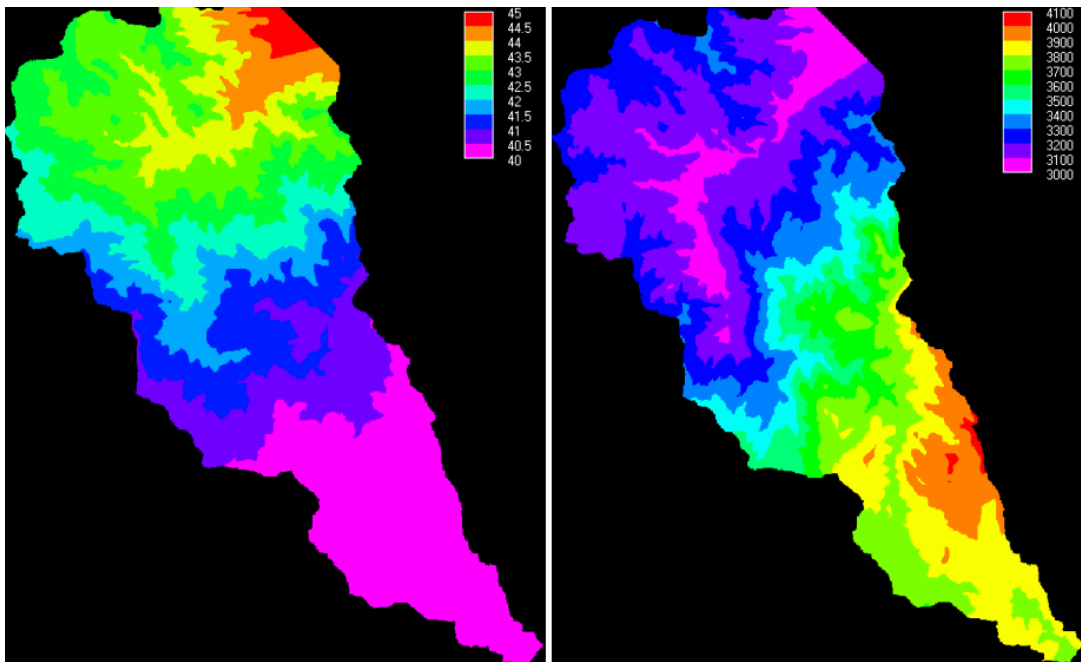


**Figure 22** Annual total rainfall (right) and coefficient of variation (%) of monthly rainfall (left)

The number of dry days (days with no rain) was calculated from a straight tension spline interpolation for the full records of the eight best stations. A spatialisation of the number of dry days indicates a strong east-west pattern with the 32% of days dry at the western limits of the catchment compared with 16% in the eastern limits (Figure 23). The rainfall per rain day (a measure of rainfall intensity), also shown in Figure 23 shows an altitudinally increasing pattern with values of 11mm/rainday in the lower parts of the catchment and up to 14mm/rain day at altitude.

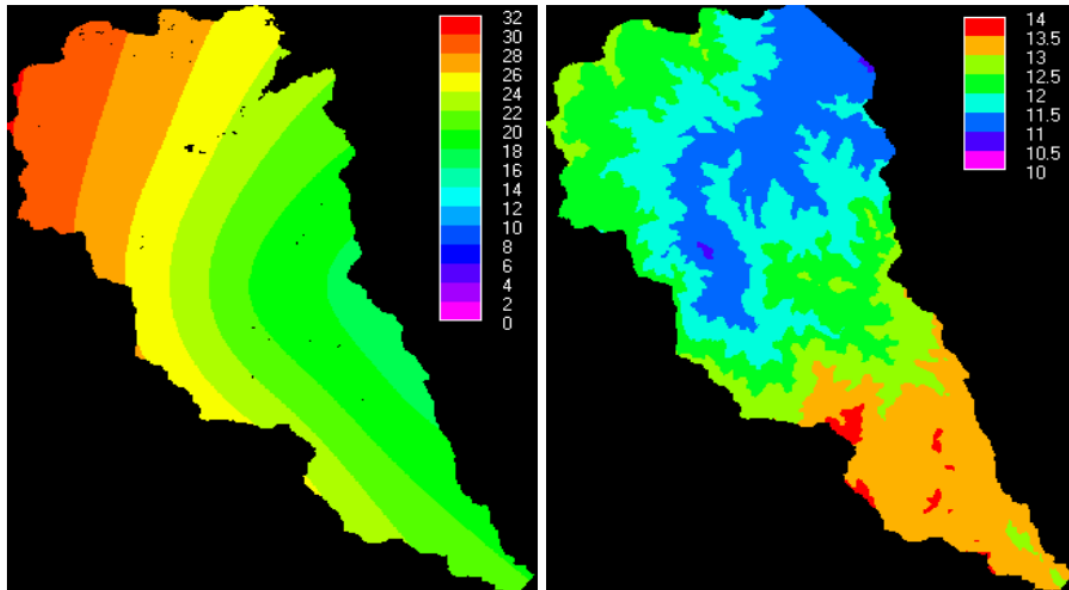


Figure 23 Percent of days with no rainfall (dry days, left) and rainfall per rainday (mm, right)

### 3.1.3.4 Wind speed

Wind speed is notoriously spatially and temporally variable. It is also not measured at all but the most sophisticated of weather stations. No satellite measurements are available over land. Wind speeds were mapped in this study from the four Chiquito stations since these provided comparable, hourly wind speed data. The stations are located as shown in Figure 29. Wind speeds were calculated as momentum averages and energy averages of u,v components of wind at the four Chiquito stations for a contiguous period from 11/2002 to 6/2003 for which good data were available from all stations. The mean wind speeds at the stations showed a clear relationship with topex values except station 3 which must reflect some wider topographic funnelling of wind (Table 4). No more sophisticated interpolation than simple splines were possible though these were enhanced by accounting for topographic exposure effects on wind speed and topographic effects on wind direction (see section 4.2).

Wind_stn (@2m)	X(degrees)	Y(degrees)	Momentum average (m/s)	Energy average (m/s)	Aspect	Slope gradient (°)	Min. TOPEX (exposure)	Exposed to
pasture	-	10.34933779	2.2	2.2	24.6	6.4		
chiq1	84.8006276	10.43088472	3.4	3.4	30.8	9.3	3.2	N
chiq2	84.8758130	10.40279443	4.5	4.5	253	17.5	-9.2	NW
chiq3	84.8520066	10.42105468	9.3	9.3	flat	flat	5.2	N
chiq4	84.9007806	10.36948000	5.6	5.6	314	22.8	-26.6	NW

Table 4 Chiquito wind stations and topographic characteristics

The *minimum TOPEX* column in Table 4 represents the minimum value of the TOPEX exposure metric for wind from any direction as calculated from the 25m DEM for the location in which the station stands. Minimum TOPEX values represent maximum exposure (to -80). The *exposed to* column represent the direction in which the

maximum exposure occurs (i.e. the slope is maximally exposed to winds from this direction). It is clear that all the stations (except station 4) are not particularly exposed, though by comparison with Figure 24 it is clear that these locations are representative of the exposure conditions of the Chiquito catchments (only around 10% of land has TOPEX more exposed than -20. The station observed direction of maximum exposure stations is also typical for the area with most slopes being maximally exposed to winds from a N, NE and E direction according to the GIS (Figure 25) and maximally sheltered to a W, SW or S direction (Figure 26).

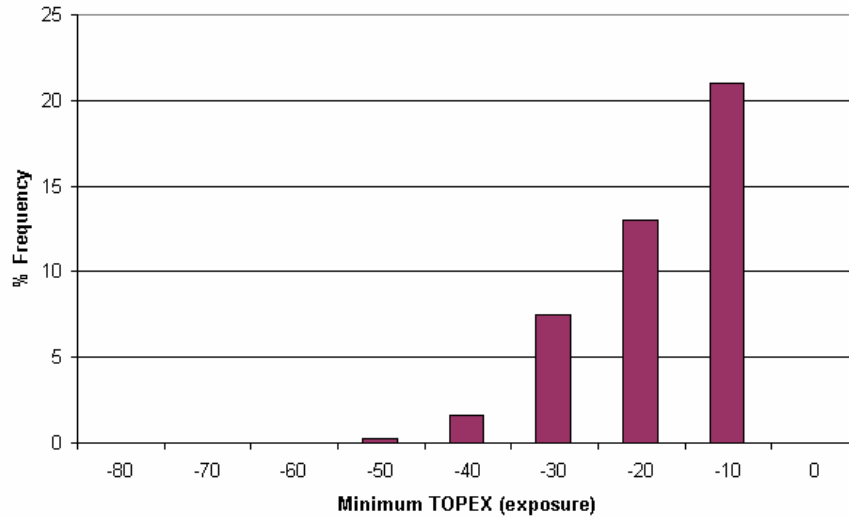


Figure 24 Minimum TOPEX exposure frequency distribution for the Chiquito catchment

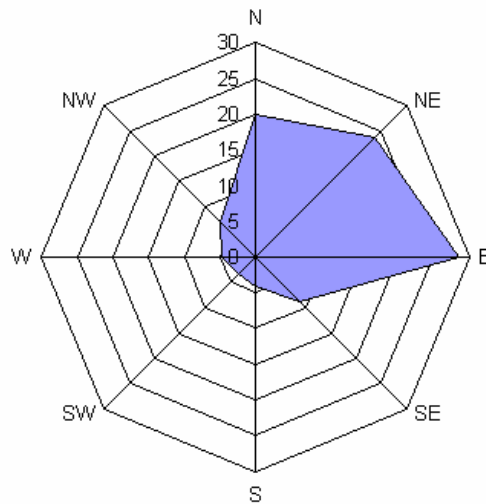
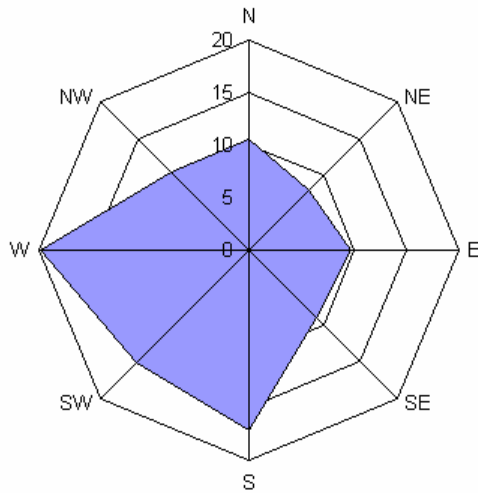
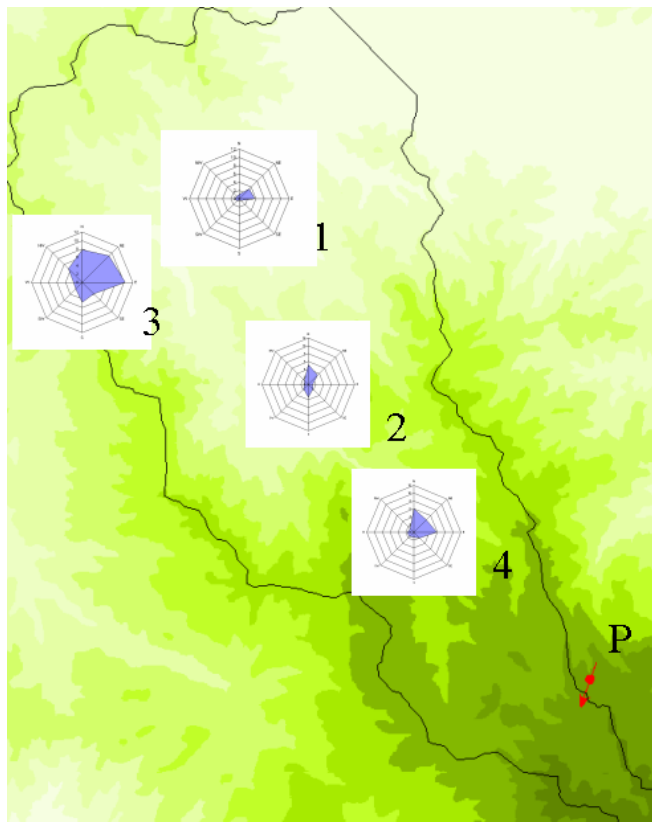


Figure 25 Direction of maximum TOPEX exposure for Chiquito slopes (% of total frequency)



**Figure 26 Direction of maximum TOPEX shelter for Chiquito slopes (% of total frequency)**

The analysis of station measured hourly wind speed by direction shown in Figure 27 shows that the higher altitude sites tend towards higher overall wind speeds (up to 12 m/s for station 3). The strongest winds are always those from the N, NE and W.



**Figure 27 Average wind speed by direction for the four Chiquito stations (all to same scale, max=12 m/s).**

Interpolation of wind speed from the four Chiquito stations and the comparable pasture station gives the surface of Figure 28 (right) in which the lowest speeds are

observed at low altitudes, close to the lake and the highest speeds are observed at some of the more exposed ridges to the west of the catchment. In order to account for topographic effects simpler (a more detailed approach is shown in 4.2) the method of Ruel et al (1996) was applied to the TOPEX values for the dominant (NE) wind. This modified the wind speeds for topographic exposure, resulting in the values shown in Figure 28 (left).

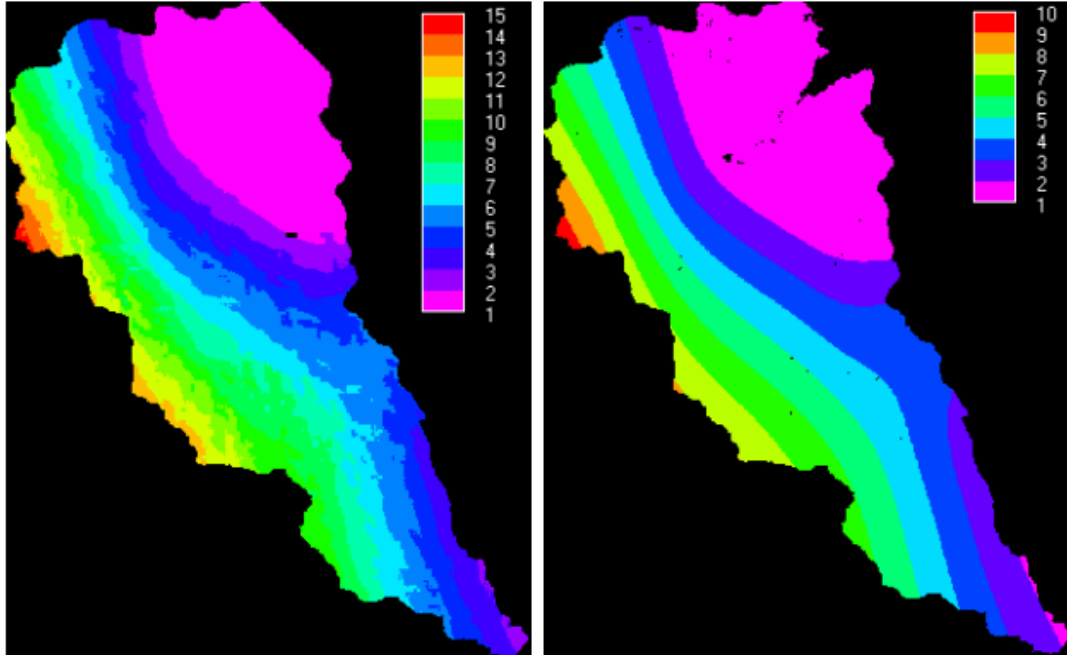
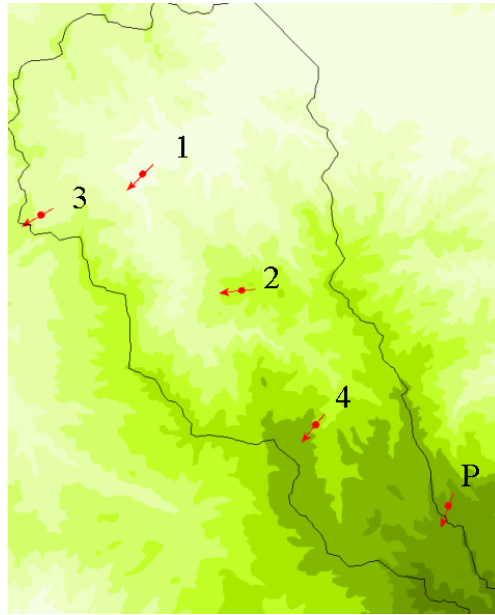


Figure 28 Raw wind speed (right) and topographically corrected wind speed (left).

### 3.1.3.5 Wind direction

Wind direction is calculated using vector averaging of the u,v components at the four Chiquito stations and the pasture site for the contiguous period 11/2002 to 6/2003. This results in the mean wind directions given in Figure 29, clearly from the NE and E as one might expect.



**Figure 29 Distribution of Chiquito stations and dominant wind directions.**

An analysis of the frequency distribution of wind directions produces the results shown in Figure 30, confirming the validity of the dominant directions described in Figure 29 (except for at station 2).

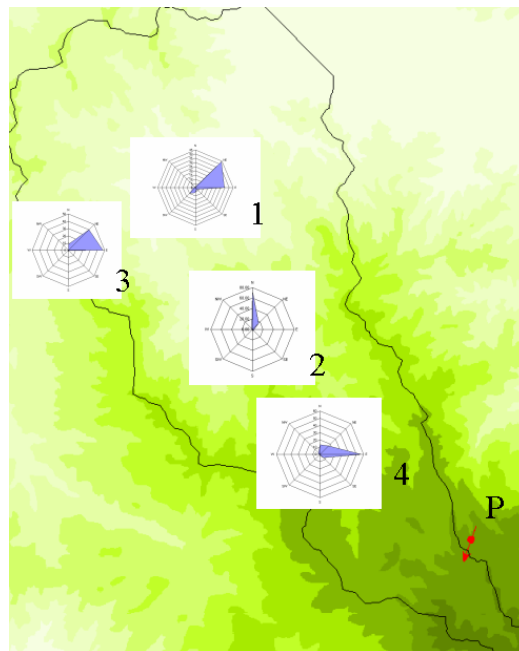


**Figure 30 Frequency distributions of wind direction (%)**

The resulting crude map of wind directions is shown in Figure 31, though this is likely to be far from representative of actual ground wind directions because of the effects of topography. Modelling topographic effects on wind directions are covered in section 4.2. and those same algorithms were used to convert these crude wind directions to topographically modified wind directions.

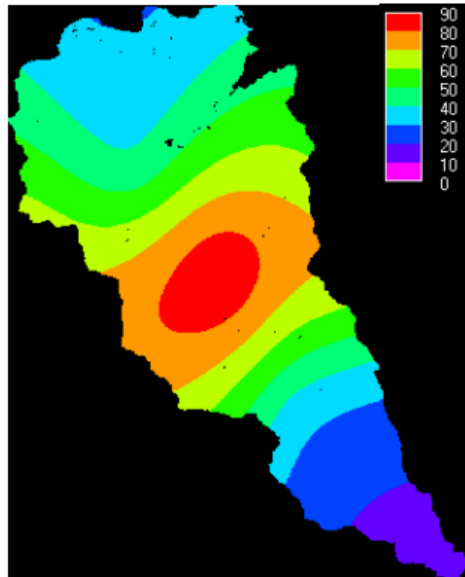


**Figure 31 Regionalised wind directions.**

### 3.1.3.6 Ground cloud (fog) frequency

Fog presence is also notoriously spatially and temporally variable and is important to understand impacts on fog interception and on reducing energy inputs for evaporational losses. Fog is difficult to separate from wind driven rain in standard fog gauges and as is the case with wind speed and direction, these are rather specialist instruments which are not routinely used, hence data on fog presence is only usually available for a few points in the landscape such as the FIESTA Chiquito stations. Since the purpose of the FIESTA models are to model fog inputs rather than measure them we reserve the measured fog input data for validation purposes and calculate fog presence on the basis of satellite measured observed cloud frequency from the MODIS cloud mask (see section 4.2.1.1). The observed cloud frequency (a mean of 400 images over a six year period) is combined with a topographic mask which rather simply converts observed atmospheric cloud frequency to observed cloud frequency by settling ground cloud frequency to zero at altitudes below 500m. Whilst this is appropriate for the Chiquito scale analysis improved methods were required for the national scale analysis (see section 4.2.1.1). In this way because all areas in the Chiquito are >500m the observed atmospheric and ground level cloud frequencies are essentially the same. An extensive analysis showed no significant relationship between observed cloudiness and any topographic property. Patterns were more complex than simple altitudinal increases in cloud cover. The resulting map of ground level cloud cover (Figure 32) shows high cloudiness in the high ridges of the catchment, especially to the east, where cloud spills over from the Atlantic slopes and much lower cloudiness in the Pacific west and the lowland parts of the catchments.

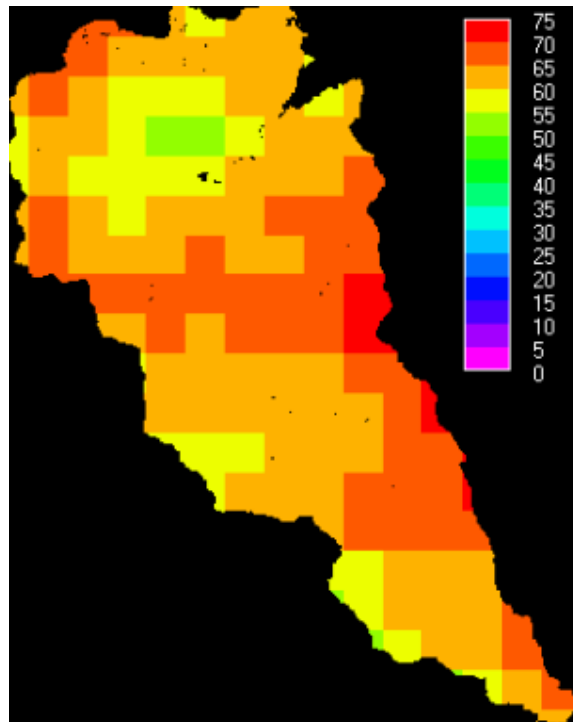


**Figure 32** Frequency of ground level cloud cover (fog)

### 3.1.4 Topographic

The following terrain indices were calculated for the modelling using standard methods and the 25m DEM<sup>3</sup> and are shown in Figure 33 : Ruggedness, Stream order (after Strahler), Catchments, Aspect, Slope Gradient. There are few rugged areas, a complex dendritic drainage network, a NE-SW aligned topography, some very steep slopes and altitudes that range from more than 500 masl through to 1900 masl in the catchment, though most of the catchment is less than 1000 masl.

---

<sup>3</sup> supplied by J. Fallas

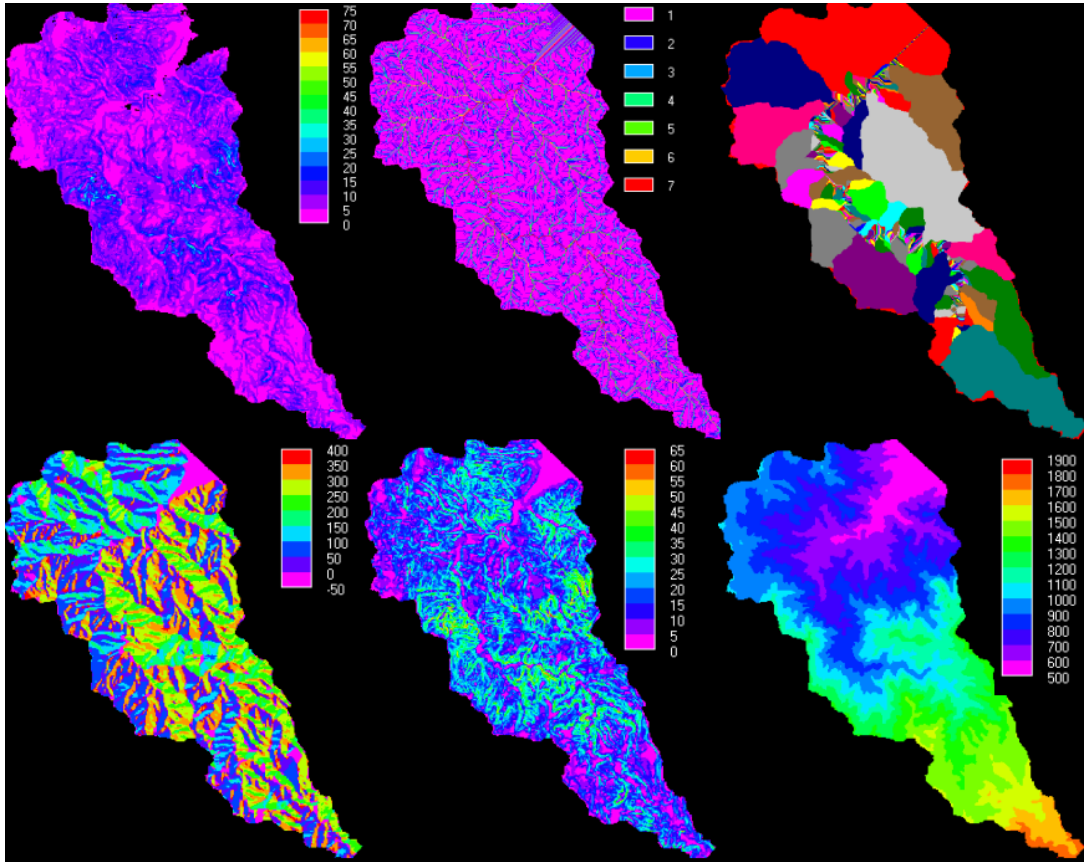


**Figure 33** Terrain ruggedness (top left), stream order (top centre), subcatchments (top, right), slope aspect (bottom left), slope gradient (bottom middle) and altitude (bottom right)

### 3.1.4.1 Topographic exposure (TOPEX)

Topographic exposure is important for the determination of wind exposure and thus fog interception. It is calculated as described in section 4.2.1.10 using the 25m Chiquito DEM. In Figure 34 green and red areas are sheltered whilst blue and pink areas are exposed to winds from the respective directions. Because of the form of the topography winds from the S or SE are fairly uniformly exposed across the landscape whereas winds from the N, NE and NW produce strong exposed/shadowed contrasts.

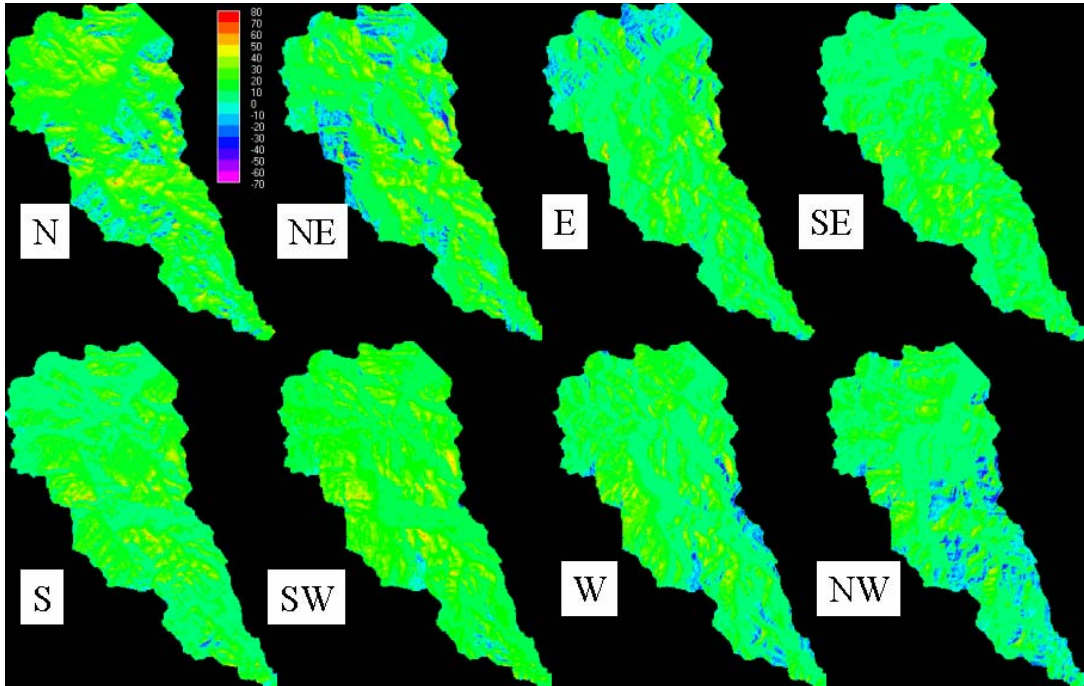


**Figure 34 Topographic exposure to winds from the main wind directions**

### 3.1.5 Human

In addition to land use the only other major human dataset used in this analysis is the distribution of roads (for the land use change scenario modelling).

#### 3.1.5.1 Roads

Landsat data are too spatially crude for the characterisation of all but the largest of roads. Thus IKONOS data were used here to characterise roads into major (paved) roads and minor (unpaved) roads by manual digitisation. Part of the IKONOS mosaic used is shown in **Figure 35**



**Figure 35 IKONOS mosaic – northern Chiquito.**

The resulting map of major and minor roads is shown in Figure 36. A dense network is clear as is the extent of pasture-isation in the vicinity of roads compared with the intervening forest blocks where there are not roads.

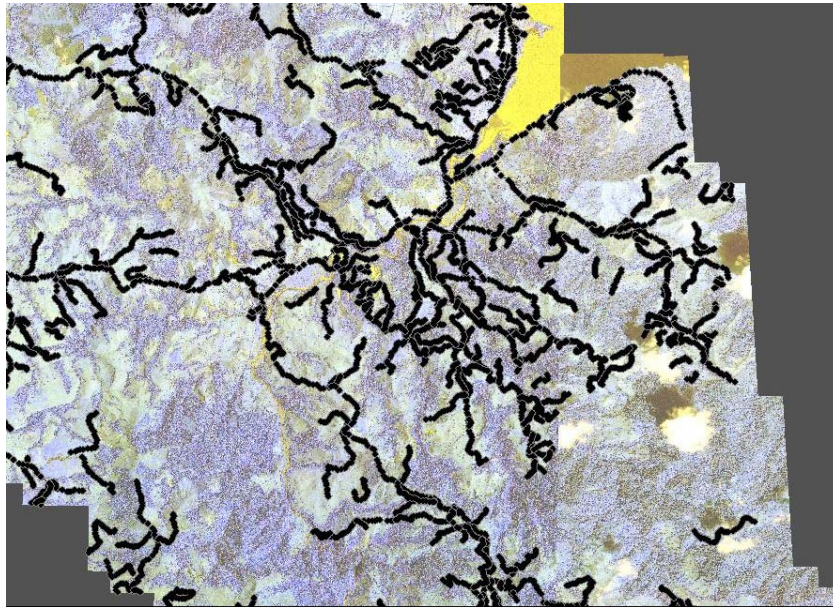


Figure 36 Road network of major and minor roads in the N Chiquito.

### 3.1.6 Sampling

Data on the locations of subcatchments (forest, pasture and secondary forest, as well as measurements sites (e.g. the chiquito stations) were also necessary and were produced using the catchment maps or field coordinates for those sites/instruments.

### 3.1.7 Vegetation

A number of vegetation characteristics are necessary in order to characterise vegetation for fog interception. These characteristics are generally beyond the crude measures of land use that can be obtained by classification of landsat data.

#### 3.1.7.1 Isolated trees

Isolated trees may be important in the interception of fog since (a) they seem to be very common in deforested landscapes and (b) they are highly exposed to fog compared with the interiors of forest blocks. Purchase, processing and analysis of IKONOS imagery enabled the production of detailed maps of forest blocks and of the number (9225), position and density of isolated trees in the catchment (Figure 37 and Figure 38). Forest blocks throughout the catchment were digitised manually and the position of each isolated tree recorded. These were then aggregated into the 25m pixels of the Chiquito GIS to produce a map of the number of isolated trees per pixel (Figure 38).

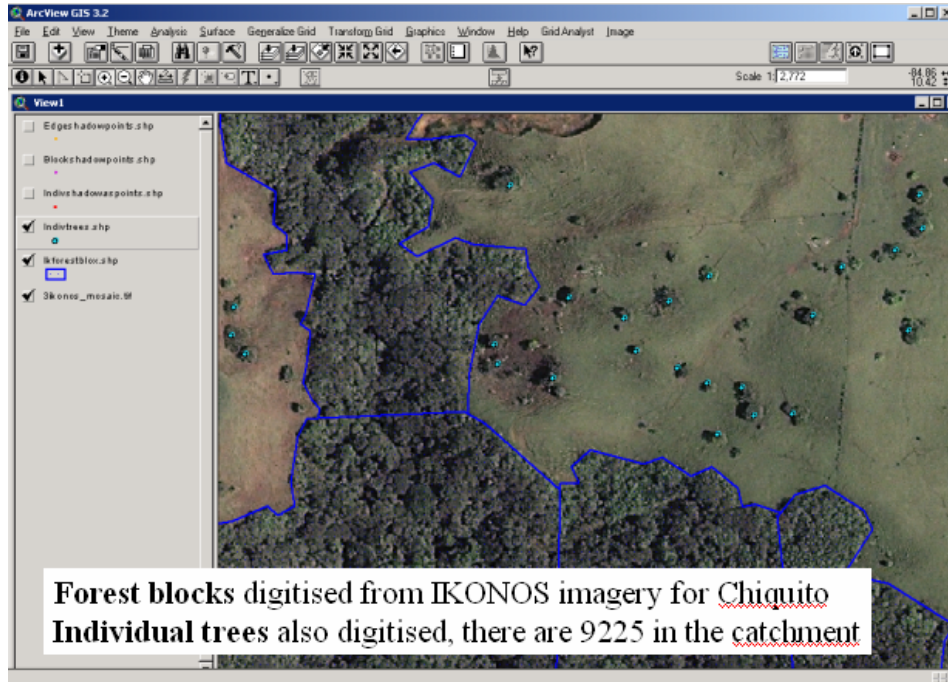


Figure 37 Digitising of forest blocks and trees for the Chiquito.



Figure 38 Resulting map of locations and density of isolated trees

### 3.1.7.2 Vegetation properties sampling strategy

For the remaining vegetation properties direct measurement from even the IKONOS imagery was not possible. The strategy developed to spatialise these properties was to set up a stratified sampling scheme using a series of terrain and RS derived properties that are likely to control these vegetation properties, to identify representative sites in

the field, measure the properties *in situ* during an intensive field programme and then look for relationships between the individual properties and either an NDVI index of the IKONOS data or terrain properties in order to spatialise the results. The sampling method can be summarised as in Figure 39. A stratified scheme is produced according to the following properties : distance to forest edge, slope gradient, slope aspect, exposure and altitude. The scheme is designed such that measurement at 30 (representing 30 different classes or combinations of the landscape variables) sites could be used to characterise 73% of the catchment area (91% for 61 sites). The 30 main sampling classes are shown in Table 5.

Class Number	% of catchment	cumulative % of catchment	exposure to fog from north east	distance from forest edge (m)	altitude (m)	topographic aspect	topographic slope
1	7.86	7.86	fairly sheltered	0-100	1000-1500	southerly	less than 30
2	6.27	14.13	fairly sheltered	0-100	1000-1500	southerly	less than 30
3	5.80	19.93	fairly sheltered	0-100	500-1000	north westerly	less than 30
4	5.07	25.01	fairly exposed	0-100	500-1000	northeast	less than 30
5	4.77	29.78	fairly sheltered	0-100	500-1000	north westerly	less than 30
6	4.52	34.30	fairly exposed	0-100	1000-1500	northeast	less than 30
7	3.61	37.91	fairly exposed	0-100	500-1000	north westerly	less than 30
8	3.36	41.27	fairly exposed	0-100	1000-1500	southerly	less than 30
9	3.24	44.51	fairly exposed	0-100	1000-1500	southerly	less than 30
10	2.95	47.46	fairly exposed	0-100	500-1000	north westerly	less than 30
11	2.50	49.96	fairly sheltered	100-300	1000-1500	southerly	less than 30
12	2.29	52.25	fairly sheltered	0-100	1000-1500	northeast	less than 30
13	2.27	54.52	fairly sheltered	0-100	500-1000	northeast	less than 30
14	1.92	56.44	fairly sheltered	100-300	1000-1500	southerly	less than 30
15	1.72	58.16	fairly sheltered	0-100	1500-2000	north westerly	less than 30
16	1.40	59.56	fairly sheltered	0-100	1500-2000	north westerly	less than 30
17	1.28	60.84	fairly sheltered	100-300	1000-1500	northeast	less than 30
18	1.20	62.04	fairly exposed	100-300	1500-2000	northeast	less than 30
19	1.15	63.19	fairly exposed	100-300	1000-1500	northeast	less than 30
20	1.12	64.32	fairly exposed	0-100	1500-2000	northeast	less than 30
21	1.07	65.39	fairly sheltered	0-100	1000-1500	southerly	30 to 55

22	1.06	66.44	fairly sheltered	100-300	1500-2000	north westerly	less than 30
23	1.03	67.47	fairly sheltered	0-100	1000-1500	southerly	more than 55
24	1.01	68.47	fairly sheltered	100-300	1500-2000	north westerly	less than 30
25	0.97	69.44	fairly exposed	100-300	1000-1500	southerly	less than 30
26	0.94	70.38	fairly sheltered	100-300	500-1000	north westerly	less than 30
27	0.93	71.32	fairly exposed	100-300	500-1000	northeast	less than 30
28	0.91	72.22	fairly sheltered	0-100	500-1000	north westerly	30 to 55
29	0.88	73.11	fairly sheltered	0-100	1000-1500	southerly	30 to 55
30	0.84	73.94	fairly exposed	0-100	1500-2000	north westerly	less than 30

Table 5 Main sampling classes for vegetation properties

One site representing each of these 30 classes is chosen in close proximity to an accessible road (using the IKONOS imagery). The site is visited in the field and its landscape properties are confirmed on the ground. Six subsites are randomly chosen within the site and the measurements taken at each of these. The mean of those measurements represents the result for that class. The following properties were measured :Tree height, stem density, LAI, gap fraction, number of bromeliads, crown epiphytism, whole tree epiphytism.

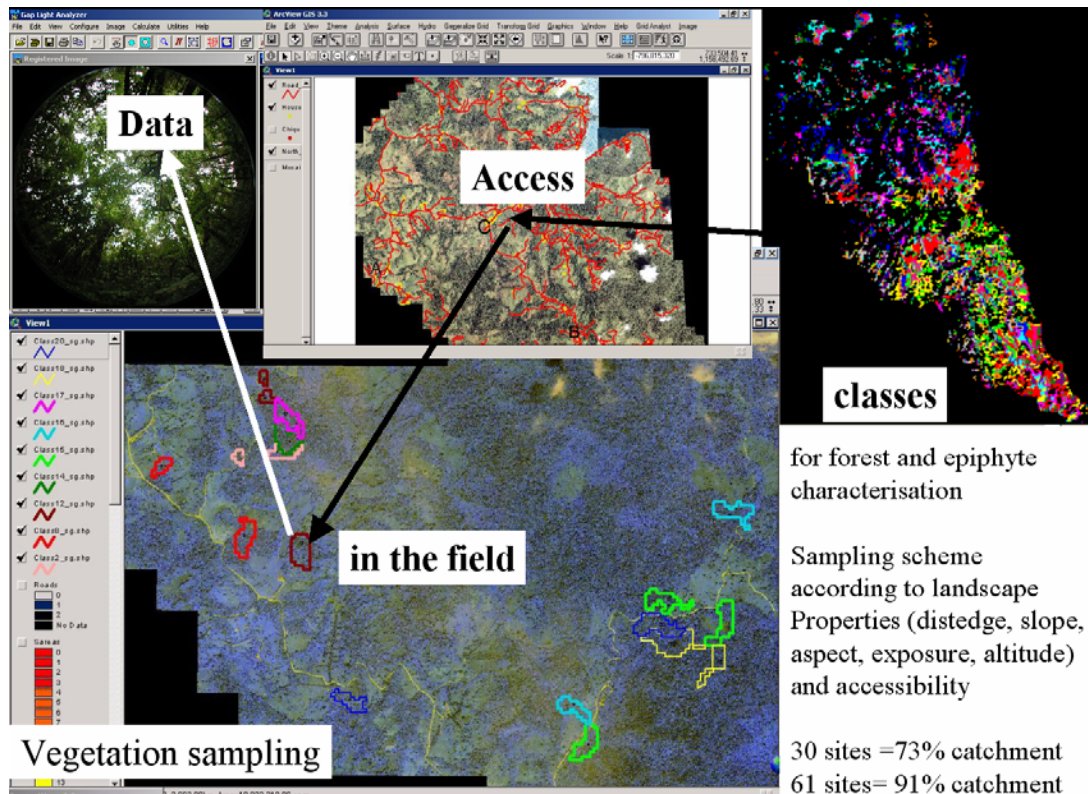


Figure 39 Vegetation properties sampling scheme

Each sampling area (six per site) is a circle with a 10m diameter defined using a rope from a central (randomly assigned) point. Tree height was measured with a laser rangefinder or else estimated if too difficult with the rangefinder. Stem density is measured by counting the number of stems (for trees > 1m tall) within the defined area. Hemispherical photographs were taken at random locations within each subsite with a NIKON 990 digital camera and NIKON fisheye lens. LAI and gap fraction were determined from the hemispherical photography with the GLA software<sup>4</sup> number of bromeliads was estimated by a rough count in each subplot. Epiphytism is estimated for a subsample of trees in each subplot by assigning the following classification : epiphyte thickness: 0-1 cm, 1-2 cm, >2 cm and percentage cover: 0-33%, 33-66%, 100%, for the trunk, main branches, smaller branches, hanging forms and leaves,. according to the different classes of tree height as in the proforma shown in Table 6.

		Tree heights (m)			3-6			6-10		
		DBH (cm)			3.5 - 8			8 - 13		
Coverage	Thickness (cm)	Trunk			main branches			smaller branches (bc)		
		Trunk	main branches	smaller branches (bc)	Trunk	main branches	smaller branches (bc)	Trunk	main branches	smaller branches (bc)
33%	0 - 1									
	1 - 2									
	>2									
66%	0 - 1									
	1 - 2									
	>2									
100%	0 - 1									
	1 - 2									
	>2									
Hanging forms	0 - 10									
	10 - 20									
	> 20									
Bromeliad Count	number									

**Table 6 Proforma epiphyte biomass data entry.**

A summary of the mean field results for all sites within a class and for all variables measured is shown in Table 7.

<sup>4</sup> <http://www.ecostudies.org/gla/>

# FIESTA Final Technical Report

CLASS	Plot	UTM, X	UTM, Y	Altitude (m)	mean crown epiphyte cover (%), DBH<5cm	mean crown epiphyte cover (%)	mean crown epiphyte thickness (cm),	mean crown epiphyte thickness (cm)	mean whole-free epiphyte cover (%), DBH<5cm	mean whole-free epiphyte cover (%)	mean length of hanging forms (cm)	mean whole free epiphyte thickness	mean whole free epiphyte thickness	mean tree height (m), DBH<5cm	mean tree height (m)	mean DBH (cm)	mean stem density (stems/ha), DBH<5cm	mean stem density (stems/ha)	mean bromeliad count	mean bromeliad/ha
1	1	737738.40	1145462.28	1454.00	34.44	33.34	0.88	0.59	34.73	33.41	7.70	0.80	0.57	8.07	4.21	5.14	3844.45	16247.74	11.54	367.30
	2	nd	nd	nd																
	3	737719.20	1145431.28	1472.00																
	4	nd	nd	nd																
2	1	737722.59	1144934.50	1479.00	44.20	36.19	1.83	0.94	42.50	36.11	8.32	1.58	0.87	8.36	4.65	5.00	5563.36	17134.58	21.75	692.21
	2	737773.85	1144933.02	1477.82																
	3	737795.90	1144925.34	1471.17																
	4	737810.18	1144913.97	1463.58																
3	1	731404.33	1157454.10	861.00	33.64	33.11	1.69	1.57	33.46	33.08	7.10	1.49	1.43	11.78	4.64	5.06	721.13	4791.71	2.37	75.36
	2	731442.96	1157474.55	865.00																
	3	731422.52	1157454.22	865.00																
	4	731375.28	1157404.06	873.00																
6	1	737613.17	1145251.75	1464.60	45.42	34.87	1.91	1.20	42.07	34.37	7.04	1.64	1.14	9.52	4.09	4.75	2732.19	16651.98	25.45	809.96
	2	737622.46	1145235.20	1462.60																
	3	737641.67	1145222.44	1462.95																
	4	737657.92	1145208.05	1465.10																
8	1	737511.88	1144453.10	1534.52	36.88	33.76	1.88	0.89	38.57	34.09	7.15	1.64	0.97	8.51	4.18	4.54	5238.36	19448.85	42.16	1342.07
	2	737517.83	1144432.94	1536.17																
	3	737537.68	1144432.93	1529.23																
	4	737551.44	1144450.46	1527.52																
9	1	737673.44	1145077.13	1445.85	44.45	36.13	1.99	0.98	40.61	35.08	11.21	1.64	0.89	10.53	5.25	6.37	2722.24	10235.61	33.50	1066.34
	2	737669.54	1145056.70	1451.03																
	3	737659.14	1145041.98	1457.70																
	4	737644.72	1145024.63	1450.62																
12	1	737916.23	1144262.69	1521.11	33.00	33.00	1.09	0.87	33.00	33.00	5.88	1.16	1.02	7.08	5.57	6.63	10536.03	16743.06	17.00	541.13
15	1	740511.00	1144033.00	1507.00	62.67	66.92	1.76	1.83	62.07	65.24	12.74	1.55	1.58	12.33	9.62	18.35	706.07	996.00	32.45	1032.96
	2	740531.23	1144030.61	1508.78																
16	1	740654.87	1144567.98	1569.35	45.93	39.95	1.92	1.48	42.49	38.30	16.07	1.65	1.39	5.85	4.58	5.71	6703.30	9174.66	1.37	43.71
	2	740666.10	1144605.18	1582.02																
	3	740681.27	1144635.18	1577.81																
	4	740684.01	1144662.51	1576.86																
20	1	739930.58	1143936.19	1596.04	35.88	35.74	1.47	1.47	35.92	36.31	7.57	1.35	1.37	7.94	4.66	6.19	4532.64	13922.10	14.35	456.89
	2	739923.29	1143953.95	1596.59																
	3	739948.79	1143913.99	1599.00																
	4	739974.76	1143897.53	1565.00																
23	1	738703.26	1143501.83	1465.00	35.60	33.72	1.11	0.64	35.51	33.70	5.40	1.11	0.71	8.18	4.60	6.45	1996.75	6943.47	6.89	219.45
	2	738678.02	1143496.90	1455.00																
	3	738597.35	1143606.76	1456.00																
	4	738615.24	1143561.80	1456.64																
29	1	735435.58	1150840.75	1176.19	35.54	34.39	1.66	1.33	36.05	34.67	13.89	1.48	1.27	6.11	4.71	7.55	6022.46	10940.61	13.46	428.54
	2	735415.80	1150856.68	1158.00																
30	1	737147.06	1144614.23	1537.00	44.10	36.49	1.54	1.04	45.60	37.91	6.73	1.42	1.06	7.92	4.77	6.81	2558.45	5945.31	44.03	1401.62
	2	737128.99	1144591.56	1547.00																
	3	737110.46	1144584.97	1543.82																
	4	737116.52	1144571.61	1544.14																
40	1	735454.83	1150818.95	1178.00	48.40	38.85	1.73	0.97	48.84	39.02	10.70	1.54	1.08	6.88	4.47	5.96	1909.85	5029.28	36.00	1145.91
42	1	737335.59	1144460.59	1548.00	42.60	35.99	1.88	0.95	40.12	35.21	6.53	1.62	0.99	8.66	4.85	7.76	2174.49	6871.30	6.13	195.21

**Table 7 Summary of field results for vegetation characterisation.**

Unfortunately, few clear relationships exist between these properties and landscape factors or satellite vegetation indices (see Table 8) so vegetation parameters could not be distributed in a continuous way according to altitude or some other terrain variable but rather had to be distributed according to the defined sampling classes. Whilst this is better than no distribution at all, because the terrain variables turned out not to be strong controls on the vegetation properties it is probably as valid to take the mean for all sites for each variable and use that as a representative, but lumped, value within all areas of forest cover.

Terrain Property	distance from forest edge	aspect	topo exposure (NE)	altitude	slope
Comments	LAI and epiphytism (both whole tree and plot scale) increase with distance from forest edge	LAI higher on south facing slopes	LAI no change	LAI highest in mid altitudes	LAI increases with slope
		Single tree epiphytism highest on NW slopes but plot epiphytism highest on NE slopes (shorter, thinner but much more stem dense trees)	Single tree epiphytism (whole tree and crown) higher in exposed areas	Single tree epiphytism increases with alt, plot epiphytism increases dramatically with alt	epiphytism same irrespective of slope, plot epiphytism highest on shallow slopes, stem density highest on shallow slopes
		NDVI highest on south facing slopes (also true for non shaded areas only)	Plot scale epiphytism also higher in orographically exposed slopes NDVI higher on exposed slopes Stem density lower, DBH higher, height similar exposed slopes	Stem density highest in mid alts NDVI increases with alt	NDVI increases with slope (veg density artefact)?

**Table 8 Relationships between landscape and RS indices and vegetation properties**

The distributions for each parameter which result from this regionalised variables scheme are shown in Figure 40. As much as possible measures were converted to units that would be most appropriate to canopy modelling *e.g.* epiphytes in m<sup>3</sup>/Ha.

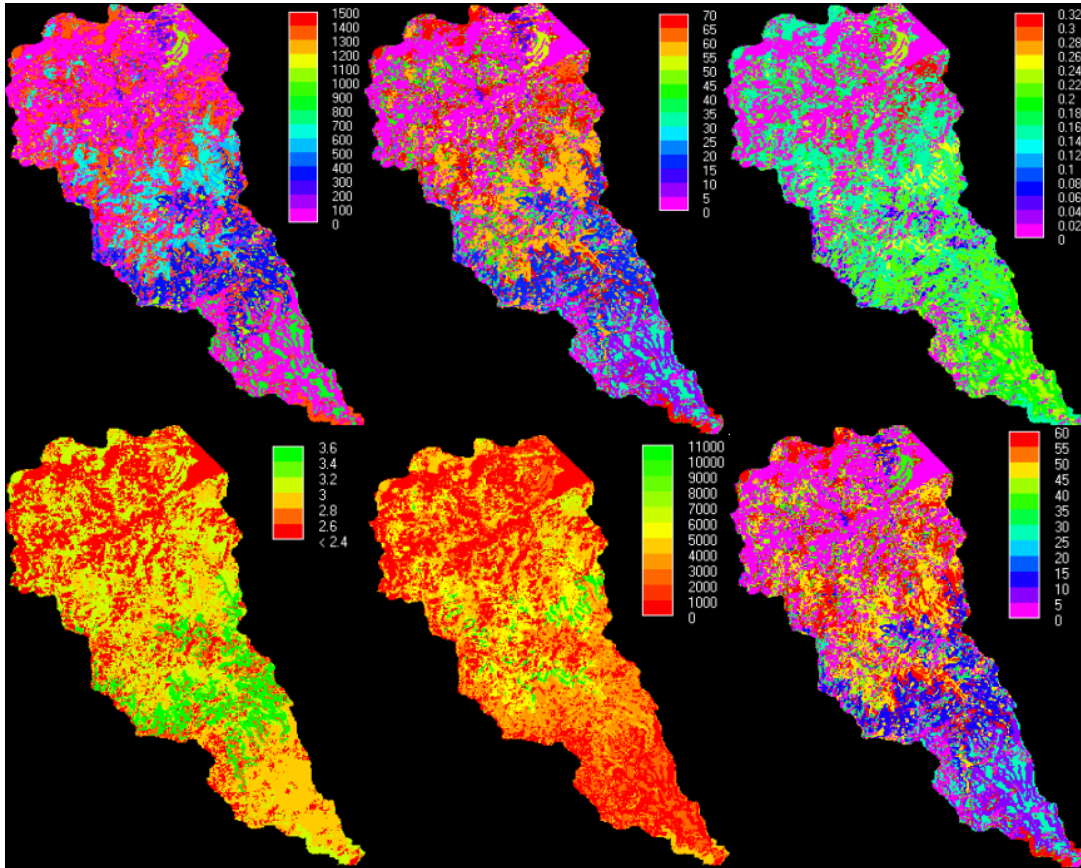


**Figure 40** Vegetation properties distributed according to the stratified (regionalised variables) scheme. Top left : Bromeliad count (individuals/hectare); top middle : crown epiphytism  $m^3$  epiphytes/Ha.; top right : gap fraction ; bottom left : LAI; bottom middle : stem density; bottom right : whole tree epiphytism ( $m^3$  epiphytes/Ha.)

### 3.1.8 Development of land use change scenaria

Land use change scenaria were generated using the 2001 land cover map as an initial condition and by employing a cellular automata-based spatial model which allows forest loss to continue from existing forest-pasture frontiers and from access routes. Access routes (major and minor roads) were mapped from the catchment wide IKONOS data. Roads in the northern part of the catchment are shown in Figure 36.

The cellular automata rules ensure that forest loss occurs from access routes and existing agricultural frontiers and that shallow slope gradients are lost in preference to steep ones. This does not take into account many of the spatially complex land title and ownership issues that can often drive land use change patterns but does capture the main pattern of land use change , that of a progressive eating away of forest remnants with access as the dominant control. The resulting scenario is shown in Figure 41 and indicates a progressive forest loss over time with only the largest continuous patch of original forest remaining in any form by the final iteration.

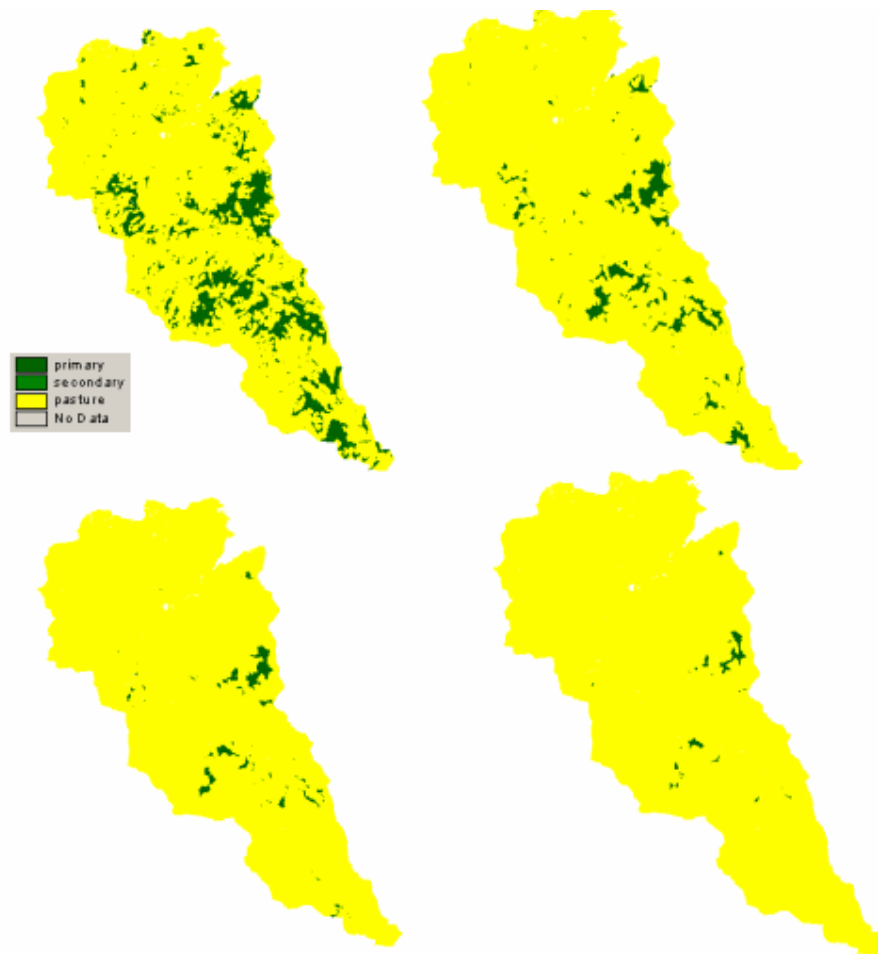


**Figure 41 Land use change scenario for the Chiquito. No timeline is given since rates of future land use change are impossible to predict. Patterns of change are more relevant here.**

A series of further scenarios were produced to indicate the impact of land use change in the cloud forest belt only, thus in these scenarios:

- (a) and use for all areas  $\leq 1400\text{m}$  remains as per 2001 and
- (b) for scenario 1 - the cloud forest belt ( $>1400\text{m}$ ) deforests according to the CA model described above
- (c) for scenario 2 - the cloud forest belt reforests over time to represent the effects of PES scenarios on cloud forest only hydrological change
- (d) for scenario 2a - reforestation of the cloud forest area occurs from the 2001 situation back to 1975 situation, all other areas remain as of 2001
- (e) for scenario 2b - complete reforestation of cloud forest area occurs, all other areas remain as of 2001.

## 4 The (Inter)National Scale

The purpose of the national scale FIESTA fog delivery (FIESTA\_delivery) model is to produce results that are generically applicable across a range of cloud forests. This does not mean that the results of the FIESTA\_delivery application in Costa Rica will hold for other (different) environments but rather that:

- (a) the national scale and small grain (90m-1km) ensures that a variety of landscapes and conditions will be modelled thus providing a range of outcomes of land use change rather than a single outcome as is possible from the single site activities
- (b) the model is designed to run from freely available data sources and thus is available for application to other areas/countries where conditions may not be the same as in Costa Rica but where the model can be parameterised from readily available data (an ongoing project is making this data available) and will still be a valid tool to investigate land use-hydrology interactions.

We will first examine the generation of necessary data for modelling before examining the model developed and its sensitivity analysis, verification and application. At the national scale two model applications were developed one with a 1km grain (based on the USGS GTOPO30 DEM<sup>5</sup>) and one with a 92m grain (based on the SRTM DEM<sup>6</sup>). The 1km application provides a less computer intensive implementation (553 MB database, 10 minute runtime on Pentium 1GHz) suitable for national scale analysis whereas the 92m version is much more computer intensive (50GB database, 1 hour runtime on dual Pentium 3GHz with 4GB memory and 64 bit operating system). The 92m version is suitable for *both* national and regional (groups of catchments) scale analysis.

### 4.1.1 Topography and derivatives

### 4.1.2 The regional context

The regional context for the Arenal and associated catchments is clear from Figure 42 which indicates the steep, exposed situation of the Penas Blancas and the more sheltered (facing away from the dominant easterly and north easterly winds and cloud banks) position of the Chiquito.

---

<sup>5</sup> <http://edcdaac.usgs.gov/gtopo30/gtopo30.asp>

The Shuttle Radar Topography Mission (SRTM) <sup>6</sup> <http://www2.jpl.nasa.gov/srtm/>

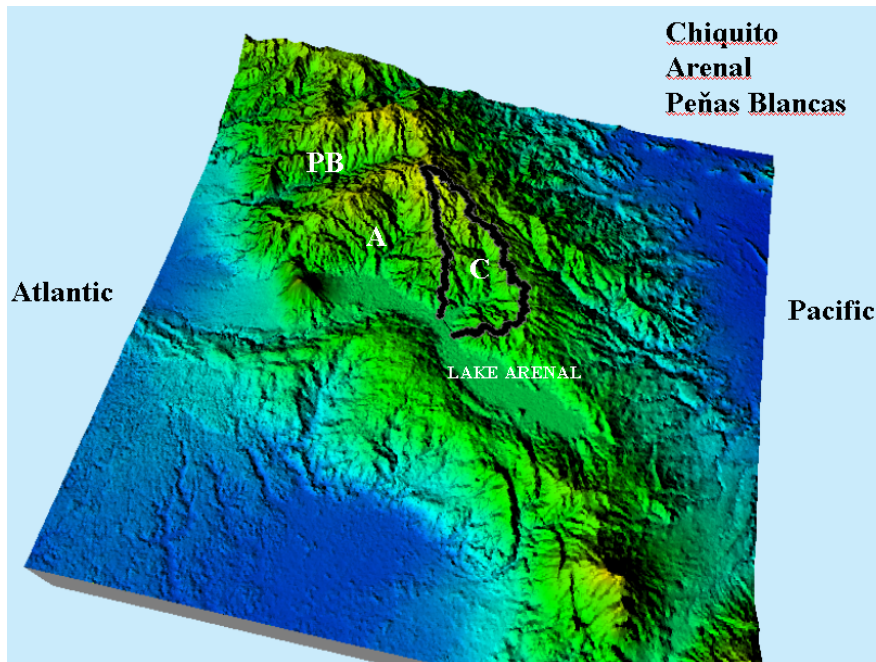


Figure 42 The regional topographic context for the Arenal catchments.

## 4.2 Climate

Climate data are interpolated from the best available data for the parameter of interest. For some parameters data are available at 1km resolution (WORLDCLIM), for others (the New et al. 2000 data) they are available as 0.5 degree resolution. Interpolation to the required resolution is carried out using thin plate (tension) splines to 1km and then simple nearest neighbour to 90m. Appendix 1 lists the climate data used and their sources and includes the following data.

### 4.2.1.1 Cloud cover

A knowledge of cloud cover frequency is essential for understanding radiation and thus evaporation dynamics and the potential for ground level cloud (fog). Cloud cover varies spatially but also seasonally and on a diurnal cycle. The MODIS cloud mask (see appendix 1) was used to assess cloud frequency. 400 images were acquired covering different seasons and times of day (from both MODIS TERRA and MODIS AQUA) and the cloud masks were processed to produce an overall frequency and frequencies for the seasons (DJF, MAM, JJA, SON) and for different periods of the day (early morning [0300,0400,0500,0600], morning [0700, 0800], afternoon [1500,1600,1700], and evening [1800,1900,2000]). The resulting data for Costa Rica is shown in

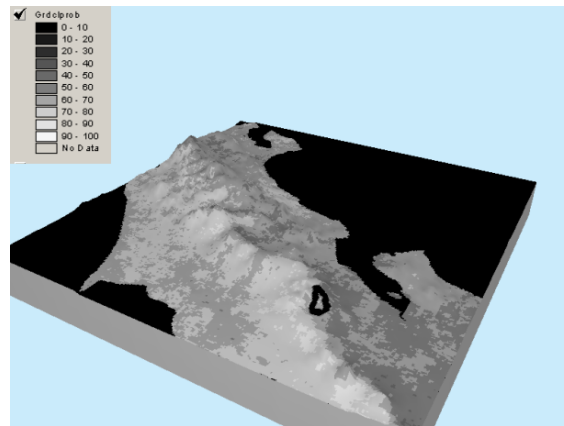


Figure 43 Mean Cloud frequency over Costa Rica. Cloudiest on the Atlantic slopes especially close to the continental divide.

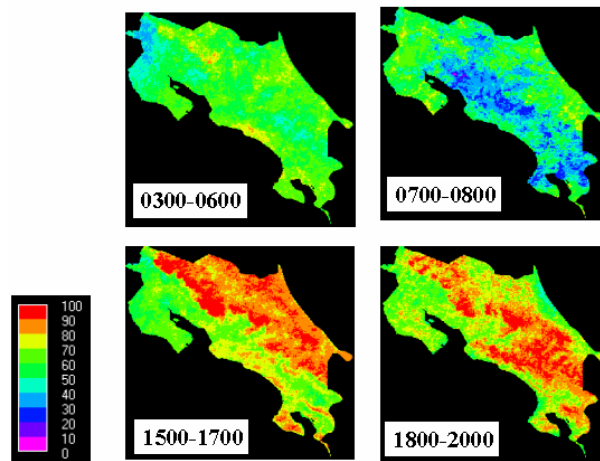


Figure 44 Cloud frequency over Costa Rica by hour. Strong diurnality with particularly strong cloud bank development on Atlantic slopes during the afternoon.

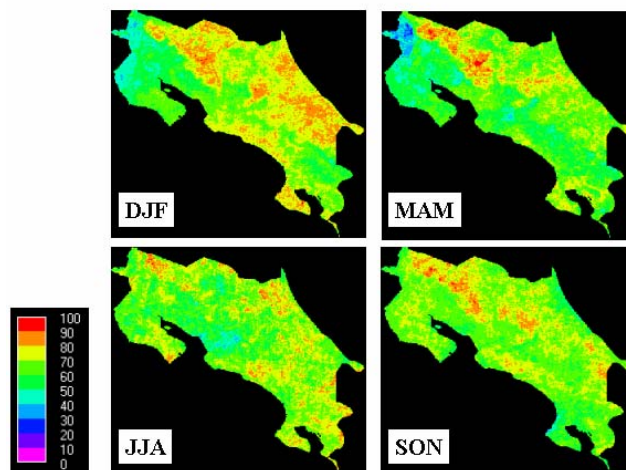
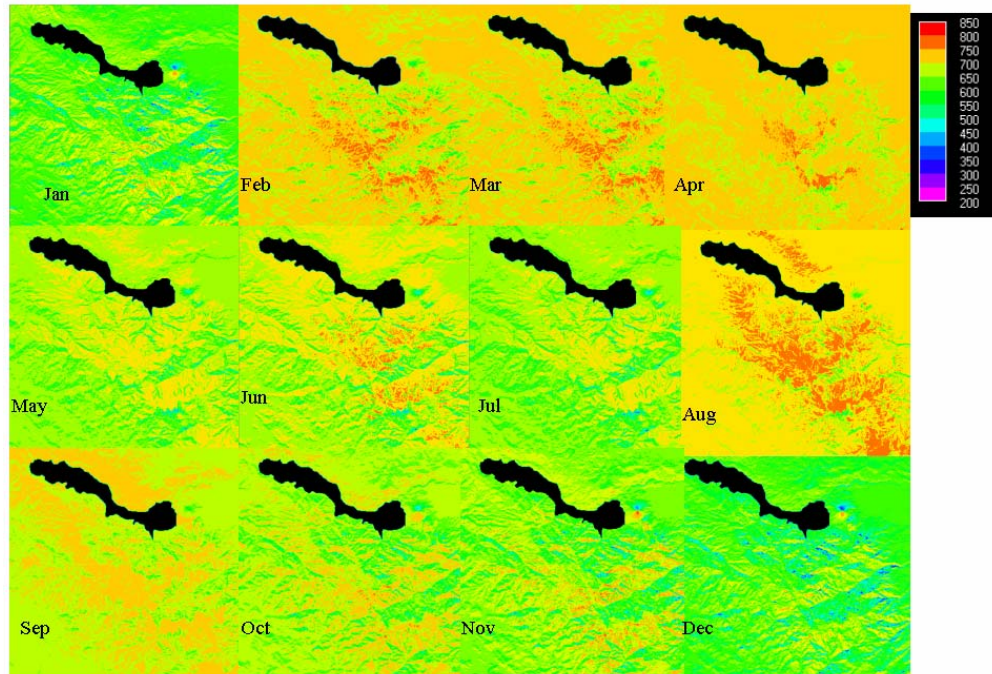


Figure 45 Cloud frequency by season for Costa Rica. Note the areas of persistent cloud close to Arenal/Monteverde.

#### 4.2.1.2 Potential solar radiation

Potential radiation is an important parameter for modelling evapo-transpiration and responds to location, time, topography, shadowing and cloud cover. Potential solar radiation is calculated here using a detailed model of solar geometry and topographic shading implemented as a PCRASTER pre-processing script. Potential radiation is calculated hourly but integrated to monthly totals for the FIESTA\_delivery model (see Figure 46). Within the FIESTA\_delivery model a cloud cover correction is applied.



**Figure 46** Seasonal pattern of top of the atmosphere solar radiation for the Arenal Area. Notice the very high spatial variation especially at low solar elevations (Dec and Jan)

#### 4.2.1.3 An analysis of the exposure of national climate network.

In order to understand better the basis upon which the climate mapping is done we first undertake a locational analysis of the 356 stations which make up Costa Rica's temperature and rainfall climatology. By analysing the landscape properties in the vicinity of these stations using the SRTM 92m DEM and derivatives and comparing these with the same properties for 360 and then 720 randomly sited locations in Costa Rica we can see (Table 9) that the stations (true\_stations) are sited somewhat non-randomly in terms of terrain properties. They are on average some 200m higher than the 360 and 720 random locations, occur on lower slope gradients than the random sites and are underexposed relative to the random points, especially for winds from the N, NE, E, NW and W. This will have implications for the representativeness of the station data.

property	topexn	topexne	topexnw	topexw	topexsw	topexs	topexse	topexe	aspect	dem	slope
true_stations	3.99	4.04	3.43	3.50	3.70	4.37	4.37	4.15	175.77	688.78	6.62
random_points_360	4.70	4.76	4.27	4.07	3.79	4.67	4.83	4.99	173.18	500.35	8.04
random_points_720	4.40	4.39	4.11	3.81	3.62	4.34	4.48	4.72	174.28	533.52	8.38
%, 720	90.61	92.08	83.37	91.85	102.28	100.56	97.54	87.80	100.86	129.10	79.03
%, 360	84.90	84.95	80.26	85.95	97.64	93.44	90.54	83.05	101.50	137.66	82.35
bias	under	<b>under</b>	<b>under</b>	under			under	<b>under</b>	over	higher	lower

**Table 9 Non-randomness of met station terrain conditions : Costa Rica**

The spatial distribution of Costa Rica’s rainfall stations (left) and temperature station (right) networks are shown in Figure 47. Some clear spatial concentrations can be seen and the network is very sparse compared with the spatial complexity of underlying delivery model simulated precipitation (left) and evapo-transpiration (right) variation.

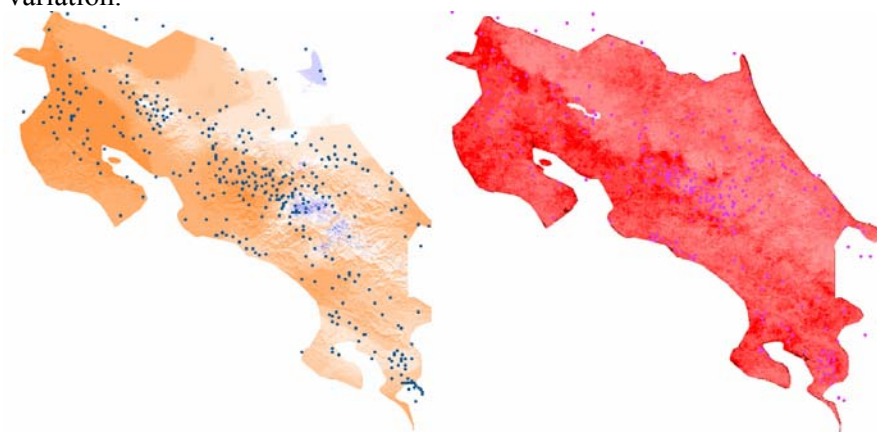


**Figure 47 Costa Rica’s rainfall (left) and temperature (right) station network compared with the underlying variation in modelled wind driven precipitation (left) and evapotranspiration (right)**

#### 4.2.1.4 Temperature and daily temperature range

Temperature data are necessary for the calculation of evaporation and for the calculation of the lifting condensation level for the formation of fog (liquid water) from humid air. Since this is a highly diurnally variable process we also need to know the diurnal temperature range. The New et al. (2000) dataset contains both temperature and diurnal temperature range (DTR) on a 0.5 degree grid globally. These data were obtained and interpolated using thin plate (tension) splines to 1km and then simple nearest neighbour to 90m. The resulting dataset for temperature is shown in Figure 48 and for DTR is shown in Figure 49.

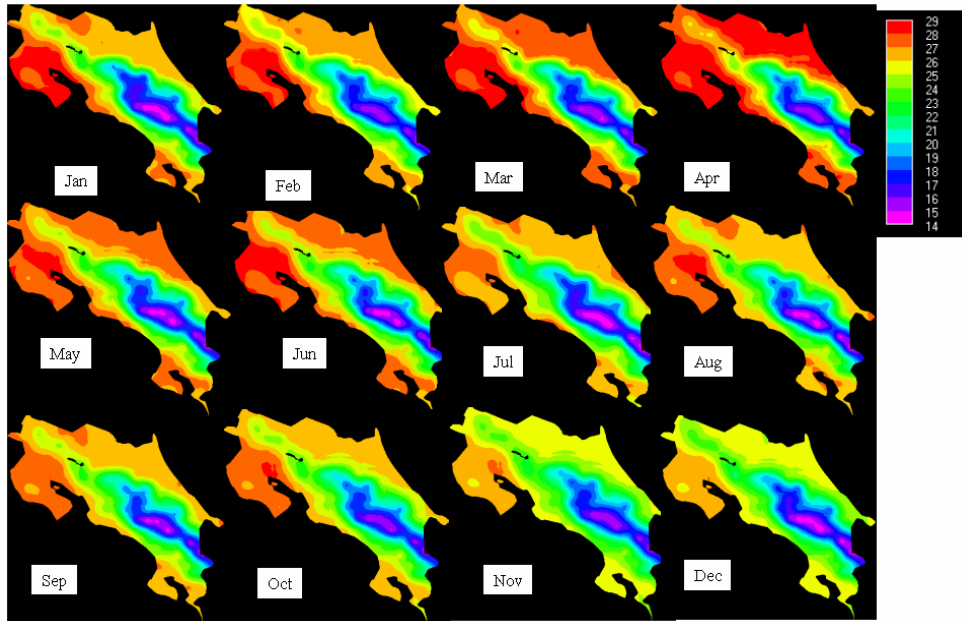


**Figure 48** Air temperature by Month. Note the strong altitudinal and Pacific-Atlantic differences.

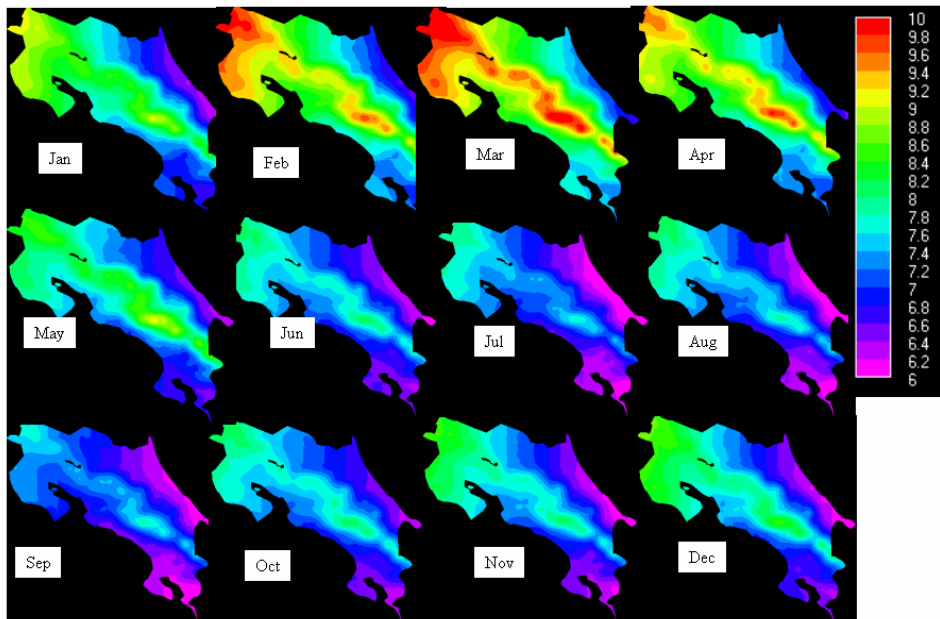


**Figure 49** Diurnal temperature range by month. Note the strong altitudinal effect and seasonality.

#### 4.2.1.5 Precipitation

Precipitation is a fundamental variable for water balance studies. There are however a number of difficulties in its interpretation since precipitation gauges in tropical mountains measure some combination of vertical rainfall, wind driven rain and fog and have different catching efficiencies for all three. The volume of each caught will depend largely on the gauge type, topographic exposure of the gauge and the prevailing wind conditions. Except under very low wind speed conditions, inputs of

fog to raingauges are likely to be low and we will assume here that gauges collect no fog (although it is likely that on leeward slopes they do). The impact of wind on rainfall is to reduce rainfall input to the gauge (compared with vertical rainfall), so highly exposed gauges are likely to significantly underestimate the actual rainfall inputs to the land. Since stations are not uniformly exposed these effects can produce important impacts on spatial interpolations especially for highly exposed mountainous regions such as we find in Costa Rica.

The WORLDCLIM dataset includes a 1km monthly rainfall field, interpolated from station data. Note that the rainfall station data (CIAT<sup>7</sup>, FAO<sup>8</sup>, GHCN<sup>9</sup>, WMO<sup>10</sup>) used by WORLDCLIM are not corrected for differences in gauge type, gauge wetting losses and gauge wind losses. Gauge losses depend upon gauge types, heights above the ground and any wind reducing structures applied as well as the local environmental conditions. We did not attempt such a correction here because of lack of information on gauge types, vegetation and other conditions in their vicinity, none were applied here, thus the gauges in highly exposed areas may be underestimating the catch of the land by a significant amount (see analysis at SG scale section 2.1.1). The station data were interpolated by WORLDCLIM using a thin plate (tension) splines to 1km and then simple nearest neighbour by AMBIOTEK to 90m. Figure 50 shows the interpolated precipitation data at 90m resolution. Note that the effects of wind and topography on the distribution of actual surface rainfall catches under prevailing conditions is included as part of the FIESTA\_delivery model (though this does not account for gauge wind losses for the reasons given above), see Arazi et al (1996).

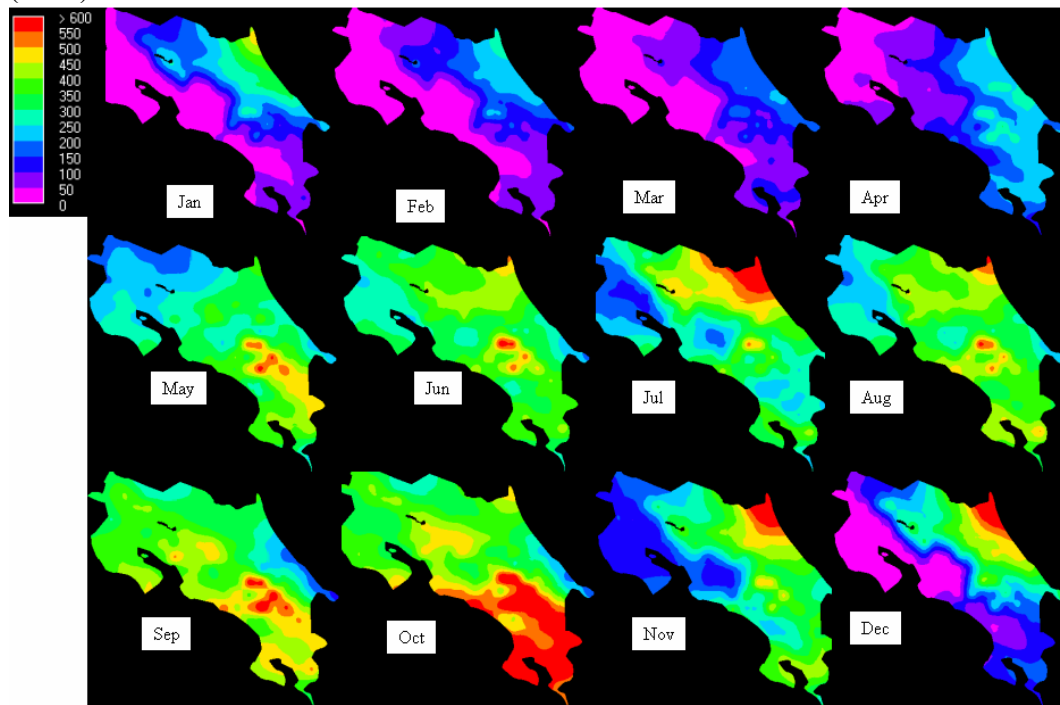


**Figure 50** Interpolated wind corrected station data for rainfall, by month.

<sup>7</sup> <http://www.ciat.cgiar.org/>

<sup>8</sup> <http://www.fao.org/>

<sup>9</sup> <http://www.ncdc.noaa.gov/cgi-bin/res40.pl?page=ghcn.html>

<sup>10</sup> <http://www.wmo.ch/>

#### 4.2.1.6 Humidity

Humidity is fundamental for the calculation of fog liquid water content and of the lifting condensation level for fog production. The New et al (2000) dataset provides monthly relative humidity based on station data and on a 0.5 degree grid. The data were re-interpolated here using grid thin plate (tension) splines to 1km and then simple nearest neighbour interpolation to 90m. Figure 51 shows the monthly progression of relative humidity for Costa Rica.

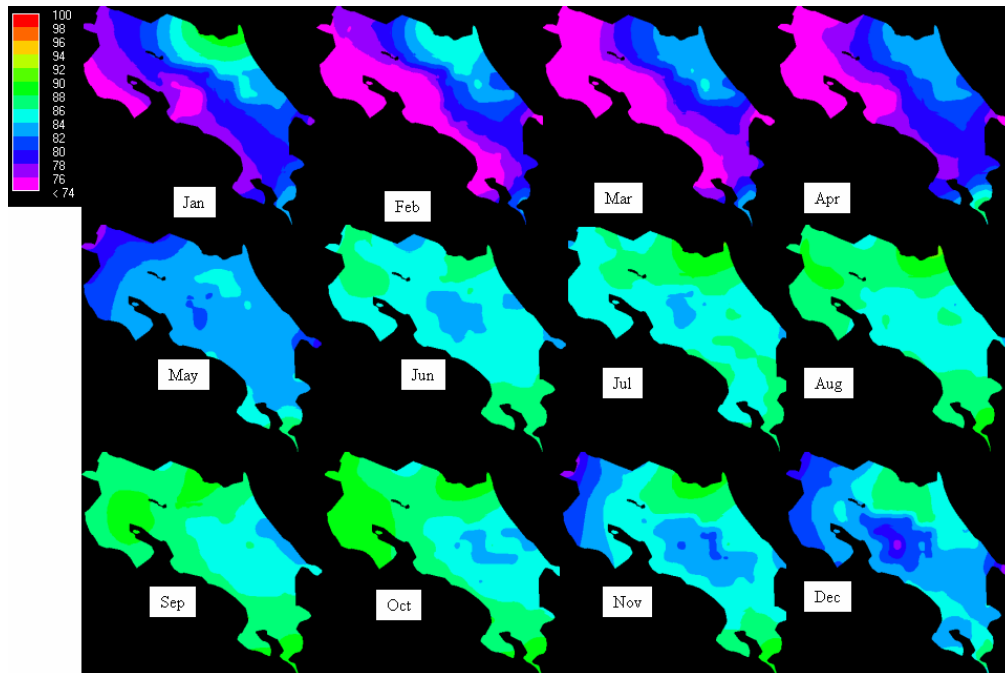


**Figure 51** Monthly patterns of relative humidity.

#### 4.2.1.7 Mean sea level pressure

Mean sea level pressure (mslp) is important in order to be able to model wind directions and lifting condensation levels (which depend in part on air density and thus mslp). Since there are no gridded or satellite based wind direction datasets over land mslp is used alongside topography to model wind direction.

#### 4.2.1.8 Wind speed

Wind speed is important for the modelling of wind driven rainfall and fog dynamics. The New et al. (2000) dataset provides monthly gridded near surface wind speed on a 0.5 degree grid. These data were re-interpolated to a 1km grid using thin plate (tension) splines and then to a 90m grid using simple nearest neighbour interpolation for input to the model. Figure 52 shows the monthly progression of wind speeds for Costa Rica.

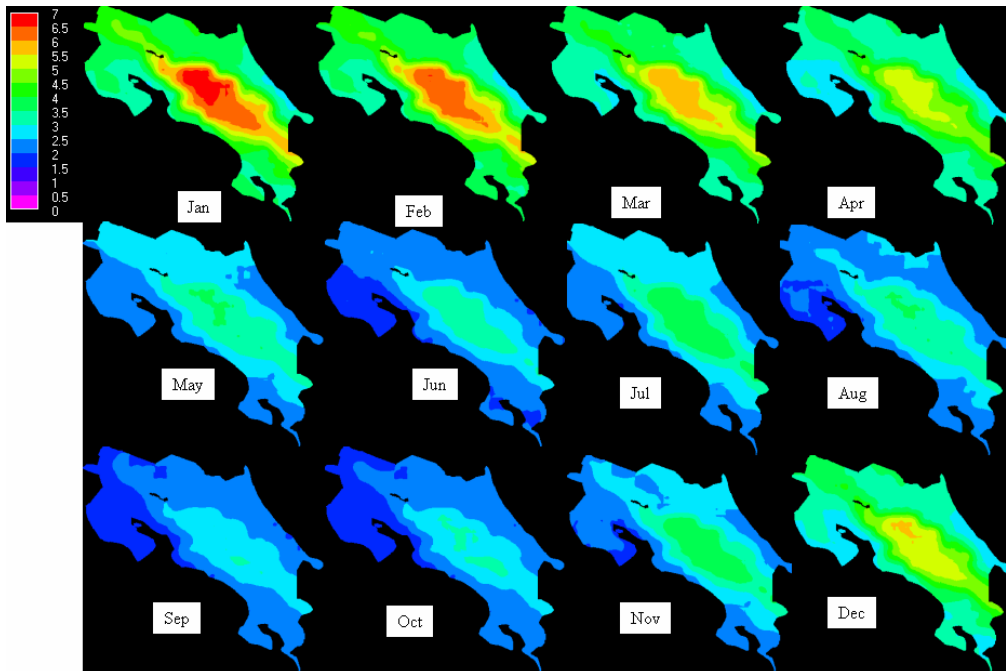


**Figure 52 Monthly progression of mean wind speeds for Costa Rica**

#### 4.2.1.9 Wind direction

Wind direction is an important variable for the calculation of exposure of land and vegetation to wind, rain and fog. There are no available wind direction datasets over land areas and wind directions are also highly locally variable according to topography. A two stage approach to the calculation of wind direction is used here. First, a boundary layer wind direction is calculated from the mslp fields. The gradient wind is calculated as the direction of the steepest gradient between mslp values using a D8 steepest drop algorithm (Burrough, and McDonnell, 1998). The geostrophic wind is then estimated by adding 45 degrees to the gradient wind (to simulate the effects of the Coriolis deflection to the right in the N hemisphere . For the southern hemisphere 45 degrees would be subtracted from the gradient wind.

The geostrophic wind directions are converted to surface wind directions which are warped to (i.e. deflected around) topography on the basis of the interaction of the boundary layer winds with local slope aspect and gradient. The algorithm used is as follows:

- (a) for each of the main (N,NE,E,SE,S,SW,W,NW) wind directions the wind direction is deflected left or rightwards dependent upon the local aspect and slope.
- (b) Where the aspect faces to the right of direction in which the wind is travelling deflection is to the right. Where the slope aspect faces to the left deflection is to the left.
- (c) The magnitude of the deflection is gradient dependent. If the slope gradient is zero the deflection is zero, if the slope gradient is 45 degrees the deflection is a maximum 90 degrees.
- (d) Where the slope faces away from the direction of travel of the wind, there is no deflection and wind passes over with direction unmodified.

- (e) In this way a series of maps are produced, one for each direction. When the FIESTA\_delivery model reads in a particular boundary layer (geostrophic) wind direction for a cell it is converted to a topography modified direction according to it's the corresponding map for that direction, see Figure 53.

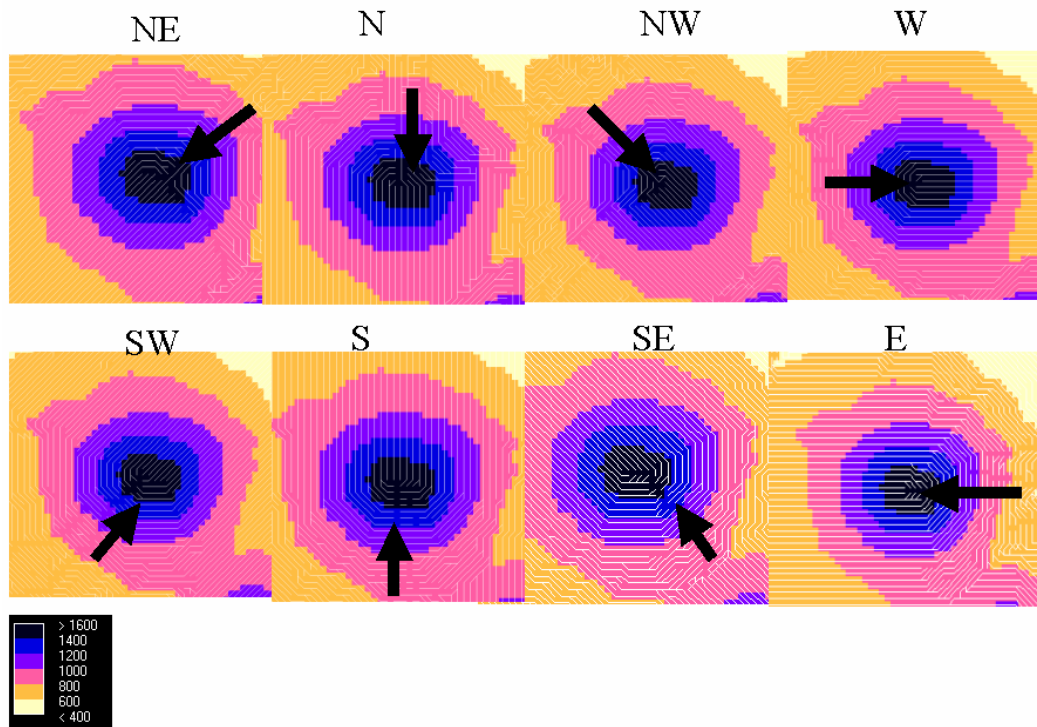


**Figure 53** Warping of winds to topography, example for Volcan Arenal

This is a simple way of representing topographic effects on surface wind directions but lacks memory so that the wind direction in a particular cell is uniquely affected by the topographic effects of that cell and has no residual effects of upstream topographic effects (except those inherent in the spatially autocorrelated landscape itself). The technique also does not represent the concentration or dispersion of flow that may accrue from topographic effects and its effects of observed wind speeds. Though simple, this technique does give an indication of landscape effects on wind direction.

#### 4.2.1.10 Wind exposure

Exposure to wind is calculated using an algorithm based on the TOPEX algorithm (Ruel et al., 2002), which determines to what extent an area is exposed or sheltered to winds from a particular direction by measuring the vertical angle (from the horizontal) from the point in question to the highest (or lowest) topographic or other feature in that direction. Assuming that winds are horizontal then negative angles are exposed from that direction whilst positive ones are sheltered. The degree of sheltering or exposure in a particular direction is proportional to the measured angle. Negative TOPEX values are exposed and positive values are sheltered. The PCRASTER horizontal function is used to calculate the maximum vertical angle from a particular direction. A TOPEX score is thus calculated for each of the eight possible wind directions to a cell. Figure 54 shows topographic exposure for an area around Lake Arenal calculated from the SRTM 90m DEM for winds from the cardinal directions.

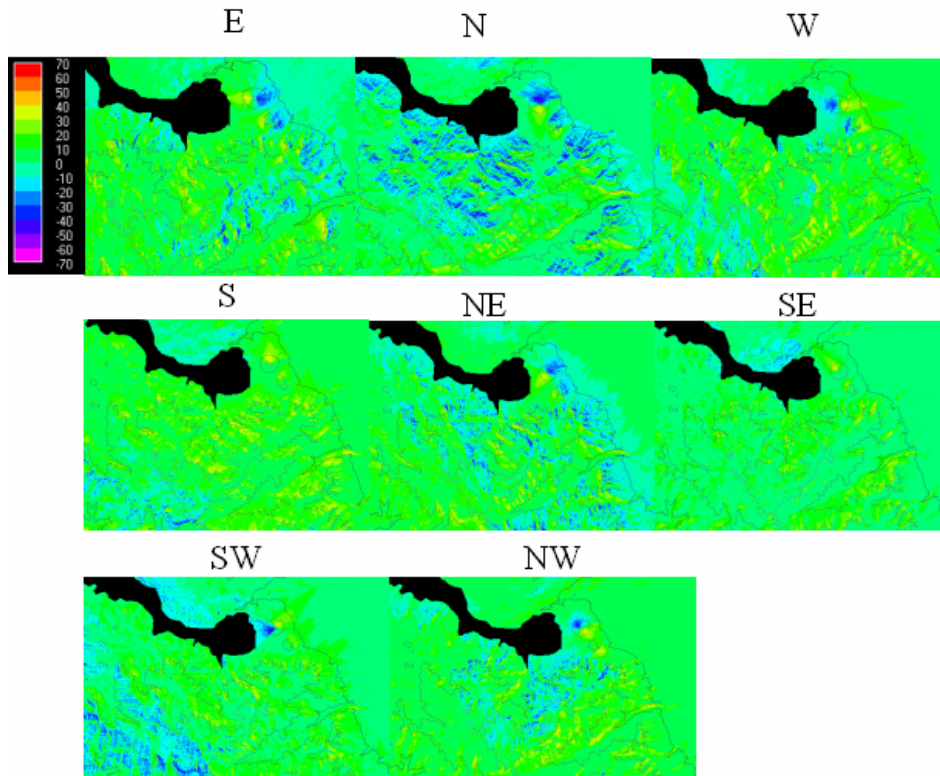


**Figure 54 Topographic exposure for winds from different directions.**

Taking the wind directions for each month in Costa Rica and passing them through this procedure, yields the map of average annual exposure in Figure 55.

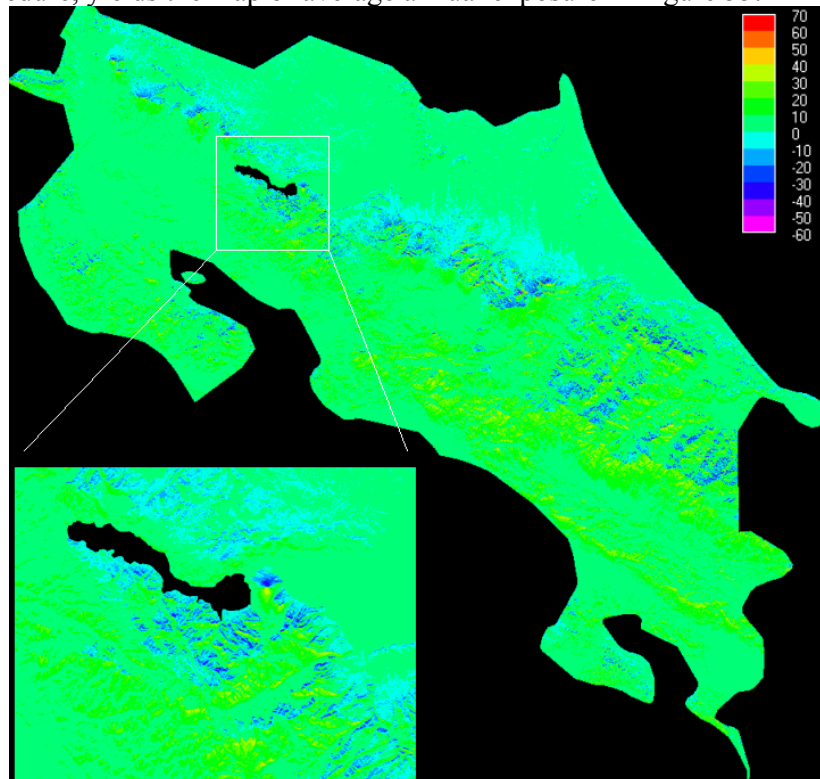


**Figure 55 Overall annual average topographic exposure for Costa Rica**

The resulting map of annual average wind speed is shown in Figure 56 and appears much more realistic than the input from the New et al. (2000) database.

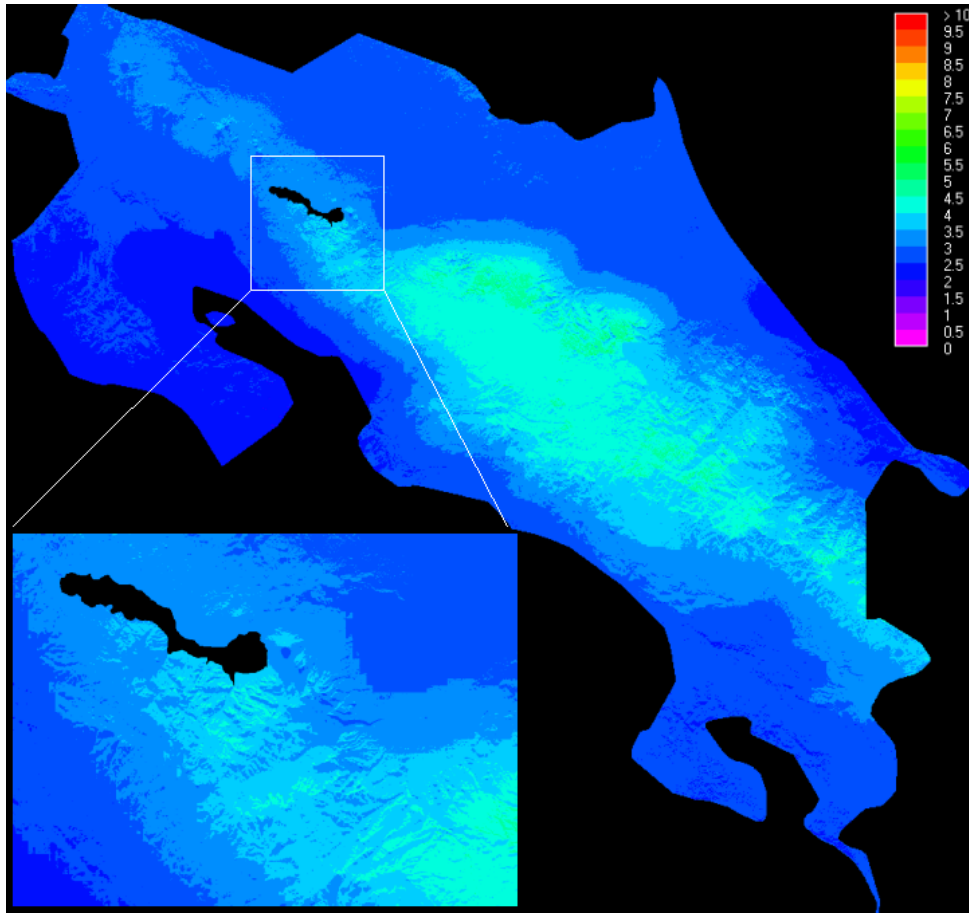


Figure 56 Annual average topography corrected windspeed.

### 4.3 Vegetation

Modelling fog inputs and the hydrological budget require spatial data on proportional cover of vegetation, in our case forest and pasture and on the fragmentation of forest and thus the number of forest edges exposed. The MODIS Vegetation Continuous Fields (VCF) are available globally at 500m grain providing information on % tree, % bare and % herbaceous cover (Hansen et al. 2003). Using continuous fields rather than land cover classifications provides a much more precise treatment of vegetation cover and avoids the choice of arbitrary thresholds separating forest and non-forest. These threshold approaches can lead to substantial errors in the estimation of forest cover (Mulligan and Burke, 2005a). Figure 57 provides a comparison of classification based approaches from two global datasets : the GLC2000 and the Global land cover characteristics (GLCC) databases<sup>11</sup>. The differing legends of the two classifications have been combined into a series of crude and comparable classes here (forest, grassland, cropland, urban....). There are clearly substantial differences in the

<sup>11</sup> <http://www-gvm.jrc.it/glc2000/>  
<http://edc.usgs.gov/products/landcover/glcc.html>

classification in terms of their representation of forest cover and grassland even though the two classifications are only 10 years apart. The MODIS derived Vegetation Continuous Fields, not only provides a more suitable representation of vegetation properties for the current work but does so with greater spatial detail and with the greater precision afforded by a continuous field rather than a classification.

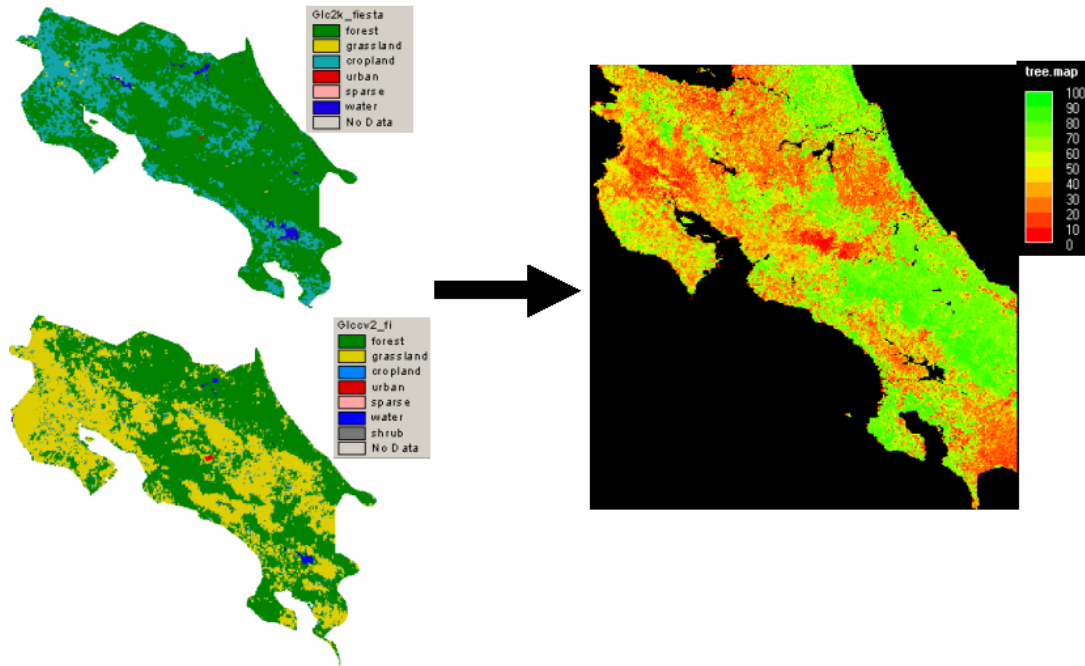


**Figure 57** GLC2k (topleft) and GLCC (bottom left) classifications of land cover for Costa Rica compared with the MODIS VCF (right).

The continuous fields have been cut and resampled to 1km and 90m resolutions here using the nearest neighbour technique. Whilst the VCF data provide information on forest cover, these are 500m samples and give no information on fragmentation and the number and direction of forest-pasture boundaries or *edges*, which are likely to be important in the trapping of fog and wind driven rain.

The technique developed to provide such information involved analysing the relationship between forest cover at 500m grains and the patchiness of forest within these 500m cells using landsat (30m grain) data for the whole of the Rio Chiquito catchment for which landsat data were available. at 25m grain size, the edges bounding forested and pasture areas are defined at the edge length calculated, an isolated patch can have the maximum edge length (100m, four sides of a pixel) whereas a section of a forest/pasture interface has an edge length of 25m. The distribution of edges in the southern part of the Chiquito catchment is shown in Figure 58.

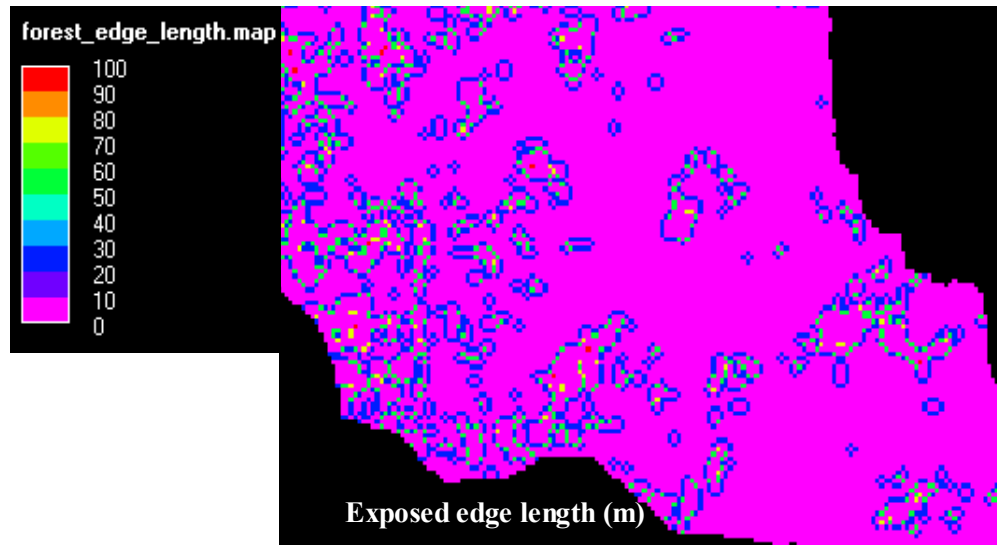


**Figure 58** Exposed edge lengths in the southern Chiquito catchment.

Comparing these edge length statistics against the MODIS VCF tree cover percentage for 500m pixels overlying these indicates that at 100% tree fractional cover in the MODIS VCF data edge length from the landsat data in m/pixel is zero. Similarly for 500m pixels with a MODIS VCF of 0% edge length is zero. The peak in edge length occurs at MODIS VCF tree covers of around 50% (Figure 59), as one might expect.

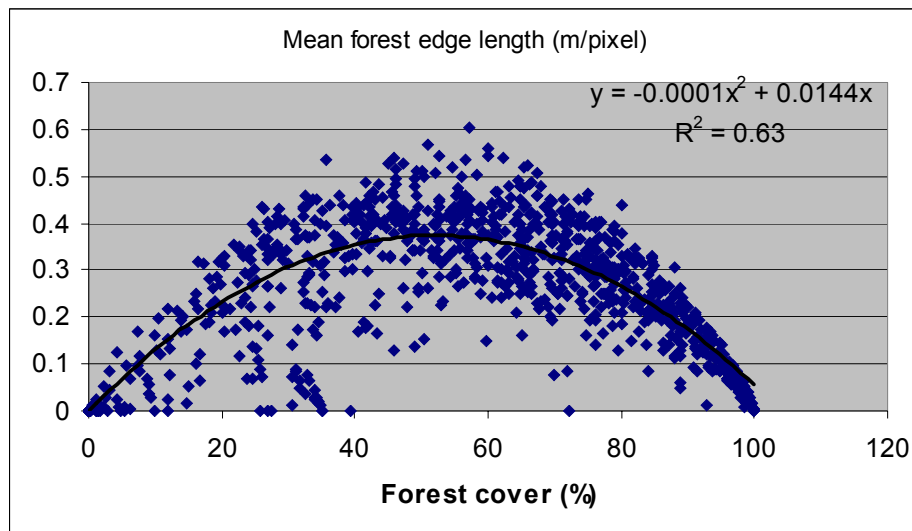


**Figure 59** Relationship between MODIS VCF cover and LANDSAT measured edge lengths.

This provides a mechanism for the calculation of edge length from MODIS VCF data. Analyses of the directionality of edges indicates that they are randomly distributed amongst the eight compass directions, at least in the Chiquito.

#### 4.4 Development of land use change scenaria

At the national scale, the land use change scenaria are rather simple. The scenaria were produced to represent the impact of PES schemes in general and of deforestation in the cloud forest belt in particular. The following scenaria were produced:

(a) BASELINE

The baseline scenario represents the land use situation as of 2001. This situation can be summarised as follows:

The average size of catchment in Costa Rica is 151 km<sup>2</sup> and the mean catchment altitude 2488m. Catchments are on average 39% forest, just under half of which (16%) is protected, though there is much variation between catchments. Assuming forest=tree cover >60%<sup>12</sup>, Costa Rica has 23,390 km<sup>2</sup> of forest of 61,815 km<sup>2</sup> terrestrial surface (making 37.8% forest cover). Some 12062 km<sup>2</sup> of forest is protected (51.5%) and 11328 km<sup>2</sup> (48.5) of forest is unprotected

(b) PES

The PES scenario represents a future in which the existing protected areas network is maintained without land use change through the provision of funds through PES schemes. Outside of the protected areas tree cover is lost at the measured historic rate -0.5 % per year. The scenario is centred on the projected situation by 2051 if this situation were sustained.

(c) NOPES

Deforestation at recent measured rates (0.5% per yr) both inside and outside of protected areas to 2055. Since there are no PES payments under this scenario the current protected area system is not sustained against land use change. The protected area system was defined according to the WDPA (World database on protected areas)<sup>13</sup>, see Figure 60.

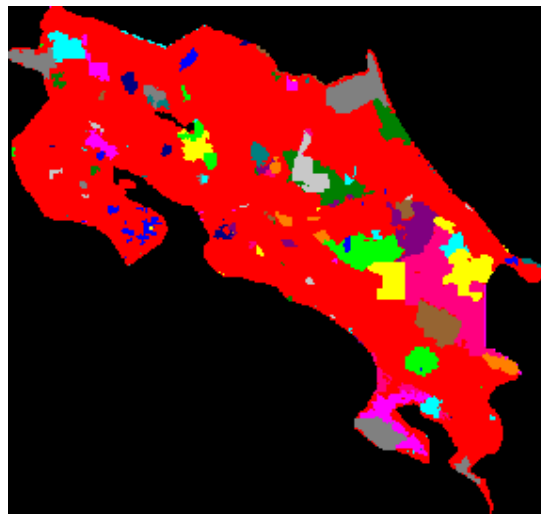


**Figure 60 Protected areas of Costa Rica**

<sup>12</sup> Though this is debatable, see Mulligan and Burke (2005)

<sup>13</sup> WDPA Consortium. "World Database on Protected Areas" 2004 . Copyright World Conservation Union (IUCN) and UNEP-World Conservation Monitoring Centre (UNEP-WCMC), 2004. Source for this dataset was the Global Land Cover Facility.

These scenarios are shown in terms of their tree cover distributions in Figure 61. Clearly the current situation shows high tree covers inside of protected areas and these are maintained in the PES scenario even though tree cover falls outside of these areas. In the PES scenario tree cover falls both within and outside of the protected areas.

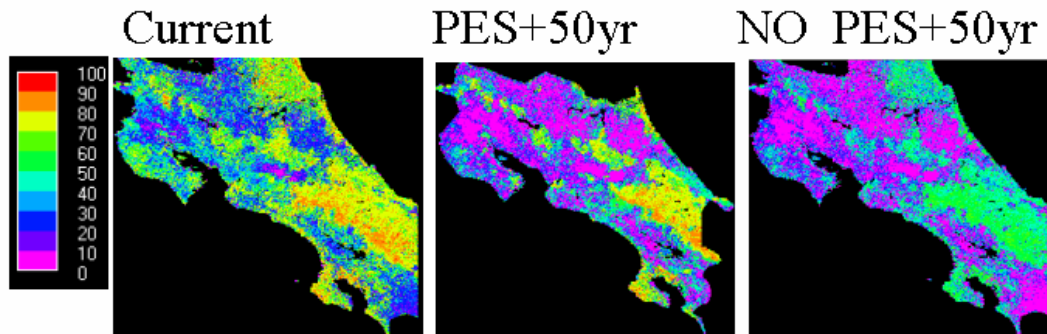


Figure 61 The FIESTA\_delivery model land use change scenaria

(d) UNPROTECTED CLOUDFOREST REMOVED

In the cloudforest removed scenario then all areas >1400 masl that are **unprotected** lose their cloud forest at the observed rate of -0.5% per year. This scenario is present to enable hydrological assessment of cloud forests only loss (rather than mixed cloud and lowland forest loss).

These are simple and extreme scenarios developed to test the effect of major changes and do not represent predictions or projections of the future. Many other scenarios are possible.

**4.5 Forest cover and forest protection in Costa Rica : by altitude**

Analysis of the forest cover and conservation status of Costa Rica (Figure 62) using the MODIS VCF, the SRTM DEM And the WDPA indicates that around half of Costa Rica’s land area lies above 200 metres altitude with the land above 1600 metres altitude having near complete forest cover. More than 80% of the land above 2100m is protected in some way and more than 80% of forests above 1700m are protected. Compared with many countries there is little scope for further protection of cloud forests in Costa Rica, hence our concentration on the maintenance of the existing protected areas network rather than its expansion through PES.

### An altitudinal conservation analysis for Costa Rica

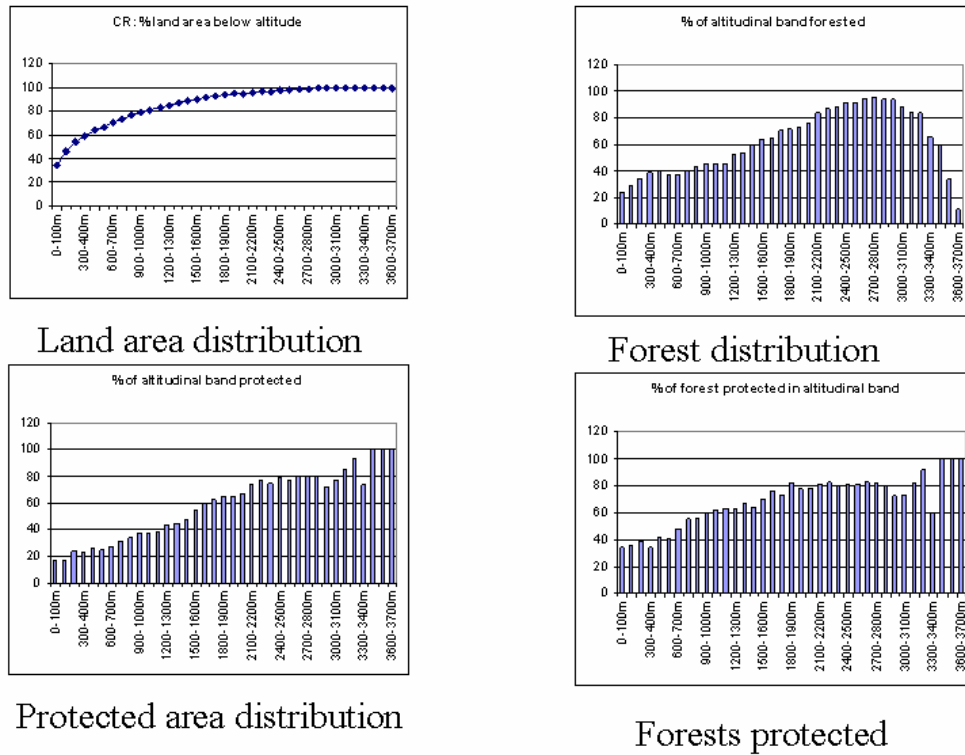


Figure 62 An altitudinal conservation analysis for Costa Rica.

#### 4.6 Climate Change Scenarios

In addition to the land use change scenarios a climate change scenario was also developed. The purpose of this scenario is to test the relative impact of climate change against that of land use change. The scenario is derived from mean temperature and precipitation change projected by two general circulation models of the atmosphere (HADCM2 and ECHAM driven by the IS92a scenario) for the grid cells overlying Costa Rica. The changes are:

Temperature change by 2050 = +1.08°C

Rainfall change by 2050 = -13.3 mm/month

This pattern of warming and drying is typical for central America (see Figure 63)

The changes are applied uniformly over space and across time (months and hours) for simplicity.

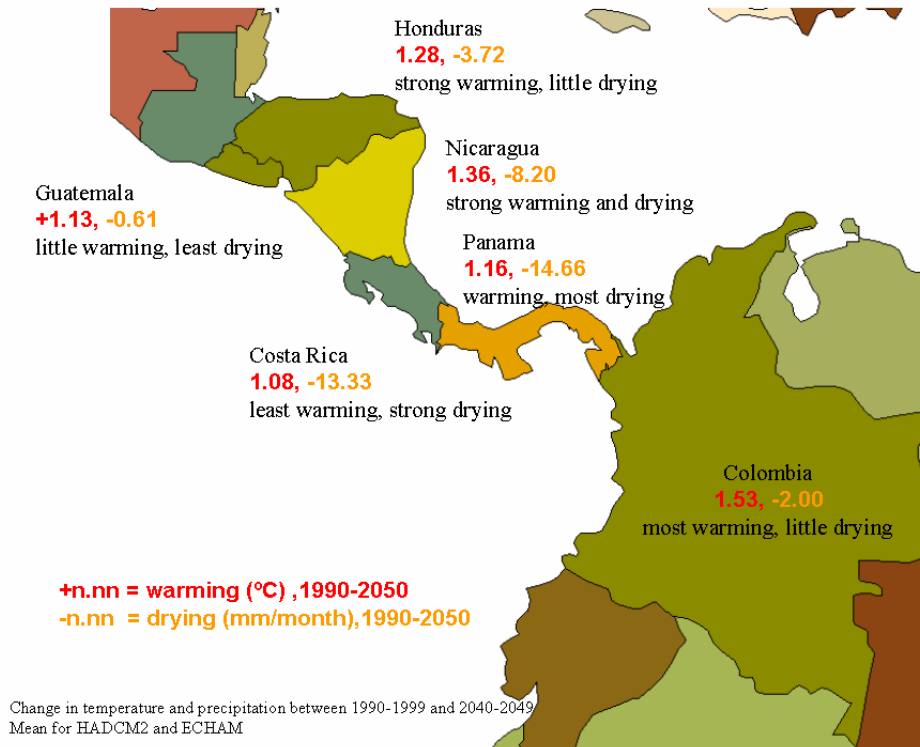


Figure 63 Expected climate change in central America

#### 4.7 Software development : PCRASTER

In order to process the datasets and permit the modelling of the high resolution 90m version of the FIESTA -delivery model (representing 6 million cells for Costa Rica), the following improvements were made to the PCRASTER software by PCRASTER ENVIRONMENTAL SOFTWARE under contract.

- (1) Implementation of -p functionality. This functionality allows the PCRASTER developer to test the memory requirements of a model being developed and thus understand better how to optimise the model and what kind of computing platform will be needed to run it.
- (2) Implementation of -m functionality. This functionality ensures that only data cells actually consume memory and computations and that cells that are no data on any input map do not consume computing resources. This can lead to an efficiency gain of up to 50% depending on the shape of the catchment/country relative to the bounding square or rectangle.
- (3) Implementation of -l. This functionality allows PCRASTER to move away from its traditional mode of operation to load all data and do all processing in RAM memory to a situation in which the software maintains a disk cache for calculations. This removes the 2 GB limit on memory (though it does slow the computations down considerably). The result is that this technique can be used to work with very large databases where the -m function is not sufficient.

- (4) Implementation of 64 bit capability. Basic 64 bit capability has been enabled so that PCRASTER can work with up to 4GB on RAM memory on a 64bit operating system. This has allowed rapid national scale simulations of the 90m model to be undertaken.
- (5) Implementation of the lookupmapstack functionality. This functionality significantly reduces memory requirements for dynamic models by only loading a single member of a temporal map stack into memory when needed.

#### **4.8 Hydro-climatic Model development**

The bulk of AMBIOTEK's effort was devoted towards the development, testing, application, experimentation with and deployment of the FIESTA\_delivery model. The model is spatial, dynamic and sophisticated in process terms. At the same time it has been developed in high spatial resolution (detail) and with a sophisticated timestep and time dynamics. Nevertheless, the 1km policy version (as opposed to the 90m research version) runs quickly (5 minutes on a reasonable computer) and is suitable for policy exercises and decision support. Considerable challenges were overcome in the:

- (a) representation of cloud interception processes,
- (b) representation of diurnal dynamics,
- (c) development using only publicly available global datasets,
- (d) testing and distribution.

##### *4.8.1 Introduction*

One of the greatest limitations of hydrological investigations is that they can usually only be applied to small scales and few locations. This is true for field research because of the prohibitive technical difficulty and high cost of instrumentation and of data collection at scales greater than the point or plot scale. It is true for modelling studies because of limitations imposed by the lack of ground-based data at scales greater than the point or plot scale.

This limitation is a serious one for policy-relevant hydrology since it means that studies are usually carried out intensively at a single or a few locations with particular characteristics and the results are then extrapolated rather crudely as 'rules of thumb' (by the policy analysts if not the scientists) to larger scales and different locations which may have very different characteristics to the study site(s). The FIESTA\_delivery model has two main objectives. First the model is intended to place the Chiquito catchment results within a national context for Costa Rica (and later an international context for Central America so that the results from the Cqflow model can be seen within the context of the Chiquito catchment and its similarities/differences with other catchments in central America (both lowland and montane). Secondly, the FIESTA model was intended to summarise the field and modelling knowledge gained from the finer scale research and 'deliver' it in the form of a model that can be used by anyone for land use and climate change hydrological impact scenario analysis in their own countries. Thus the model operates in a freely

available software environment and using globally available (mainly remotely sensed) data.

The FIESTA delivery model is a process model, which simulates the hydrological balance including inputs of wind driven precipitation and fog and outputs of evapotranspiration. The resulting balance is cumulated along river flow networks to give an indication of runoff. It is cumulated water balance rather than runoff since it does not account for infiltration, baseflow and returnflow but these effects are usually quite small compared with downstream cumulated water balance at the very large scales of operation of the delivery model. The model operates at a monthly timestep using a long-term monthly mean climatology and thus shows the mean hydrological balance and seasonal variation. Within this monthly timestep a diurnal timestep also operates in order to properly simulate the dynamics of fog incidence and interception. The model is a grid-based spatially distributed model, which can operate at a 1km grain or a 90m grain, depending on the computing resources available. The 1km version is intended for policy application and the 90m version is more appropriate for research applications. Results between the two versions differ a little in magnitude and pattern as one might expect since the 90m version represents 100 times the spatial variability. The two models do not differ in the overall outcomes of the model for any parameter. They are the same in terms of process and only differ in terms of input data.

#### *4.8.2 Policy application*

All data are supplied for the whole of Costa Rica and work is underway to make the necessary data available for the whole tropics. The model comes with a series of policy exercises designed to investigate the impacts of scenaria for forest conservation, land use change and climate change. The scenaria include a baseline (run\_baseline) representing conditions in 2001, a PES scenario (run\_pes, representing the situation after 50 years of continued forest protection from PES funds) a no PES scenario (run\_nopes, in which forest protection is less possible and land use change occurs also within area under protection in 2001), a cloud forest loss scenario (run\_cloudforestremoved, in which unprotected cloud forests only receive continued land use change) and a climate change scenario (run\_climch, in which the GCM derived temperature and precipitation trends for Costa Rica are applied to the 2001 baseline). A series of postprocessors (named compare\_all) compare the results of the scenaria with the baseline and display the impacts of the scenaria on fog interception and hydrological balances in general.

#### *4.8.3 Model Summary*

For a national scale model the FIESTA delivery model is very sophisticated and accounts for many processes that are not usually simulated in many hydrological models including :

##### *4.8.3.1 Temporal*

- Unique diurnal cycle-in month timestep to capture daily and seasonal cycles in computationally efficient manner

#### 4.8.3.2 Spatial

- The model is operable from globally available free datasets. The following are amongst those required:
- SRTM digital elevation model (90m) or GTOPO30 DEM (1km) and derivatives
- MODIS satellite derived cloud cover frequency and diurnal/seasonal derivatives
- WORLDCLIM-derived monthly meteorological inputs (precipitation, temperature, diurnal temperature range)
- Monthly relative humidity, mean sea level pressure, wind direction, wind speed and derivatives developed for this project and available at 1km resolution at <http://www.ambiotek.com/fiesta/fiesta.kml>
- Fractional tree, herb and bare vegetation cover from MODIS VCF (Vegetation Continuous Fields)
- Capable of application at scales from 1km (for continental extent) to 90m (for national extent)
- Calculation and use of true surface areas (rather than planimetric areas) for all area calculations
- Representation of land use as a more precise fractional coverage of trees per cell rather than a binary forest/nonforest classification

#### 4.8.3.3 Simulated Processes

- Calculation of spatially distributed direct and diffuse solar radiation receipt accounting for slope, aspect and topographic shadowing effects. Solar radiation corrected for cloud cover and fog attenuation. Net radiation calculated from solar radiation on the basis of land cover type (forest or pasture)
- Wind driven rainfall calculated for each cell on the basis of measured rainfall inputs corrected for local windspeeds and topography
- Fog incidence is calculated as a function of the observed frequency of observed atmospheric cloud and the propensity for condensing conditions to exist at the land surface
- Calculation of wind direction on the basis of mean atmospheric pressure fields and modification for local topographic funneling
- Spatial distribution of wind speeds on the basis of regional wind speeds corrected for topographic exposure to winds from the relevant local wind direction
- Separation of fog interception into deposition and impaction components on the basis of wind speed and calculated surface areas according to angle of fog impact for forest and pasture. Calculation of forest-pasture edges and emergent tree exposure to fog and their role in fog interception. Total fog interception is thus the sum of vertical deposition and horizontal impaction to forest and grass surfaces, edges and emergents. We do not model water vapour condensation to leaves in the delivery model as this is considered minor in these very cloudy environments.
- Representation of self-shading for fog interception and for evaporation for both forest and grassland
- Evapotranspiration driven by available energy (net radiation) intercepted by the land and vegetated surfaces
- Water balance calculated as sum of fog inputs plus wind driven rainfall minus evapotranspiration and then cumulated downstream. Fog and other water

balance components can be expressed as a proportion of the water balance at a point and integrated downstream along the hydrological flowpaths

- Variables can be analysed raw (for each grid cell) or aggregated by altitudinal band, catchment, protected area, continental divide, mountain areas only (>1000masl), identified field sites and provinces

Some simplifications had to be made in working at these scales and with the data sources available and as such:

- The evapotranspiration model is a simple energy driven model which takes little account of vegetation properties other than LAI
- No soil moisture, groundwater or canopy water balance are produced so no baseflows are represented in the model : it calculates on the water balance precipitation-evapotranspiration and though this balance is also cumulated downslope it is not entirely equivalent to runoff

#### **4.9 Detailed outline of the FIESTA\_delivery model**

Here we describe the conceptual basis and application of the model. Details of how it may be operated (a user manual) and a description of the policy exercises are given in Part II of this document. The model application can be separated into a series of steps

- (a) Data pre-processing/generation (described earlier, not necessary for central America since the datasets have been prepared)
- (b) Modelling
- (c) Postprocessing/scenario evaluation

The model processes can be summarised as shown in Figure 64.

## ‘FIESTA Delivery’ model : processes

- Monthly wind directions calculated from 5° gridded mean pressure fields
- Monthly T,  $T_{DR}$ , RH, P and U at 1km from 10’ CRU database
- Wind directions warped to topography.  $R_s$  and  $R_N$  calculated including effects of slope, shading and cloud cover.
- Wind speeds corrected for exposure, rainfall wind-driven
- Dewpoint, LCL(mb) and LCL(metres) calculated.
- Fog where  $DEM \geq LCL$  with MODIS cloud frequency,  $LWC \propto AH$
- Fog settling according to Stokes Law
- Impaction: Deposition ratio  $f(U, \text{Settling velocity})$
- Capture efficiency  $f(LAD, \text{inclination angle})$
- Capture area for deposition=cell, for impaction=edge length  $f(\text{cover}), \text{veg height}$
- Total fog flux  $f(\text{flux}, \text{capture efficiency}, \text{capture area})$

Figure 64 Summary of the FIESTA\_delivery model processes.

The basic fluxes simulated in the model are simplified in Figure 65. These are simulated within each grid cell of the modelled area.

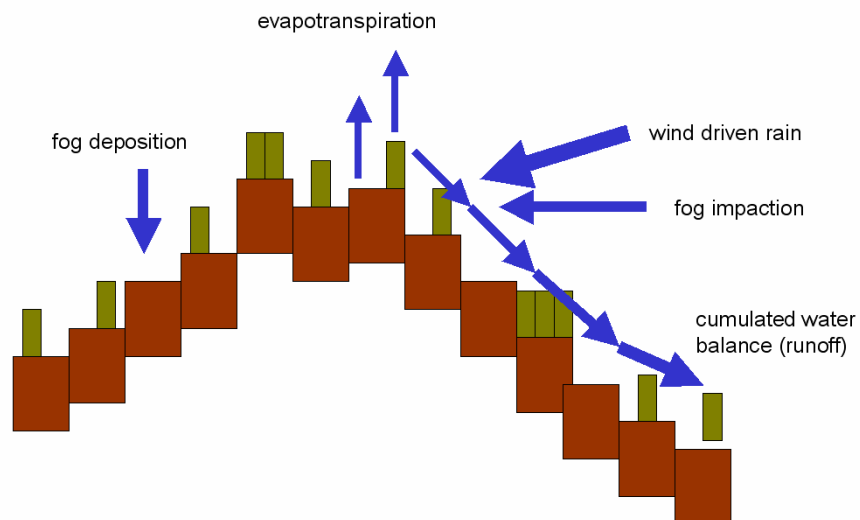


Figure 65 Basic fluxes simulated in the FIESTA delivery model

#### *4.9.1 Intention*

The model essentially simulates the water balance by simulating the above ground components of the hydrological cycle. It is these components for which we can access good spatial data. If we were to have to simulate infiltration and runoff generation then detailed soil and subsurface data would be required. Since these types of data cannot readily be remote sensed they tend not to be available at the scale and detail at which we would require them. Thus the delivery model calculates the water balance by accounting for spatially distributed inputs of wind driven rain and fog and outputs of evapotranspiration according to spatially variable topographic, climatic and vegetation properties. Though we do cumulate the water balance downstream, this is only an indication of runoff potential since it does not account for baseflows, changes in local storage and associated time lags. Since the model calculates on the basis of long-term average climatologies, the cumulated water balance should be close to the long term average runoff (since changes in local storage will not appear strongly in long term data). Whilst the model cannot be used to predict river flow regimes it can be used to better understand the impacts of climate, land use and topography on the water productivity of environments and thus potential yields to downstream communities.

The model is intended as a tool to better understand the outcome of processes and thus has no calibration parameters and is used without calibration. If the model does not work well on application to a new region then the model processes should be adapted rather than any model parameters calibrated. The model is sophisticated in process even though it can be run at large scales on readily available data. This process sophistication facilitates model realism and ensures that where better data are available they can be utilised or the model applied at smaller spatial scales, as required.

#### *4.9.2 Timestep*

Most globally available datasets are available at 1km spatial resolution or worse and with monthly timesteps. Though a monthly timestep is sufficient to capture seasonal variability, we also need to capture diurnally varying processes if we are to simulate fog interception. Thus the timestep we use is a diurnal step (4 times per day, 1=2400, 2=0600, 3=1200, 4=1800) embedded within a monthly timestep. Results can be output at the end of the simulation only or for midday each month but are based on these 48 (12 times 4) timesteps which capture the diurnal and seasonal variation of climate and other processes.

#### *4.9.3 Spatial scale*

The model is applied at a 1km grain for national international extents or at a 90m grain for national extents only. Only technical (computing) limitations prevent larger extent application at 90m or continental application at 1km since the required data are available. These limitations could be overcome with further investment in software development. Results are output as raw cellular data or aggregated according to defined catchments, sites, provinces altitudinal bands, protected areas or other.

#### 4.9.4 Processes simulated

##### 4.9.4.1 Surface area

*Key assumption : that DEM generated surface areas are representative of land surface areas*

(1) True surface areas (as opposed to planimetric areas) are calculated with the triangle method (Jenness, 2004). These are important for the accurate representation of surface area in montane environments. True surface areas can be three times the planimetric surface area for very steep rugged slopes.

##### 4.9.4.2 Vegetation cover

*Key assumption : That this vegetation data is sufficient to represent the main fog catching processes and different types of vegetation can be effectively considered only as their proportional representation in these classes.*

(2) Tree, herb and bare percentages from MODIS VCF are converted to fractions

##### 4.9.4.3 Fog settling

*Key assumption : That fog settling occurs under calm conditions and upwards fog turbulent diffusion is limited compared with this downward flux.*

(3) Fog settling velocity is calculated according to Stokes Law based on the mean particle size for fog.

$$\text{FogSettlingVel} = (980 * ((7.5 / 10000) ** 2) * (1 - 0.0013)) / (18 * 0.000185)$$

#### Equation 2

where 7.5 = fog droplet size in um

##### 4.9.4.4 Forest edges

*Key assumption : That forest edges are important and can be represented as catching surfaces. That, as in the Chiquito, there is a random directionality of forest edges.*

(4) Forest is given an one sided LAI=3 and pasture LAI=2

(5) Forest edges are calculated according to the tree fractional cover as :

$$\begin{aligned} \text{forestededgefrac} &= -3E-05 * \text{Tree} ** 2 + 0.0036 * \text{Tree}; \\ \text{forestedgelenm} &= \text{forestededgefrac} * ((\text{CellSize} * \text{CellSize}) / (25 * 25)) * 100 ; \\ \text{emergentedgeelenm} &= (0.05 * \text{TreeFrac}) * ((\text{CellSize} * \text{CellSize}) / (25 * 25)) * 100 \\ \text{forestedgelenfacingm} &= (\text{forestedgelenm} / 4); \\ \text{emergentedgeelenfacingm} &= (\text{emergentedgeelenm} / 4); \end{aligned}$$

#### Equation 3

so that the empirical equation derived from Figure 59 provides the fractional forest edge length on the basis of tree fractional cover, this is converted to an actual length based on the cellsize of the grid compared with the original landsat grid. The fraction of exposed emergent trees is calculated as a 5% fractional of the area covered by tree. The division by four accounts for the fact that only one edge of a grid cell will face a wind from a particular direction. Figure 66 shows forest edge fractions for an area around Lake Arenal.

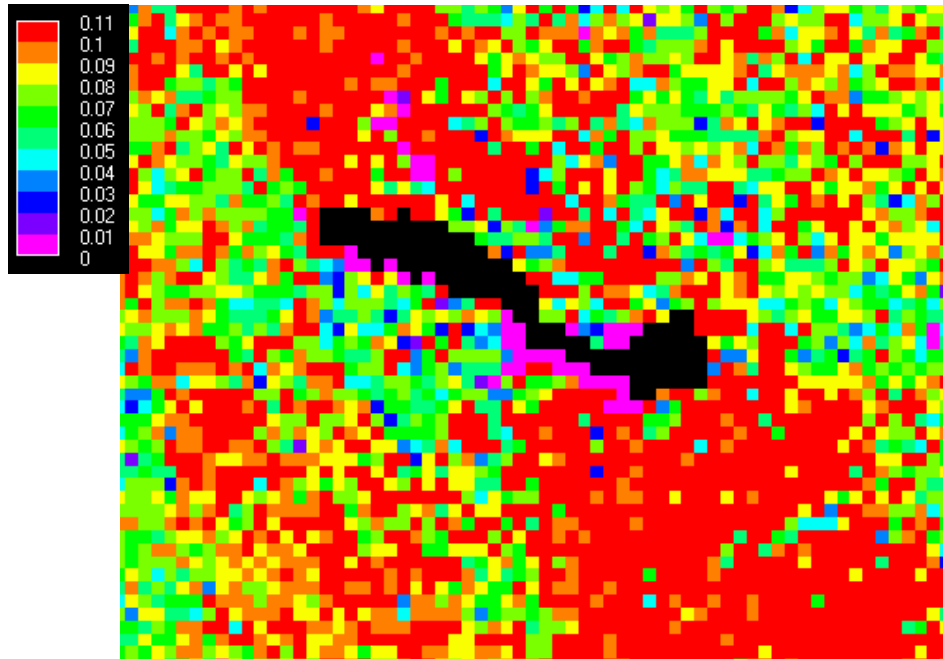


**Figure 66 Forest edge fractions around Lake Arenal.**

#### 4.9.4.5 Sedimentation surface area

*Key assumption : That the whole unshaded (one sided) leaf surface area is available for sedimentation (deposition)*

(6) The surface area available for fog deposition (sedimentation) is calculated as:

$$\begin{aligned} \text{ForestTrappingSfcArea} &= (1 - (\exp(-0.7 * 0.3 * 10))) \\ \text{PastureTrappingSfcArea} &= (1 - (\exp(-0.7 * 6 * 0.5))) \\ \text{DepositionFrac} &= (\text{TreeFrac} * \text{ForestTrappingSfcArea} * \text{ForestLAI}) + ((1 - \text{TreeFrac}) * \text{PastureTrappingSfcArea} * \text{PastureLAI}) \end{aligned}$$

#### Equation 4

Fractional trapping areas for forest and pasture are calculated first (on the basis of leaf self shading). These are then multiplied by the fractional covers of tree and pasture for the grid cell and the available LAI.

#### 4.9.4.6 Intercepted energy fractions

*Key assumption : That evapotranspiration is effectively modelled at this coarse spatial and temporal scale from consideration of energy availability and atmospheric demand for water only. Leaf area is sufficient to represent plant processes and aerodynamic resistances can safely be ignored.*

(7) For simplicity and parsimony the model does not account for stomatal behaviour but rather defines the evapotranspiration differences between forest and pasture to be a function of the radiation intercepted by the canopy since this is the driver of both transpiration and wet canopy evaporation.

$$\begin{aligned} \text{ExpLAI} &= (1 - \exp(-0.7 * \max(1, \text{ForestLAI}))) \\ \text{EtFrac} &= \text{TreeFrac} * \text{ExpLAI}; \# \text{ forest} \\ \text{ExpLAI} &= (1 - \exp(-0.7 * \max(1, \text{PastureLAI}))) \\ \text{EtFrac} &= \text{EtFrac} + ((1 - (\text{TreeFrac} + \text{BareFrac})) * \text{ExpLAI}); \end{aligned}$$

#### Equation 5

Thus the overall intercepted energy for ET is the sum of energy intercepted by tree leaves and by pasture in the grid cell.

The model now iterates between four diurnal and 12 mensual timesteps (4 in each month) for a total of 48 timesteps for a complete run.

#### 4.9.4.7 Input climate data

*Key assumption : Winds bend around topography, taking the path of least resistance. It is sufficient to model these changes in direction without accounting for concentration (funnelling effects)*

(8) Wind directions are read and converted to the appropriate topographically affected wind direction (see Figure 53) by reading the appropriate wind direction file. Based on this wind direction, the appropriate TOPEX value is read from the topeX files. Note that the wind direction file BLWind mis the directions that wind is going to whereas in the delivery model windspeeds are specified as directions that wind is coming from.

(9) Relative humidity, temperature, diurnal temperature range, wind speed precipitation and extraterrestrial solar radiation are read from the appropriate files

#### 4.9.4.8 Input cloud cover data for time of day and season

*Key assumption : The MODIS data represents well the pattern of atmospheric cloud, where atmospheric cloud has formed and terrain level conditions are condensing (i.e. above the cloud base), this cloud is likely to be present at ground level.*

(10) MODIS derived cloud cover is read with the overall annual average value modified by seasonal and diurnal correction factors based on the maps in Figure 44 and Figure 45.

#### 4.9.4.9 Temperature, dewpoint and liquid water content

*Key assumption: Cloud liquid water content is proportional to absolute atmospheric humidity.*

(11) Temperature is modified according to the diurnal temperature range as follows:

```

Tmp=if(Hour eq 1 then Tmp-(0.25*DiurnalTRange) else
      if(Hour eq 2 then Tmp else
      if(Hour eq 3 then Tmp+(0.25*DiurnalTRange) else
      if(Hour eq 4 then Tmp
      ))));
    
```

#### Equation 6

(12) Dewpoint and vapour pressure are calculated according to:

```

es=exp(26.66082-0.0091379024*(Tmp+273.15)-(6106.396/(Tmp+273.15)));
e=(RH/100)*es;
    
```

#### Equation 7

where

Tmp = temperature (C)

Es = saturated vapour pressure (mb)

RH = relative humidity (%)

E = vapour pressure (mb)

(13) Air density and absolute humidity are calculated as:

$$\text{AirDensity} = (\text{MSLP} * 100) / ((\text{Tmp} + 273.15) * 287);$$

$$\text{AH} = (e * 100) / ((\text{Tmp} + 273.15) * 461.5);$$

**Equation 8**

Where

AirDensity = kg/m<sup>3</sup>

MSLP = mean sea level pressure (mb)

(14) Liquid water content is distributed rather simplistically as :

$$\text{LWC} = (\text{AH} / \text{mapmaximum}(\text{AH})) * 0.0002$$

whereby LWC varies linearly with AH under the assumption that the maximum AH observed at any one time is equivalent to the usually observed maximum LWC (0.0002 kg m<sup>3</sup>). Such a simplification is necessary because conversion of AH to LWC is complex depending on cloud condensation nuclei and cloud physics.

(15) Dewpoint is calculated as:

$$\text{btemp} = 26.66082 - \ln(e);$$

$$\text{Td} = ((\text{btemp} - \sqrt{(\text{btemp} ** 2) - 223.1986}) / 0.0182758048) - 273.15;$$

**Equation 9**

where

Td = Celsius

4.9.4.10 Lifting condensation level

(16) This means that the lifting condensation level (LCL) becomes

$$\text{lcl} = (1 / (((\text{Newtemp} - \text{Td}) / 223.15) + 1) ** 3.5) * \text{MSLP};$$

$$\text{lcl} = \max((44.3308 - 4.94654 * ((\text{lcl} * 100) ** 0.190263)) * 1000, 0);$$

**Equation 10**

Where

Newtemp = ground temperature (c)

The first part of Equation 10 produces the LCL in mb and the second part in masl

4.9.4.11 Ground level cloud (fog) occurrence

(17) Fog occurs where the ground altitude is greater than the LCL:

$$\text{fog} = \text{scalar}(\text{Dem} \text{ gt } \text{lcl})$$

**Equation 11**

Where

Dem = elevation (m)

4.9.4.12 Radiation receipt and correction for cloud and fog

*Key assumption : The radiation reductions observed under cloud and fog at the FIESTA sites are representative for other sites also.*

(18) Extra terrestrial radiation receipts are now converted to ground level radiation receipts by correction for dimming due to the presence cloud and fog using:

$$\text{TransmissionLoss} = \text{if}(\text{fog} \text{ eq } 1 \text{ then } (\text{CloudFreqFrac} * 0.678) + ((1 - \text{CloudFreqFrac}) * -0.143) \text{ else } (\text{CloudFreqFrac} * 0.525) + ((1 - \text{CloudFreqFrac}) * -0.143));$$

$$\text{SolarMJ} = \text{SolarMJ} * (1 - \text{TransmissionLoss});$$

**Equation 12**

The empirical parameters for the effect of fog and cloud on radiation receipts were taken from the analysis of the hourly radiation dataset for the pasture site. In particular the measured radiation was compared with modelled extraterrestrial radiation for a the 1m pasture site pixel in which the weather station sits. The difference between modelled extraterrestrial and received land surface radiation by hour is a function of the transmission losses by cloud and fog. Thus these transmission losses were grouped according to those periods where the pasture site fog gauges were recording fog and those when they were not. This enabled the calculation of a mean transmission loss under cloudy conditions (no fog but  $R_{meas} \ll R_{model}$ ) and foggy conditions (fog present and  $R_{meas} \ll R_{model}$ ). Data were also analysed for clear conditions because the station recorded slightly lower values than the modelled values possibly because of more humid atmosphere above the station than parameterised in the atmospheric transmission component of the solar radiation model.

4.9.4.13 Net radiation

*Key assumption : The solar to net radiation conversion functions measured under forest and grassland are representative for larger areas and other covers of similar density.*

(19) Solar radiation inputs are set to zero at night, converted to  $W/m^2$  and used to calculate Net radiation as a function of the tree fractional cover:

```
SolarWm=(SolarMJ*1000000)/(SecondsInMonth/2);
NetMap=((Tree/100)*(-27.9+(0.90*SolarWm)));
NetMap=NetMap+((1-(Tree/100))*(-27.5+(0.8*SolarWm)));
```

**Equation 13**

Again, the empirical constants for the simple linear regression of net with solar radiation for sensors above a forest and a pasture cover (see Figure 67 and Figure 68).

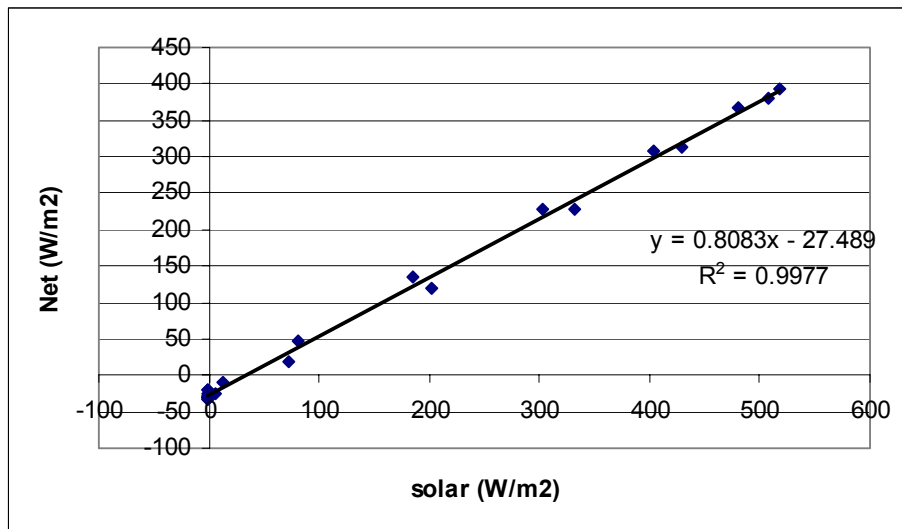


Figure 67 Relationship between incoming solar and net radiation for the pasture site.

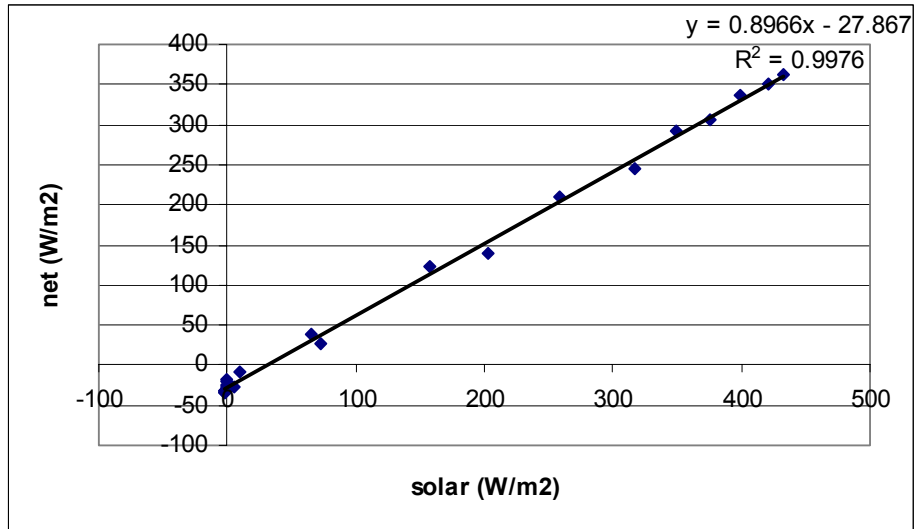


Figure 68 Relationship between incoming solar and net radiation for the forest site.

#### 4.9.4.14 Wind speeds modified for exposure

*Key assumption : The empirical parameters determined by Ruel (from wind tunnel studies) are representative. Exposure can be measured effectively from a DEM.*

(20) Wind speeds are now modified for local wind direction dependent exposure using an approach modified from Ruel et al. (2002)

```
ExposureWindSpdRatio=-0.005*TOPEXWind+1.0;
windspd=windspd*ExposureWindSpdRatio*scalclon.map;
```

#### Equation 14

Where

TOPEXWind = topeX values for the appropriate wind direction of the cell of interest

(21) Rainfall is now modified for wind-driven effects using:

```
TanRainfallInclination=if(Prec gt 0 then windspd/DropTermVeloc else 0);
WindSlopeCorrectionfactor=if(Prec gt 0 then 1+Grad
*TanRainfallInclination*cos(AspectDeg-WindDirDeg) else 0);
WindSlopeCorrectionfactor=max(WindSlopeCorrectionfactor,0);
Prec=Prec*WindSlopeCorrectionfactor;
```

#### Equation 15

where

Prec = monthly precipitation (mm)

Grad = slope gradient

AspectDeg = slope aspect (°)

WindDirDeg = wind direction (°)

#### 4.9.4.15 Impaction fluxes

*Key assumption : The windspeed reductions within forest and rough pasture measured at the FIESTA sites are generally representative*

(22) Fluxes of fog available for impaction are now calculated. The model has no spatial memory or budgeting of fog so fog passing through a forest is not necessary depleted along the flowpath – rather the model assumes that there is limitless availability of fog from the near surface atmosphere (when and where fog is present) thus no budget of atmospheric moisture is maintained. Impaction fluxes are calculated as:

```
WindFlux=(windspd*0.6053*3600)*forestedgedelenfacingm*10;
EdgeImpactionFlux=LWC*WindFlux;
```

**Equation 16**

The 0.6053 is a factor which reduces wind speeds as a result of frictional losses with the forest and is calculate from comparison of forest and pasture site vertical wind profiles. The 10 represents the mean height of forest edges (10m). This equation calculates the kg/hr/cell of water passing through forest edges.

The amount of water passing emergents is then calculated as:

```
WindFlux=(windspd*3600)*emergentedgedelenfacingm*1.5;
EmergentImpactionFlux=(LWC*WindFlux);
```

Wind speed at the grid scale is assumed unaffected by passing through occasional emergents. 1.5 is the average height of emergents above the surrounding canopy (1.5m). The factors influencing fog inputs to forest and pasture are summarised in (Figure 69).

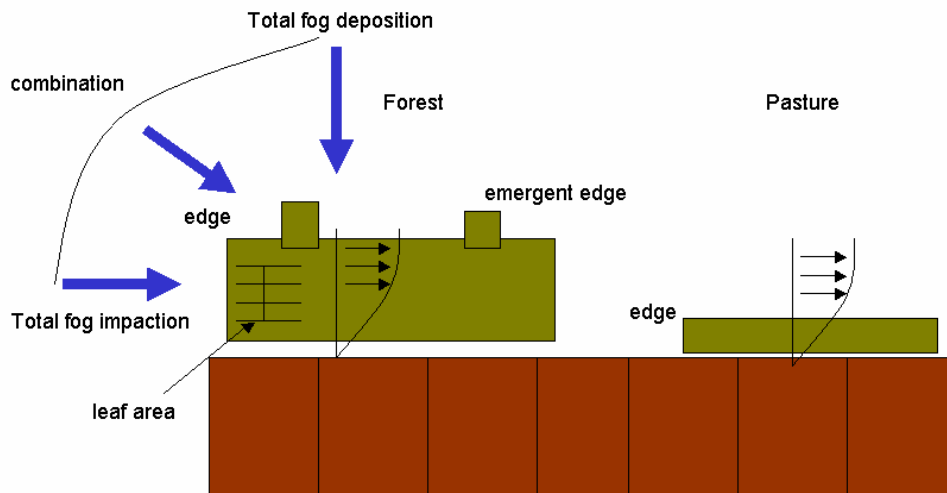


**Figure 69 Factors influencing fog inputs to forest and pasture**

Finally the amount of water passing pasture is calculated using the correction for observed wind speeds at pasture heights and the height of pasture assumed to be 0.5 m. A fog inclination angle for fog inputs over forest and pasture is calculated, based on their respective wind speeds. A vertical flux is calculated as the fog settling velocity over the whole cell surface area (rather than any vertical catching surfaces). The

proportion of fog inputs that are deposited rather than impacted depends upon the cosine of the fog inclination angle over grassland and forest fractions.

```
WindFlux=(windspd*0.5030*3600)*(1-TreeFrac)*CellSize*0.5;
GrassImpactionFlux=(LWC*WindFlux);
ForestFogInclinationAngle=scalar(atan((windspd*0.6053)/FogSettlingVel));
PastureFogInclinationAngle=scalar(atan((windspd*0.5030)/FogSettlingVel));
GravityFlux=(FogSettlingVel*3600)*Celltruearea;
DeposProportion=((cos(ForestFogInclinationAngle))*TreeFrac)+
((cos(PastureFogInclinationAngle))*(1-TreeFrac));
ImpactionProportion=1-DeposProportion;
```

**Equation 17**

4.9.4.16 Vegetation areas for fog interception

*Key assumption : Fog impaction occurs to all non shaded leaves according to the geometrical relationships between the angle of incoming fog (wind speed dependent) and the leaf area. Impaction only occurs on windward forest edges whereas fog passes over forest canopies or falls as sedimentation on leeward (topographically sheltered) forests.*

Next the actual intercepting area of vegetation for fog is calculated because this will be combined with the previously calculated fog fluxes in order to calculate the fog interception. Surface areas for interception depend upon the leaf area density of the vegetation and the angle of incoming fog relative to leaves. The equations are:

```
ForestTrappingSfcArea=(1-(exp((-0.7*0.3*TreeFrac)/cos(ForestFogInclinationAngle))));
PastureTrappingSfcArea=(1-(exp((-0.7*6*(1-TreeFrac))/cos(PastureFogInclinationAngle))));
ImpactionFrac=(AirRising*ForestTrappingSfcArea);
ImpactionFlux=(EmergentImpactionFlux+EdgeImpactionFlux+GrassImpactionFlux);
SettlingFlux=LWC*GravityFlux;
```

**Equation 18**

First the forest trapping surface area is calculated as the self shaded area of leaves exposed to fog droplets arriving at a particular angle (for the tree fraction of the cell). Pasture trapping surface area is calculated in a similar way (also according to pasture leaf area density and observed wind speeds).

The impaction fraction is the fraction of the total potential impaction fluxes (to emergents, to edges and to grassland) that is trapped and so depends on the calculated forest trapping surface area. Importantly impaction only occurs in the model when air is rising because the model assumes that air flows close to the ground when moving uphill (usually in windward exposed) but above the ground in the leeward, more sheltered situations slopes, the parameter air rising is true for situation where upwind elevations are greater than the downwind cell (see Figure 70).

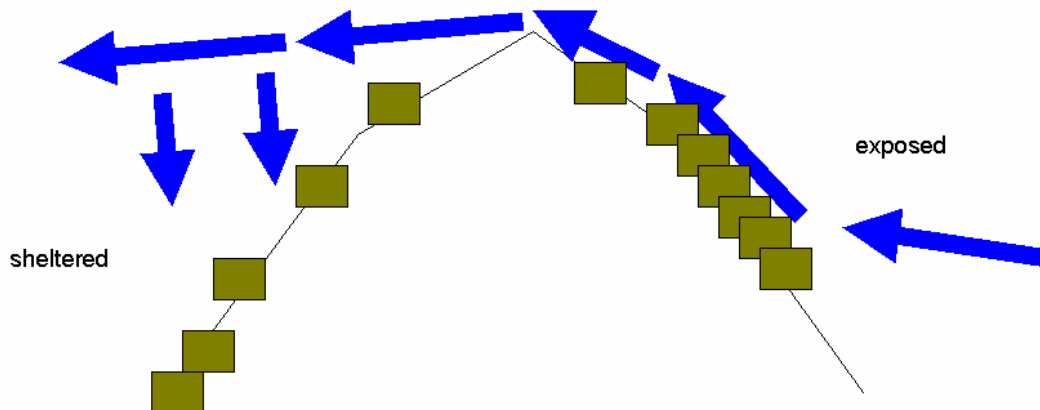


**Figure 70 Impaction dynamics and topography.**

4.9.4.17 Ratio of impaction to sedimentation

*Key assumption : the balance between impaction and deposition depends upon the fluxes of water, the tendency towards lateral or vertical flow and the intercepting areas for horizontal and vertical fluxes.*

(23) The proportional flux that will be deposited compared with that that will be impacted is calculated as:

```
DeposInterc=fog*(SettlingFlux*DeposProportion)*DepositionFrac;
ImpactionInterc=fog*(ImpactionFlux*ImpactionProportion)*ImpactionFrac;
```

```
FogInterc=DeposInterc+ImpactionInterc;
```

where the ‘flux’ is the volume of water passing by the representative surface area, the ‘frac’ is the fraction of that surface area that will intercept fog and the ‘proportion’ is the proportion of the flux that is horizontal and vertical (dependent of the balance between local horizontal wind speed and settling velocity). The parameter ‘fog’ denotes areas above the LCL for that timestep so where there is no fog there will be no fog flux. The units of FogInterc, DeposInterc and ImpactionInterc are kg/m<sup>2</sup>/hr. They are converted to mm/hr and multiplied by the cloud frequency to take account of those periods where the site may be above the LCL but no cloud generation has occurred:

$$\text{FogIntmm} = (\text{FogInterc} / \text{Celltruearea}) * (\text{CloudFreqFrac})$$

**Equation 19**

Monthly total fluxes are the cumulation of the four monthly diurnal; fluxes and the 144 simulation hours that they represent :

$$\text{Fogtotalmm.map} = \text{Fogtotalmm.map} + (\text{FogIntmm} * 6 * 30)$$

**Equation 20**

4.9.4.18 Evapo-transpiration

*Key assumption : Water availability is less significant in determining evapotranspiration than energy available*

(24) Evapo-transpiration is calculated on the basis of the energy available (the net radiation received) and the surface area available for transpiration and wet canopy evaporation. Because of the time and space scales used surface, soil and wet canopy water balances were not possible so a water availability term could not be added to the model. Since available surface area (LAI) is a good surrogate for the availability of water through transpiring stomata or wet canopy evaporation, this was used here. The equations are:

```
Ea=(611*exp((17.27*Newtemp)/(273.15+Newtemp)))/1000;
SlopeSatCurveK=(4098*Ea)/sqr(273.15+Newtemp);
PotEvap=(SlopeSatCurveK/(SlopeSatCurveK+0.066))*NetMap;
PotEvap=PotEvap*(60*60/1000000);
PotEvap=if(PotEvap gt 0 then (PotEvap/2.45) else 0);
ActEvap=if(PotEvap gt 0 then PotEvap*EtFrac else 0);
```

**Equation 21**

where

Newtemp = air temperature (C)

$E_a$  = vapour pressure (KPa)

SlopeSatCurveK = slope of the saturation vapour pressure curve (KPaC)

NetMap = Net radiation receipt ( $W/m^2$ )

2.45 = latent heat of vapourisation of water (MJ/kg)

Thus evaporation is calculated on the basis of available energy and atmospheric demand to give potential evaporation and this is then combined with the non self shaded surface area available for the interception of radiation/evaporation of water to give something closer to actual evaporation, which is responsive to vegetation type and cover as well as climate conditions.

#### 4.9.4.19 Water balance calculation

*Key assumption : at these time and space scales losses to canopy, soil and groundwater are much less significant than the fluxes of rainfall and evapotranspiration*

(25) Precipitation is converted to mm/hr and the budget is calculated as :

$$\begin{aligned} \text{Precmmh} &= \text{Prec} / (24 * 30); \\ \text{Budget} &= ((\text{Precmmh} + \text{FogIntmm}) - \text{ActEvap}); \end{aligned}$$

#### Equation 22

#### 4.9.4.20 Runoff calculation and summary

(26) Finally downstream cumulated water balance or ‘runoff’ is calculated using the PCRASTER accuflux function. Separately net fog inputs are also cumulated downstream once fog evaporation has been calculated. Evaporation from fog is in proportion to its contribution to available water. Assumes evaporation processes of fog water and rain water are similar.

$$\begin{aligned} \text{Runoff} &= \text{accuflux}(\text{ldd.map}, \text{max}(0, \text{Budget})); \# \text{mm/hr} \\ \text{FogIntmmMinEvap} &= \text{FogIntmm} - ((\text{FogIntmm} / (\text{max}(\text{Precmmh} + \text{FogIntmm}, 0.00000001))) * \text{ActEvap}); \\ \text{Fogriver} &= \text{accuflux}(\text{ldd.map}, \text{max}(0, \text{FogIntmmMinEvap})); \end{aligned}$$

#### Equation 23

Water balances can be negative allowing for correct cumulation of flows downstream (i.e. ‘evaporation’ of upslope contributed water in downstream cells with a high demand) – this is important to consider given the long timestep (i.e. opportunity time)

(27) Finally the state variables and fluxes are integrated over the various units (catchments, protected areas, provinces, altitudinal bands...). Fog as a percentage of water balance and of Fog as a percentage of water balance and fog generated runoff of total generated runoff are then calculated.

### 4.10 Model verification

Model verification involves the testing of model outcomes and results against a commonsense knowledge of how the simulated environment should behave and what magnitude stores and fluxes should be. This process was carried out throughout the period of submodel and model development. For process models verification is often much more important than validation, especially for large scale models where in the



A clearer view of the distribution of stations around Lake Arenal is given in Figure 72. Clearly the Rio Chiquito is well served (with six stations) whereas the Penas Blancas has no stations in the WORLDCCLIM database. In fact there are no stations in the upper reaches of the Atlantic catchments and very few in the upper reaches of the Pacific catchments in the vicinity of Lake Arenal.

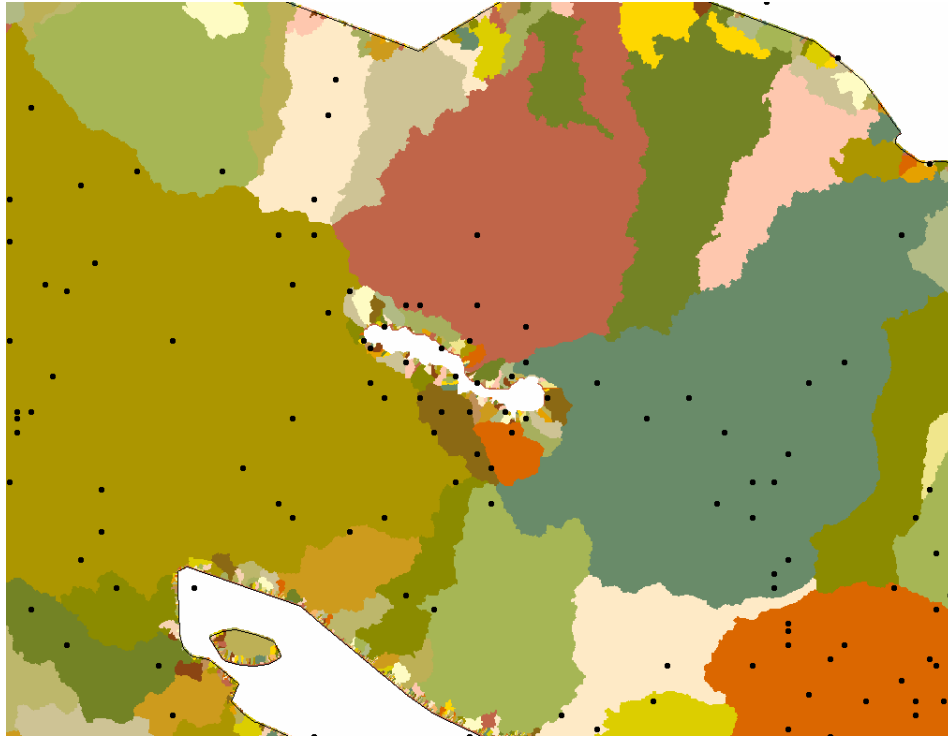


**Figure 72** Rainfall stations in the WORLDCCLIM database in the vicinity of Lake Arenal.

One of the difficulties of working with large extent, distributed spatial models is that validation data are usually not available and even if they are available, they are not easily compared with the model results because of differences in the scale of measurements (e.g. points for the field measurement versus grid for the model). Whilst the model has been thoroughly verified, validation has only been possible for certain aspects of the model.

Three initial attempts at model validation are made here though more could be possible if the fiesta\_delivery model were applied at the San Gerardo and Chiquito spatial scales (grains) for which an extensive dataset for validation are now available. The validation attempts made were : (a) comparison of evapotranspiration with Chiquito model and San Gerardo field data, (b) comparison of model results with the analysis of Zadroga (1981) and (c) comparison of model flows with those observed from the network of Costa Rican runoff stations.

#### *4.12.1 Evapotranspiration validation*

Since evapotranspiration (ET) is one of the key fluxes and also one of the fluxes which is most poorly known (especially in tropical mountains) and which responds greatest to forest cover change, it was important to provide a thorough validation that

the rather simple ET model used in *fiesta\_delivery* produced suitable results (especially for cloud forest environments). This was achieved first of all by comparison of the delivery model results with those of CQflow and secondly by comparison of the delivery model results with those obtained from the field campaign.

When comparing estimates of evapotranspiration for *fiesta\_delivery* and *fiesta\_Cqflow* one should bear in mind that the models operate with different input climate data (*fiesta\_delivery* = long term average, CQflow = one year) and with different processes (*fiesta\_CQflow* contains a canopy hydrology and soil hydrology module) as well as different approaches to modelling ET. Nevertheless, the two estimates are reasonably similar. The delivery model produces somewhat lower ET values for the Chiquito than CQflow (781 compared with 955 mm/yr) giving a difference of 174 mm (18%) on average over the catchment. This is largely due to lower radiation (cloud cover and fog corrections) as used in the Delivery model compared with Cqflow.

Comparison of the *fiesta\_delivery* model estimates for the grid cells containing the forest and pasture stations with measured values at those stations is equally encouraging. The 90m version of the delivery model produces the following values for annual average evapotranspiration for the forest and pasture station grid cells compared with the field measurements:

Station	Delivery model	Field measurement	Difference
Pasture AWS	774mm/yr	854mm/yr	-80mm/yr
Forest tower	729mm/yr	785mm/yr	-56mm/yr

**Table 10 Comparison of delivery model and field ET estimates**

The model performs reasonably well for the two sites. Some differences are to be expected, not least because within the two SG sites there is considerable spatial variability (Figure 733) in the modelled ET because of slope aspect and topographic shading effects (especially at the forest site, Figure 733). Moreover there are likely to be more differences between the model representation of forest ET and the equivalent field measurement than for pasture. Application of the delivery model at finer resolution to the SG sites could be a valuable next step.

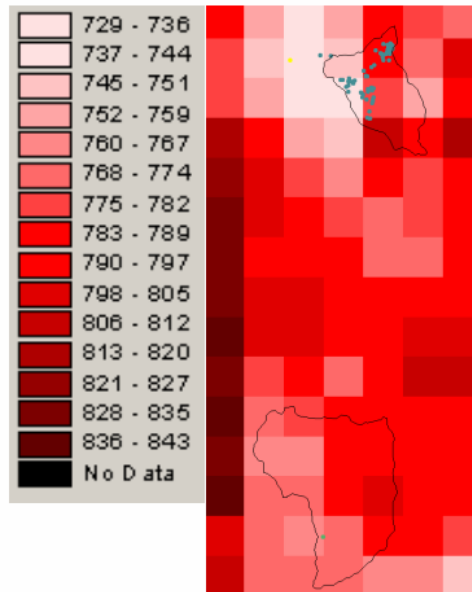


**Figure 73 Delivery model ET estimates for the pasture and forest sites (mm/yr)**

*4.12.2 Validation versus FIESTA Rio Chiquito flow data*

A much better attempt at validation is provided by the availability of flow data collected by the FIESTA project for a precisely known location on the Rio Chiquito (a well defined catchment). Data collected for the period 01/07/2003 to 01/07/2004 provides a flow of 2685 mm/yr assuming a catchment area of 100 km<sup>2</sup>. The actual planimetric catchment area according to the 90m SRTM DEM is 91.1 km<sup>2</sup> and according to the 25m topographically generated DEM is 97.7 km<sup>2</sup>. In fact the Chiquito measurement station is some way before the catchment outlet and only drains a planimetric area of 81.94 km<sup>2</sup> according to the 25m DEM. However the best estimate of actual land area is achieved by calculating the true surface area rather than the planimetric area. According to the method of triangles performed on the 25m DEM this yields a true surface area to the measurement point of 96.04 km<sup>2</sup>. If we use the true surface area to the measurement point (since this is closer to the representation used in the delivery model with its corrections for surface area and wind driven rain) then the measured flow becomes 2795.6 mm/year compared with 2757.9 mm/year for the delivery model, a difference of only 38mm. This gives us some confidence that fog inputs generated by the delivery model are of the correct order of magnitude and that, where there are a reasonable number of stations in the WORLDCLIM database (i.e. the rainfall inputs are correct) the model balances will be reasonably correct. If we use the planimetric surface area instead of true surface area then the measured runoff to the measurement point is 3276 mm (a difference of 518mm/yr or 15.8% from the modelled value). Thus, how one treats surface area in montane environments also makes quite a difference. Where good quality validation data have been available the model has performed well at least for the rather sheltered Chiquito catchment. We now attempt a further validation for the more exposed Penas Blancas catchment.

*Validation versus Penas Blancas flow data*<sup>14</sup>

A ten year daily streamflow record was provided by Julio Calvo for the Pocosol station on the Rio Penas Blancas. This record (1994-2003) yields an average of 19.86 cumecs over the period. The area of the catchment to the Pocosol measurement point is 158.09 km<sup>2</sup> when calculated planimetrically from the SRTM data and 183.9 km<sup>2</sup> if true surface areas are calculated using SRTM. On the basis of the planimetric catchment area the measured runoff is 3966 mm/year whereas if true surface area is used the runoff is 3408 mm/year. The fiesta\_delivery modelled runoff is 2869 mm/year. Thus the difference from the more compatible true area measured runoff value is -539mm – a 15.8% underestimate of flows by the model. This difference may represent differences in the periods of input data between the model and the validation data, differences in the definition of the catchment in the model and in reality or subsurface flows (leakage) into the catchment but are more likely to be the result of underestimation of rainfall inputs to the catchment. We can confirm whether the latter is true by comparing the values of rainfall measured at a number of stations within the catchment<sup>15</sup> with the wind driven rain values produced by the model for those points (Table 11.). The field measurements at all stations are underestimated by the WORLDCLIM interpolation and the wind driven corrections to it. The greatest underestimate is for the highest station at Fila Toro. This reflects the fact that the WORLDCLIM database has no stations in the Penas Blancas or anywhere else in the high altitude vicinity. Moreover the wind driven rain corrections underestimate the measured rainfall even further at these specific points (but wind driven rainfall is highly spatially variable and thus the differences could be due as much to the precision of the station locations as the wind corrections themselves). *It is not surprising therefore that the model validation is much weaker than for the Chiquito catchment (which has 6 stations in the WORLDCLIM database). The underestimate of runoff is 15.8% whereas the WORLDCLIM underestimate of rainfall for these stations is -33%.*

Station	Altitude	Years	Measured (raw) <sup>16</sup> rainfall (mm/yr)	Input worldclim rainfall (mm/yr)	Difference (measured to WORLDCLIM (mm/yr) and (%))	Modelled wind driven rain (mm/yr)	Difference (measured – to wind driven) (mm/yr)	Wind exposure (TOPEX)
Aleman	960	1995-2003	4260	3110	-1150 (-26.9)	3024	-1236 (-29%)	23.7
Audubon	760	1995-2003	5703	3378	-2325 (-40.8)	3834	-1869 (-32.7%)	7.7
Fila Toro	1630	1995-2003	5832	3119	-2713 (-46.5)	1907	-3925 (-67.3%)	17.3
Poco Sol	329	1995-2003	4977	3553	-1424 (-28.6)	1787	-3190 (-64.1%)	39.4
SP Penas Blancas	312	1995-2003	4599	3552	-1047 (-22.7)	2558	-2041 (-44.4%)	16.6
<b>Mean of points</b>			<b>5074.2</b>	<b>3342</b>	<b>-1732 (-33.1)</b>	<b>2622</b>	<b>-2452.2 (-48.3%)</b>	<b>20.94</b>

**Table 11 Measured versus modelled rainfall for the Penas Blancas stations**

<sup>14</sup> data generously provided by Julio Calvo

<sup>15</sup> data generously provided by Julio Calvo

<sup>16</sup> that is, uncorrected for wind and wetting losses

The average wind exposure of the stations is 20.9 (quite sheltered) whereas the mean exposure for the catchment is 8.5 (less sheltered), hence the wind driven rain corrections are negative (reductions). Thus we cannot place too much emphasis on the underpredictions of wind corrected values because of spatial uncertainty in the station locations – and thus exposure which means that at-a-point values are difficult to compare. It is indicative that although the wind corrected values are often much lower than the worldclim values at these station locations, the catchment average wind corrected value is higher than the worldclim value (Table 12) indicating the overall exposed nature of the catchment.

Even with four stations in the Penas Blancas there is still a great deal of uncertainty as to the actual areal rainfall inputs since there are significant areas between these stations over which to interpolate and these upper Atlantic catchments are clearly highly exposed and very spatially variable in rainfall inputs (4000 to nearly 6000 mm at only 5 points). Figure 74 to Figure 77 show the results of four different approaches to quantifying this spatial variability in the PB. The first approach results from the spline interpolation performed for the WORLDCLIM stations (though there are none of these within the PB catchment boundaries). The results are an (unrealistic) altitudinal decrease in rainfall in the catchment from 3500 in the lower parts to 2900 in the uppermost reaches.

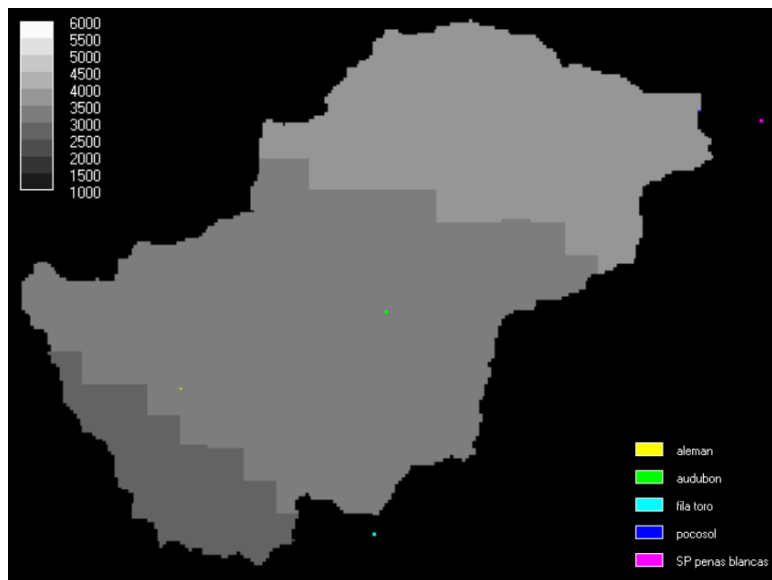


**Figure 74 Raw WORLDCLIM interpolation for the PB with the PB stations (not in the WORLDCLIM database) shown.**

Correcting these data for wind driven rain effects in the *fiesta\_delivery* model produces the much more complex spatial pattern shown in Figure 75 with stronger exposure based contrasts than altitudinal ones and values varying from less than 1000mm in highly sheltered spots to more than 6000 in highly exposed areas. There is clearly considerable variation around the PB station locations such that if these patterns are realistic then the mean catchment rainfall estimated from a small number of stations will be highly dependent on the location of those stations. Most of these seem, logically, to be in areas that are neither highly exposed nor highly sheltered.

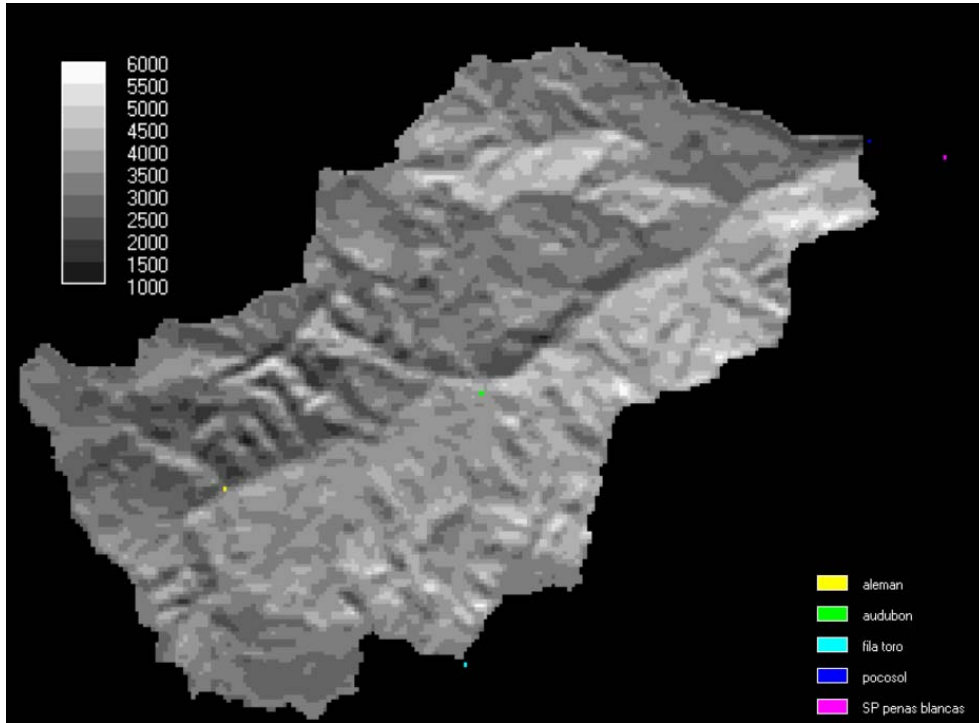


**Figure 75 Modelled wind driven rain receipts from the gauge-loss uncorrected WORLDCLIM surfaces with the PB stations (not in the WORLDCLIM database) shown**

In Figure 76 we produce an interpolation from the PB station data rather than the WORLDCLIM database. The interpolation is by simple Thiessen polygonds and indicates generally higher rainfalls than those derived from WORLDCLIM and a central band of high rainfall sdriven by Fila Toro and Audubon stations , with the lowest rainfall around Aleman station in the upper reaches (but not the highest altitude part of the catchment).

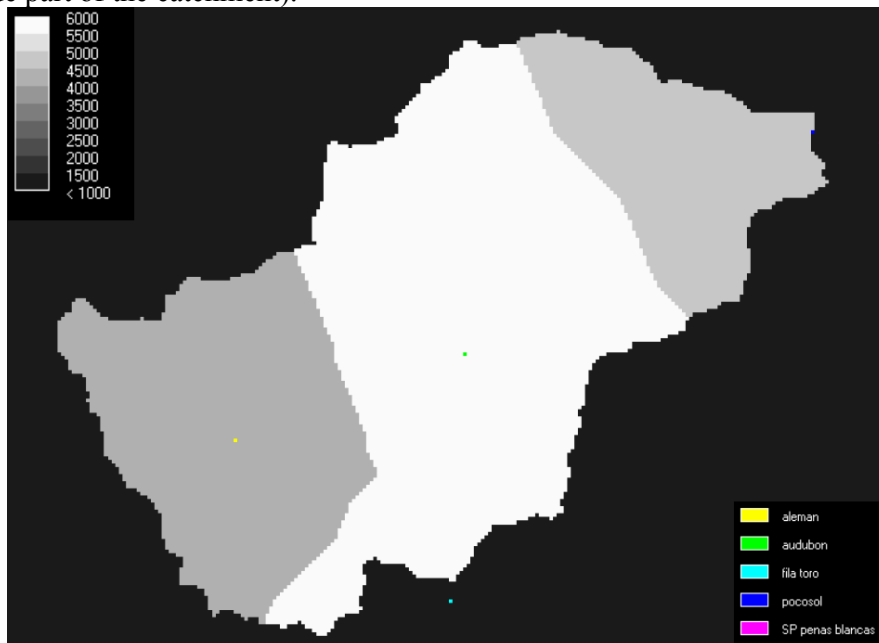


**Figure 76 A simple Thiessen polygon interpolation between the five PB rainfall stations, with the PB shown**

Our final interpolation is a simple linear regression of precipitation versus altitude for the five stations which produces the following relationship  $\text{Rainfall}(\text{mm}/\text{yr}) = 0.639\text{Altitude} + 4564.6$  for the data available, though with some considerable scatter ( $R^2=0.2$ ). The resulting map shows values in excess of 5500 mm/yr in the highest peaks of the catchment.

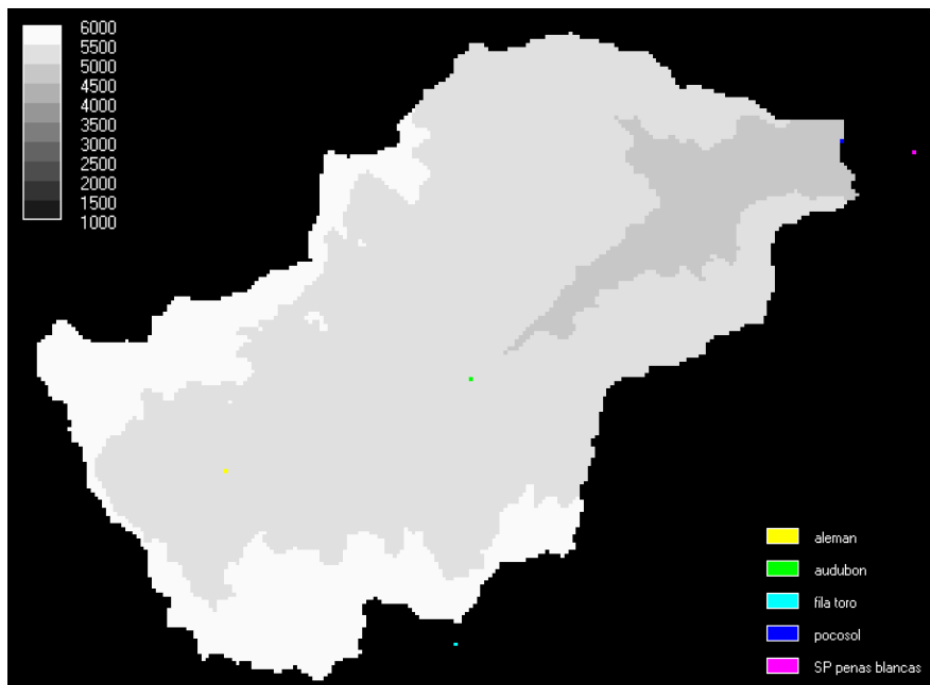


**Figure 77 An altitudinal regression relationship based rainfall interpolation from the five PB stations with the PB stations shown**

If we now calculate the mean rainfall over the entire catchment according to these four methods we see some considerable differences based on data source - between the WORLDCLIM and PB station data - (with the WORLDCLIM values 2000mm lower). The different interpolation methods, though they produce very different patterns of rainfall, show relatively small catchment average differences with WDR corrections adding 71 mm on average to the WORLDCLIM values and Thiessen polygon versus Altitudinal regression differing from 137mm for the PB station data.

Interpolation	Mean catchment rainfall (mm/year)	Difference from altitudinal regression based on PB stations(%)
Raw input rainfall (worldclim)	3328	-37.22
Modelled WDR (worldclim)	3399	-35.88
Thiessen polygon	5164	-2.58
<b>Altitudinal regression</b>	<b>5301</b>	<b>-0.00</b>

**Table 12 Catchment average rainfall estimates for the Penas Blancas for different data sources and interpolation methods.**

It is thus unsurprising that the model underestimates runoff by around 15% for the PB since the input rainfall is underestimated by around 35%. Clearly the patterns of rainfall in these exposed catchments are likely to be so complex compared with the paucity of station data that, even after this analysis we still cannot be certain which (if any) of these rainfall figures is closest to the truth for the PB.

#### 4.12.3 Runoff Validation vs National runoff station database

The best validation of a large scale model is comparison of the estimated runoff against measured runoff for a *wide range* of catchments in different environments. Thus the next stage in our validation process is to compare *fiesta\_delivery* against the Costa Rican national runoff database as held at the Global Runoff Data Centre (GRDC)<sup>17</sup>. The GRDC provides long term average flow data for gauged basins and it is those that were used here for comparison with the *fiesta\_delivery* model. The major difficulty in doing so is locating the exact location of the gauging stations and deriving the correct hydrologic catchments from them. The coordinates given by GRDC are neither precise nor accurate enough for comparison with the 90m resolution DEM and most of the gauge locations as specified were some distance from the rivers that they represented. These stations were taken to the nearest location on the appropriate river according to the naming provided by the *vmap* data coverage<sup>18</sup>. This produced the 44 gauged catchments identified in Figure 78.

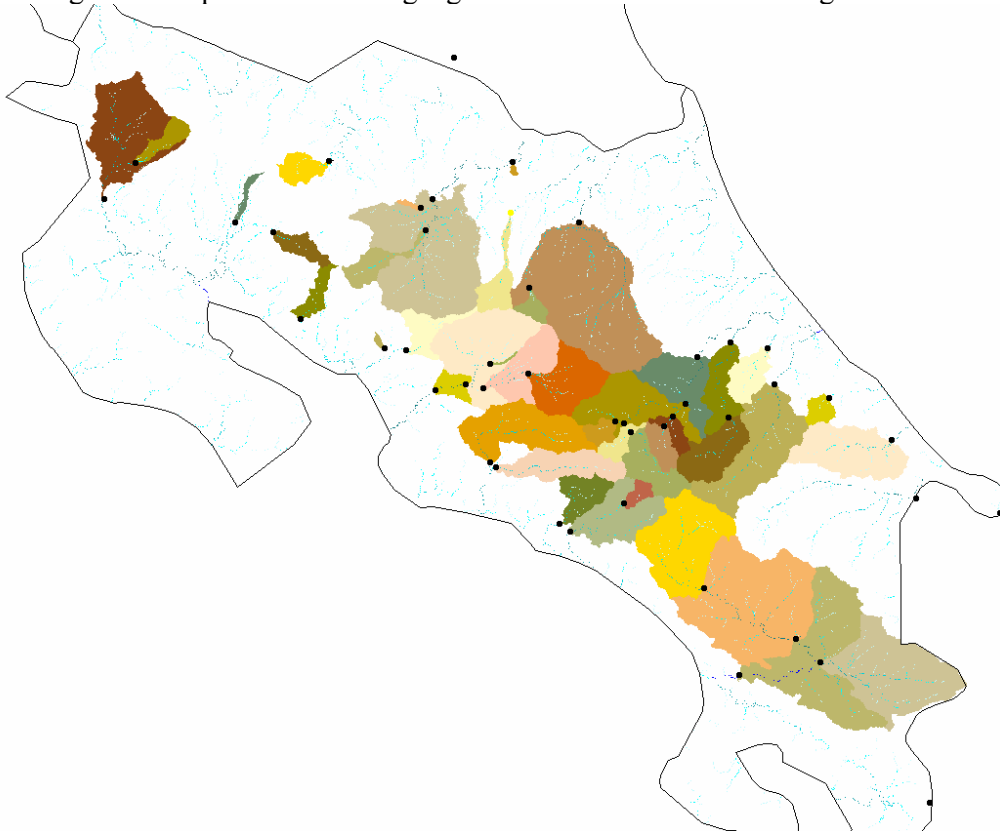


**Figure 78 Gauging stations and upstream catchments for Costa Rica.**

<sup>17</sup> <http://www.bafg.de/grdc.htm>

<sup>18</sup> [http://www.mapability.com/index1.html?http&&&www.mapability.com/info/vmap1\\_download.html](http://www.mapability.com/index1.html?http&&&www.mapability.com/info/vmap1_download.html)

In order to verify the accuracy of the (re-)location of the gauging stations we compared the GIS-derived catchment area with the catchment area defined by GRDC for each station. Those stations with GIS-derived areas within 10% of the GRDC-supplied areas were retained for further analysis and amounted to 17 catchments (Figure 79). Clearly the remaining 27 catchment gauges are either incorrectly positioned or their drainage networks are not sufficiently precisely defined in the DEM. Those catchments need field validation of location and of the upstream river network before they can be used. For the good 17 catchments we can be fairly confident that the area measured by the gauge is the same as that modelled by the `fiesta_delivery` model (so the catchments are properly defined in the `FIESTA_delivery` model GIS). Nevertheless a number of measurement uncertainties remain:

- (a) The flow records are only measured estimates of actual flow (since many of these are large rivers without flow structures),
- (b) there are still small differences between the GRDC reported and actual GIS-measured catchment areas which will have impacts on the actual areas modelled versus measured which can be important in a spatially variable environment.
- (c) The periods of the station records differ from each other and from the model period and this may be important within the context of climate variation
- (d) The possibility of (unmeasured) subterranean inter-basin transfers still exists

As such this validation can only be seen as a first attempt until such a time as better georeferenced gauge locations for the remaining gauged catchments can be obtained.

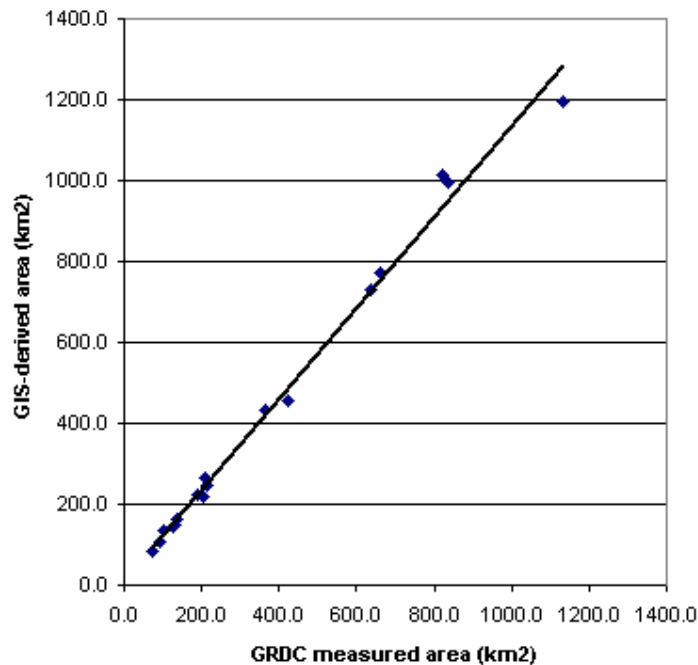


**Figure 79** GIS-derived true surface areas compared with GRDC measured catchment areas for the 17 best catchments.

A summary of the characteristics of these 17 validation stations and their corresponding model results are given in Table 13.

Catchment name	Station		GRDC area (km <sup>2</sup> )	GRDC water volume (km <sup>3</sup> /yr)	GRDC_runoff (mm)	GRDC_runoff true area (mm/yr)	Delivery model precipitation (mm)	GIS derived area (km <sup>2</sup> ) (planimetric)	GIS-derived true surface area (km <sup>2</sup> )	Delivery model runoff (mm/yr)	Ratio GIS-derived to GRDC catchment size	Absolute error	Relative error %
<b>BARRANCA</b>	<b>GUAPINOL</b>	<b>Pacific</b>	<b>203</b>	<b>0.2</b>	<b>1129</b>	<b>1170.6</b>	<b>2765.6</b>	<b>196.5</b>	<b>219.4</b>	<b>2043.2</b>	<b>1</b>	<b>872.6</b>	<b>74.5</b>
<b>CANAS</b>	<b>LIBANO</b>	<b>Pacific</b>	<b>129</b>	<b>0.1</b>	<b>811</b>	<b>831.4</b>	<b>2750.5</b>	<b>132.3</b>	<b>148.7</b>	<b>1956.3</b>	<b>1</b>	<b>1124.9</b>	<b>135.3</b>
<b>COLORADO</b>	<b>COYOLAR</b>	<b>Pacific</b>	<b>128</b>	<b>0.1</b>	<b>699</b>	<b>700.7</b>	<b>2009.8</b>	<b>128.4</b>	<b>142.2</b>	<b>1073.6</b>	<b>1</b>	<b>372.9</b>	<b>53.2</b>
COTO BRUS	CARACUCHO	Pacific	1131	1.9	1702	1812.1	3271.9	1065.1	1197.6	2471.9	0.9	659.8	36.4
GENERAL	LA CUESTA	Pacific	836	1.9	2305	2229.8	3447.1	865.6	995.8	2757	1	527.2	23.6
GRANDE DE CANDELARIA	EL REY	Pacific	661	0.7	1090	1081.2	2101	665.9	772	1304.5	1	223.3	20.7
<b>LAGARTO</b>	<b>YOMALE</b>	<b>Pacific</b>	<b>104</b>	<b>0.1</b>	<b>930</b>	<b>823.2</b>	<b>2360.6</b>	<b>121.5</b>	<b>135.9</b>	<b>1402.2</b>	<b>1.2</b>	<b>579.1</b>	<b>70.3</b>
NARANJO	LONDRES	Pacific	210	0.8	3851	3656.7	3127.1	221.5	264.9	2450.7	1.1	-1206	-33
PIRRIS	BIJAGUAL	Pacific	422	0.9	2150	2342.5	2673.1	388.5	455.7	1922.6	0.9	-419.9	-17.9
BANANO	ASUNCION	Atlantic	91.4	0.4	4431	3828.9	3778.1	90.3	107.1	3255	1	-573.9	-15
BARBILLA	BARBILLA	Atlantic	212	0.8	3583	3555.3	3461	213.8	246	2826.4	1	-728.9	-20.5
CHIRRIPO	PLAYA HERMOSA	Atlantic	821	1.9	2293	2211.1	3794	850.3	1013	3214.2	1	1003.1	45.4
ESTRELLA	PANDORA	Atlantic	635	1.4	2122	2127.6	3170.2	634.5	729.3	2450	1	322.4	15.2
<b>PACUARE</b>	<b>PACUARE</b>	<b>Atlantic</b>	<b>367</b>	<b>0.9</b>	<b>2401</b>	<b>2396</b>	<b>4456.7</b>	<b>367.3</b>	<b>430.3</b>	<b>3881.9</b>	<b>1</b>	<b>1485.9</b>	<b>62</b>
PEJIBAYE	EL HUMO	Atlantic	137	0.5	3875	3860.3	5140.5	137.3	161.9	4573.8	1	713.5	18.5
SARAPIQUI	CARIBLANCO	Atlantic	73	0.3	4113	3937.4	3725.6	76.2	86	3121.8	1	-815.6	-20.7
TORO	VERACRUZ	Atlantic	191	0.8	4040	3975.1	3720.1	193.7	222.1	3134.5	1	-840.6	-21.1

**Table 13 Characteristics of the validation stations and their model results.**

Comparing the measured runoff versus the model-generated runoff for these 17 catchments (Figure 80) - using measured runoff calculated with the GRDC measured planimetric area of the catchments - indicates that the model tends to overpredict yields. Since the delivery model represents processes according to true surface area rather than planimetric area, a more consistent validation is achieved by calculating the measured runoff over the true surface area for the catchments rather than the planimetric area. These results are shown in Figure 81 and still indicate an overall overestimation of flows which may indicate that precipitation inputs are overestimated, deep percolation is significant enabling flows to travel from the mountainous zone to the coastal plains unmeasured by the stream gauges or that evapotranspiration in the model is too low under certain conditions (though that was not the case for the Chiquito and does not seem to be the case for Zadroga’s catchments, section 4.16).

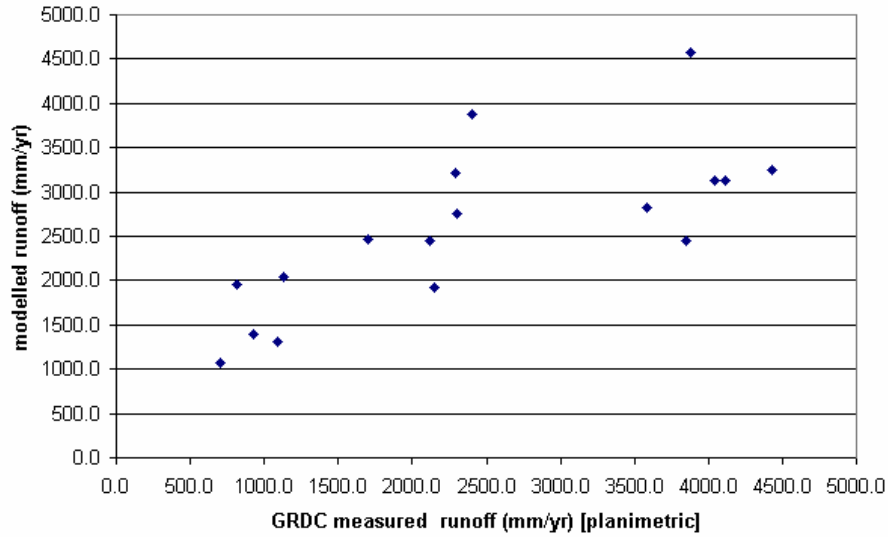


**Figure 80 Comparison of measured and modelled runoff on the basis of planimetric calculation of measured runoff.**

Using true surface areas tends to slightly decrease model overestimation of yields in the uplands (which have higher true surface areas than planimetric areas and thus reduced true area measured yields compared with those calculated planimetrically)

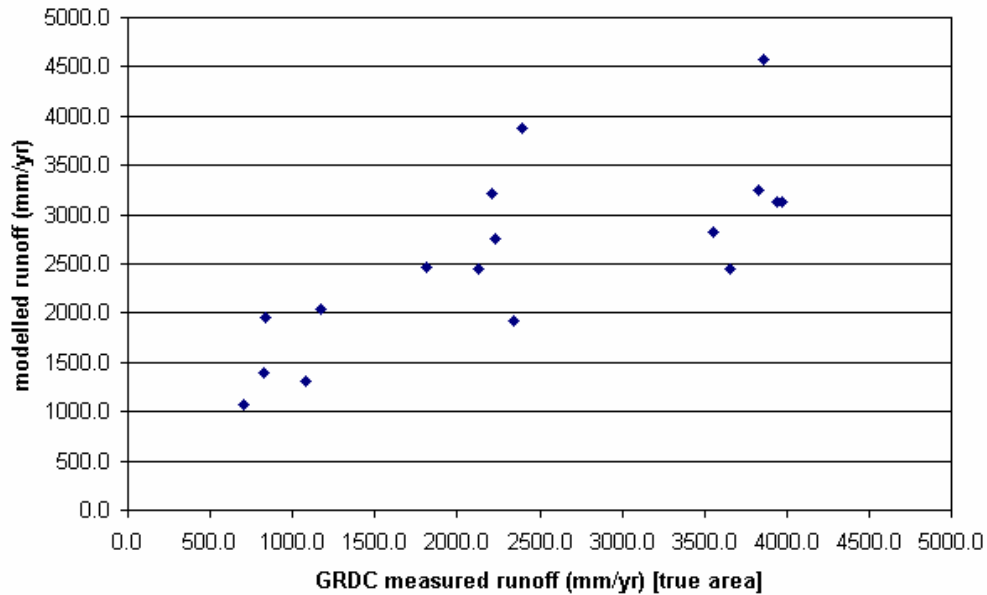


**Figure 81 Comparison of measured and modelled runoff on the basis of true surface area calculation of measured runoff.**

Figure 82 shows a series of the most useful measures of model predictive uncertainty for the validation set shown in Figure 81. The coefficient of determination ( $R^2$ ) is not well suited to the assessment of model error (Mitchell, 1997; Legates and McCabe, 1999) and is not used here. The Index of agreement (D) varies from 0 for a poor model and 1.0 for a perfect model and represents the ratio between the mean square error and the potential error and overcomes the insensitivity of correlation based

measures to differences in observed and modelled means and variances (Wilmott, 1984). The original index of agreement (D2) is sensitive to outliers since it uses the sum of squared differences between observed and predicted. The Legates and McCabe (1999) modification (D1) removes this sensitivity by using a power of 1 instead of 2. The coefficient of efficiency (CE) is the ratio of the mean square error (MAE) to the variance in the observed data. If the error is as large as the variability in the data then CE=0, if the error exceeds the observed variability then CE<0 (so the mean of the observations will be a better predictor of an observation than the model prediction). A value of 1.0 denotes the perfect model. Again CE2 is the original formulation (Nash and Sutcliffe, 1970) but is sensitive to outliers so CE1 is a better alternative (that uses power one not power two of the errors), again suggested by Legates and McCabe (1999).

Overall agreement is good. The model mean is only 194 mm/yr greater than the observed mean across all catchments (i.e. the bias is 8 % of the observed mean) though the observed SD is 288mm greater than the modelled SD. The MAE is 733 mm/yr. Even with the original indices (outliers weighted) performance is good (CE2=0.53, D2=0.83, CE1=0.27, D1=0.58). Much of the error results from six anomalous catchments with much higher modelled runoff than measured. These catchments are the Barranca, Canas, Colorado, Lagarto, Pacuare and the Chirripo. If these catchments are removed from the validation, the MAE falls to 413mm, the bias becomes 125mm and the D1 and CE1 become 0.61 and 0.35 respectively.

Measure		Value (ATLANTIC catchments)	Value (PACIFIC catchments)	Value (all catchments)
Index of agreement (after Legates and McCabe, 1999)	D1	0.31	0.50	<b>0.58</b>
Coefficient of efficiency (after Legates and McCabe, 1999)	CE1	-0.09	0.15	<b>0.27</b>
Mean absolute error	MAE	810.47	665.08	<b>733.50</b>
Root mean square error	RMSE	870.31	737.50	<b>802.74</b>
Observation mean	Omean	3236.44	1627.56	<b>2384.68</b>
Observation sd	Osd	833.76	979.32	<b>1211.96</b>
Model mean	Pmean	3307.19	1931.34	<b>2578.79</b>
Model SD	Psd	652.03	577.23	<b>923.95</b>
Mean bias (of measurement)	BIAS	-70.75	-303.77	<b>-194.12</b>
Index of agreement	CE2	-0.25	0.36	<b>0.53</b>
Coefficient of efficiency	D2	0.53	0.75	<b>0.83</b>

Figure 82 Measures of predictive uncertainty for the GRDC catchments.

Model performance differs between the Atlantic and Pacific catchments. MAE is 145 mm greater for the Atlantic catchments than the Pacific. The model overpredicts for both Atlantic and Pacific catchments (by 71 mm/yr for Atlantic catchments and 304 mm/yr for Pacific catchments). The various model performance measures are much higher for the Pacific catchments than the Atlantic, probably reflecting the difficulty of accurate spatial rainfall estimation for the Atlantic catchments.

If we examine the predictive error on a catchment by catchment basis in relation to the mean physical characteristics of the catchments (Table 14), no obvious patterns emerge except that the model overpredicts (positive errors) runoff for half of the Pacific catchments but underpredicts (negative errors) for a number of Atlantic catchments. There appears to be little relationship between the magnitude of the residual and any discrepancy between measured and GIS-derived catchment size except for Lagarto which is 20% different in size in the FIESTA GIS compared with the GRDC estimate (data not shown). There is no obvious relationship between relative prediction error and catchment altitude, exposure to wind driven rain, fog inputs or catchment average rainfall inputs. The spatial distribution of relative error by catchment is shown in Figure 83 but gives no further clues as to the reasons behind the errors that exist.

Catchment name	Station		WORLDCLIM climate stations	Cloud frequency (%)	Altitude (masl)	Difference between input and WDR (mm/yr)	Fog inputs (mm/yr)	Mean exposure (TOPEX)	Total precipitation (mm/yr)	Absolute error (model-measured)	Relative error(model-measured/measured) %
<b>CANAS</b>	<b>LIBANO</b>	<b>Pacific</b>	<b>2.0</b>	<b>60.4</b>	<b>798.3</b>	<b>-45.8</b>	<b>140.9</b>	<b>7.2</b>	<b>2811.4</b>	<b>872.6</b>	<b>74.5</b>
<b>COLORADO</b>	<b>COYOLAR</b>	<b>Pacific</b>	<b>2.0</b>	<b>56.4</b>	<b>676.9</b>	<b>15.9</b>	<b>110.0</b>	<b>5.7</b>	<b>2734.6</b>	<b>1124.9</b>	<b>135.3</b>
<b>COTO BRUS</b>	<b>CARACUCHO</b>	<b>Pacific</b>	<b>4.0</b>	<b>61.6</b>	<b>1244.3</b>	<b>-108.8</b>	<b>79.4</b>	<b>8.7</b>	<b>2118.6</b>	<b>372.9</b>	<b>53.2</b>
GENERAL	LA CUESTA	Pacific	4.0	65.8	1414.3	-134.8	101.9	9.7	3406.7	659.8	36.4
GRANDE DE CANDELARIA	EL REY	Pacific	4.0	61.2	1136.4	-165.8	109.0	11.7	3612.9	527.2	23.6
LAGARTO	YOMALE	Pacific	1.0	56.7	519.9	16.3	109.9	10.5	2084.7	223.3	20.7
<b>NARANJO</b>	<b>LONDRES</b>	<b>Pacific</b>	<b>0.0</b>	<b>69.6</b>	<b>1318.0</b>	<b>-60.3</b>	<b>48.4</b>	<b>7.8</b>	<b>2420.9</b>	<b>579.1</b>	<b>70.3</b>
PIRRIS	BIJAGUAL	Pacific	2.0	63.4	1659.6	-114.0	113.8	14.6	3241.1	-1206.0	-33.0
BANANO	ASUNCION	Atlantic	0.0	76.1	884.1	-25.6	111.2	12.1	2698.7	-419.9	-17.9
BARBILLA	BARBILLA	Atlantic	0.0	74.0	650.0	322.5	189.6	0.3	3455.6	-573.9	-15.0
CHIRRIPO	PLAYA HERMOSA	Atlantic	3.0	70.1	1575.2	151.7	151.4	3.4	3309.3	-728.9	-20.5
ESTRELLA	PANDORA	Atlantic	3.0	71.9	596.2	210.3	156.7	6.7	3583.7	1003.1	45.4
PACUARE	PACUARE	Atlantic	4.0	69.9	1701.5	12.5	90.7	8.3	3157.8	322.4	15.2
<b>PEJIBAYE</b>	<b>EL HUMO</b>	<b>Atlantic</b>	<b>4.0</b>	<b>71.6</b>	<b>1556.6</b>	<b>288.9</b>	<b>162.6</b>	<b>3.4</b>	<b>4167.9</b>	<b>1485.9</b>	<b>62.0</b>
SARAPIQUI	CARIBLANCO	Atlantic	1.0	68.0	1851.5	372.0	163.8	6.6	4768.5	713.5	18.5
TORO	VERACRUZ	Atlantic	0.0	73.0	1326.7	299.6	187.5	-3.2	3426.0	-815.6	-20.7

**Table 14 Relationships between model error and catchment characteristics.**

The problem with model validation, especially at large scales, is that it becomes impossible to separate deficiencies of the model from deficiencies of the data and as a result one is never sure whether model performance is any better tested through the validation process than through the verification process. Applying the delivery model at the SG catchment scale for which we now have large volumes of data and close to closed hydrological budgets could provide a better validation. Overall we have seen that predictions are good on average across the region but that the model can underestimate flows in very exposed areas with few or no rain gauges and can underestimate evapotranspiration (overestimate flows) in dry, cloud free lowlands. These characteristics should be borne in mind when interpreting the model simulations but it should also be borne in mind that the model is designed primarily to

assist in process understanding and directionality of change after land use and not necessarily designed for great predictive success (if so then a simpler empirical approach would have been used). Moreover, under circumstances where the validation data are most detailed and sound (SG scale analysis and Chiquito scale analysis), the model performed rather well.

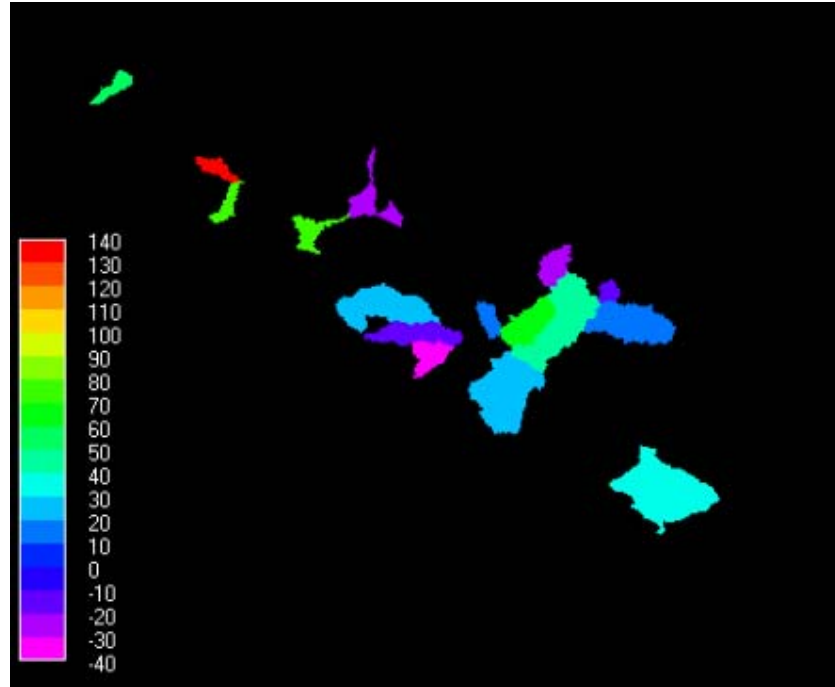


**Figure 83** The spatial distribution of relative error (%)

### 4.13 Model simulations : General outcomes

In this section we present results of the FIESTA\_delivery model using a set of 90m simulations for both baseline conditions and the various scenarios. We focus on countrywide patterns for Costa Rica as well as the more regionally specific patterns in the area of Lake Arenal. We first examine the general outcomes of the model before concentrating in more detail on any further process understanding which it gives.

#### 4.13.1 Fog inputs.

Figure 84 shows fog inputs and clearly indicates that all mountainous areas within Costa Rica receive fog inputs of the order of 50-150 mm/yr with a few (spatially restricted) areas receiving more (250-400 mm/yr) especially to the NW of Lake Arenal and the Atlantic slopes. For readers critical on the notion that fog interception could occur in the Nicoya peninsular, please see Figure 86. Looking in greater detail at the area around Lake Arenal indicates that highly exposed areas generally receive 300-500 mm/yr but these are spatially restricted to exposed ridges and N and E facing areas whereas the majority of sheltered areas (leeward slopes) receive 100-150mm. Low, flat and very sheltered areas receive 50-100 mm/yr.

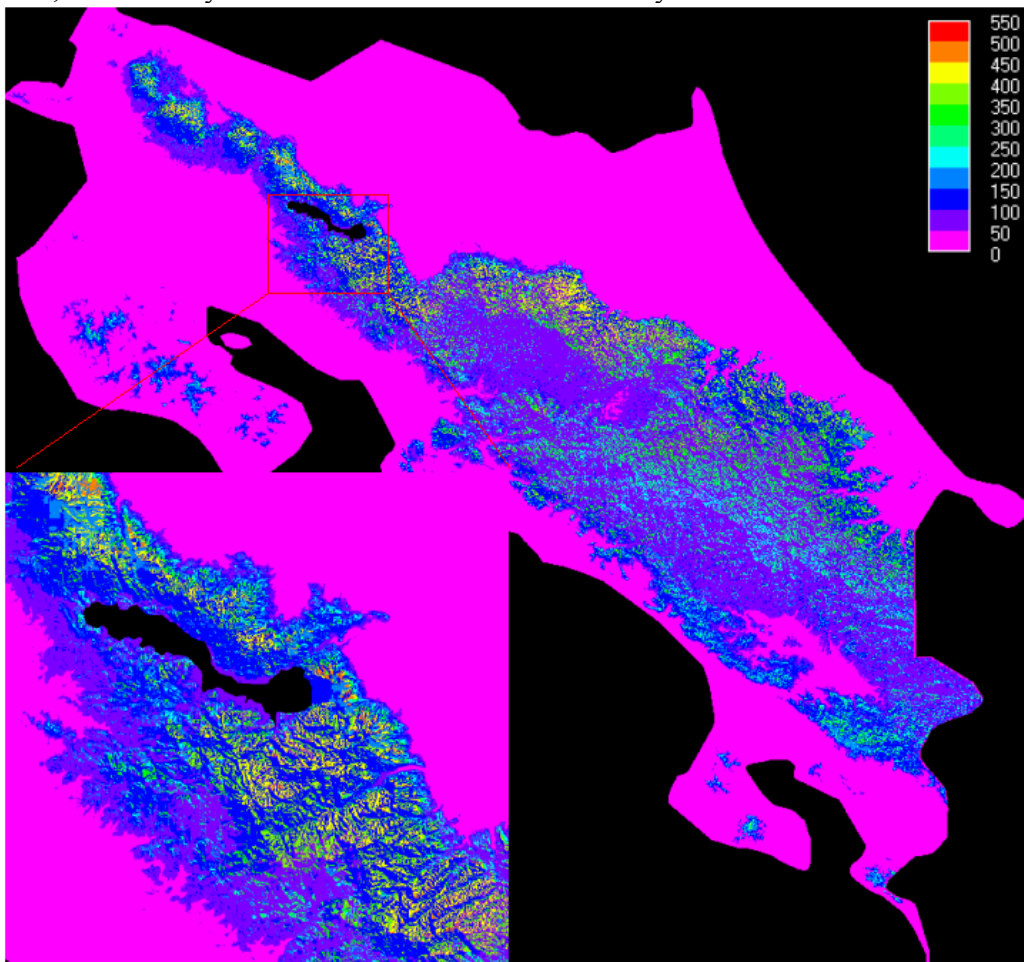


Figure 84 Annual total of fog interception (mm/yr)

4.13.2 *Fog as a proportion of rainfall*

As a proportion of rainfall, the modelled fog inputs are always low, generally from 0-6%, slightly higher on the drier, lower Pacific and southern Atlantic slopes and the Nicoya Peninsular (6-9%) and highest in the exposed Atlantic areas where fog inputs are greatest (still less than 15%). Values are 0-3% in the wettest parts of San Jose and Puntarenas provinces. The exposed eastern slopes of Penas Blancas have larger contributions than the western slopes.

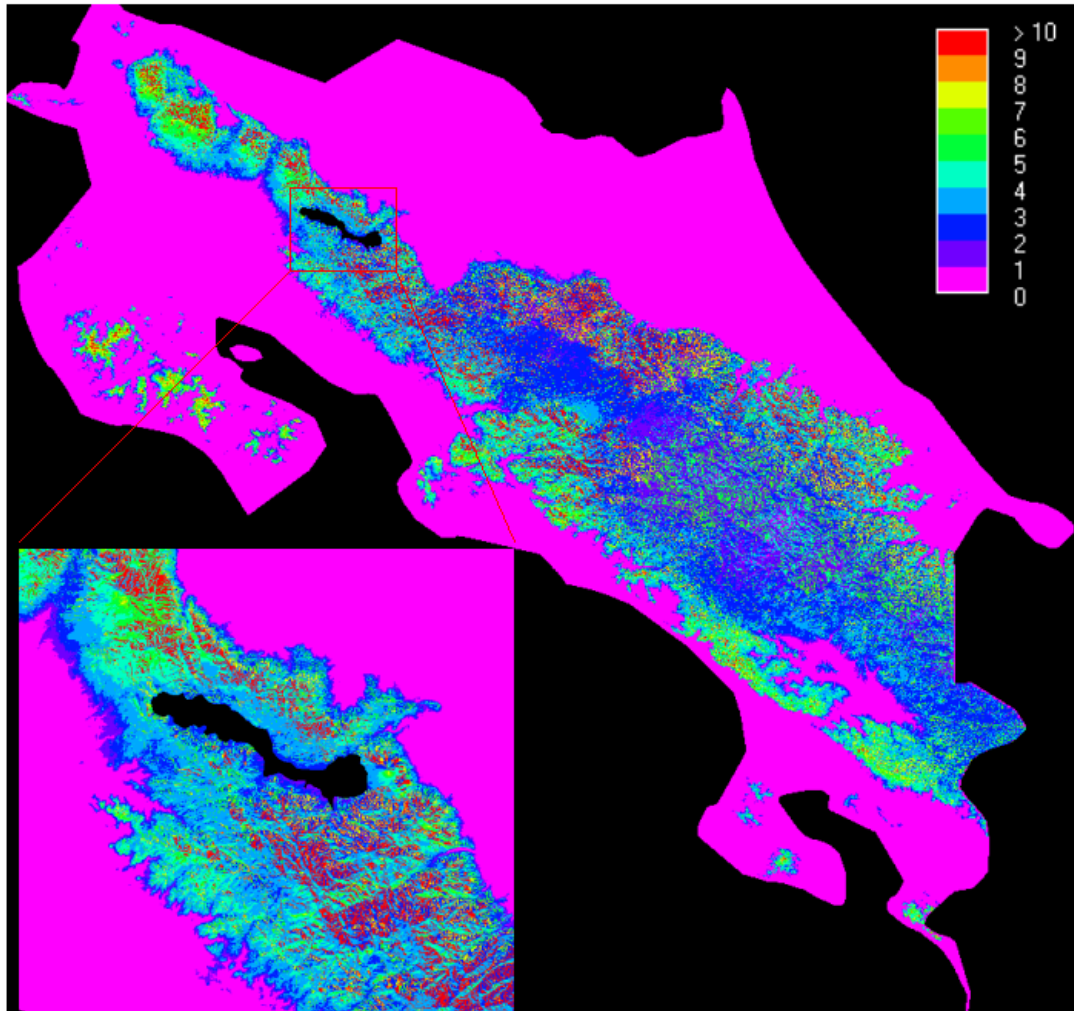


Figure 85 Fog as a percentage of rainfall.



**Figure 86 Cloud interception in the Nicoya Peninsular (photo by Arnoud Frumau)**

Calculating fog as a percentage of rainfall instead of precipitation (rainfall+fog) increased the observed values by around 0.1%-1% but has no appreciable outcome on the spatial patterns.

#### *4.13.3 Fog as a proportion of water balance*

As a proportion of the water balance, fog inputs are, again small, 0-2% in the wettest provinces, 2-10 % over the most exposed parts of the Atlantic slopes and 4-6% over the remaining mountain regions. Contributions are higher (10-14%) in parts of the drier Pacific slopes and the Nicoya Peninsular. The highest contiguous contributions (10-15% and sometimes >20%) are observed in the very cloudy vicinity of the Rincon de la Vieja volcano on the borders of Guanacaste and Alajuela. Closer examination of the area around Lake Arenal indicates exposed areas with contributions of 8-12% and less exposed areas with 3-4% of the observed water balance.

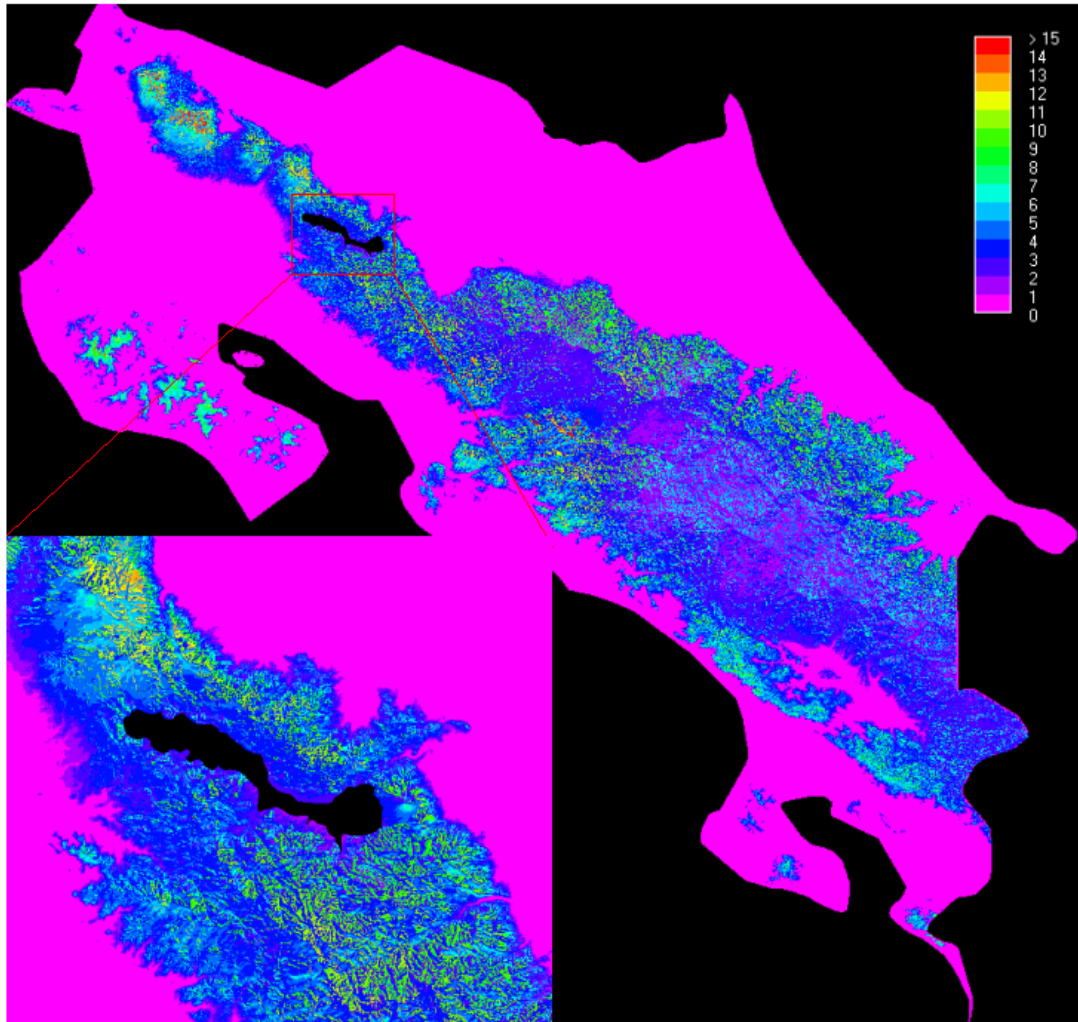


**Figure 87 Fog as a percentage of annual water balance**

#### 4.13.4 Wind driven rain

Patterns of rainfall are shown in Figure 50 and show a strong altitudinal pattern, also varying up to around 7000mm. The pattern of wind driven rain from the FIESTA\_delivery model is shown in Figure 88. The effect of wind is clear even at the national scale with the Atlantic slopes receiving rainfall inputs in excess of 6000mm/yr whilst the leeward Pacific slopes receive much less (around 3000 mm/yr. Receipts are particularly high on NE facing slopes. The detail for the Arenal area indicates that in this region N facing slopes receive the greatest rainfall with S facing slopes being sheltered and thus drier: the difference can be up to 4000 mm and is particularly clear for the Arenal Volcano. Isolated locations with up to 10000 mm of rainfall are consistent with the reports from individual ICE stations (e.g. Zadroga, 1981, p. 65).

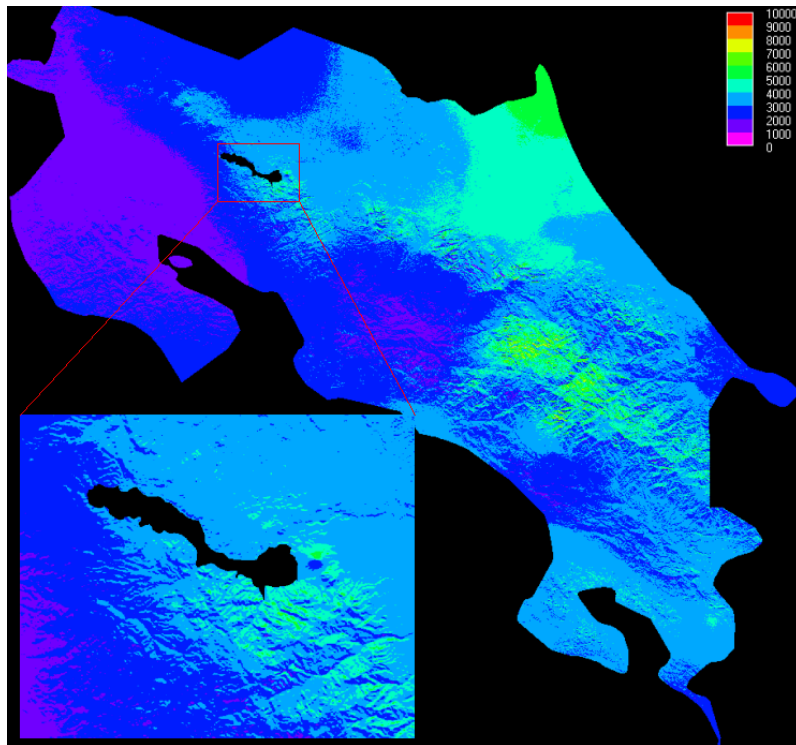


**Figure 88 Annual total wind driven rainfall, mm/yr**

Figure 89 shows the difference between input rainfall and wind corrected rainfall and generally indicates enhancement by wind on the Atlantic slopes and reduction on the Pacific slopes, also clear in the area around Lake Arenal.

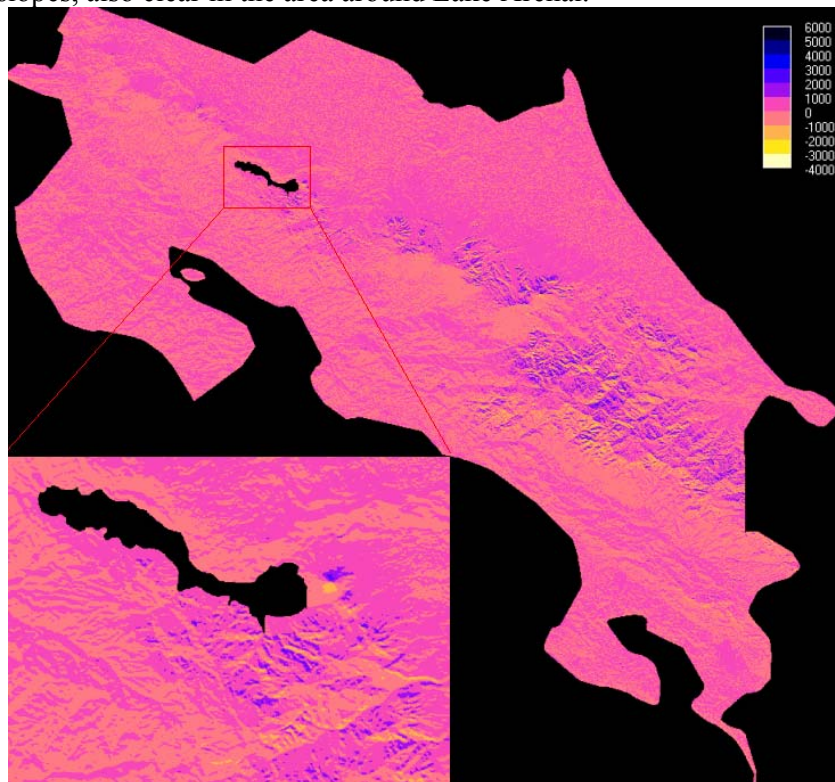


**Figure 89 Difference between input annual rainfall surface and wind corrected rainfall, mm/yr**

#### 4.13.5 Evapotranspiration

Evapotranspiration (ET) is the second major flux, behind rainfall. The delivery model results for ET are shown in Figure 90. Values are clearly highest 1000-1400 mm in the Guanacaste area because of low cloud cover and consequently high solar radiation loads. These figures are greater than those reported by ICE in Zadroga (1981, p.66), which, if right, would indicate that the general overestimation of flows by the delivery model for Pacific catchments is not the result of underestimated lowland ET. Higher cloud cover leads to lower values on the Atlantic lowlands though this is in part compensated for by greater forest cover (which increases ET compared with other land uses because of the lower albedo and greater surface area for ET). So, values are overall 700-1200 on the Atlantic lowlands. Because of cloud cover and fog presence, values are lowest in the central mountain range (generally 600-700 mm/yr) and occasionally lower.

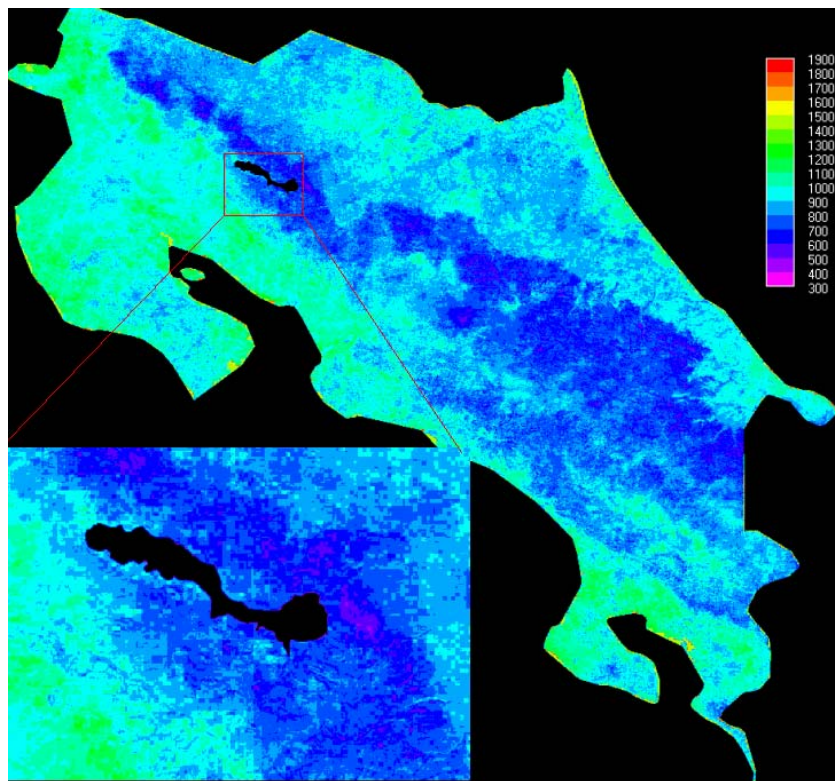


**Figure 90 Annual total actual evapotranspiration, mm/yr**

#### 4.13.6 Water balance

Coupled with the generally high and spatially variable rainfall and fog inputs, the water balance (rainfall+fog –evapotranspiration) is also highly spatially variable and varies from 0 in the drylands of lowland Guanacaste to more than 6000 mm in the high precipitation, low evapotranspiration montane areas of San Jose province and the SE of Lake Arenal, especially those slopes exposed to the N and E (Figure 91). Small isolated ridges of a few hundred square metres have balances up to 10 000 mm/yr because evapotranspiration losses are offset by fog inputs so almost all of the rainfall becomes effective rainfall.

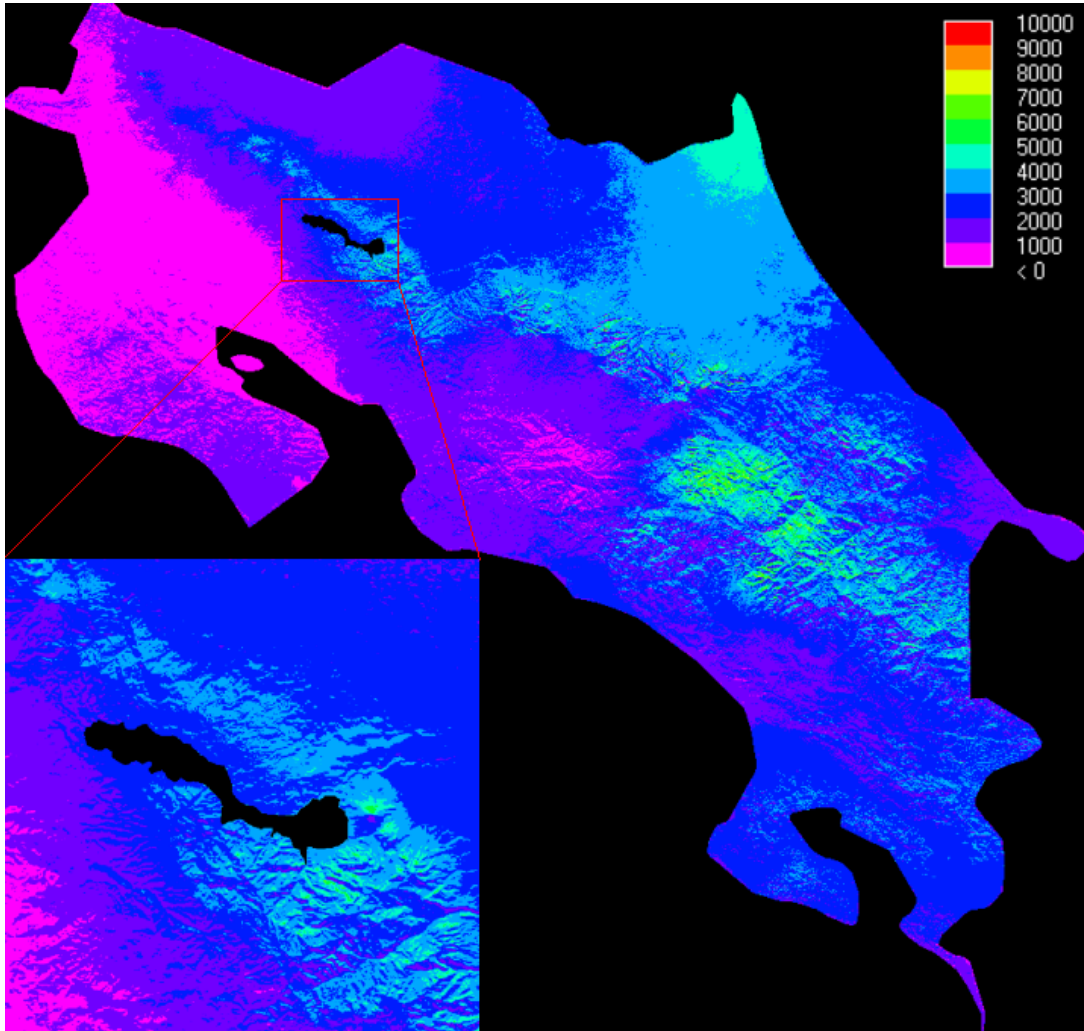


**Figure 91** Annual water balance, mm/yr

#### 4.13.7 Analysis by catchment

Aggregating fluxes by catchment (for all catchments draining to the sea or inland water bodies provides a better indicates of the area average fluxes (Figure 92). Fog inputs are clearly greatest for small catchments in the mountains so catchment average values of up to 240 mm/year can be observed for the catchments draining into Lake Arenal (the highest values in the country, largely because they are small mountain only catchments). Dominantly lowland catchments on the Atlantic or Pacific slopes have inputs close to zero and mixed upland-lowland catchments have values from 40-120 mm and, at the catchment scale, are similar on the Pacific and Atlantic slopes. Wind driven rainfall is invariably highest for the Atlantic catchments but also for the exposed Chiquito and Cano Negro catchments. Evapotranspiration at the catchment scale is lowest for those Atlantic catchments with significant montane contributions and highest for solely lowland and Pacific catchments. Evapotranspiration is also low for the small catchments draining into Lake Arenal by nature of their size and location largely within a cloudy, foggy region. Entirely lowland Atlantic catchments have higher evapotranspiration. This means that, by catchment, water balance is lowest

(less than 1000mm) over the majority of Guanacaste, is less than 2500mm for most Pacific catchments and from 2000-4000 for most Atlantic catchments.

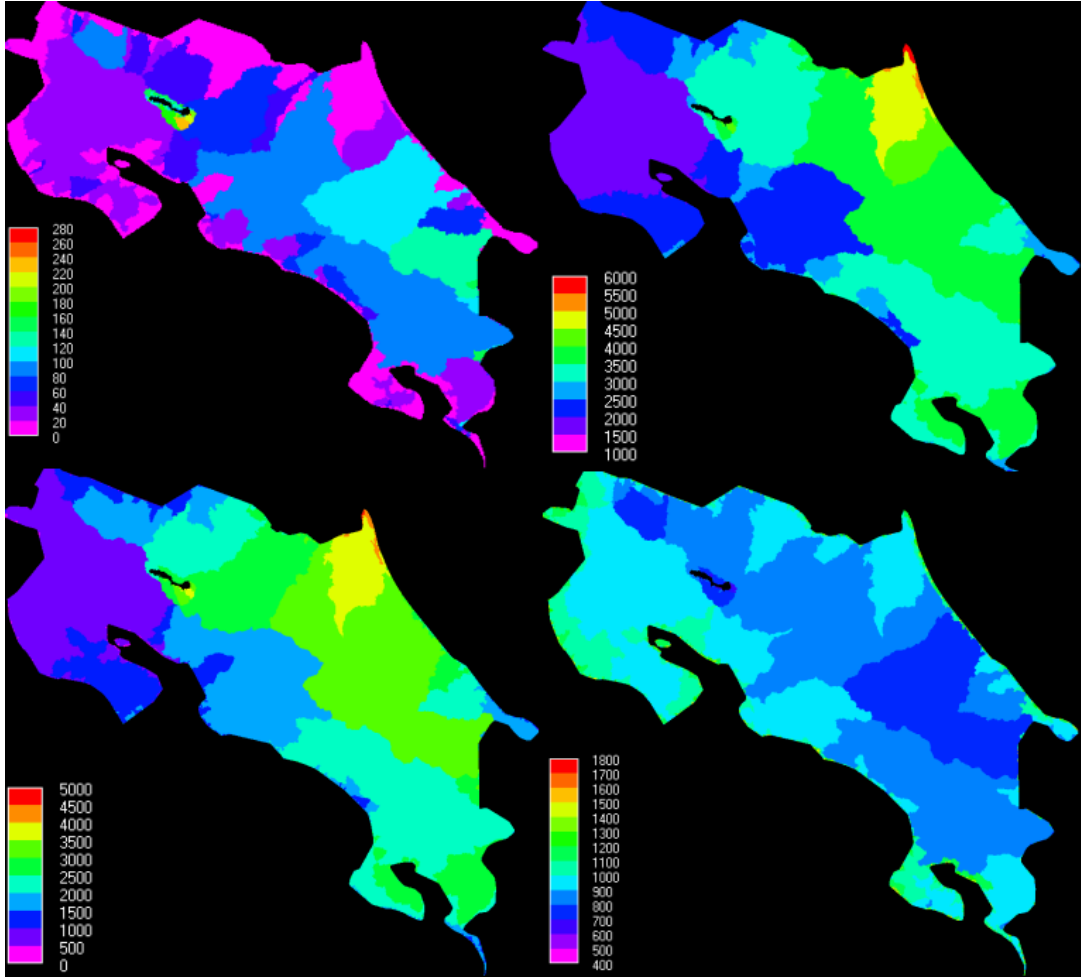


**Figure 92 Total fog inputs (top left) wind driven rainfall (top right), water balance (bottom left) and evapotranspiration (bottom right) by catchment, mm/yr**

An analysis of fog as a percentage of water balance by catchment (Figure 93) indicates that, at the catchment scale, fog is always <7% of the water balance and is greatest (4-7%) in the small catchments draining into Lake Arenal and the Rios Barranca, Segundo and Parris (Parrita) draining into the Pacific (in a very low rainfall area in the central Pacific of Costa Rica). Larger Atlantic catchments have fog contributions of 1-3.5% and larger Pacific catchments 1.5-4%.

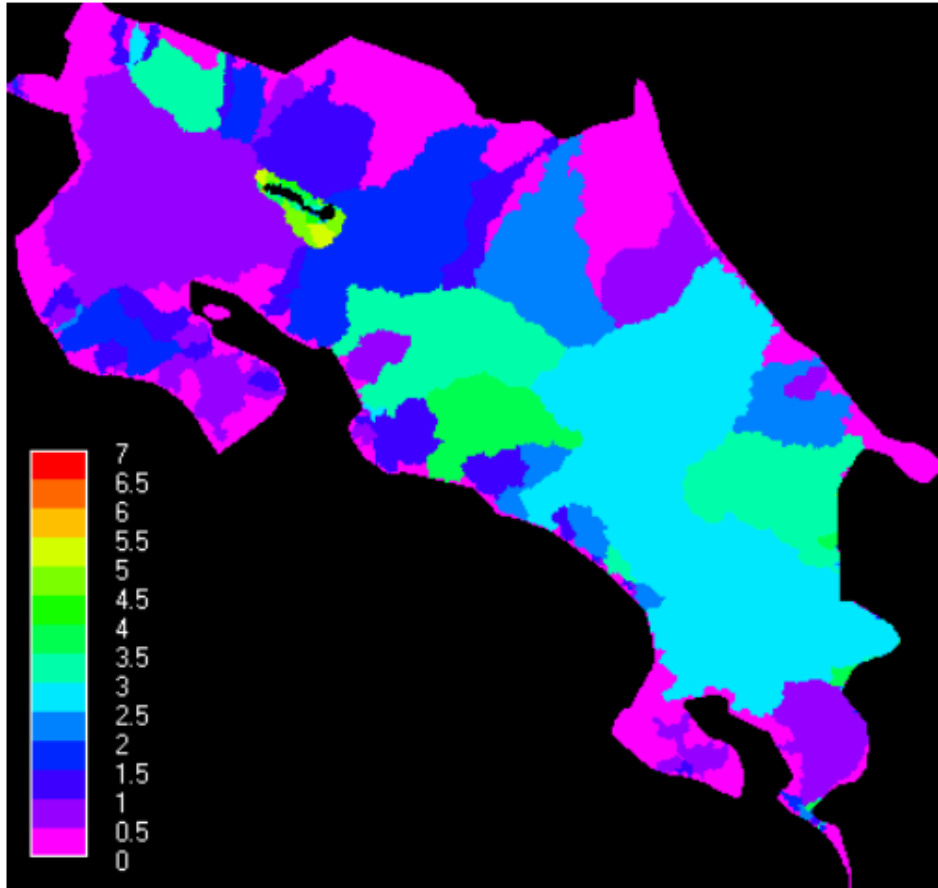


**Figure 93 Fog as a percentage of water balance, by catchment.**

#### 4.13.8 Analysis by protected area

Integration of the key fluxes by protected area indicates the conservation areas that contribute the greatest water and have the greatest fog inputs. Figure 94 indicates that the most water productive parks are Humedal Caribe Noreste, Barra del Colorado and Tortugero, since they have very high rainfall inputs. These do not have high downstream populations whereas the highly productive Chirripo, Rio Macho and Los Santos parks (3500-4000mm/yr) do. The remaining montane protected areas from Tenorio in the North through to the Arenal-Monteverde complex to the Talamancas in the South all produce in excess of 3000mm of water. Even the dry forests of the Nicoya peninsular produce 1000mm over a small area. The parks with the greatest proportional contribution of fog to the water balance are Carraigres in the dry Pacific (6%) and the Monteverde-Arenal complex (5.5%) through to Tenorio in the North (7%). Taking the mean water balance and fog contribution to water balance for individual protected areas (Table 15), Arenal-Monteverde is rank 19<sup>th</sup> in terms of water provision and 9<sup>th</sup> in terms of the fog contribution to that water balance.

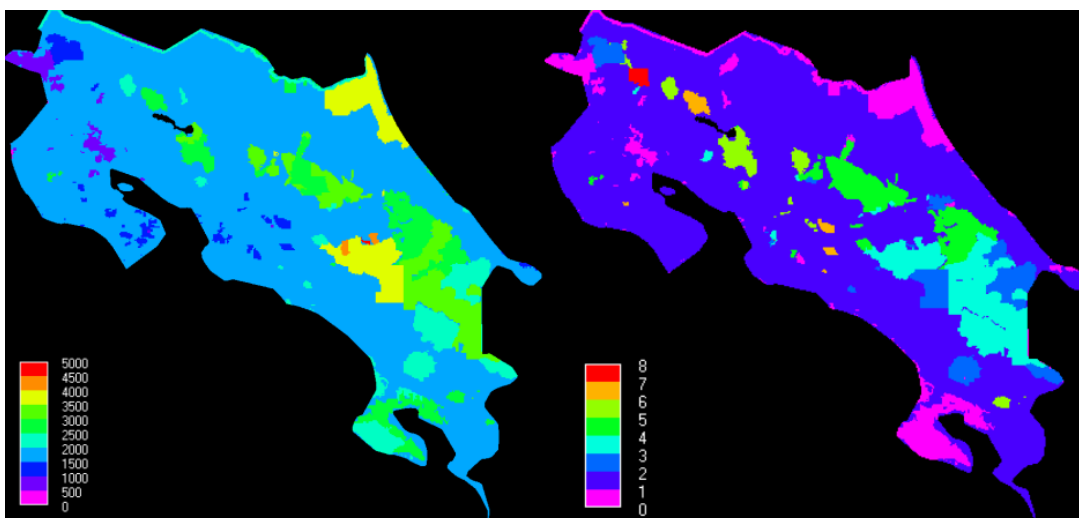


**Figure 94** Water balance by protected area (left) and percentage of water balance contributed by fog by protected area (right), mm/yr

Name	Mean water balance (mm/yr)	Name	Mean fog contribution to water balance (%)
Cuenca Río Tuis	4402	Rincón de la Vieja	6.8
Tapantí	4246	Tenorio	5.8
Barra del Colorado	3865	Cerros de Escazú	5.7
Humedal Caribe Noreste	3857	Río Grande	5.6
Río Macho	3687	Quitirrisí	5.4
Tortuguero	3576	Caraigres	5.3
Chirripó	3473	Miravalles	5.1
Acuíferos Guácimo y Pococí	3251	San Ramón	5.0
Zona de Emergencia Volcán Arenal	3226	Arenal-Monteverde	5.0
La Selva	3198	Coto Brus	5.0
Braulio Carrillo	3092	El Rodeo	4.5
Internacional La Amistad	3091	Barbilla	4.5
Talamanca Range-La Amistad Reserves	3091	Juan Castro Blanco	4.4
Juan Castro Blanco	3087	Cerro Atenas	4.3
Cordillera Volcánica Central	3055	Braulio Carrillo	4.2
Bajo Chirripó	2987	Acuíferos Guácimo y Pococí	4.2
Telire	2976	Cordillera Volcánica Central	4.1
Río Pacuare	2908	Zona de Emergencia Volcán Arenal	4.0
Arenal-Monteverde	2884	Río Navarro y Río Sombrero	4.0
Barbilla	2800	Cerros de la Carpintera	3.8
Volcán Poás	2789	Bajo Chirripó	3.8
Abrojo - Montezuma	2774	Cerro de La Cangreja	3.6
San Ramón	2750	Telire	3.4
Coto Brus	2656	Volcán Poás	3.3
Nairi Awari	2622	Internacional La Amistad	3.2

Golfito	2610	Talamanca Range-La Amistad Reserves	3.2
Tenorio	2604	Cerros de Turrubares	3.2
Matina	2595	Hitoy-Cerere	2.9
Río Indio Maíz	2591	Los Santos	2.9
Golfo Dulce	2573	Río Macho	2.8
Tayni	2571	Volcán Irazú	2.7
Hitoy-Cerere	2535	Tapantí	2.7
Guaymí de Osa	2521	Cuenca Río Tuis	2.7
Volcán Irazú	2508	Ujarrás (Cabécar)	2.6
Ujarrás (Cabécar)	2499	El Chayote	2.5
Poly: Talamanca - contains Bribri & Cabcar	2479	Las Tablas	2.5
Los Santos	2461	Guanacaste	2.5

**Table 15 Protected areas in rank of (left) water balance and (right) fog contribution to water balance.**

#### 4.13.9 Analysis by province

Analysis by province indicates that Cartago, Heredia and Limon have the highest water balances, all in excess of 3000 mm, whilst Guanacaste has the lowest (997 mm). Fog contributions to this balance are highest for San Jose (3.6%) and lowest for Guanacaste (0.8%) and Heredia (1.1%).

Region	Mean fog input (mm/yr)	Mean water balance (mm/yr)	Fog as a % of water balance
Guanacaste	19.9	997	0.8
Alajuela	59.7	2202	1.8
San Jose	101.7	1998	3.6
Puntarenas	41.6	2102	1.3
Heredia	43.3	3032	1.1
Cartago	143.7	3100	3.7
Limon	61.7	3062	1.6

**Table 16 Analysis of fog contributions and water balance by province.**

An analysis by continental divide is shown in Table 17 which shows that, fog inputs are 17 mm/yr (26%) higher on the Atlantic slopes. Actual evaporation is higher for the Pacific slopes and rainfall much lower so that the overall water balance is much higher for the Atlantic slopes. This has little to do with fog inputs though as these are less than 2% of the budget and are fairly equal relative to the budget for Atlantic and Pacific slopes.

Variable	Pacific	Atlantic
Fog input (mm/yr)	49.3	66.2
Potential evapotranspiration (mm/yr)	1176	1037
Actual evapotranspiration (mm/yr)	952	846
Rainfall(mm/yr)	2586	3574
Water balance(mm/yr)	1683	2794
Fog as a % of precipitation/water balance	1.73	1.71

**Table 17 Hydrological fluxes and fog contributions across the continental divide**

4.13.10 Fog runoff as a percentage of runoff

The best way to understand the significance of fog inputs to cloud forests in the wider hydrological context is to calculate fog inputs cumulative downstream (fog runoff) as a proportion of the rainfall generated runoff. Fog runoff is fog inputs minus fog evapotranspiration, cumulated downstream. It is important to remember that both fog runoff and runoff represent runoff *generation* from current rainfall and do not include runoff which results from release of soil and groundwater stores from previous rainfall (i.e. baseflow). The inclusion of baseflows would tend to further reduce the fog runoff percentages suggested here, especially in the dry season (though some of that baseflow would also be derived from previous fog). Fog runoff as a percentage of rainfall runoff is shown for part of Costa Rica in Figure 95. Clearly the highest contributions to runoff (up to 18%) are highly localised to very exposed slopes. Throughout the mountain zones fog contributions to runoff are 2-6% in line with its contribution to the local water balance. As one travels downstream (out of the highlands), the contribution of fog soon becomes less than 5% and for most rivers approaches zero before the river reaches the sea (because of the much larger volumes of non-fog generated water from the lowlands). Fog inputs are thus less than 3% for much of the long profile of a typical river (depending on the area of cloud forest drained). Figure 96 shows this in detail for the upper reaches of the San Carlos river.

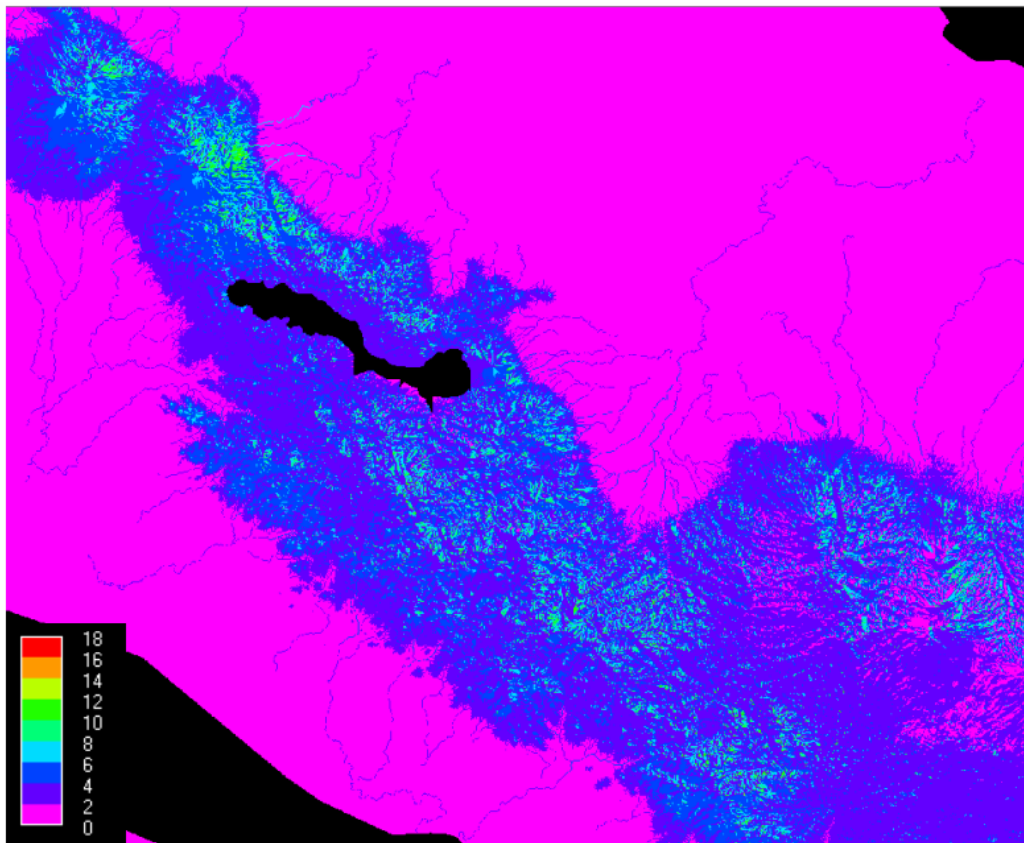
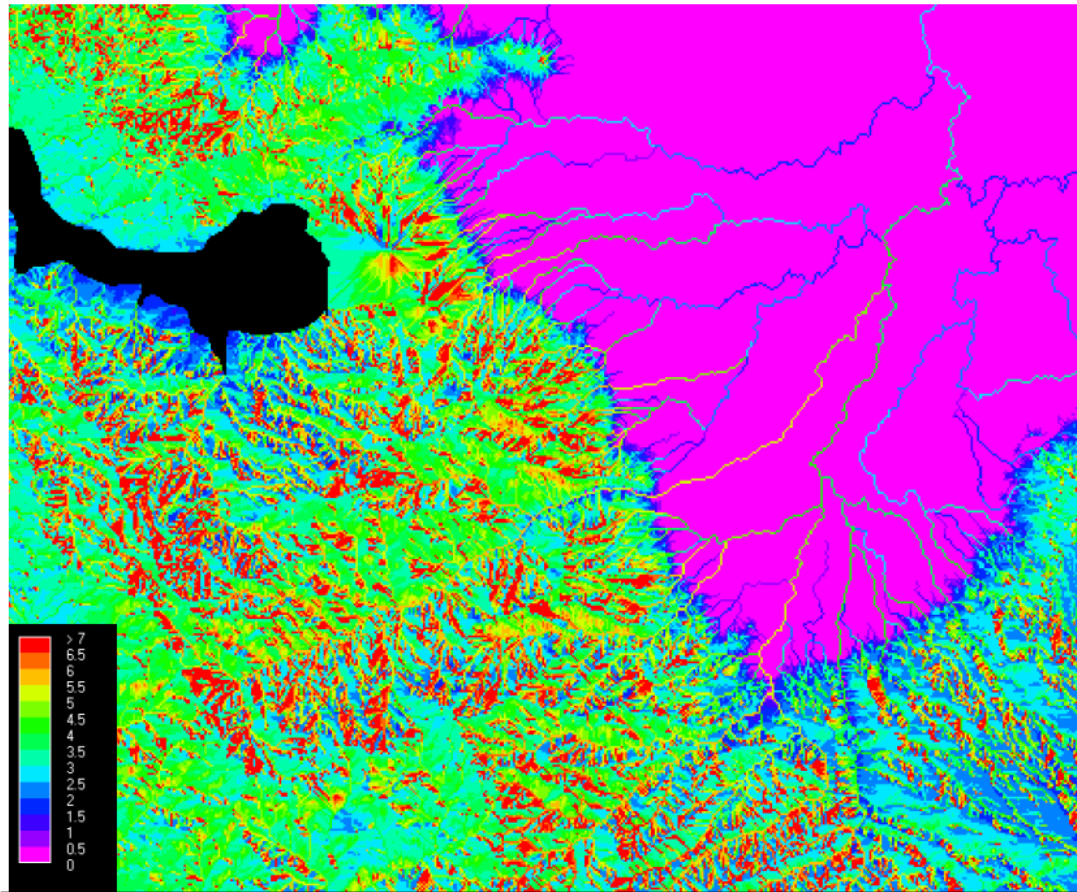


Figure 95 Fog runoff as a percentage of rainfall runoff.



**Figure 96 Fog runoff as a percentage of rainfall runoff : detail for upper San Juan river**

#### *4.13.11 Seasonal variation*

Though annual total figures do not point to a large contribution of fog interception to water balances in Costa Rica, climate is highly seasonal here (as in many places) and thus it is important to analyse the seasonality of fog contributions to the water balance. It is important to reiterate here that the runoff and fog runoff figures do not account for baseflows (which are not simulated) and so the seasonal fog-runoff as a percentage of rainfall runoff figures given in this section (as in others) may be slightly inflated in areas where baseflows are significant (though it is important to remember that baseflows are also generated in part from fog), especially in the dry season. Nevertheless we do get a good picture for the contribution of fog to runoff *generation*, if not total runoff. Figure 97 shows fog runoff as a percentage of rainfall runoff by month. Where there is no fog runoff or no rainfall runoff, a value of zero is given (the pink areas) because percentages would be unrepresentative.

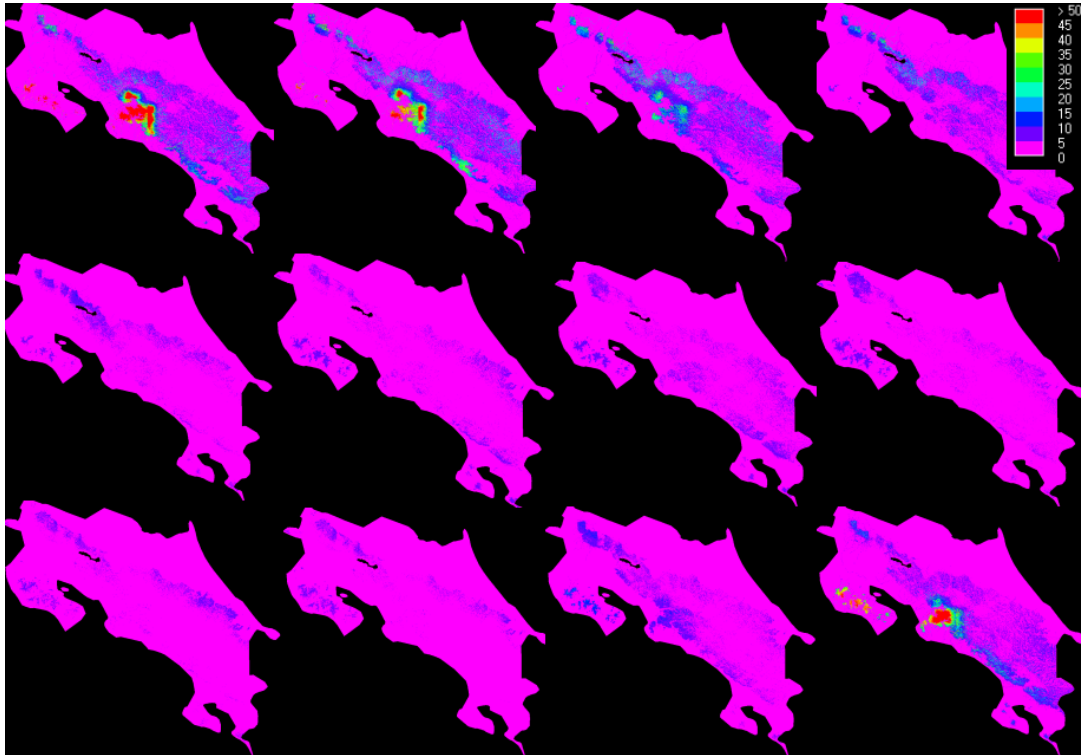


**Figure 97 Annual progression of monthly fog contribution to runoff : top left=January, bottom right=December.**

In January there are peaks of fog contribution in the north and in the central Pacific areas and over the Nicoya Peninsula, some of the rivers draining to the Pacific in the very north and south of the country reach fog contributions of 25-35% of the rainfall contribution (20-23% of the total runoff from fog) and the streams within cloud forest themselves can reach >50% fog contribution. This continues through February and declines in intensity in March. By April there is a shift towards greater contributions of fog to Northern Atlantic flows. In May and June the contribution to all rivers is a fraction of one percent outside the mountain areas. From May to October contributions are low <15% locally in the cloudforests. The contributions are also spatially restricted to Atlantic or Pacific foothills. There are changes to the spatial distribution of montane contributions but contributions to lowlands rivers remain a fraction of one percent for the Atlantic and Pacific during this period. By November local contributions increase in extent (but are still <15% in magnitude) and are concentrated once more in the central Pacific rivers, the most northerly mountains and the Nicoya Peninsula but with little in the way of contribution to the lowland rivers which emanate from those uplands. By December we have a similar situation to January with >50% in the central Pacific peaks and over the Nicoya Peninsula and 10-25% elsewhere in the Pacific.

Given the importance of maintaining stable seasonal river flows in climatically seasonal environments (for ecological and for water resource reasons), perhaps the best indicator of the importance of fog inputs are their maximum annual contribution to runoff (i.e. their contribution to runoff in the month in which it is greatest). This is shown in Figure 98 and shows low but significant (10-15%) maximum monthly

contributions for the mid and southern Atlantic rivers (so fog is never really very important to those rivers, even seasonally). However maximum monthly contributions to the N Atlantic catchments are much higher 25-35% as they are for some of the mid and N Pacific rivers. Locally to the montane areas and montane rivers, contributions can be significantly higher in seasonally dry (low rainfall) areas.

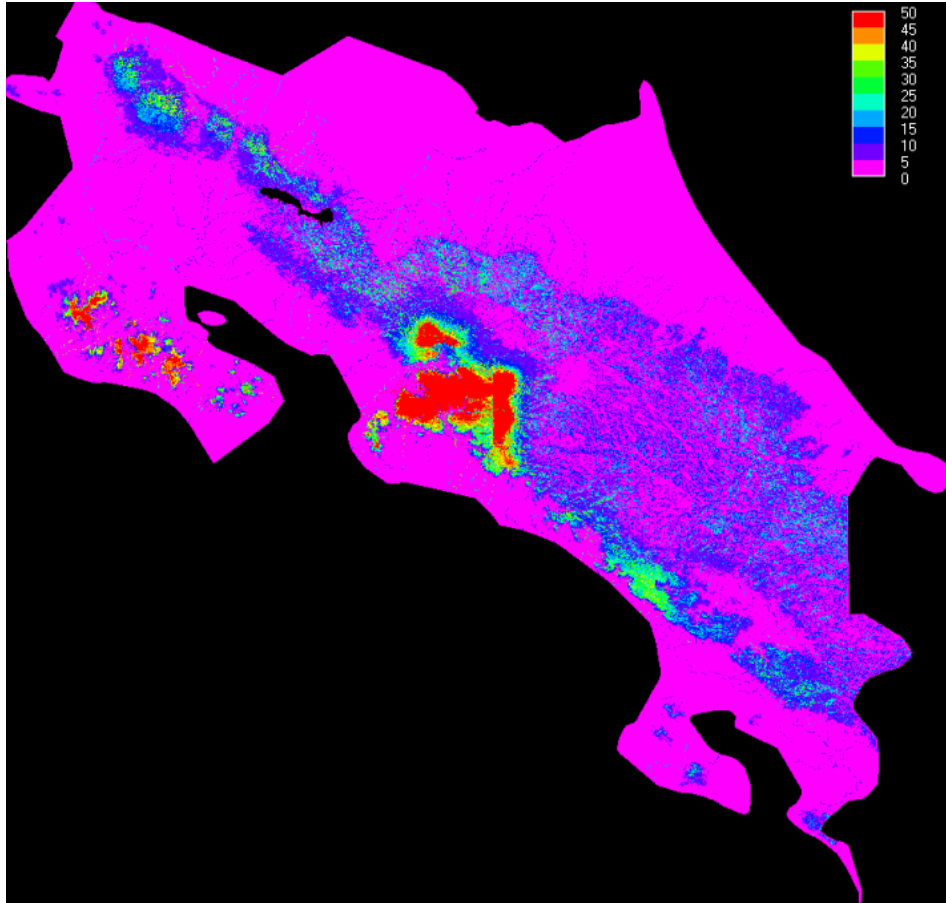


**Figure 98 Maximum monthly contribution of fog runoff to as a percentage of rainfall runoff.**

Looking at this image in greater detail (Figure 99) for the area around the Arenal Lake we see that the maximum monthly contribution of fog is 20-25% of rainfall runoff (16-20% of total runoff) for the upper Chiquito (occurring in April), falling to around 15-20% (13-16% of total runoff) in the lower parts (in the month of March). The Cano Negro has values of 20-30% (16-23% of total runoff) extensively occurring in March and April as does much of the upper reaches of the Penas Blancas (occurring in March). These values clearly fall as one moves further downstream but are at a maximum of 15-20% (in March) even in the lowland Rio San Carlos.

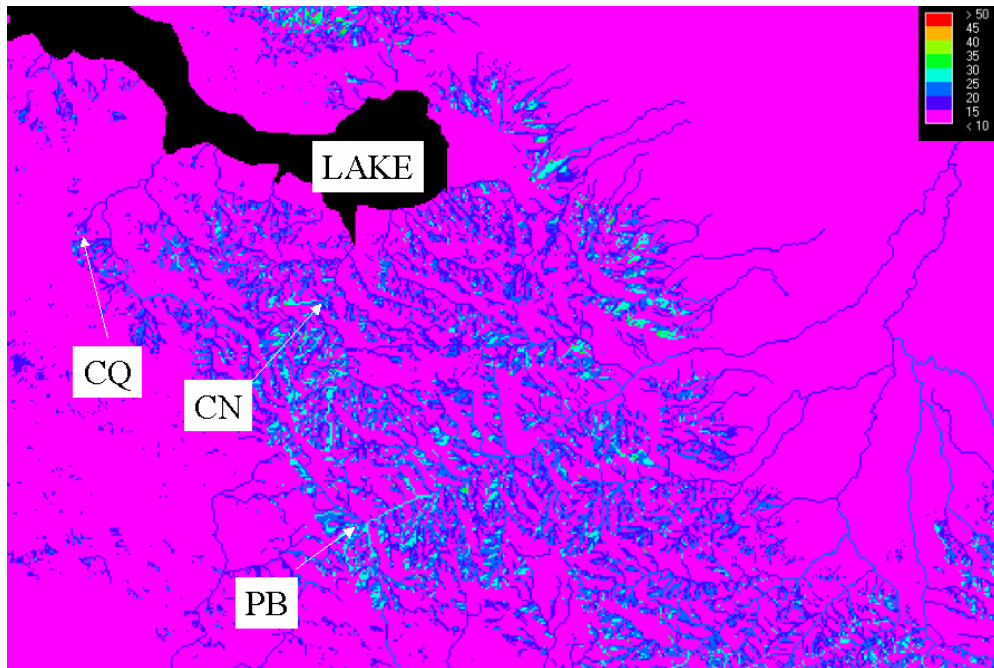


**Figure 99 Maximum monthly contribution of fog runoff to as a percentage of rainfall runoff.**

Finally we examine the month of greatest contribution of fog to flows. This is April for most Atlantic slopes, March for much of the southern Atlantic and Pacific slopes, February for the central Pacific slopes, October to December for Nicoya and June for much of the area draining into Lake Arenal. These are the months when the fogrunoff:runoff ratio is highest.

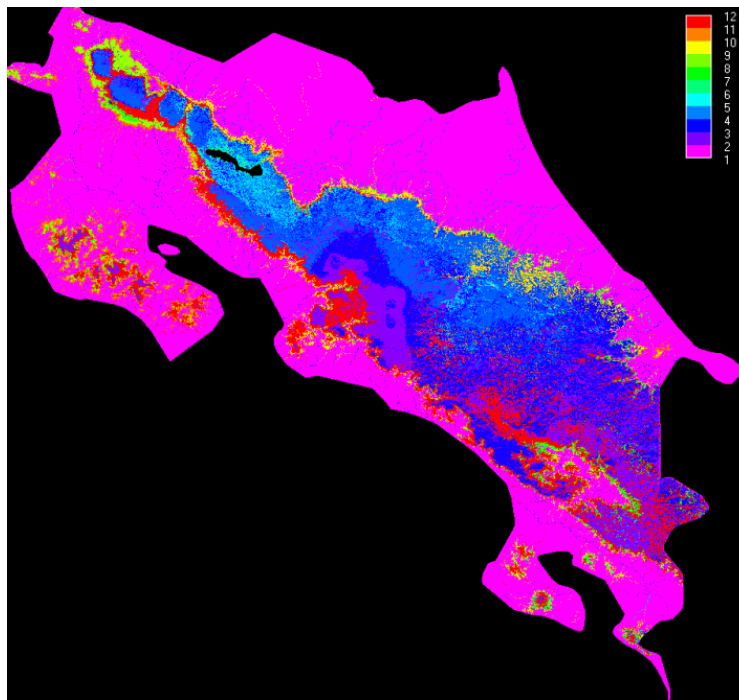


**Figure 100 Month of maximum fog contribution to runoff**

Examining the area around Lake Arenal in more detail (Figure 101), we see that there are some exposure and slope aspect effects (resulting from changing wind directions and solar inputs) which mean that NE exposed areas tend to have the highest fog contribution to runoff in May instead of April for the NE sheltered slopes. There is also a clear altitudinal pattern according to the seasonality of the cloud base level (especially on the shallower gradient Pacific slopes) with greatest fog contributions in December on lower slopes. For rivers reaching the lowlands, the month of their greatest fog contribution depends largely on the altitudinal zone in which they have greatest occupancy.

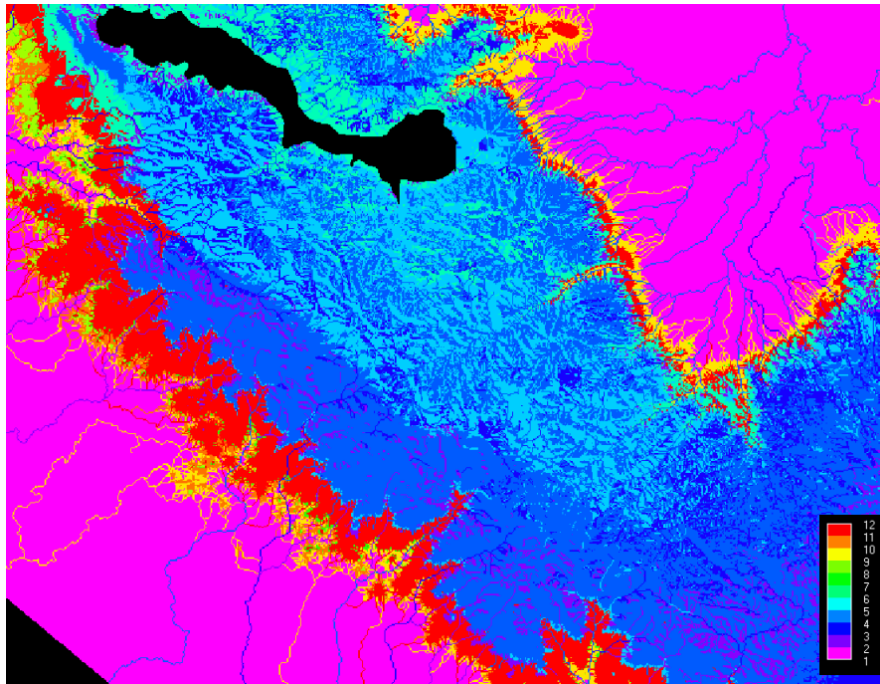


**Figure 101 Month of maximum fog contribution to runoff : detail around Lake Arenal.**

In summary volumetric fog contributions are low except in some small, highly exposed areas. These contributions are usually only a few percent of the water balance for areas of Costa Rica. The contribution of fog to flows is a few 10's of percent in cloud forest rivers and streams but soon declines to a few percent or less as one travels downstream through the lowlands. Nevertheless in some seasonally dry areas monthly contributions of fog (in the lowest rainfall month) both locally and to downstream lowlands can remain high (10% or greater for upper reaches of the Atlantic lowlands and for the entirety of some Pacific streams).

#### **4.14 An examination of model processes**

Here we take some examples of process insights gained through application of the `fiesta_delivery` model.

Flux mechanisms

Figure 102 shows the inputs of fog according to different flux mechanisms (impaction versus deposition) for the whole country. Clearly impaction is highly spatially isolated but can reach high magnitudes - up to 500mm per year, though this tends to be in very exposed areas (where rainfall inputs are also very high). Impaction is highly dependent on exposure to cloud bearing winds and to vegetation fragmentation. Deposition on the other hand is much more extensive but lower in magnitude (50-150mm mainly) and much less spatially variable being less dependent on exposure. So the fog inputs to an area will be scale-dependent with majority of inputs tending to result from deposition (at large spatial scales) but from impaction (at the local scale). On the other hand, most field measurements of fog inputs tend to concentrate on impaction processes (where gauges are used) or deposition processes (where canopies are used since most canopy studies occur away from forest edges where impaction is dominant). Rates of impaction to gauges are not very scaleable since they are spatially very variable (according to exposure etc). Rates of deposition to forests are more scaleable spatially but ignore the inputs from impaction and are greatest under conditions where impaction is least. The important point here is that these two processes of fog interception differ in significance depending on terrain conditions and on the spatial scale of the study and deposition (which is rarely measured, even in raingauges unless bundled with rainfall<sup>19</sup>) can be the greater contributor at larger (and thus more significant) scales.

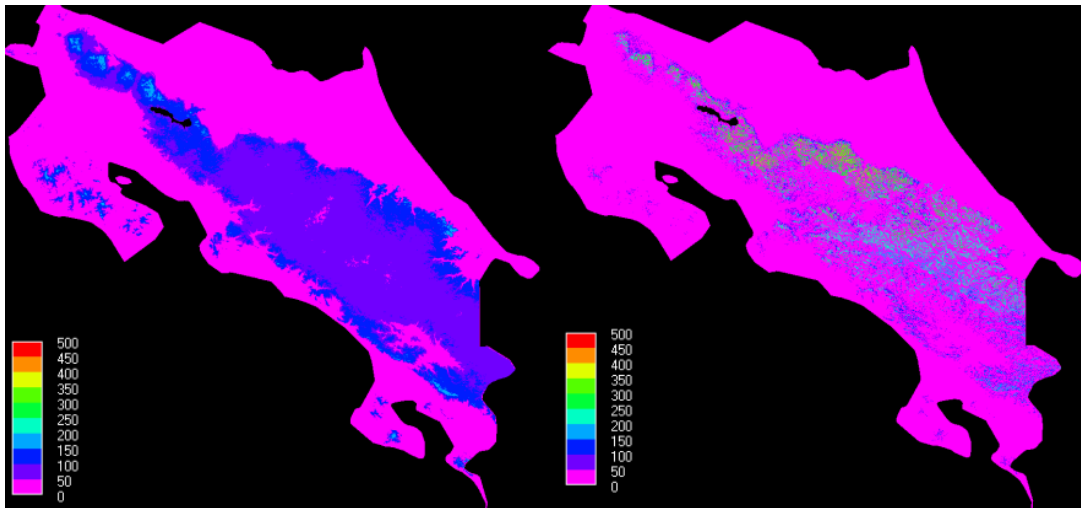


**Figure 102 Flux mechanisms for fog. (mm/yr)**

The detail of deposition and impaction for an area around Lake Arenal is shown in Figure 103 with topographic contours overlaid and indicates the dependence of both impaction and deposition on cloud frequency, of deposition to topographic shelter and, of impaction to topographic exposure and vegetation patterns.

<sup>19</sup> Deposition is measured by raingauges since deposition is vertical. It is however highly subject to evaporational losses at the gauge because it remains as droplets in the gauge funnel. Moreover unless it occurs on days in which rainfall also occurs fog deposition is likely to be too little to measure accurately and thus considered as a dry day and not included in total rainfall statistics.

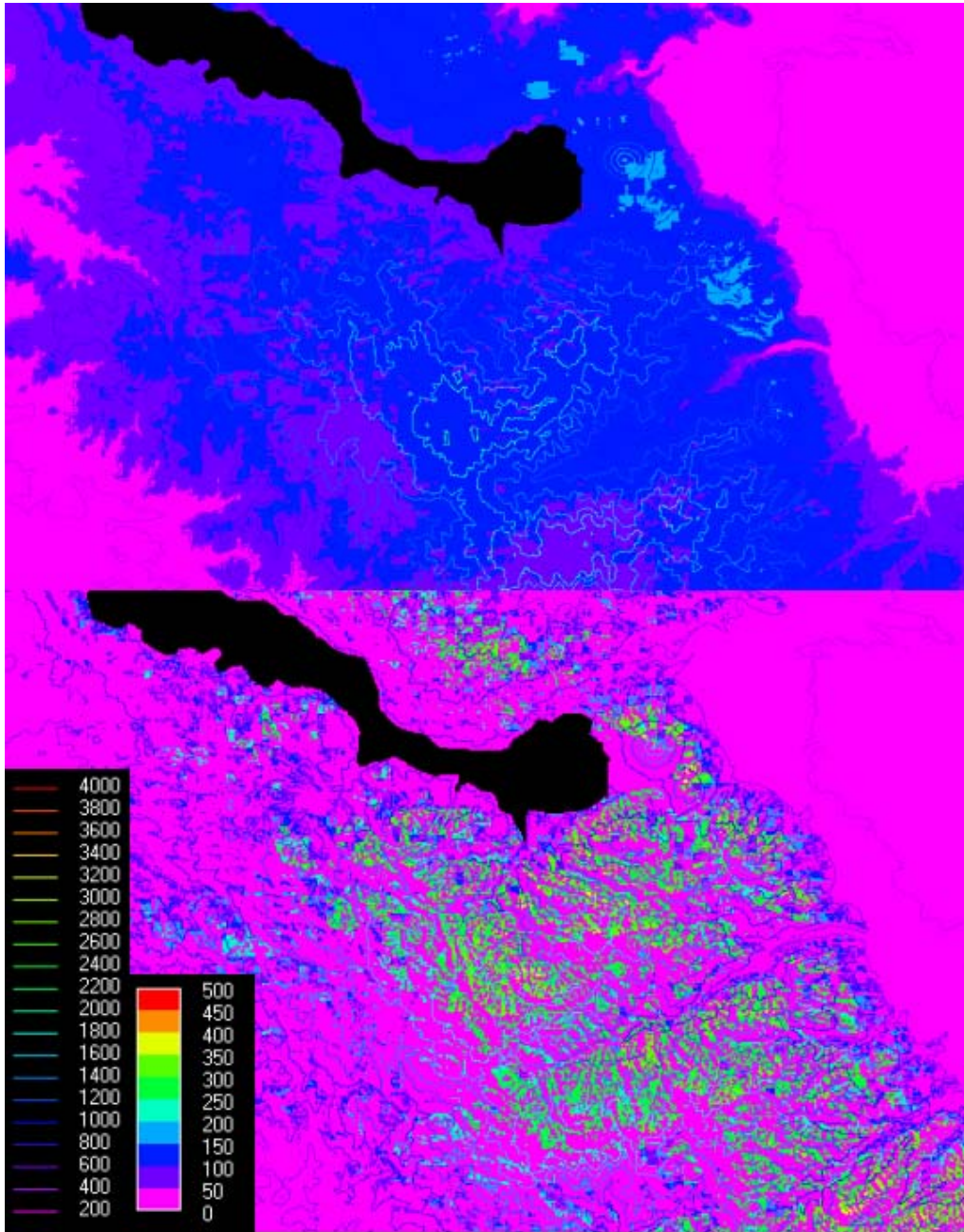


**Figure 103** Detail of deposition (top) and impaction fluxes (mm/year) for an area around lake Arenal.

#### 4.14.1 Wind driven rain

As we have seen, wind effects, as well as reducing gauge catches, can have significant effects on the spatial distribution of rainfall in windy and mountainous terrain. Figure 104 shows wind driven gains and losses by sub-catchment and indicates that for the area around Lake Arenal, Southern (N facing) catchments do show a net increase in rainfall as a result of wind effects (142 mm for CQ, 289 mm for Cano Negro, 96 mm for the larger Penas Blancas), whilst northern (S facing) catchments show a net loss of the same magnitude. The effect is greater for smaller catchments and tends to be much less for larger catchments, which are more likely to contain a variety of

exposures. In a country like Costa Rica (with a sharp continental divide across which the dominant winds pass), the effect is still apparent at the national scale with Atlantic slopes showing net gain and Pacific ones net loss. These are the result of non vertical rains interacting with non-flat slopes whereas the input rainfall values interpolated from stations values are interpolated on the basis that the stations catch vertical rain only, that only vertical rain falls and that the landscape, like the raingauge orifice is also flat. To a certain extent, at the national scale the kinds of topographic patterns observed in the WDR maps are already measured by the station data, this work converts those station values to values representing the catch of the true land surface rather than the gauge orifice.

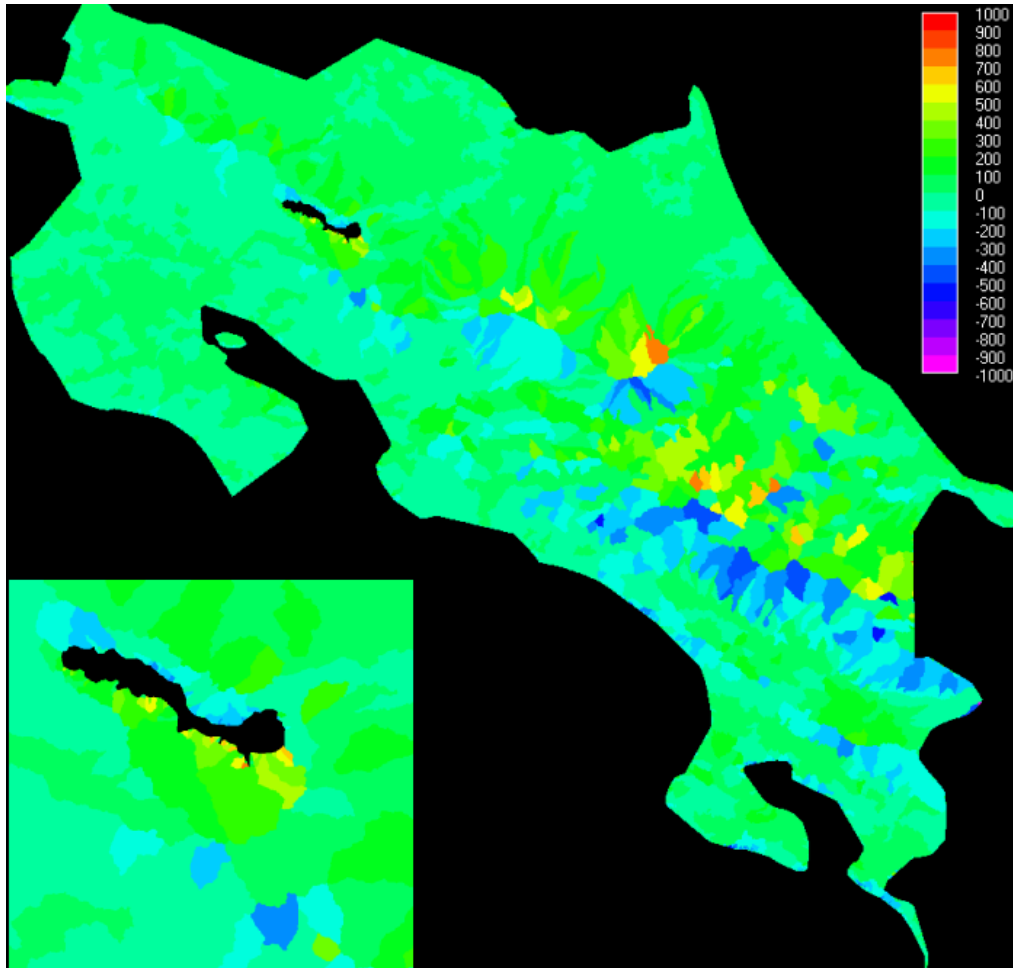


Figure 104 Integrating wind driven rain effects up to the catchment scale (mm/yr)

#### 4.15 Results of scenario runs

Here we analyse the hydrological differences between the baseline scenario run and the various land use change scenaria, starting with the payments for environmental services scenario. The purpose of these runs is to understand better the hydrological impacts at a variety of scales of complex patterns (but simple scenarios) of land use change.

##### 4.15.1 PES Scenario

In this scenario land use change is allowed to continue at current rates outside of protected areas but within the current protected areas system PES payments maintain a situation in which no land use change is allowed to occur. Figure 105 shows the differences in fog inputs between the baseline and PES scenario, negative values indicate a loss in fog inputs as a result of the land use change whereas positive values indicate a gain in fog inputs. First, it is clear that changes in fog inputs occur only outside of protected areas (because this is where land use has changed). The changes represent an average of  $-20$  mm/yr in the deforested areas (because of the reduced leaf area for interception of sedimenting fog over large areas). The change in fragmentation that resulted from land use change produced a highly complex pattern of (mainly) fog impaction reductions of up to  $-200$ mm for individual pixels and  $-100$  for larger areas with some small areas also showing increases in fog by impaction (because of new edges being created), though these areas are restricted to areas under full forest cover in the baseline scenario and thus fragmented (rather than totally deforested) in the PES scenario.

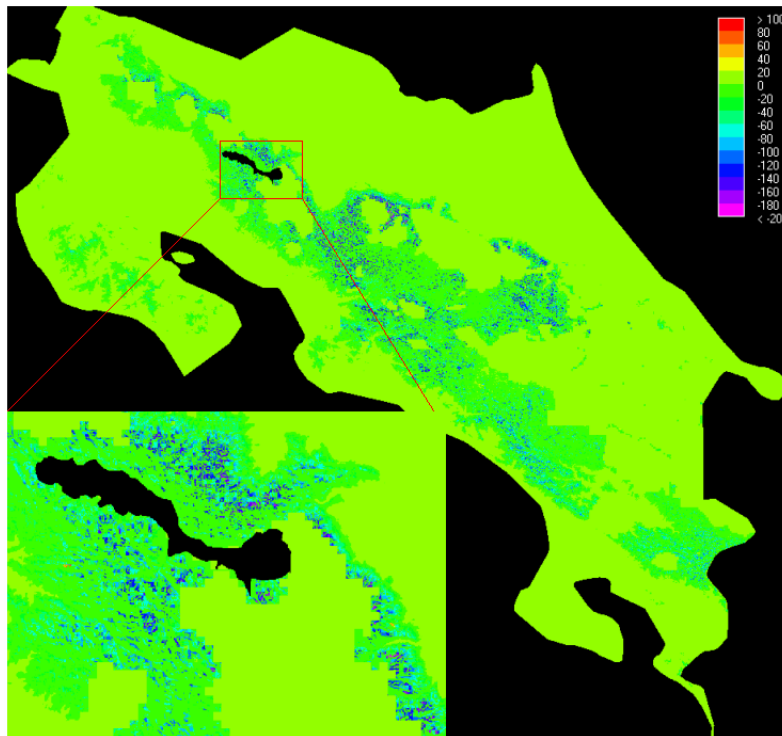
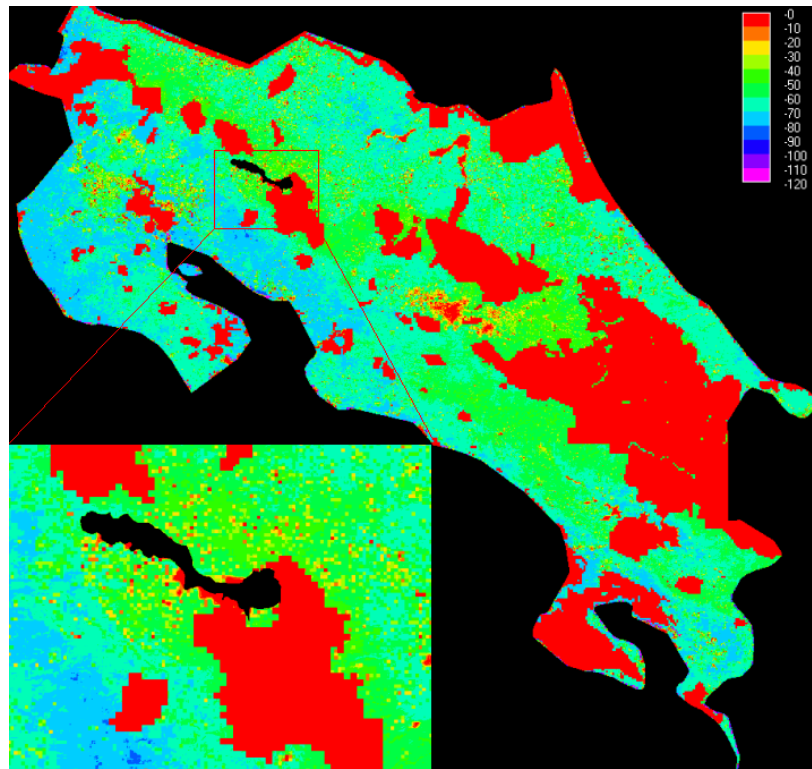
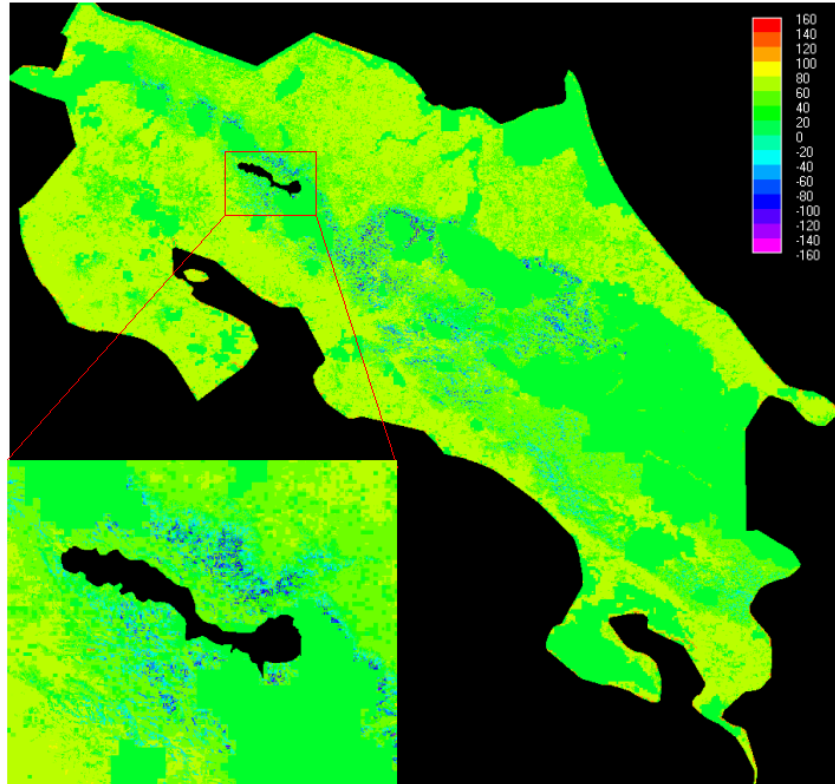


Figure 105 Difference in fog inputs between baseline and PES scenario (mm/yr).

Figure 106 shows the change in evaporation from the baseline to the PES scenario. Once again there is no change in the protected areas since there is no deforestation in these. Outside of the protected areas there are reductions in evapotranspiration consequent with the replacement of forest cover with pasture. The reductions are greatest in the lowlands, particularly in Guanacaste since in these areas evapotranspiration is not energy (radiation) limited. Reductions are lower in the mountain areas because forest cover is initially high so some forest remains under PES but also because the vegetation takes on less significance where energy is limiting (because of high cloud cover).



**Figure 106** Difference in actual evapotranspiration between baseline and PES scenario (mm/yr).



**Figure 107 Difference in water balance between baseline and PES scenario (mm/yr).**

The resulting change in water balance is shown in Figure 107 and indicates no change in the protected areas, slight increases of the order of 40-50 mm/yr in the non-protected mountainous areas (because of reduced evaporation), and stronger increases of the order of 60-70 mm/yr in the unprotected lowlands. In a few spatially restricted montane slopes, changes in forest fragmentation have led to stronger declines in fog interception as a result of forest loss than the declines in evaporation and in these - highly exposed - areas an overall reduction in water balance is observed, but they are rather rare.

The change in runoff resulting from the PES scenario (Figure 108) shows no change in protected areas, a small increase in runoff outside of protected areas and a small localised decrease in runoff in exposed, unprotected cloud forests areas. Overall the increases in runoff dominate so that rivers tend to show an increasing difference in runoff between the scenaria as one moves downstream, to a maximum of 4.5 cumecs (142 Mm<sup>3</sup>/yr) for the largest rivers.

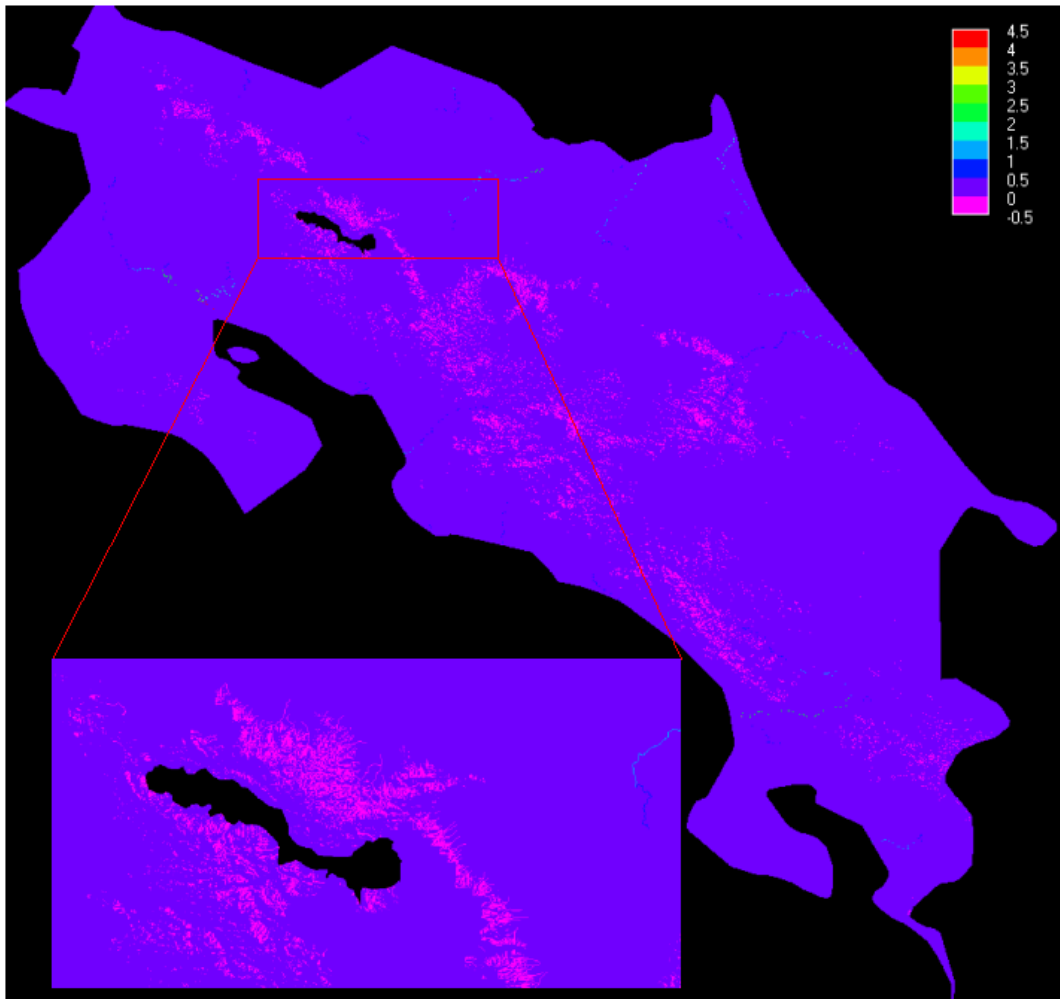


**Figure 108 Difference in runoff between baseline and PES scenario (cumecs).**

Fog runoff (Figure 109) shows an increase of up to 0.1 cumecs in a few isolated highly exposed areas, no change in protected areas and a small decrease over most of the montane zone. Thus the overall effect is a decrease in fog inputs to runoff as a result of forest loss. The decrease is of up to  $-1.2$  cumecs near the mouths of the largest rivers originating in the mountains, especially in the central Pacific.

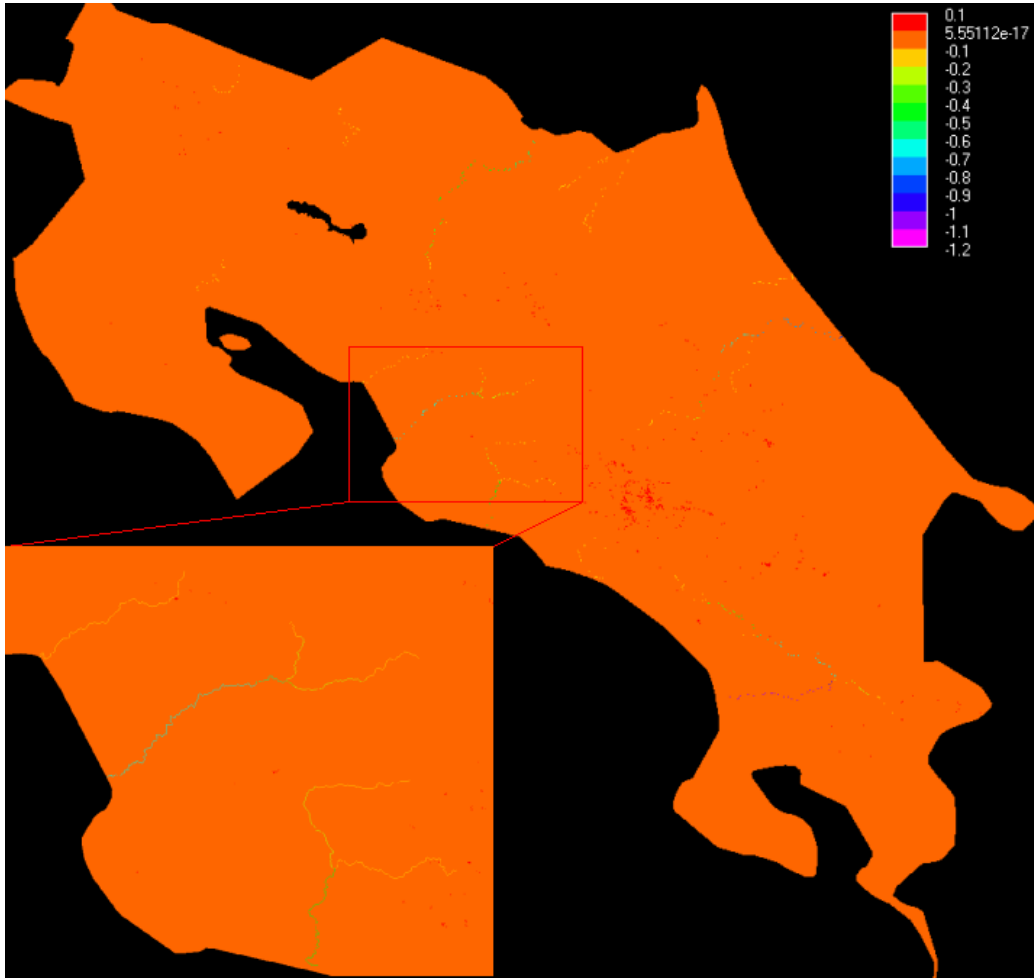


**Figure 109** Difference in the contribution of fog to runoff between the baseline and PES scenarios (cumecs)

#### 4.15.2 *NOPES scenario*

In the NOPES scenario, PES payments are not provided for conservation of the current protected areas system and thus deforestation continues at recent rates both outside and inside of the current protected areas.

Basically the same patterns emerge (Figure 110 and Figure 111) in this scenario as for the previous scenario, except that the effects of deforestation occur also in protected areas and so the national scale effects are greater. Evapotranspiration declines both in the lowlands but also, to a lesser extent, throughout the montane region. This results in an increase in the water balance of around 40-60 mm in the mountains and 80-100mm in the lowlands, but a decrease in water balance (-40 to -100) in a few isolated, exposed cloud forest areas (where the decline in fog inputs is greatest). The impact on runoff is to produce localised declines in a few exposed cloudforest areas but overall increases throughout the country. There is an overall decrease in fog runoff throughout the mountain zone (except a few isolated, exposed patches) and these cumulate to produce flow reductions of up to -1.5 cumecs for the largest rivers.

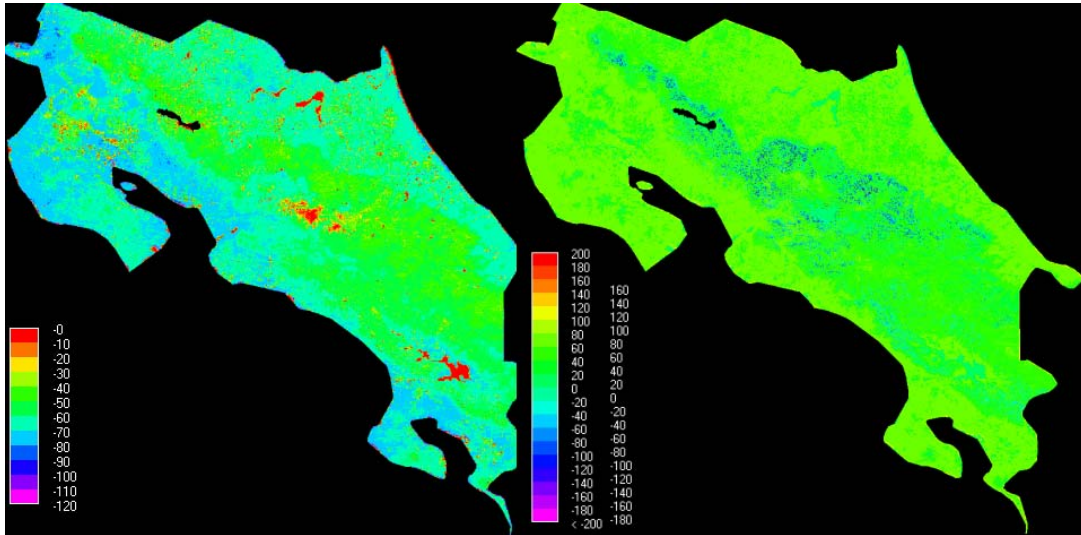


**Figure 110** Difference in evapotranspiration (left) and water balance (right) between the baseline and NOPES scenarios (mm/yr)

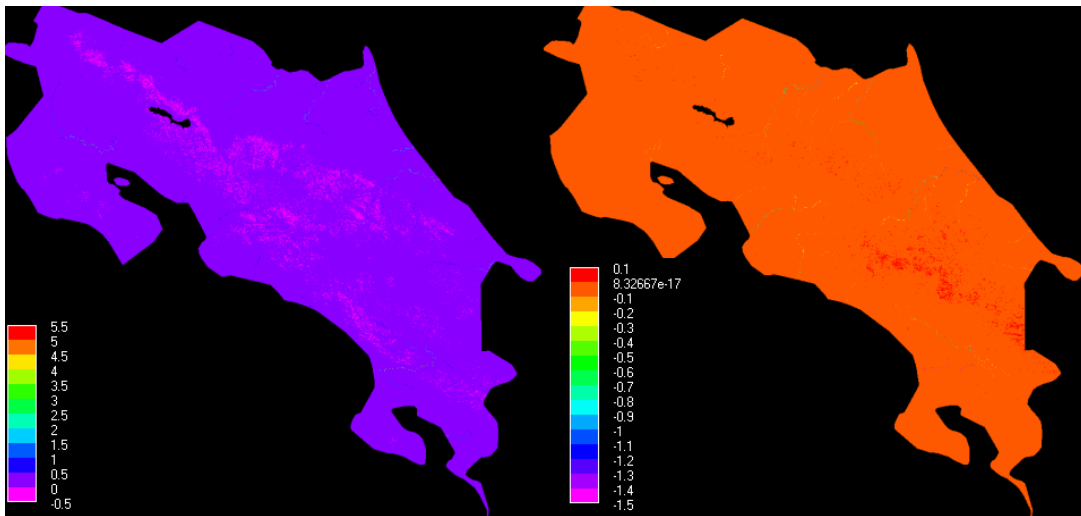


**Figure 111** Difference in runoff (left) and fog contribution to runoff(right) between the baseline and NOPES scenarios (cumecs)

#### 4.15.3 Cloud forest only removed scenario

In the cloud forest only scenario, land use change occurs at recent rates but only in unprotected forests above 1400m (cloud forests). This leads to fog losses of only  $-3.5$  mm/yr over much of the cloud forest area,  $-50$ mm over more exposed sites and  $-130$ - $200$  mm/yr over very exposed sites where impaction is the dominant process and thus the difference between forest and pasture is considerable. The impact on water balance (combining the fog and evapotranspiration effects) produces increases in water balance of between  $60$ - $100$  mm/yr over much of the cloud forest belt (where deposition of fog is the dominant process) because of reduced evapotranspiration under grassland (compared with little change between grassland and forest in the effectiveness of fog deposition). In isolated areas where forest loss reduces fog

impaction, the overall effect can be a reduction in water balance, mainly in the region of 0-60 to  $-120$  mm/yr (Figure 112).

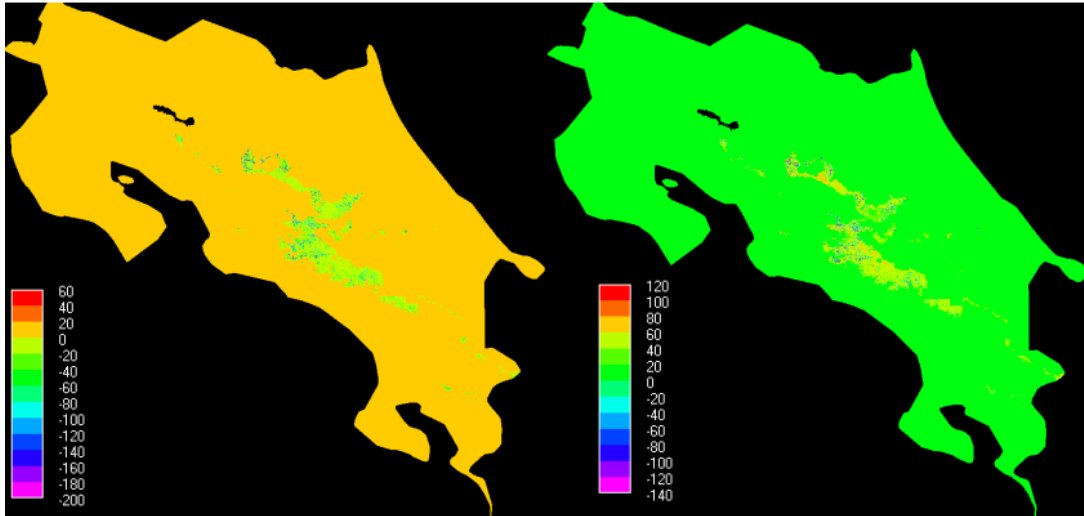


**Figure 112** Difference in fog inputs (left) and difference in water balance (right) between the baseline and unprotected cloud forest only removed scenarios (mm/yr)

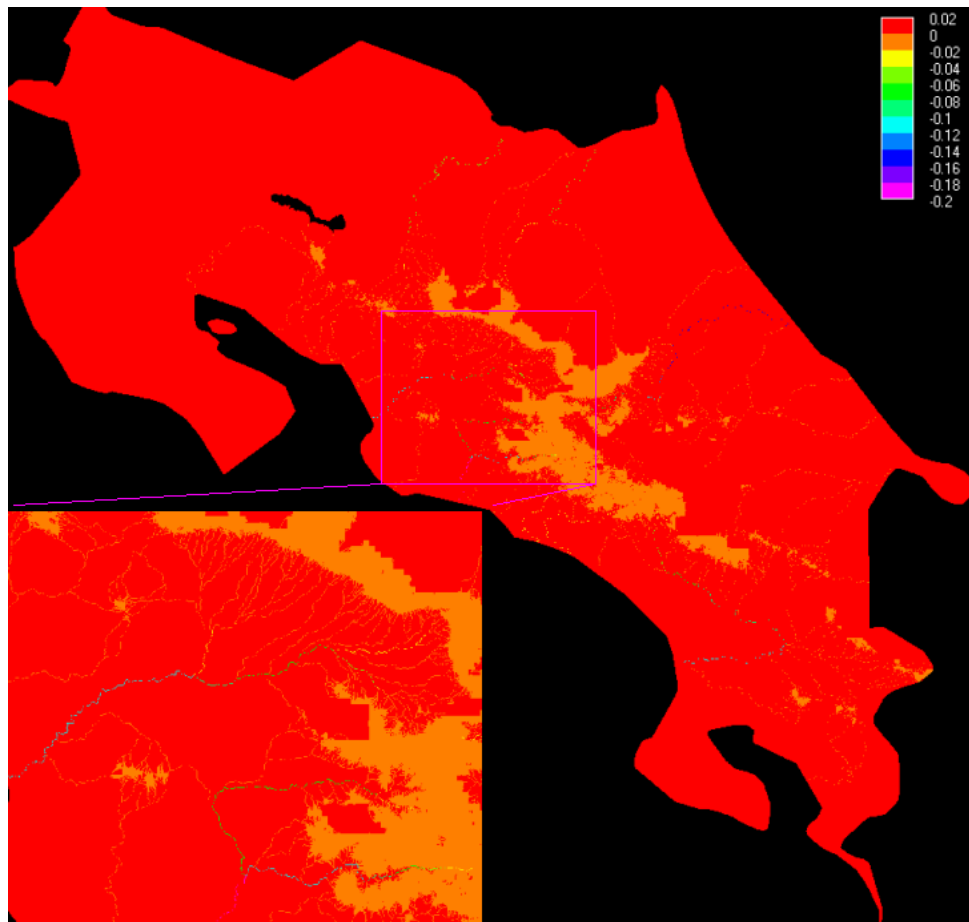


**Figure 113** Difference in fog contributions to runoff between the baseline and unprotected cloud forest only removed scenarios (cumecs)

The impact in terms of fog runoff (Figure 113) are small reductions throughout the cloud forest belt, cumulating to reductions in fog contributions to runoff of up to  $-0.2$  cumecs ( $6.3 \text{ Mm}^3$  annually) for the largest rivers.

The impact on runoff (combining the fog and the evapotranspiration effects) represents a small decline of up to  $-0.05$  cumecs in the most exposed cloud forests and the upper reaches of the streams that emanate from them. At a larger scale, the evapotranspiration effect takes over and streams show an increase in flow of a fraction of a cumec, incrementing downstream to near half a cumec for the largest rivers.

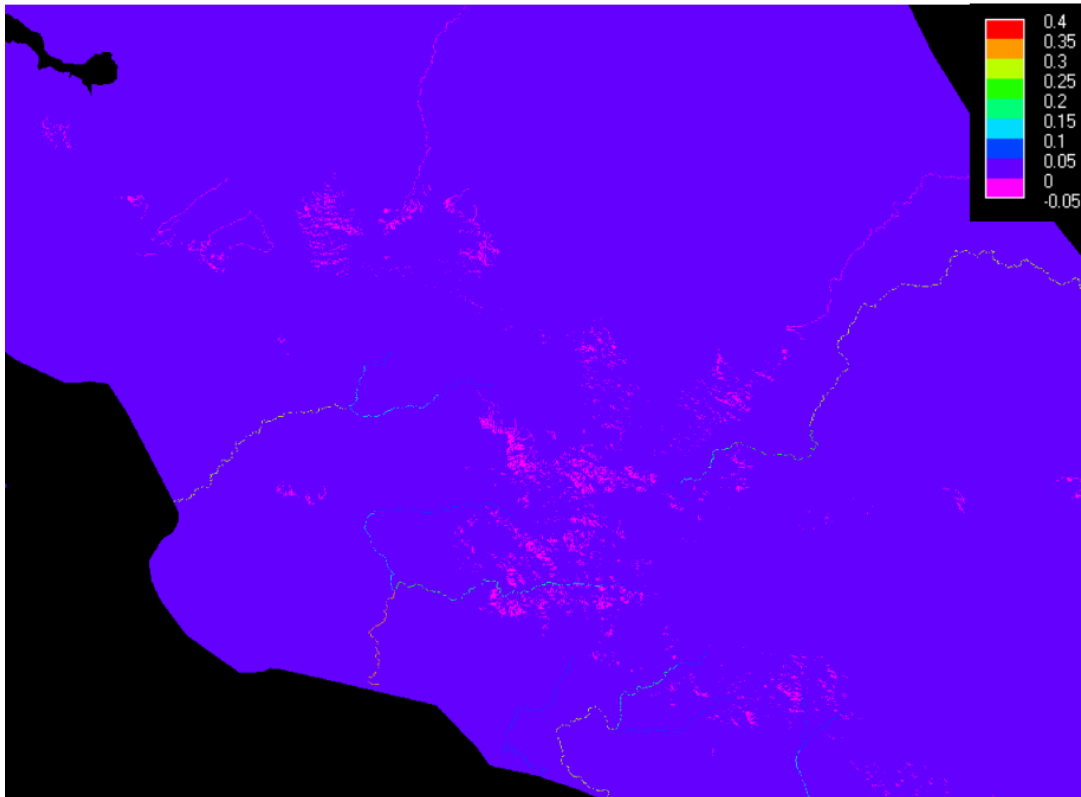


**Figure 114 Difference in runoff between the baseline and unprotected cloudforest only removed scenarios (cumecs)**

#### 4.15.4 Climate change

In the climate change scenario Costa Rica is subjected to the decrease in rainfall and increase in temperature projected by the current generation of climate models. The main effect of climate change on fog inputs accrues from the change in lifting condensation level that results from higher temperatures (the lifting cloud base level). This is evidenced in Figure 115 which shows the change in fog inputs as a result of the climate change scenario. Essentially fog inputs are reduced in a narrow band of altitudes as the cloud base levels rise. The reductions in fog input are mainly a few mm but can be more, up to  $-70\text{mm}$  but are mainly around  $-10 \text{ mm/yr}$ .

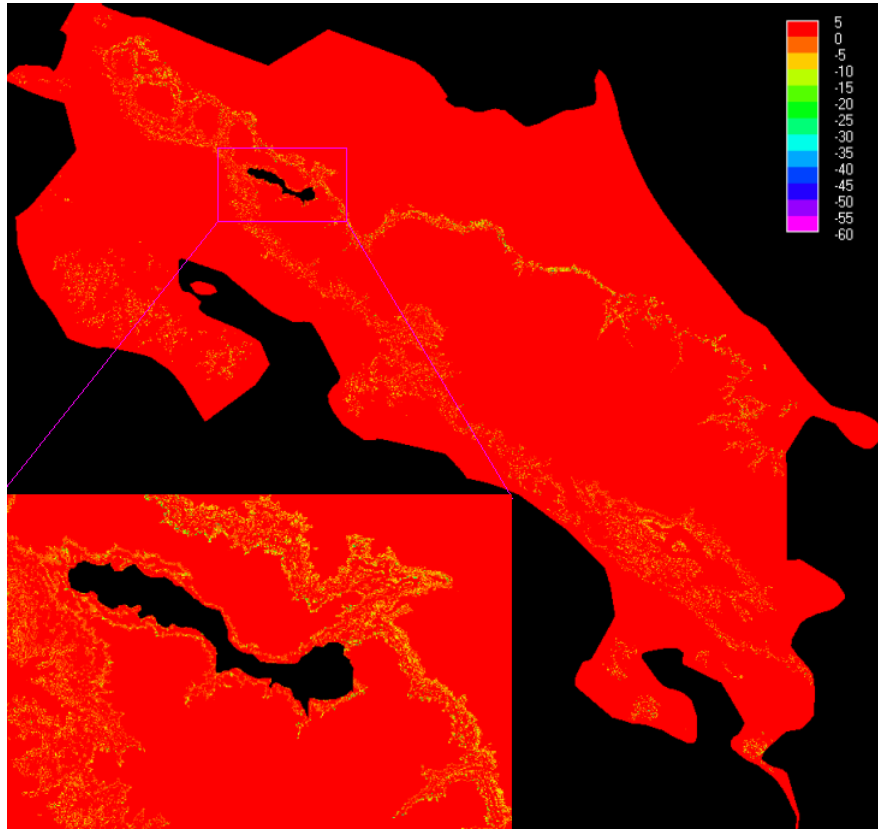


**Figure 115** Difference in fog inputs between the baseline and the climate change scenarios (mm/yr).

Climate change also affects evapo-transpiration in two ways in this model, first areas in which the cloud base has risen receive more insolation and thus evapotranspiration increases, secondly the increased temperatures increase the atmospheric demand for water. These are both clear from Figure 116 which shows overall increases in evapotranspiration of 10-20 mm/yr across most of the country but 20-25 mm/yr in areas which have seen a rise in the cloud base and thus less fogginess (but not necessarily less cloud cover in the atmosphere). Since fog reduces radiation inputs more than atmospheric cloud, this becomes significant. . The areas showing the least change in evapotranspiration (<10mm) are the cloudiest peaks, which are radiation limited and have low ground temperatures which - even with climate change - do not become high enough to have a significant impact on atmospheric demand for water vapour.

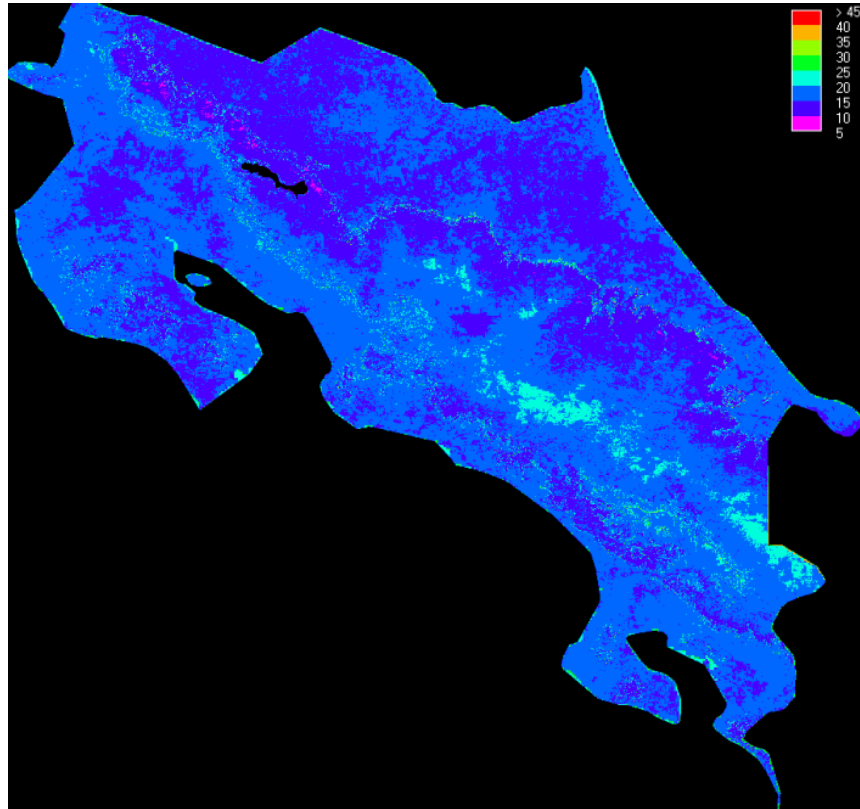


**Figure 116** Difference in evapotranspiration between the baseline and the climate change scenarios (mm/yr)

The differences in water balance (Figure 117) largely reflect climate change induced rainfall declines (which have a much greater effect than the temperature or cloud base changes). Thus the overall water balance decline is 100 to 150 mm/yr with greater changes (around -300 mm/yr) on rainfall exposed slopes and lesser changes (-100 mm/yr) on sheltered slopes. So the wettest patches in the landscape dry out proportionally the same as the drier areas. Though there will be other impacts of climate change (affecting wind speeds, radiation inputs, storminess) projections for these are not available at this scale for Costa Rica and the main hydrological impacts are likely to be driven by rainfall and temperature (as considered here).

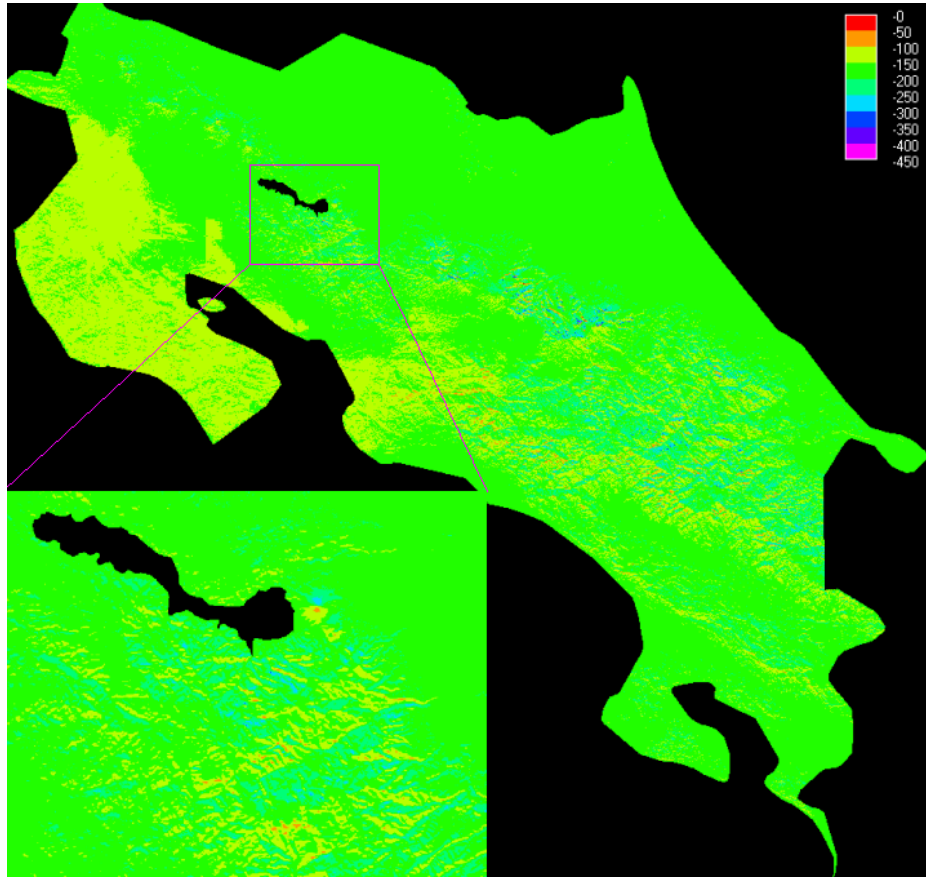


**Figure 117** Difference in water balance between the baseline and the climate change scenarios (mm/yr)

The overall impact of this climate change on runoff and fog contributions to runoff is shown in Figure 118 and Figure 119. Fog contributions to runoff fall locally in the area within which the cloud base height has lifted (the whole zone above the minimum cloud base) and these declines (of the order of  $-0.000005$  cumecs) aggregate and propagate downstream along rivers with significant presence in this zone. The impacts of climate change on runoff are substantial and result in decreases in flow of  $-21$  cumecs downstream for many of the larger rivers on both Atlantic and Pacific sides and  $-28$  cumecs for some (Figure 119).

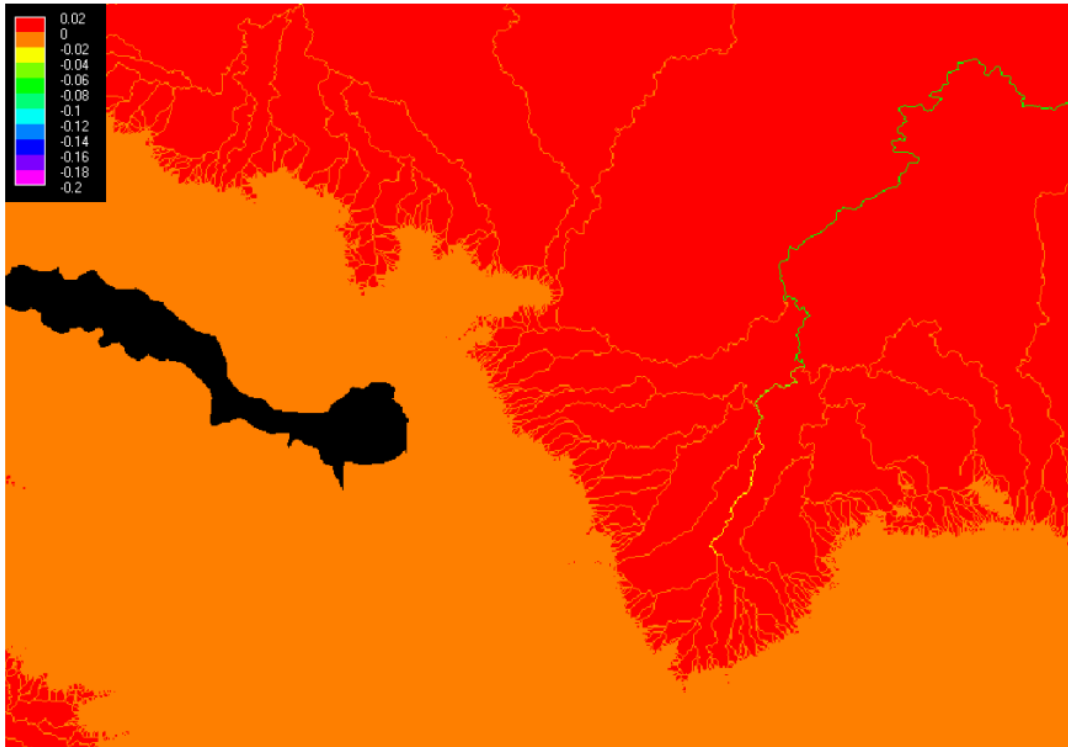


**Figure 118 Difference in fog contributions to runoff between the baseline and the climate change scenarios (cumeecs)**

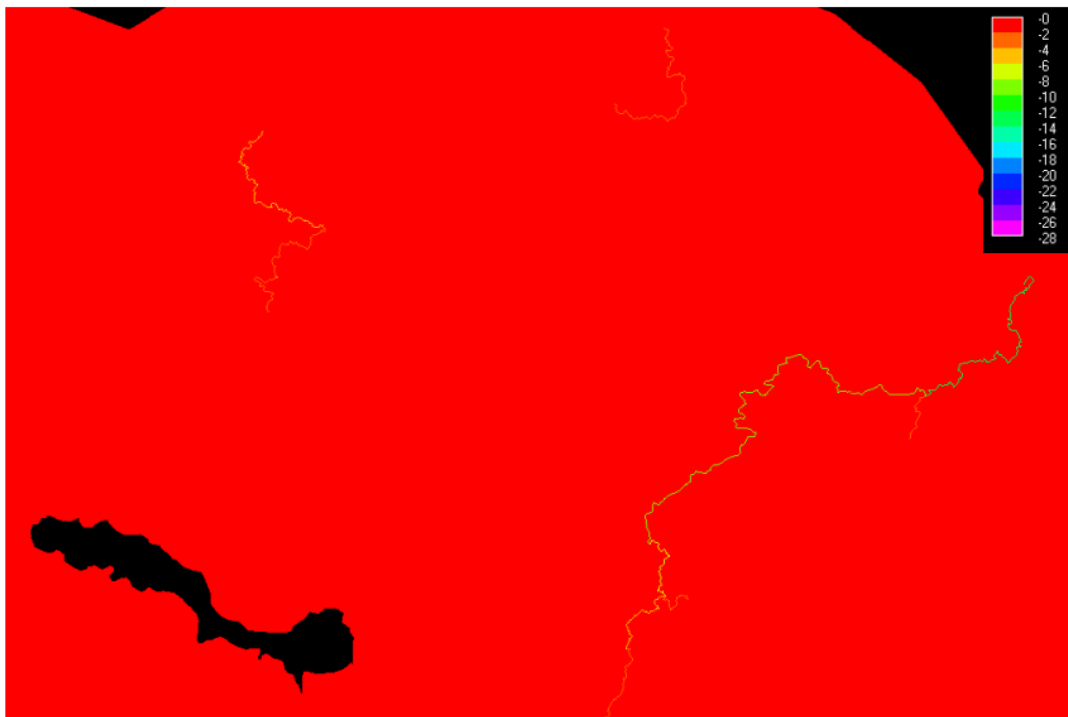


**Figure 119 Difference in runoff between the baseline and the climate change scenarios (cumeecs)**

#### 4.16 Comparison with the work of Zadroga

One of the most heavily cited works in cloud forest hydrology is that of Zadroga (1981) who undertook a comparison of measured rainfall and runoff for a series of Atlantic and Pacific catchments in Costa Rica in order to understand the impact of fog interception. His work showed a runoff ratio (runoff/rainfall) of  $>1.0$  for July, August, September, October, November, March and April for Atlantic catchments and less than 1.0 for all months for Pacific catchments (except February and April, the dry season when flows are likely fed by the drawdown of soil moisture reserves, baseflow, instead of rainfall). Overall the mean annual runoff ratio for Atlantic catchments was 102% and Pacific catchments was 34%. Zadroga attributed the fact that more runoff was measured than rainfall received to (a) the paucity of rainfall stations on the Atlantic side and thus inability to accurately quantify rainfall inputs and (b) unmeasured inputs by fog interception on the Atlantic side. He also indicated that the density of rainfall stations was also poor on the Pacific side (in which observed runoff ratios were normal – i.e. less than 100%) so that the inadequacy of the station network might not be the only explanation. Zadroga's work is widely cited as experimental evidence of the large contribution of fog interception to flows in cloud forest environments. Other possible explanations suggested here include :

- (a) a more dense network of raingauge is necessary to quantify rainfall to highly wind exposed environments (the Atlantic slopes) than sheltered ones because of the spatial variability of non vertical (wind-driven) rainfall,
- (b) the catchments are not closed and leakage occurs into the Atlantic catchments from other, surrounding, Atlantic catchments.,
- (c) significant gauge wind losses occur on the Atlantic slopes because of high wind speeds around the raingauges
- (d) significant enhancements of rainfall to typical slopes (compared with that measured by normally sheltered gauges) occur on the Atlantic slopes because of exposure to wind driven rain which preferentially hits exposed slopes at the expense of sheltered ones (where gauges are likely to be sited)
- (e) there is some altitude based bias in the distribution of rainfall stations on the Atlantic side which means that rainfall is underestimated (Zadroga himself indicated that very few stations were present in the exposed ridges which are likely to receive most rainfall),
- (f) some combination of the above.
- (g) The Atlantic catchments have very low ET and the extra few % of runoff over rainfall results from the various measurement uncertainties in rainfall and runoff.

Mechanism (b) could account for the observed seasonality of ratios  $>100\%$  because such flows are more likely to occur in heavy rainfall months. Mechanisms (a) and (c) could account for the observed seasonality because an exposure bias would have differing effects with wind speed and rainfall (wind speed is low in most  $>100\%$  months but rainfall is high), (d) could reproduce the observed seasonality for the same reason as (c) and might explain why we have  $>100\%$  months during periods of high

rainfall, low wind (Jul-Dec) and low rainfall, high wind (Dec-Apr). Mechanism (e) could reproduce the observed seasonality if the rainfall-altitude relationship changes seasonally relative to the station locations. Mechanism (g) would tend to produce >100% ratios in months with the lowest temperatures and radiation receipts. This is not observed.

The catchments are contrasted as Atlantic and Pacific but may also have other, more significant, differences that are not to do with the ocean which they face or their forest hydrology but nevertheless are important to their hydrological comparison e.g. differences in size, soils, slope gradient, altitude, topographic exposure.

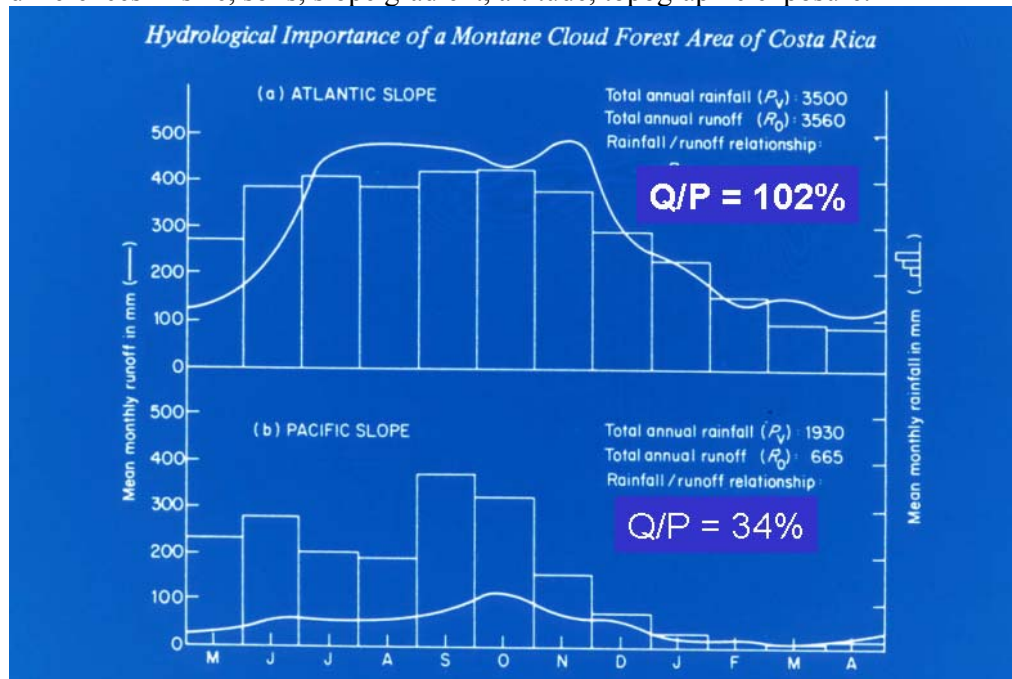


Figure 120 Runoff ratios for the Atlantic and Pacific slopes of Costa Rica, from Zadroga (1981)

In this analysis we compare the hydrological budgets estimated by Zadroga for point measurements from a series of catchments with the budgets estimated from the fiesta\_delivery model aggregated over those same catchments. The objective is to throw more process insight into Zadroga’s observations. The catchments used by Zadroga were Chiquito, Cano Negro, Penas Blancas, and Jabillos (Atlantic) and Santa Rosa, Corobici and Canas (Pacific) and are shown in Figure 121. A comparison of the catchment characteristics for the Pacific and Atlantic catchments (Table 18) indicates some considerable differences that are not necessarily to do with the ocean to which they face. The Pacific catchments are much lower (by 300m), have shallower slopes, represent half the area and have less topographically exposed (more positive TOPEX) slopes (to the known winds), though not very significantly so.

<b>Variable</b>	<b>Atlantic</b>	<b>Pacific</b>
Altitude (m)	906	607
Slope gradient (°)	14.5	9.5
Planimetric Area (km <sup>2</sup> )	547.5	254.5
True surface area (km <sup>2</sup> )	627.8	283.5
Topographic Wind Exposure (TOPEX)	3.7	5.6
Number of worldclim rainfall stations	6	5
Mean altitude of worldclim rainfall stations	1040	766
Altitude bias of stations	+134 (13%)	+159(26%)

**Table 18 Comparison of Zadroga’s Atlantic and Pacific catchment characteristics.**

Table 19 compares Zadroga’s figures for the hydrological fluxes with the figures from the delivery model averaged over the same catchments. For the Atlantic catchments Zadroga’s raw rainfall estimate is similar to that given by the delivery model. This is all the more surprising because of the paucity of WORLDCLIM rainfall stations for the delivery model in the larger and more exposed Atlantic catchments, see Figure 121. If we consider the delivery model precipitation estimates to be underestimates for the Atlantic catchments (see section 4.12.3) then we must consider Zadroga’s rainfall values to be underestimates too. It is not apparent how he arrives at these estimates because the isohyets shown in his paper (pg 65) appear to show much higher rainfall. There is also an altitude bias for both catchments with the delivery model stations being around 150m higher than the average altitude of the catchments. However Zadroga’s rainfall value is significantly lower than the delivery model estimate for the Pacific catchments (probably because we interpolate rainfall across the full range of altitudes whereas Zadroga may have used at-a-station values (though this is not clear from his paper) possibly for one of the low altitude stations on the Pacific side (Figure 121). With the wind driven rainfall (WDR) effect included, the delivery and Zadroga catchments for the Atlantic slopes become very close (within 47mm). Both are likely to be underestimates of the actual rainfall receipt for the more exposed Atlantic catchments (see section 0). Zadroga’s figures remain 633mm (25%) lower than the delivery model WDR estimate for the Pacific slopes. The wind driven rain effect on rainfall receipt in the delivery model has a small positive effect over the Atlantic catchments and a small negative effect over the Pacific ones.

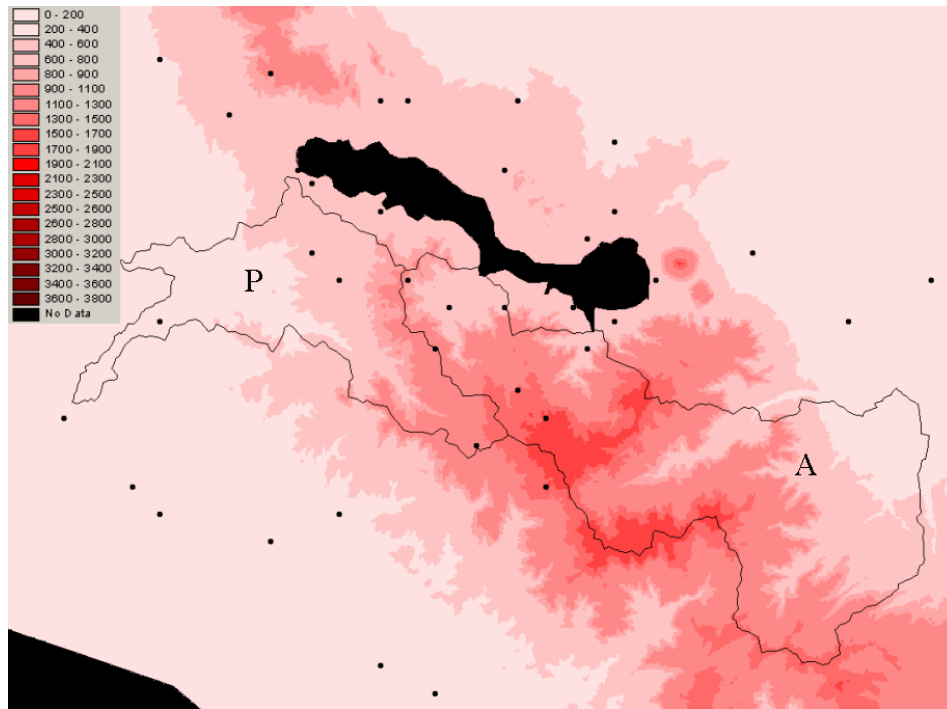


**Figure 121** Catchments used by Zadroga 1981. Dots are worldclim rainfall stations. Altitudes in m

Zadroga's measured runoff is some 599 mm (16.8%) greater than the delivery model estimate for the Atlantic slopes but some 1075 mm lower for the Pacific catchments in line with the rainfall differences between the two approaches. The difference between total precipitation and runoff (i.e. the evaporative and other losses) are negative for the Atlantic slope according to Zadroga's figures but positive to the tune of 766 mm for the delivery model figures. For the Pacific slopes calculation from Zadroga's figures produce an estimate for evapotranspiration of 1265, some 349 mm/yr greater than those of the delivery model but then Zadroga's rainfall for these catchments is much lower than that of the delivery model. The exact stations used and methods of mean rainfall calculation are never precisely given in his paper, though a map of isohyets and an actual evapotranspiration surface (Thornthwaite methodology), produced by ICE at scale 1:500000, are given. A visual inspection of the evapotranspiration map indicates that the Pacific catchments lie mainly between the 700 and 1000mm contours so the origin of Zadroga's 1265 mm (rainfall-runoff) is unclear. Zadroga does not attempt to reconcile the observed rainfall and runoff with the ICE evapotranspiration figures in order to close the budget ( $\text{Runoff} = \text{Rainfall} - \text{ET}$ ). If he did he might have found that the ICE figures and the budget figures did not agree. The Thornthwaite method is likely to underestimate ET in cloudy and foggy environments in which temperatures remain fair but incoming radiation is significantly reduced.

Runoff ratios are calculated for the delivery model separately for all effects combined (using total precipitation), for raw rainfall only (using the input rainfall data), for wind driven rainfall and for wind driven rainfall and fog combined in order to examine the effect of each aspect. Incorporating all effects the delivery model runoff ratio for Atlantic catchments is 87.3% compared with Zadroga's 102%. For Pacific catchments the delivery model estimate is 67.4% compared with 35% for Zadroga.

For the Atlantic slopes the contribution of fog inputs to the ratio as estimated by the delivery model is +5.3 % whereas the contribution of the wind driven rain effect is +3.7%. For the Pacific slopes the WDR effect contributes -0.1% to the ratio whereas fog contributes +3.1%. The delivery model runoff ratio is thus 14.7% lower than Zadroga's estimate for the Atlantic catchments and 32.4% higher for the Pacific catchments.

These differences may be due to differences in the definition of the catchments but are more likely the result of differences in the representation of spatial variability between the two approaches (and thus real differences). We have shown that if the delivery model results are reasonable Zadroga's 102% **cannot** be the result of:

- (a) fog inputs to the Atlantic (which are small),
- (b) wind driven rain effects (which are also relatively small)
- (c) zero evaporation rates in the Atlantic (very unlikely given the results presented)

That leaves the following possibilities if the 102% is true:

1. Both Zadrogas and the delivery rainfall interpolations are significant underestimates of the reality for the Atlantic as a result of gauge wind losses which are not accounted for in either approach.
2. As above but because of an inadequate density and bias of stations which becomes all the more important where rainfall is highly spatially variable (e.g. because of wind driven rain effects on the Atlantic slopes). The analysis of Table 9 does indicate that Costa Rica's stations tend to be underexposed and at higher altitude than the landscape in general. Figure 121 indicates that the stations used by the delivery model and likely also by Zadroga are dominantly in the more sheltered parts of the Atlantic catchments and there are very few.
3. There are subterranean inputs to the Atlantic catchments flows from other catchments (leakage)

Either 1 or 2 are most likely and require further study. It is thus likely that the 102% is incorrect and simply the result of rainfall stations underestimating rainfall receipt in this highly spatially variable environment. Moreover these catchments are montane, headwater catchments and any runoff ratio >1 is unlikely to be maintained further down the river networks into the lowlands (as shown previously) and that fact is also important to bear in mind when discussing the implications of Zadroga's work.

From the delivery model, fog inputs are surprisingly not all that different between Zadroga's Pacific and Atlantic catchments (185.8mm/yr for the Atlantic catchments compared with 79.4 for the Pacific catchments). There are hotspots of fog in the Atlantic catchments (Figure 122) because of exposure to fog impaction as well as deposition, whereas deposition occurs everywhere except in the lowest parts of the Pacific. Though the Atlantic catchments are cloudier, the Pacific catchments are also cloudy 50-70% of the time (Figure 123) so the two sets of catchments are not that different in terms of cloud inputs as might first appear (though they are in terms of rainfall).

VARIABLE (all mm/yr)	ZADROGA	DELIVERY
<b>ATLANTIC</b>		
RAIN	3500	3393
RAIN (with wind effect), WDR	n/a	3542
TOTALPREC <sup>20</sup>		3727
RUNOFF	3560	2961
”EVAP” <sup>21</sup>	-60	766
RATIO (including fog and wind effects i.e. runoff/totalprec) %	102	87.3
Ratio (fog effect only , i.e. runoff/WDR) %		83.6
Ratio (neither fog nor wind included i.e. runoff-fogtotal/(WDR)) %		78.3
Contribution of WDR effect( %)		+3.7
Contribution of fog effect(%)		+5.3
<b>PACIFIC</b>		
RAIN	1930	2575
RAIN (with wind effect), WDR		2572
TOTALPREC		2652
RUNOFF	665	1736
”EVAP”	1265	916
RATIO (all effects) %	35	67.4
Ratio (fog only effect) %		67.5
Ratio (no fog no wind) %		64.4
Contribution of WDR effect(%)		-0.1
Contribution of fog effect(%)		+3.1

**Table 19 Comparison of the work of Zadroga (1981) with the fiesta\_delivery model.**

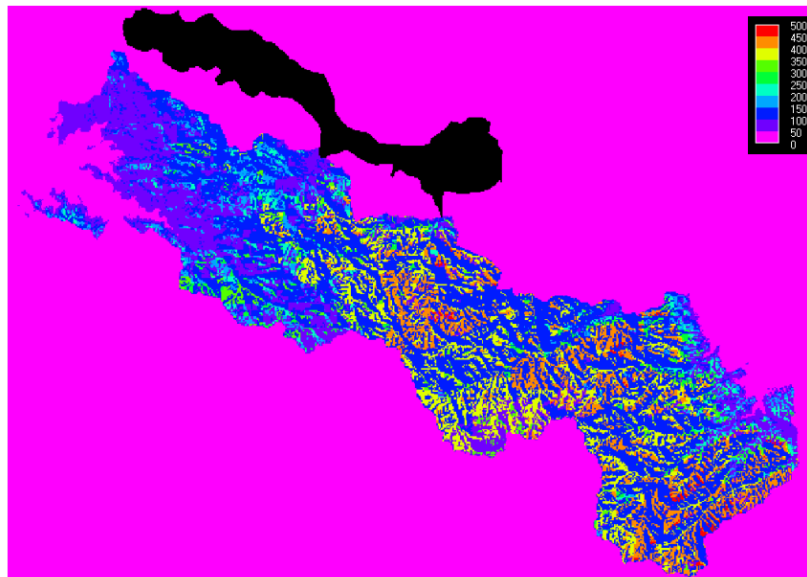


**Figure 122 Annual fog inputs to Zadroga’s catchments(mm)**

<sup>20</sup> WDR+fog

<sup>21</sup> TOTALPREC-RUNOFF

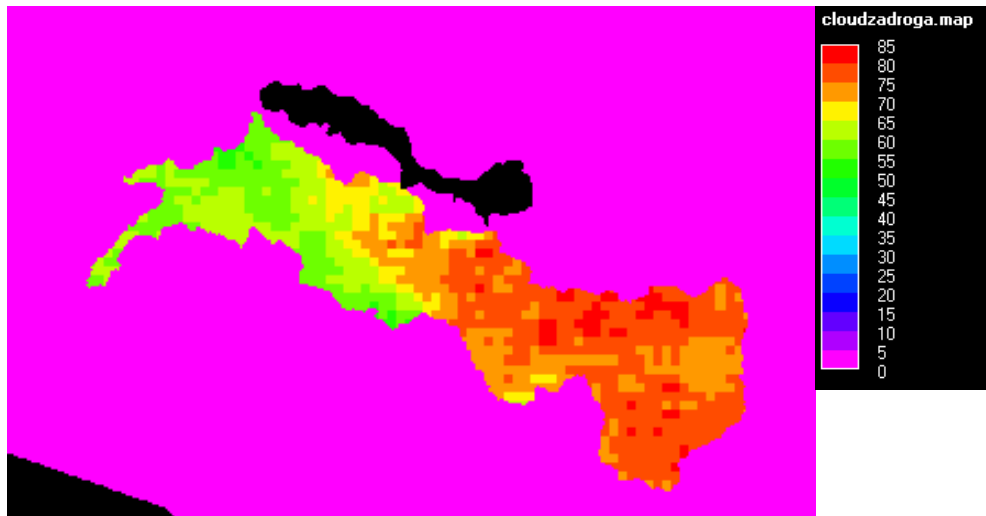


**Figure 123 Measured frequency cloud cover to Zadroga's catchments (%)**

We now compute the runoff ratio (runoff/measured rainfall) for the delivery model for all of the subcatchments of Costa Rica (subcatchments are defined from all confluences of Strahler order >5). Clearly the lowest runoff ratios (30-50%) coincide with the high evaporation areas of Guanacaste (Figure 124). The remaining Pacific catchments have ratios 50-70% as do lowland Atlantic catchments. Upland Atlantic catchments have ratios 80-100% with some of the higher altitude small catchments reaching 90-100% (indicating low evaporation and high inputs of WDR and fog compared with the rainfall gauge catches). Zadroga's catchments are thus typical of Atlantic and Pacific conditions in Costa Rica. The higher of these ratios are likely to be overestimates because of underestimate of rainfall (even with WDR and fog added) rather than high magnitudes of fog inputs (which are contributing only a few % to the ratios even in the most exposed catchments).

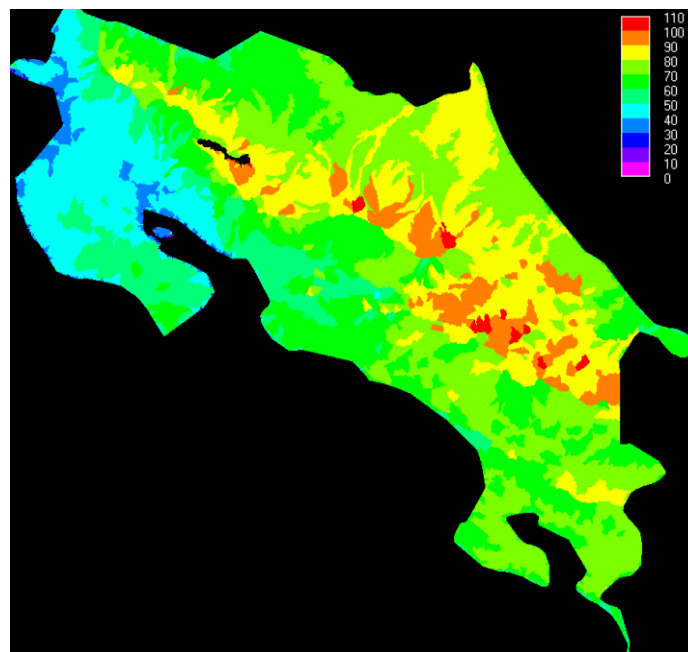


**Figure 124 Runoff ratio for national subcatchments (%)**

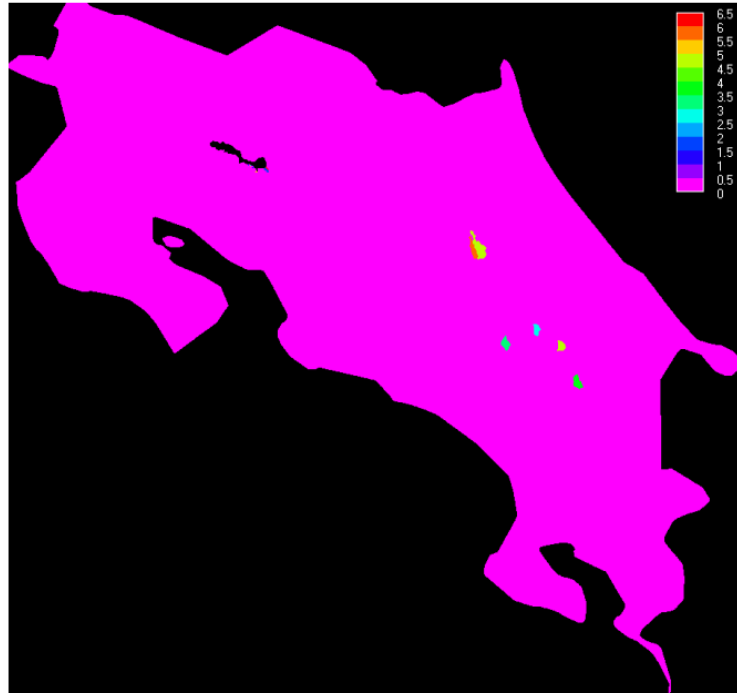


**Figure 125 Catchments with runoff ratio greater than 100% (compared with measured rainfall) and percentage over 100%**

A few small catchments do have ratios a few % over 100% (Figure 125), these are rare, high rainfall, highly exposed Atlantic subcatchments and the high ratio has more to do with underestimated wind driven rainfall receipt than fog receipt.

#### **4.17 Extending Zadroga’s analysis across Costa Rica**

We will now extend the analysis that Zadroga made across a series of other gauged catchments throughout the country (which we previously used in model validation). We thus calculate the runoff ratio on the basis of measured (and later modelled) runoff for these catchments in relation to the best estimate for their spatial rainfall inputs (provided by the delivery model). We remember that these rainfall estimates are likely underestimates for some highly exposed, high altitude Atlantic catchments.

Table 20 shows the results for 17 catchments. The runoff ratios calculated are similar conceptually to those calculated by Zadroga since they use measured runoff and interpolated rainfall on a catchment basis for Pacific and Atlantic catchments. The only difference is that the rainfall values used here are spatialised wind driven rainfall based on the worldclim surfaces interpolated from the local gauges (between 0 and 4 per catchment) rather than the as yet unclear source of rainfall data used by Zadroga. We have seen from the Penas Blancas validation that these rainfall totals may be underestimates for some high altitude, exposed Atlantic catchments with few or no gauges but as we showed in the previous sections, Zadroga’s rainfall estimates are also likely to be underestimates in those areas.

Catchment name	Station		Runoff ratio (measured, planimetric)	Runoff ratio (measured, true area)	Runoff ratio (modelled)	Runoff ratio error
BARRANCA	GUAPINOL	Pacific	0.4	<b>0.4</b>	0.7	0.33
CANAS	LIBANO	Pacific	0.3	<b>0.3</b>	0.7	0.42
COLORADO	COYOLAR	Pacific	0.3	<b>0.3</b>	0.5	0.21
COTO BRUS	CARACUCHO	Pacific	0.5	<b>0.6</b>	0.7	0.13
GENERAL	LA CUESTA	Pacific	0.7	<b>0.6</b>	0.8	0.16
GRANDE DE CANDELARIA	EL REY	Pacific	0.5	<b>0.5</b>	0.6	0.13
LAGARTO	YOMALE	Pacific	0.4	<b>0.3</b>	0.6	0.28
NARANJO	LONDRES	Pacific	<b>1.2</b>	<b>1.2</b>	0.8	-0.44
PIRRIS	BIJAGUAL	Pacific	0.8	<b>0.9</b>	0.7	-0.19
<b>Mean</b>			0.57	<b>0.57</b>	<b>0.68</b>	<b>0.11</b>
BANANO	ASUNCION	Atlantic	1.2	<b>1</b>	0.94	-0.06
BARBILLA	BARBILLA	Atlantic	1	<b>1</b>	0.85	-0.15
CHIRRIPO	PLAYA HERMOSA	Atlantic	0.6	<b>0.6</b>	0.90	0.30
ESTRELLA	PANDORA	Atlantic	0.7	<b>0.7</b>	0.78	0.08
PACUARE	PACUARE	Atlantic	0.5	<b>0.5</b>	0.93	0.43
PEJIBAYE	EL HUMO	Atlantic	0.8	<b>0.8</b>	0.96	0.16
SARAPIQUI	CARIBLANCO	Atlantic	1.1	<b>1.1</b>	0.91	-0.19
TORO	VERACRUZ	Atlantic	1.1	<b>1.1</b>	0.90	-0.20
<b>Mean</b>			0.88	<b>0.85</b>	<b>0.90</b>	<b>0.05</b>

Table 20 Runoff ratios for Pacific and Atlantic catchments in Costa Rica.

In this analysis based on measured data we find relatively little difference between runoff ratios where the runoff is calculated on the basis of planimetric or true area. The average measured runoff ratio for Pacific catchments is 57% compared with Zadroga’s 34.5. The measured ratio for Atlantic catchments is 85% compared with Zadroga’s 102%. The delivery model rainfall estimates for Zadroga’s Pacific catchments were greater, which would tend to produce a lower runoff ratio, yet the measured ratios based on delivery model rainfall estimates here produce runoff ratios which are higher than Zadroga’s.

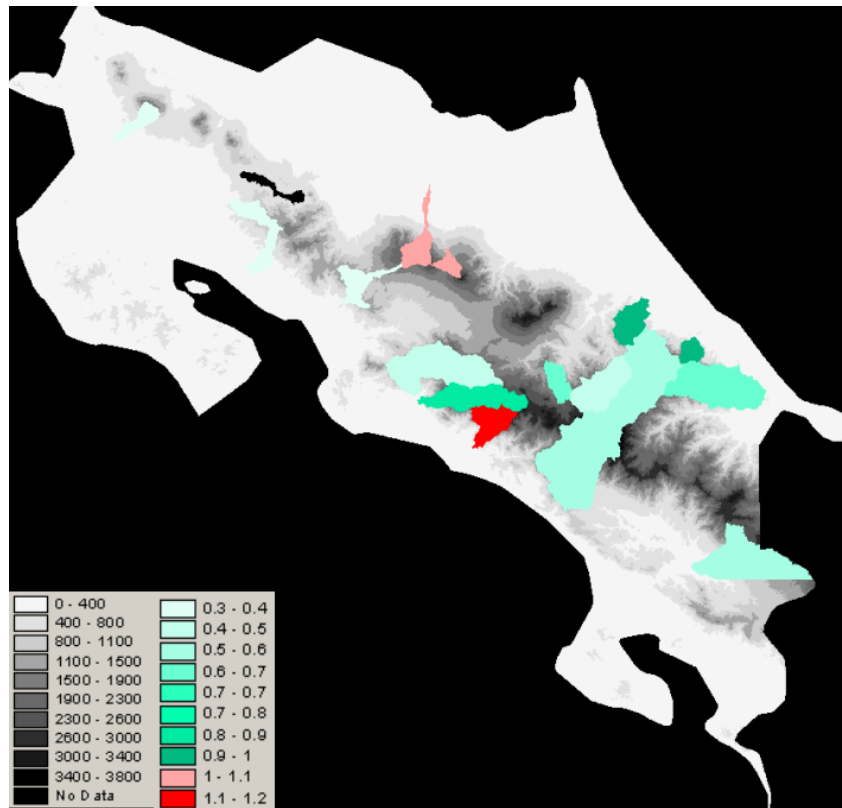
We find no evidence for an average ratio > 100% for the Atlantic (at least on an annual, rather than seasonal) basis. With measured ratios of 85% on average, to reach ratios >100%, we would need evaporation to be close to zero **and** rainfall to be significantly overestimated (though the reverse is more likely) or fog inputs to be >>15% (531 mm/yr for these catchments with their average wind driven rainfall of 3542 mm/yr). Both seem unlikely and the average measured runoff ratio of 85% being correct seems more plausible. Three out of seventeen catchments do have ratios >1, the Naranjo in the Pacific and the Sarapiqui and Toro in the Atlantic (though the upper reaches of others may also have). All of these ratio >1 stations are based on interpolated rainfall data with no or only one stations in the catchments themselves which may result in a rainfall underestimation since they are also high altitude, exposed and cloudy catchments. The ratios >1.0 are thus not likely to be real and if so are even less likely to be the result of fog inputs. Figure 126 shows the distribution of catchment runoff ratios.

Table 21 shows the physical characteristics of these catchments in relation to others. Naranjo is the cloudiest Pacific catchment with cloud frequencies similar to many of

the Atlantic catchments. It is also one of the highest altitude Pacific catchments but has the lowest modelled fog inputs for the Pacific catchments because it is also the least exposed of the Pacific catchments. It is a medium-large catchment (210 km<sup>2</sup>) and must have a measured ratio >1 because of underestimation of rainfall inputs or poor runoff data. The Sarapiqui is a smaller catchment also high altitude, high cloud cover and fog inputs and wind exposed. The Toro has one of the highest cloud cover frequencies, high altitude, high wind exposure and high fog inputs. It is possible that these last two stations have high runoff ratios (because of these characteristics) even if the input rainfall were not underestimated, but it seems unlikely that they would be >1. It seems clear that the very type of catchments in which forest *could* lead to enhanced runoff ratios (though fog interception) compared with pasture are usually lacking in rainfall gauges and underestimate rainfall inputs which may make it appear that they have high fog inputs even when they do not. If ratios are >1 it is likely to be because of underestimation of rainfall, low evaporation and high (unmeasured) wind-driven rain inputs more than because of high fog inputs.

Catchment name	Station		WORLDCLIM climate stations	Cloud frequency (%)	Altitude (masl)	Difference between input and WDR (mm/yr)	Fog inputs (mm/yr)	Mean exposure (TOPEX)	Total precipitation (mm/yr)	Absolute error (model-measured)	Relative error(model-measured/measured) %
<b>CANAS</b>	<b>LIBANO</b>	<b>Pacific</b>	<b>2.0</b>	<b>60.4</b>	<b>798.3</b>	<b>-45.8</b>	<b>140.9</b>	<b>7.2</b>	<b>2811.4</b>	<b>872.6</b>	<b>74.5</b>
<b>COLORADO</b>	<b>COYOLAR</b>	<b>Pacific</b>	<b>2.0</b>	<b>56.4</b>	<b>676.9</b>	<b>15.9</b>	<b>110.0</b>	<b>5.7</b>	<b>2734.6</b>	<b>1124.9</b>	<b>135.3</b>
<b>COTO BRUS</b>	<b>CARACUCHO</b>	<b>Pacific</b>	<b>4.0</b>	<b>61.6</b>	<b>1244.3</b>	<b>-108.8</b>	<b>79.4</b>	<b>8.7</b>	<b>2118.6</b>	<b>372.9</b>	<b>53.2</b>
GENERAL	LA CUESTA	Pacific	4.0	65.8	1414.3	-134.8	101.9	9.7	3406.7	659.8	36.4
GRANDE DE CANDELARIA	EL REY	Pacific	4.0	61.2	1136.4	-165.8	109.0	11.7	3612.9	527.2	23.6
LAGARTO	YOMALE	Pacific	1.0	56.7	519.9	16.3	109.9	10.5	2084.7	223.3	20.7
<b>NARANJO</b>	<b>LONDRES</b>	<b>Pacific</b>	<b>0.0</b>	<b>69.6</b>	<b>1318.0</b>	<b>-60.3</b>	<b>48.4</b>	<b>7.8</b>	<b>2420.9</b>	<b>579.1</b>	<b>70.3</b>
PIRRIS	BIJAGUAL	Pacific	2.0	63.4	1659.6	-114.0	113.8	14.6	3241.1	1206.0	-33.0
BANANO	ASUNCION	Atlantic	0.0	76.1	884.1	-25.6	111.2	12.1	2698.7	-419.9	-17.9
BARBILLA	BARBILLA	Atlantic	0.0	74.0	650.0	322.5	189.6	0.3	3455.6	-573.9	-15.0
CHIRRIPO	PLAYA HERMOSA	Atlantic	3.0	70.1	1575.2	151.7	151.4	3.4	3309.3	-728.9	-20.5
<b>ESTRELLA</b>	<b>PANDORA</b>	<b>Atlantic</b>	<b>3.0</b>	<b>71.9</b>	<b>596.2</b>	<b>210.3</b>	<b>156.7</b>	<b>6.7</b>	<b>3583.7</b>	<b>1003.1</b>	<b>45.4</b>
PACUARE	PACUARE	Atlantic	4.0	69.9	1701.5	12.5	90.7	8.3	3157.8	322.4	15.2
<b>PEJIBAYE</b>	<b>EL HUMO</b>	<b>Atlantic</b>	<b>4.0</b>	<b>71.6</b>	<b>1556.6</b>	<b>288.9</b>	<b>162.6</b>	<b>3.4</b>	<b>4167.9</b>	<b>1485.9</b>	<b>62.0</b>
SARAPIQUI	CARIBLANCO	Atlantic	1.0	68.0	1851.5	372.0	163.8	6.6	4768.5	713.5	18.5
TORO	VERACRUZ	Atlantic	0.0	73.0	1326.7	299.6	187.5	-3.2	3426.0	-815.6	-20.7

Table 21 Relationships between model error and catchment characteristics.



**Figure 126 Measured runoff ratios for Costa Rican catchments**

For comparison we also include in Table 20 the runoff ratio as calculated by the delivery model as modelled runoff/measured (input) rainfall. The values are higher than the measured values for the Pacific catchments (because modelled runoff is higher than the measured value).

#### 4.18 International patterns

In this next set of simulations we apply the 1km resolution version of the same delivery model to a much larger area using the same baseline datasets in order to place the Costa Rican conditions within a continental context so as to better generalise the results from the model to other environments and conditions, place the Costa Rican results in context and extrapolate more intelligently than by generating rules of thumb based on the Costa Rican conditions. With sufficient time and computing resources, the same could be achieved for the whole tropics. We will first examine the baseline outputs and then apply an historic land use scenario in order to better understand the impact that recent land use change in the region has had on water resources.

Figure 127 shows the absolute volumes of fog input for the region. Fog inputs are high in montane Costa Rica but comparable with montane N Panama, Colombia, Venezuela, Honduras and Guatemala. Inputs are lower in Mexico (but contribute a greater proportion of runoff because of lower rainfall and higher evapotranspiration in Mexico). The highest inputs occur in particular in wind exposed areas (from the Atlantic in central America but from the Pacific in S Mexico and Colombia). The highest observed values are around 320 mm/yr.

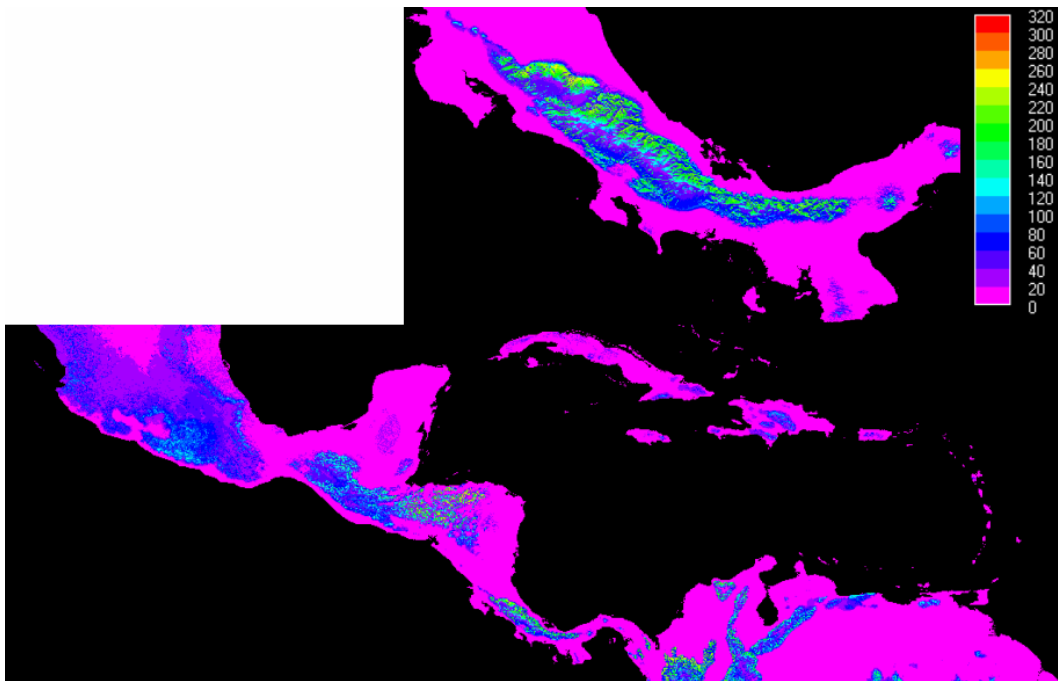


**Figure 127 Annual fog inputs for central America with detail for Costa Rica (mm/yr)**

Figure 128 shows the fog contribution to runoff. Costa Rica is at the low end of the spectrum for fog contributions to runoff. Even though its absolute fog contributions are similar or higher to those for other countries, they are dwarfed by the rainfall inputs so that even in the foggiest parts of Costa Rica fog inputs are less than 10% of runoff. Other countries have much more extensive (Mexico), intensive (Venezuela) or both (Honduras) contributions by fog. In parts of Venezuela, Honduras and

Mexico, contributions up to 15% are common with smaller areas having fog contributions to runoff in excess of 25% locally.

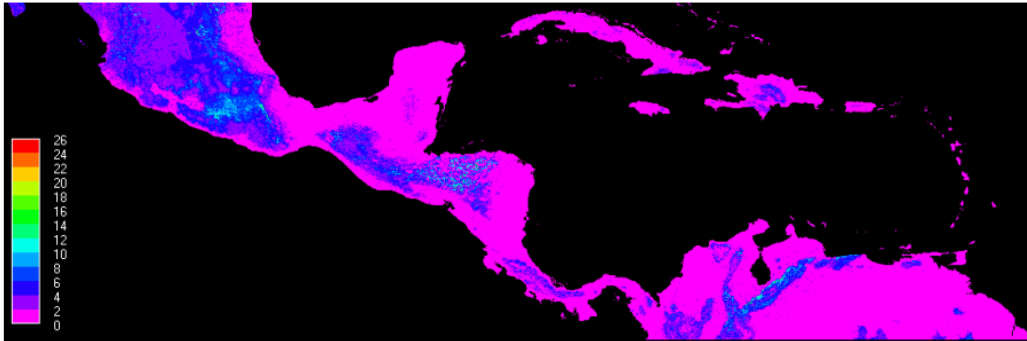


**Figure 128 Proportion of runoff derived from fog for Central America**

The following figures provide more detail on the regional patterns of fog contributions to runoff. The legends differ and are set to highlight differences in the lowland river system contributions. Fog volumes are only significant (around 6%) locally to cloud forest areas and propagate relatively little downstream because they are swamped by higher magnitude or area lowland rainfall. Rivers with significant presence in cloud forest zones e.g. the Monteverde-Arenal cloud forests have fog contributions around 3% in their upper reaches and 1.5% further downstream.

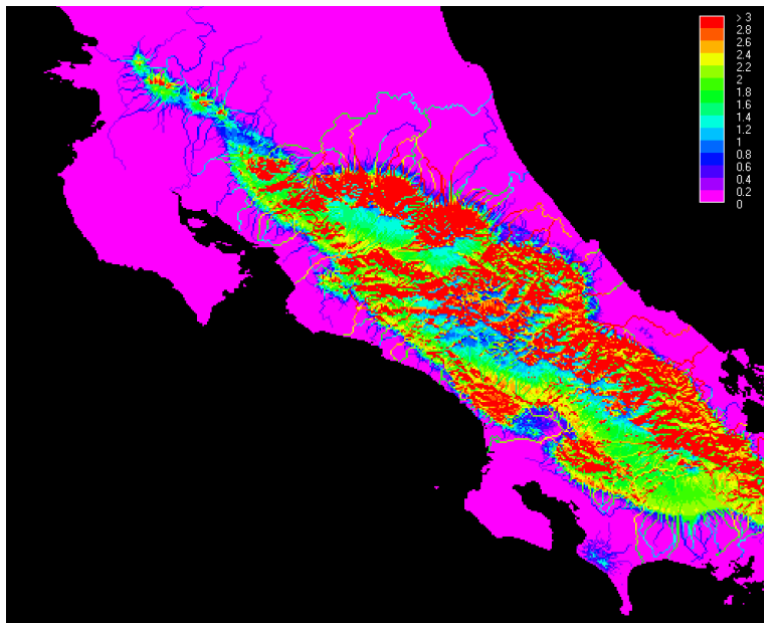


**Figure 129 Percentage of runoff derived from Fog – Costa Rica**

The situation in Honduras (Figure 130) is somewhat different with local fog contributions to runoff being 10-25% in exposed areas and 8-10% for the upper reaches of many rivers and fog representing 2-5% of the flow of most large rivers all the way to their Atlantic outlets. Fog is thus a much more significant contribution to water resources in Honduras than in Costa Rica.

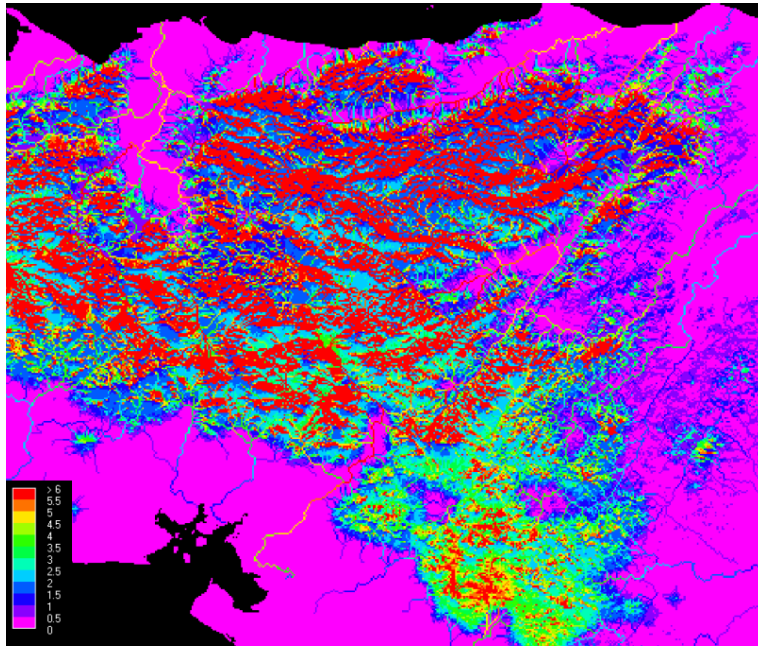


**Figure 130 Percentage of runoff derived from fog -Honduras**

The situation is similar for Guatemala (Figure 131) with fog contributions to runoff representing up to 10-25% in localised highly exposed areas, 5% over much of mountain zone but contributions being dwarfed by rainfall outside of the cloud forest areas so that fog contributes less than 4% to the upper reaches of some rivers but <2% downstream of these reaches.

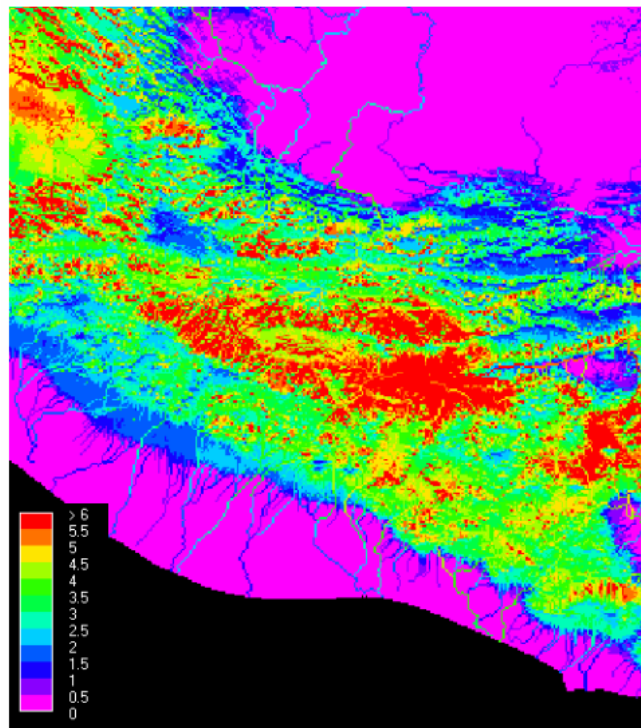


**Figure 131 Percentage of runoff derived from fog - Guatemala**

Southern Mexico has fog contributions to runoff concentrated in the Chiapas uplands with some isolated areas of 8-10% contribution but mainly 4-6% of runoff is fog in the uplands. This contribution is soon dwarfed by rainfall for most rivers but fog is 3-4% of flows for most of the course of the Quiotepec river.

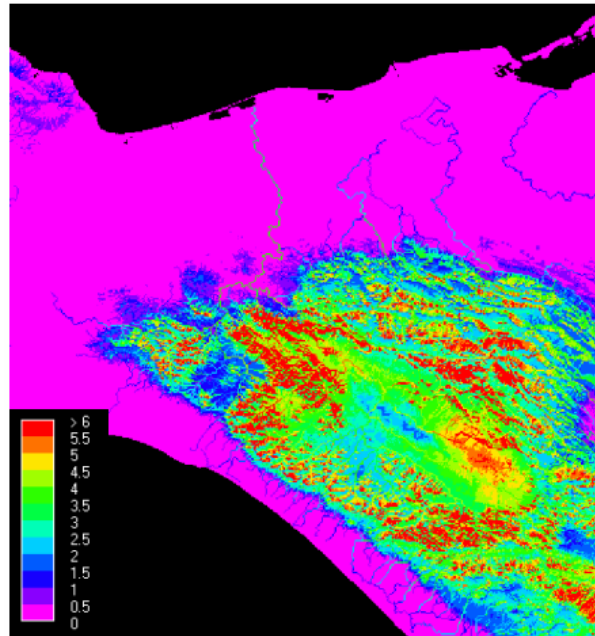


**Figure 132 Percentage of runoff derived from fog - Southern Mexico**

For Northern Mexico fog contributions are in excess of 10-12% for some isolated zones and 2-4% or 4-6% throughout much of the Mexican uplands. Again contributions are only significant in the upper reaches of most rivers but 5% for the whole course of some rivers e.g. the Rio Tepalcatepec draining into the Pacific.

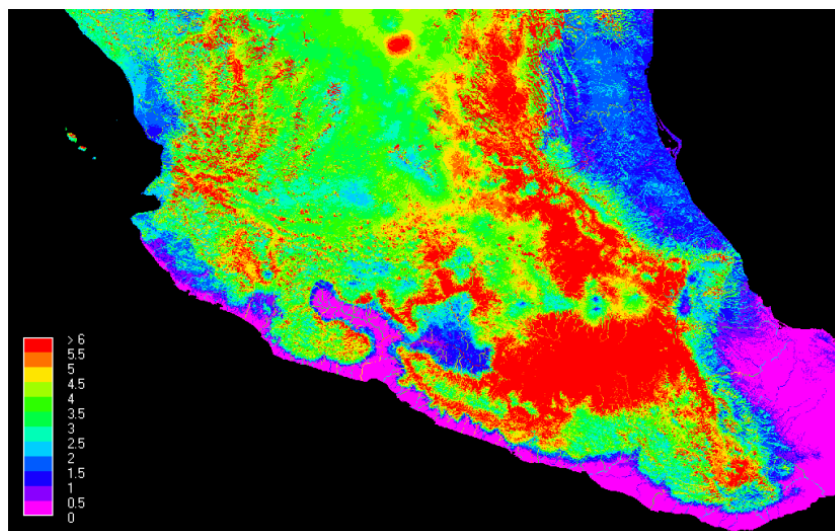


**Figure 133 Percentage of runoff derived from fog : Northern Mexico**

For N Colombia and Venezuela fog contributions to runoff are highest in eastern Cordillera especially in Venezuela with local contributions in excess of 10% and a

contribution of 3-10% in the upper reaches of most rivers draining from the cordillera into the Llanos or Caribbean. High contributions are also observed on the western and northern flanks of the Sierra Nevada de Santa Marta (Figure 134). The rivers of the Llanos receive a few percent of their flows from the surrounding cloud forests.

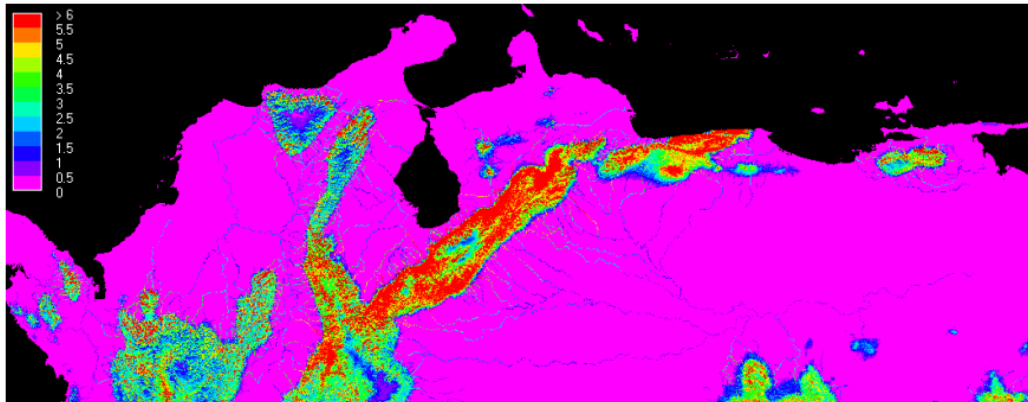


**Figure 134 Percentage of runoff derived from fog : N Colombia and Venezuela**

The overall contribution of fog to runoff in the Caribbean islands is shown in Figure 135. The highest contributions are to be found in eastern Cuba and Jamaica, in Haiti and the Dominican Republic and in the Puerto Rican highlands, but these values are still only 5-6%.

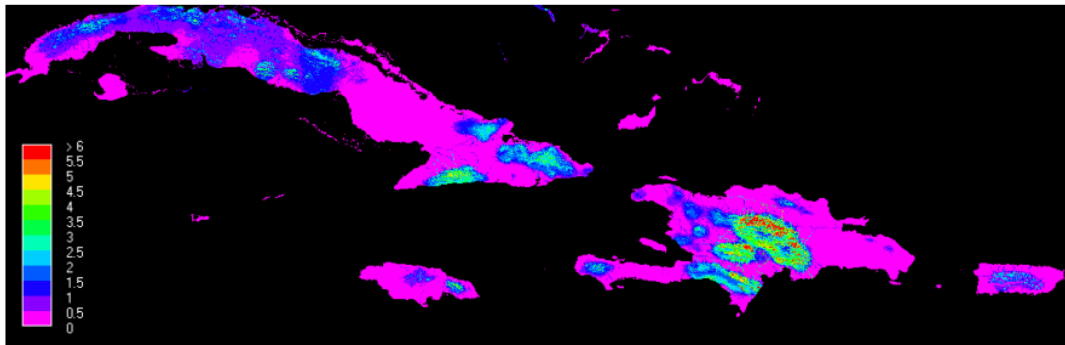


**Figure 135 Percentage of runoff derived from fog : Caribbean islands**

#### 4.18.1 Seasonal patterns

As we did with the national scale model, we will now look at the seasonal (monthly) variation in fog contributions to runoff since even if fog contributions are not significant towards annual totals they may be seasonally important. Figure 136 to Figure 147 show monthly fog contributions to runoff (%) for the region. Seasonality is clearly apparent and at greater magnitudes than we saw for Costa Rica. In January we have fog contributions of 15-20% for much of upland southern Mexico, >30% for the Guatemalan highlands and 15-20% in exposed areas through Honduras, Costa Rica, Colombia and particularly Venezuela.

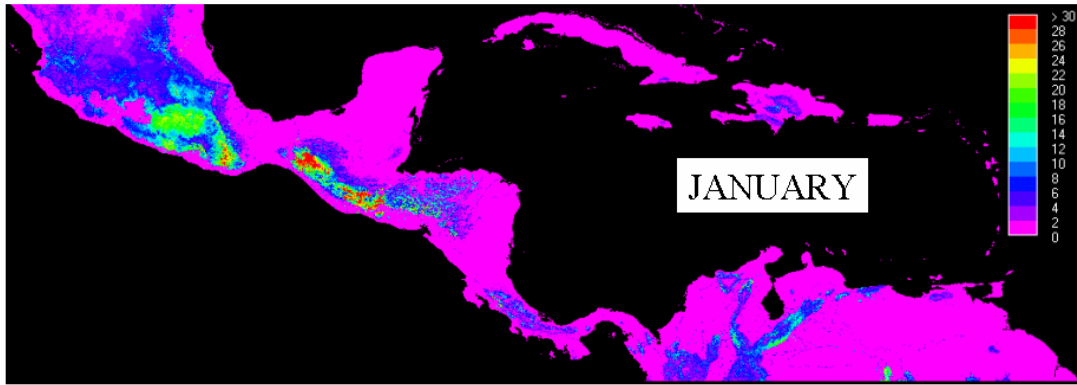


**Figure 136 Fog runoff contributions to rainfall generated runoff : January**

The same spatial pattern exists in February and March though magnitudes are higher (>30%) in Mexico and less extensive in Honduras, we have some small but important areas also in Costa Rica, Panama and Venezuela.

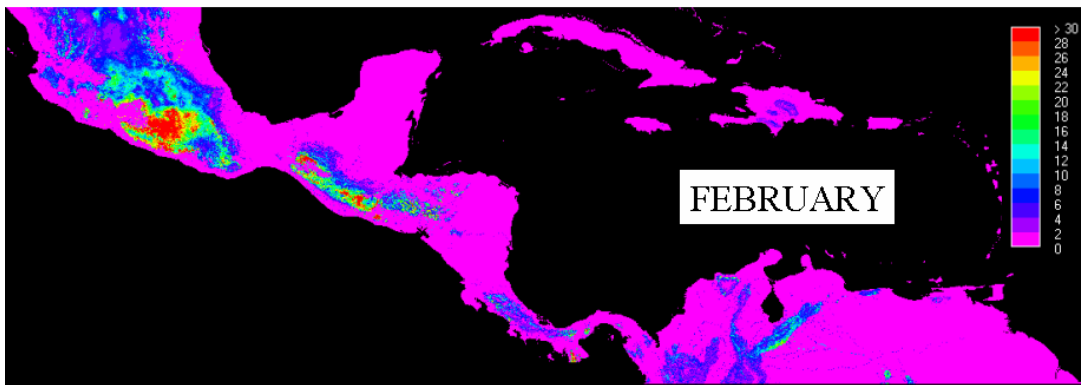


**Figure 137 Fog runoff contributions to rainfall generated runoff : February**

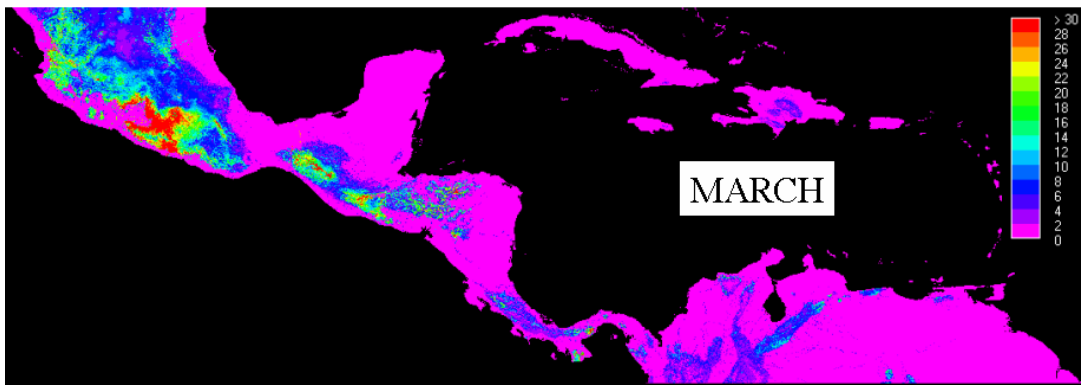


**Figure 138 Fog runoff contributions to rainfall generated runoff : March**

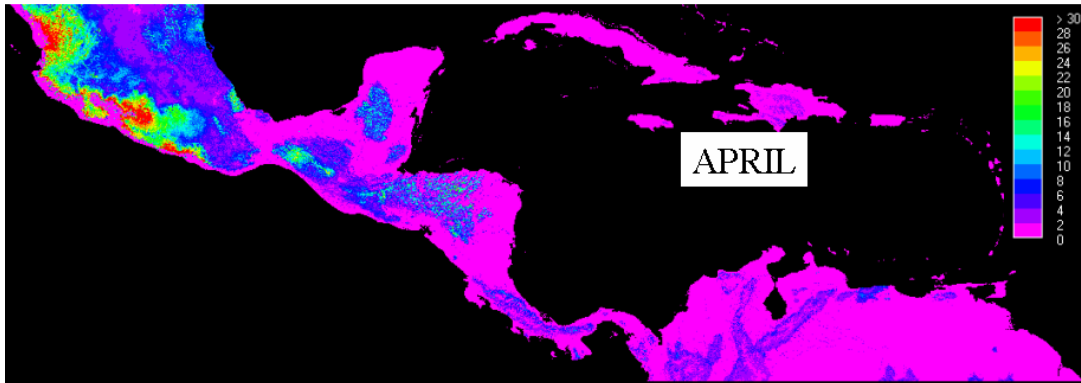


**Figure 139 Fog runoff contributions to rainfall generated runoff : April**

By April and May the greatest contributions in Mexico are much more coastal and contributions are much less in central America and northern South America.

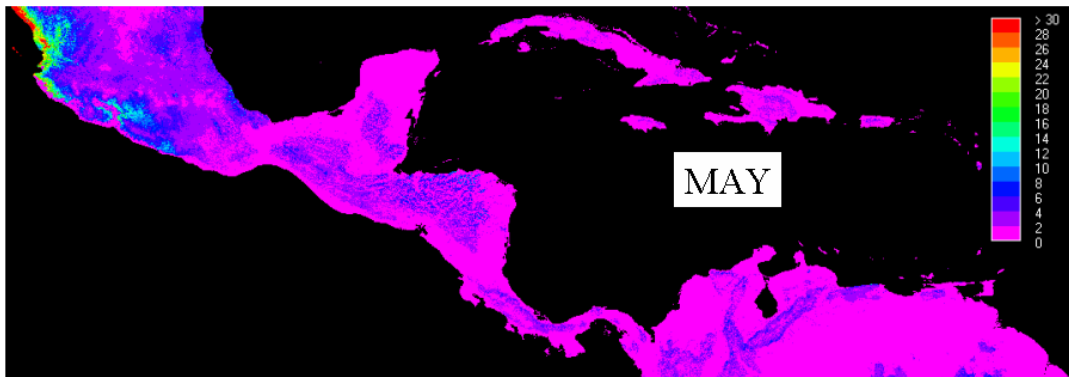


**Figure 140 Fog runoff contributions to rainfall generated runoff : May**

June to October show remarkable constancy with low fog contributions <10% throughout the countries. It is these months, which result in the low overall annual contribution of fog to runoff.

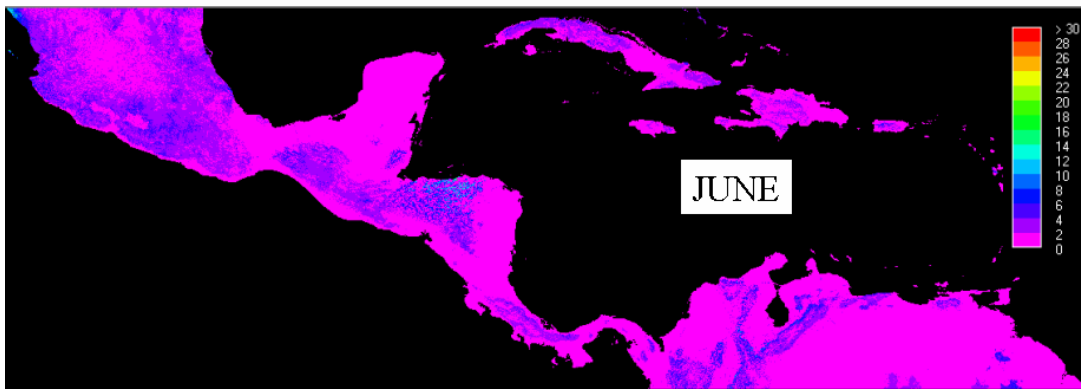


**Figure 141 Fog runoff contributions to rainfall generated runoff : June**

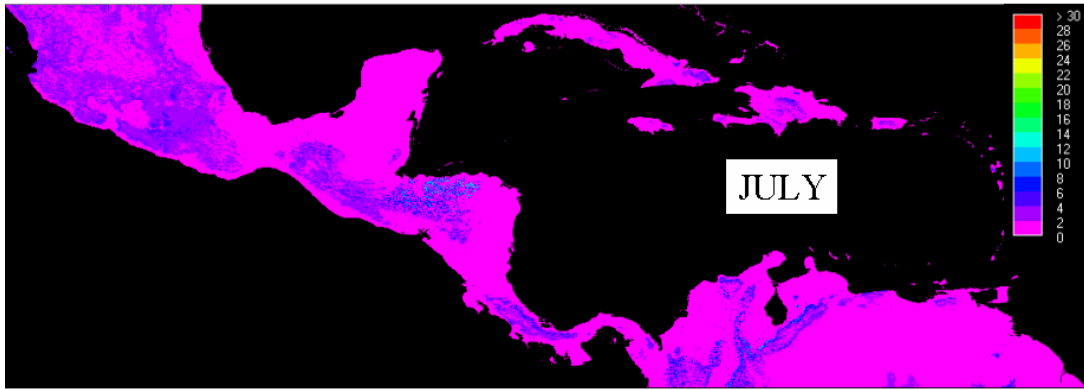


Figure 142 Fog runoff contributions to rainfall generated runoff : July

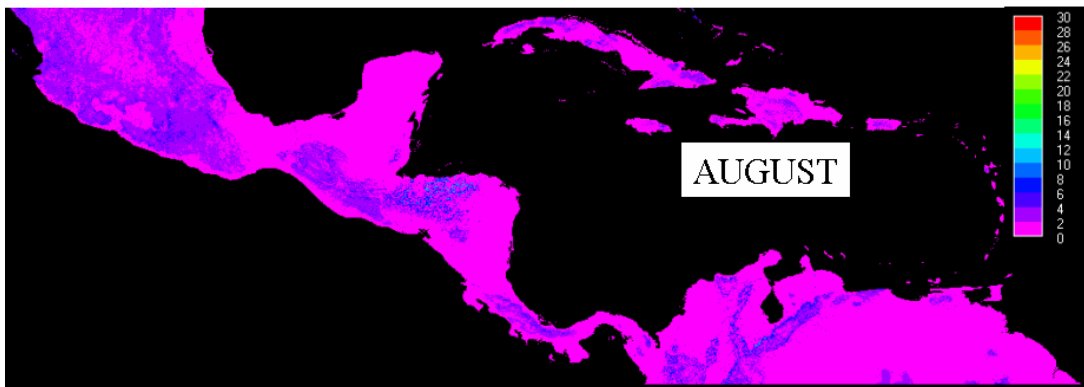


Figure 143 Fog runoff contributions to rainfall generated runoff : August

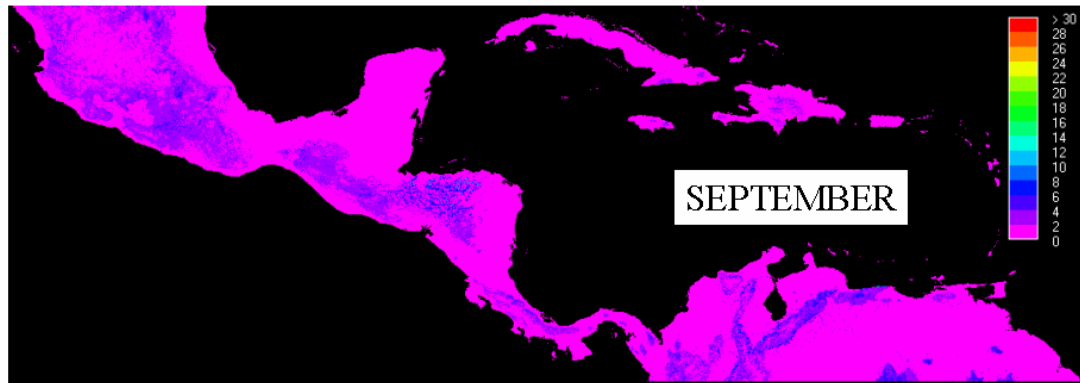
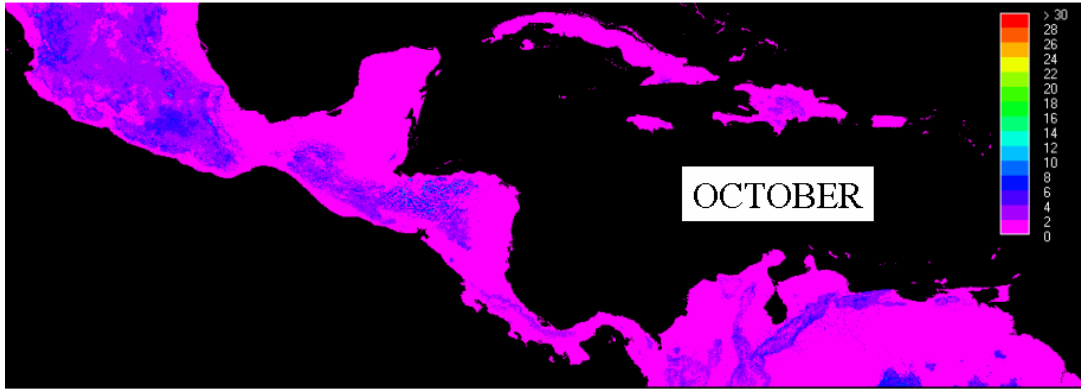
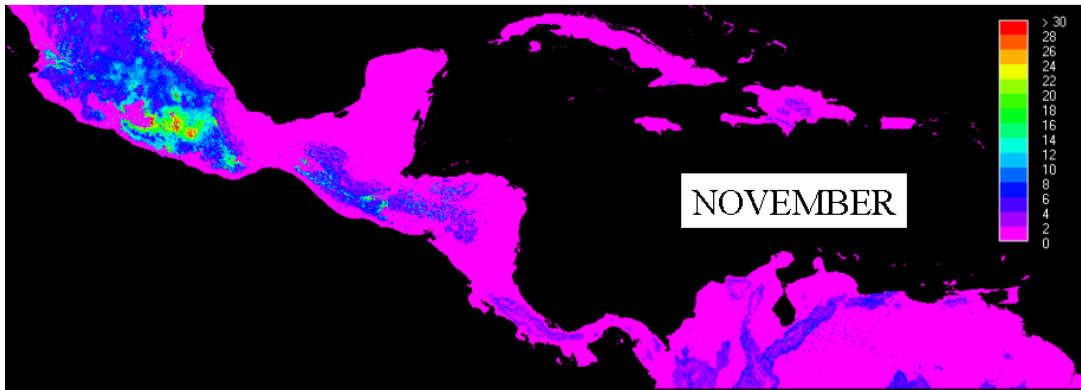


Figure 144 Fog runoff contributions to rainfall generated runoff : September



**Figure 145 Fog runoff contributions to rainfall generated runoff : October**

By November the dry season pattern returns with high inputs (20-30%) throughout northern central American uplands, further expanding in December.

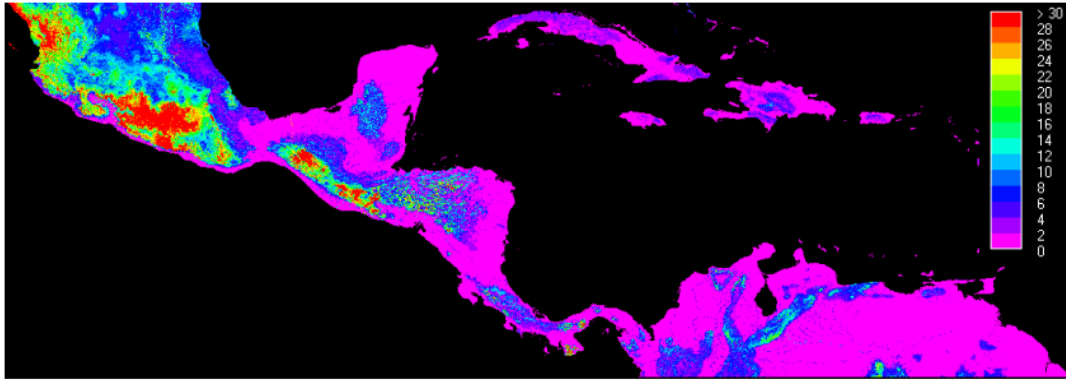


**Figure 146 Fog runoff contributions to rainfall generated runoff : November**



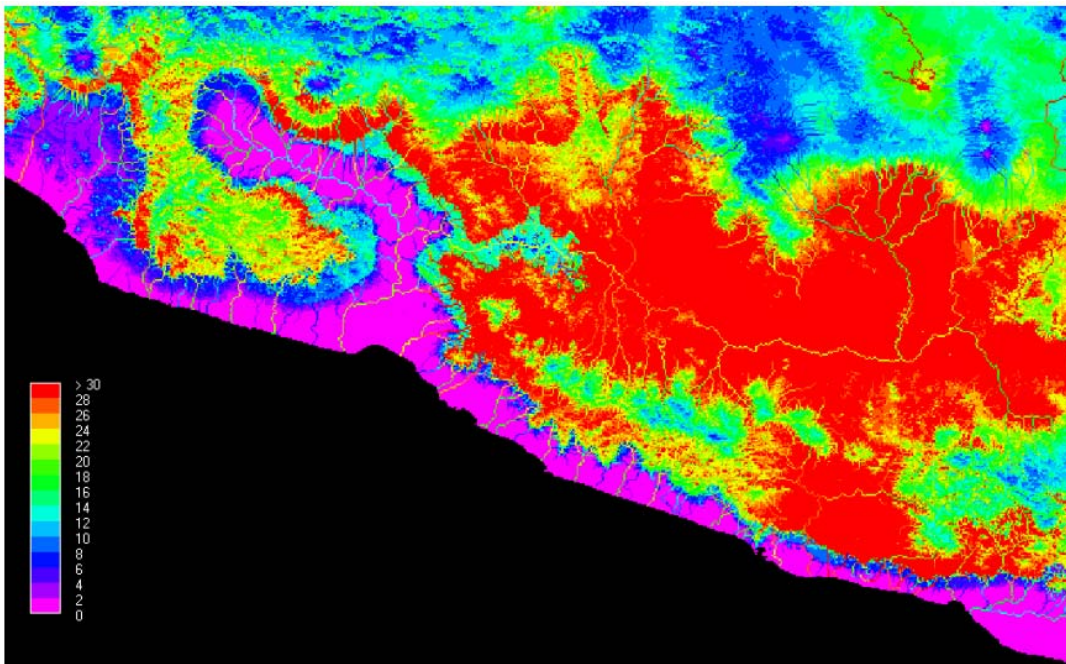
**Figure 147 Fog runoff contributions to rainfall generated runoff : December**

Figure 148 shows the magnitude of fog contribution to rainfall runoff for the month in which it is greatest and indicates that, at least seasonally, fog contributions can be extremely important to flows, particularly in Pacific Mexico and Guatemala.



**Figure 148 Monthly maximum fog runoff contribution to rainfall runoff**

Though contributions in the mountains are in excess of 30% (around 40% in S Mexico), the contributions to lowland rivers are usually less depending on the altitude occupancy of the river (see Figure 149).



**Figure 149 Monthly maximum fog runoff contribution to rainfall runoff : detail for southern Mexico**

The month in which this peak of contribution occurs varies greatly spatially : May in lowland Mexico, April for the mid altitudes and December for the highest altitudes and similar patterns throughout central America. In the Colombian Andes the greatest contributions are in January and in February in Venezuela.

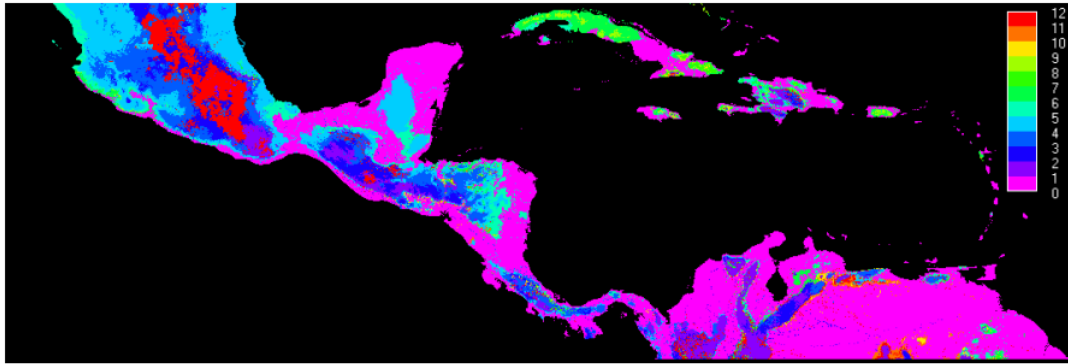


**Figure 150 Month of maximum fog runoff contribution to rainfall runoff**

Locally these patterns are, however, quite complex, with rivers sourced at different altitudes having their maximum fog contributions in different months as is clear for the rivers sourced in the Venezuelan cloud forests (Figure 151).

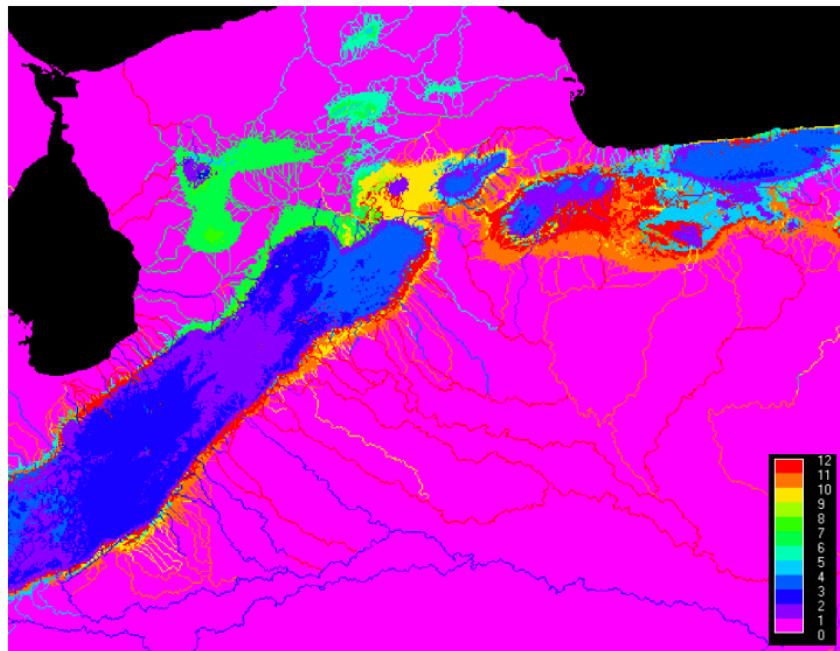


**Figure 151 Month of maximum fog runoff contribution to rainfall runoff : detail for Venezuela**

Overall we have seen that, at the continental scale, fog contributions to runoff (flows) are generally higher than those observed in Costa Rica (which has very high rainfall). Particularly in Mexico, Guatemala, Honduras and Venezuela, fog inputs can be an important addition to local flows in cloud forest areas and further downstream for certain rivers. This is true even though the magnitudes of fog input in mm/year are generally similar to or lower than those observed in Costa Rica. Moreover these fog contributions to flows are particularly important in the dry season during which they might contribute more than 30% to flows in mountain streams and 0-30% of the flows for lowland rivers in a particular month (depending upon the magnitude of their occupancy in cloud forest). 30% contributions are largely observed for rivers with a small lowland occupancy (where mountains are close to the coast) whereas maximum monthly contributions are closer to 10-20% for more extensive lowland rivers. The

seasonal timing of those contributions varies on a large spatial scale (latitudinally) with the climate but can also vary from one river to the next because of the altitudinal occupancy of those rivers.

#### 4.19 International historic land use change scenario

We now apply a simple land use change scenario to this region in order to simulate the spatially varying impact of forest cover change on the hydrological outputs with a particular emphasis on fog contributions. The land use scenario used is an historic one that compares the original (pre-human or natural) forest cover distribution in the region based on the GFW<sup>22</sup> database (see Mulligan and Burke, 2005a) with the present distribution of tree cover based on MODIS VCF. We run the *fiesta\_delivery* model for both original and current forest cover with all climate and other inputs equal. The purpose is to examine the impact that observed historic forest cover change has had on water balances and how these vary regionally. Figure 152 and Figure 153 shows the original, current and change in forest cover historically. Forest cover change represents a reduction in tree cover in most areas especially in the lowlands. A number of (largely montane) areas of forest remain particularly in S Mexico, Honduras, Costa Rica and Colombia. In the model tree cover is parameterised as for forest whereas non tree cover is parameterised as for rough pasture except in areas of bare soil.

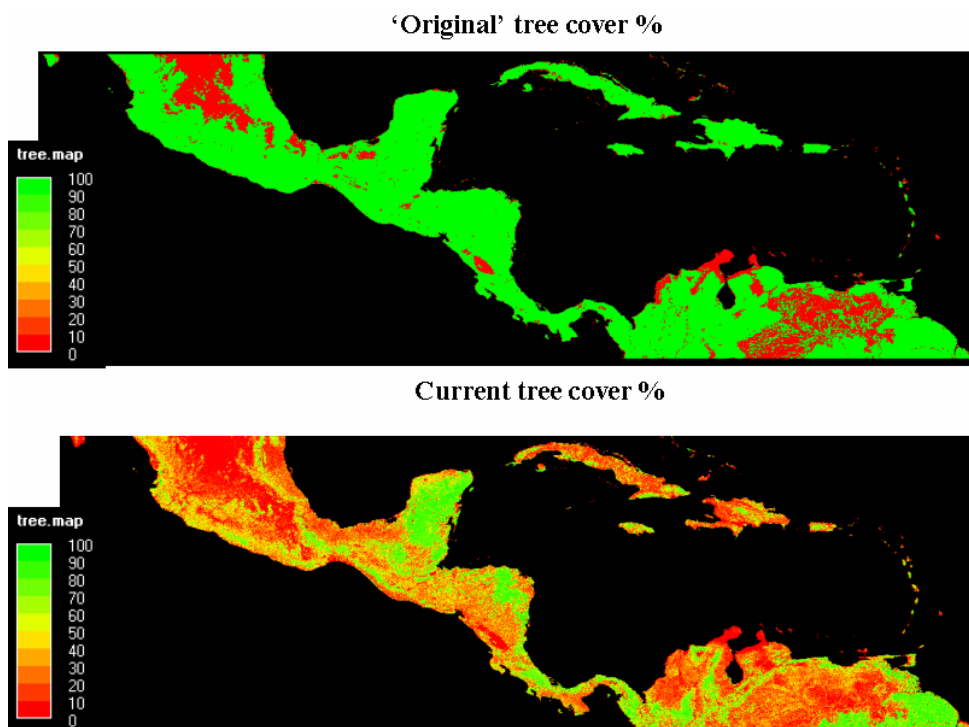
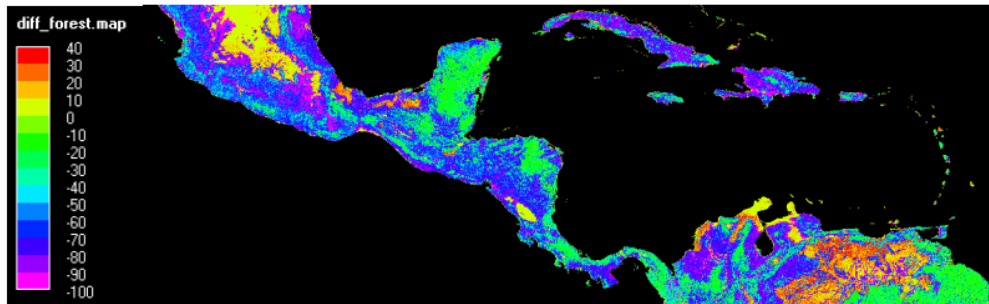


Figure 152 Comparison of historic (per-human) and current tree cover for central America

<sup>22</sup> <http://www.globalforestwatch.org/english/index.htm>



**Figure 153** Change in forest cover %

We will now look at the change in hydrological conditions between the historic simulation and the current forest cover simulation, starting with fog inputs (Figure 154). Interestingly where forest loss has occurred on windward slopes we get increases in fog inputs +80 mm/yr (because there are more edges for fog impaction in fragmented landscapes compared with the original complete forest cover (see the Atlantic slopes of Costa Rica for example). On leeward slopes we get decreases in fog inputs after forest loss because of the reduction in surfaces for intercepting fog deposition (-100 mm/yr) which is more important in sheltered areas. These changes are rather spatially restricted to highly exposed and sheltered areas.

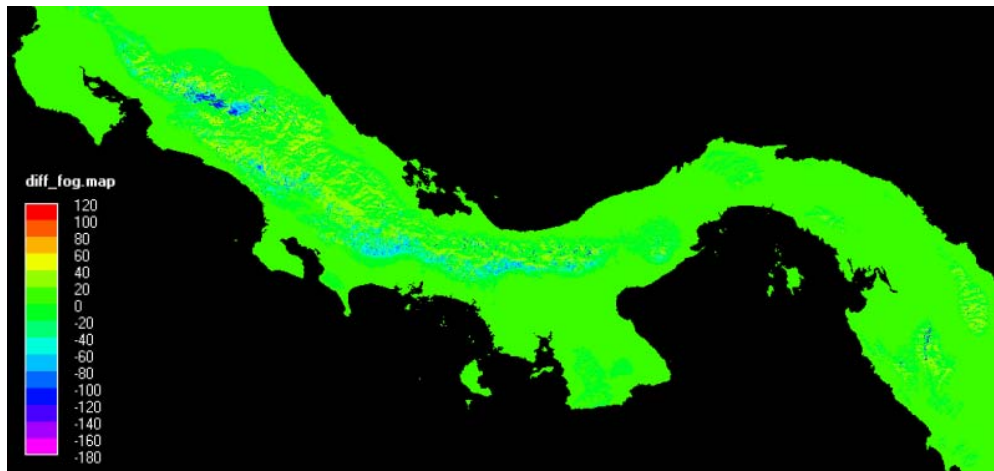


**Figure 154** Change in fog inputs (mm/year)

The changes in evapotranspiration that have resulted from this forest loss are shown in Figure 155. Evapotranspiration decreases greatest where forests loss occurs in high radiation lowland areas (-250 –300 mm/year). The impact of forest cover change is lower in upland areas (-100 –200 mm/year). Zero change occurred over water bodies and areas without forest historically and today e.g. central Mexico (not shown). Also in some parts of the Venezuelan Llanos (also not shown) increases in evapotranspiration are observed (forest cover increased in those areas in the scenario).

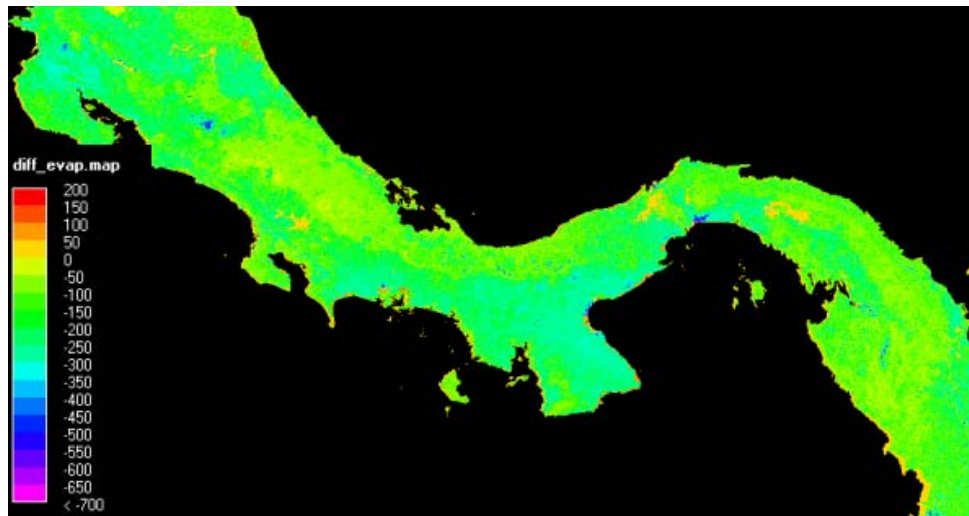


**Figure 155 Change in evapo-transpiration (mm/year)**

The resulting change in water balance (Figure 156) shows significant increases in water quantity available for runoff where forest loss has been significant for example in many of the central American lowlands (+300-400 mm/yr). The effect is much less in areas with less forest loss has occurred or in mountain areas. Stationarity or very small decreases are observed in water balance in areas with no forest loss or small forest cover increases.

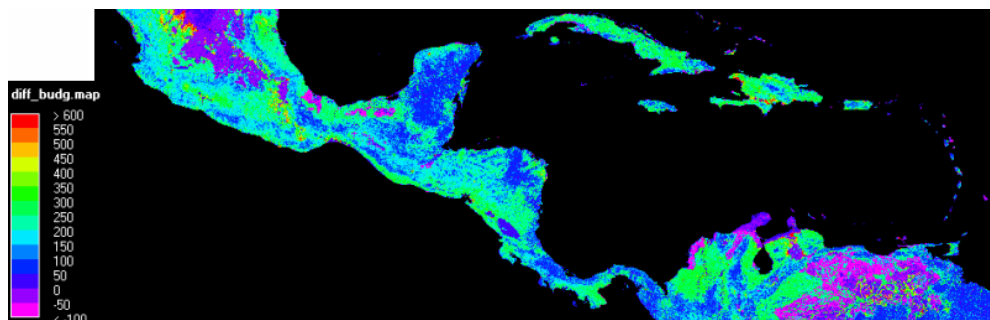


**Figure 156 Change in water balance (inputs – evap, mm/year)**

The results of these balance changes for runoff production are shown in (Figure 157). The effect is overwhelmingly an increase in flows after forest loss (because of the greater effect of widespread reduced evaporative losses compared with the spatially restricted changes to fog inputs). The effect cumulates downstream and is small for most rivers (+2 cumecs) but can be up to +400 cumecs for large rivers in heavily deforested areas. At the local scale in exposed cloud forests there are small decreases in runoff as a result of cloud forest loss but these are a maximum of 5% (in low rainfall environments) and less in higher rainfall environments. These minor reductions in runoff over some cloud forest areas (-0.029 cumecs) are dwarfed by overwhelmingly positive changes in runoff in lowlands and many uplands which lead to positive effects on flows overall and, the larger the river the larger the positive effect.

Thus we can expect regional water losses by evapotranspiration to be much lower under current forest cover than under historic forest cover and, as a result, the largest rivers are carrying a lot more water now than they were before land use change!

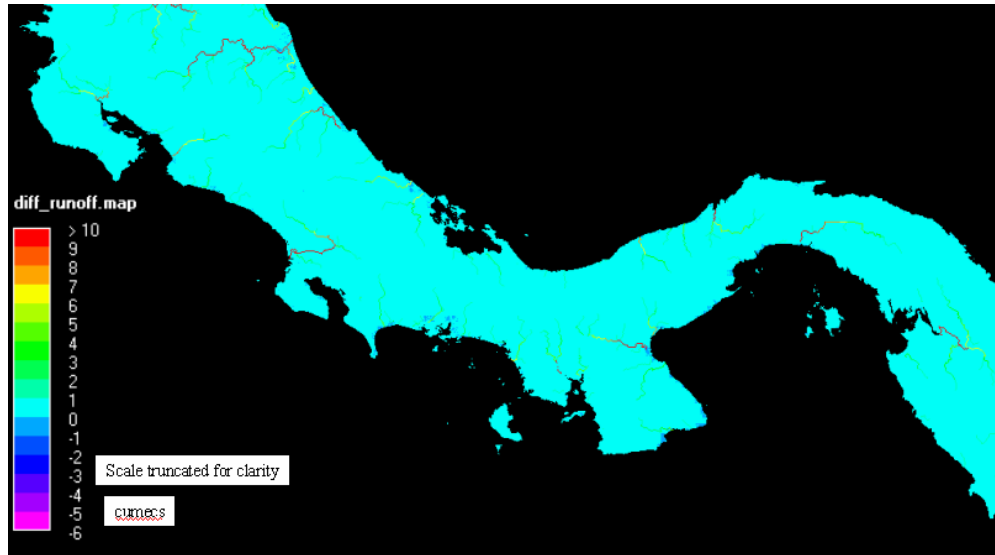


**Figure 157 Change in water balance (inputs – evap, cumecs) cumulated downstream**

Let us now examine the impacts of this forest cover change in fog inputs in more detail. Figure 158 shows fog contributions to runoff under current forest cover indicating a contribution of 0% in lowlands, <5% across majority of uplands, 5-10% in exposed uplands and 10-45% in low rainfall and exposed uplands eg Mexico.

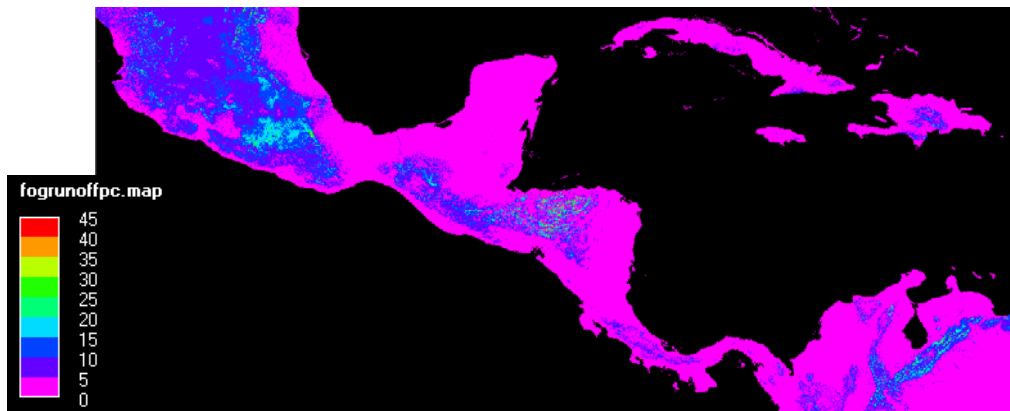


**Figure 158 Fog contributions to runoff under current forest cover**

Under the original forest cover (Figure 159) fog contributions to runoff would have been slightly higher because of a greater leaf area for deposition processes and higher evapotranspiration.

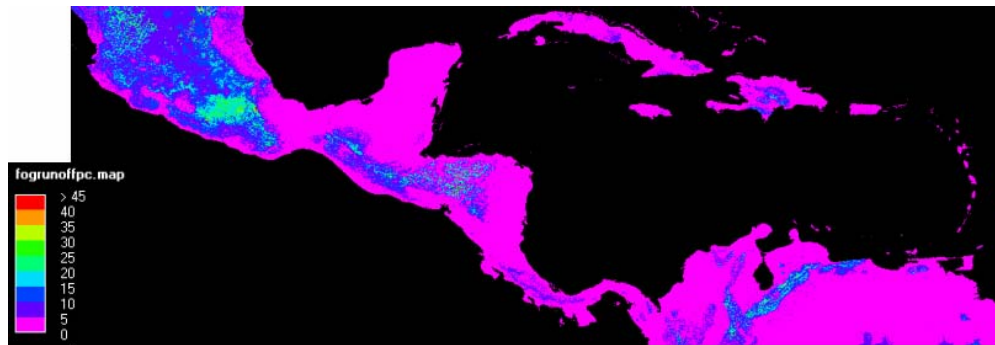


**Figure 159 Fog contributions to runoff under original forest cover**

Historic deforestation has led to widespread reduction in fog contribution to runoff of around -5% in mountains and along the rivers emanating from them. Greater impacts are observed in small isolated exposed patches in Mexico, Guatemala, Costa Rica and Venezuela.

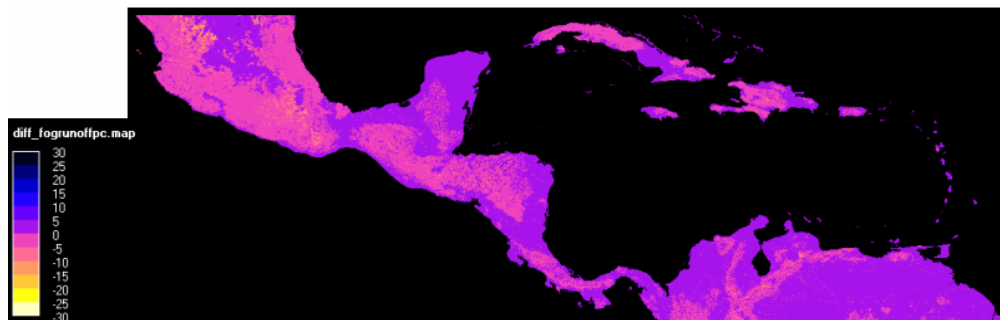


**Figure 160 Change in fog contributions to runoff, %**

#### 4.19.1 Summary of Central American simulation results

In summary, forest loss to date through human impact has led to localised reductions in fog inputs on leeward slopes which are a little higher than the increases in fog inputs observed on windward slopes (because of the fragmented forest ‘edge effect’). More significant changes in fog inputs are highly localised. The much more significant effect of forest loss is the overall reduction in evapotranspiration losses, a reduction which is higher in some climate zones than others.

This has led to increases in local water balance especially in highly deforested lowlands. When cumulated downstream the spatially extensive nature of the reduction in evaporative loss compared with the spatially restricted nature of changes in fog inputs always result in increases in flows except at a very local scale where fog effects can dominate (at exposed sites). The larger the river, the greater the observed increase in flows, since it is proportion to the absolute area of forest lost in the catchment. Fog contributions to runoff are generally 5-15% but up to 20% in highly cloud-exposed but otherwise dry (low rainfall) areas. Fog inputs were higher under full forest cover overall because of enhanced deposition. The observed land use change has reduced fog inputs by 0-5% over most cloudforests and this effect permeates downstream especially in ‘dry’ areas (e.g. the Colombian/Venezuelan

Llanos). The effect is dwarfed by the evaporation effect though so that at large scales increases in flows are the dominant result of this land use change.

#### 4.20 Economic Implications

Figure 161 shows the water balance losses and gains (mm/year) between a future in which land use change is restricted in protected areas (because of PES payments) and a future in which it is not (because of a lack of PES payments), see section 4.15. The difference between the two scenarios indicates the gain or loss in water balance as a result of the forest conservation on a sub-catchment basis.

The net result of fog inputs and lower evapotranspiration in cloud forest environments is that cloud forest areas show smaller increases in water flows on forest loss than do lowland forests, see Figure 161, (because evaporation is limited by available energy not forest cover in the mountains so it is less sensitive to forest cover). This means that in water limited areas, cloud forest removal will not significantly increase flows compared with lowland forest removal. In high rainfall areas cloud forest landscapes are very water productive as a result of reduced evapotranspiration and this, combined with their steep slopes and topographic capacity for flow concentration, makes them much more susceptible to water erosion than their lowland counterparts. The soil protective effects of forest (where they occur) thus become more important in these environments.

(4) Figure 162 is Figure 1 in monetary terms assuming a water cost of 0.19 \$/m<sup>3</sup> (Castro, 2004) assuming that the water is used. The gains and losses are thus economic gains and losses through not conserving forest in USD per hectare. The greatest gains are in the lowlands (100-150 USD/Ha./yr), gains are much lower in the mountains (0-50 USD/Ha./yr and are losses of up to -350 USD/Ha./yr in some isolated cloudforest areas.. The key issues are (a) whether these gains could be realised (very unlikely because only a fraction of water can be used – especially if it comes through more rapidly as a result of forest loss) and (b) whether the various hydrological disbenefits of forest loss (increased peak flows, reduced dry season flows, reduced water quality, increased erosion) would outweigh these (very likely). Those issues really are critical to the economic and policy consequences of these water losses/gains and require deeper investigation in future projects.

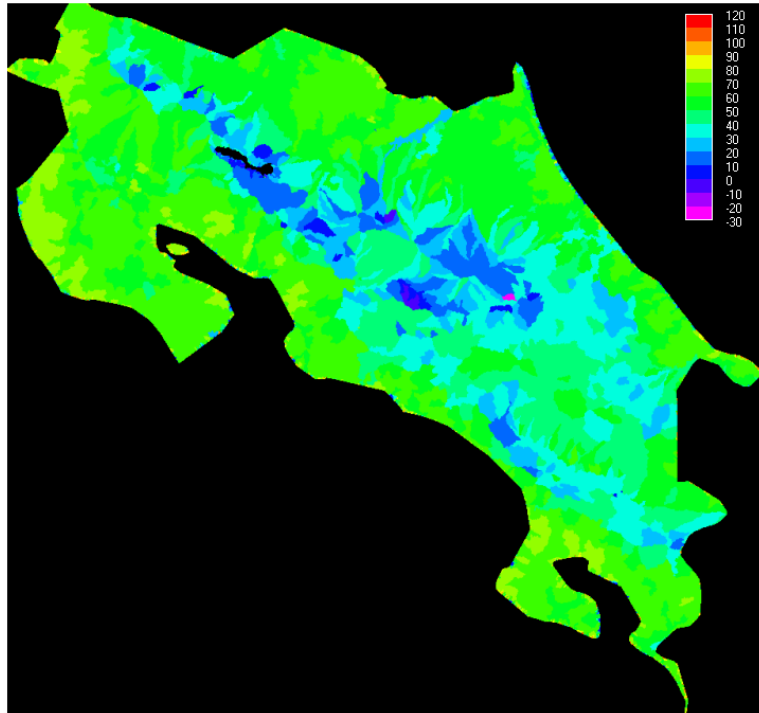


**Figure 161** Difference in water balance (mm/year) between a PES conservation future and a NOPES (no conservation) future on a sub-catchment basis (see section 4.15.)

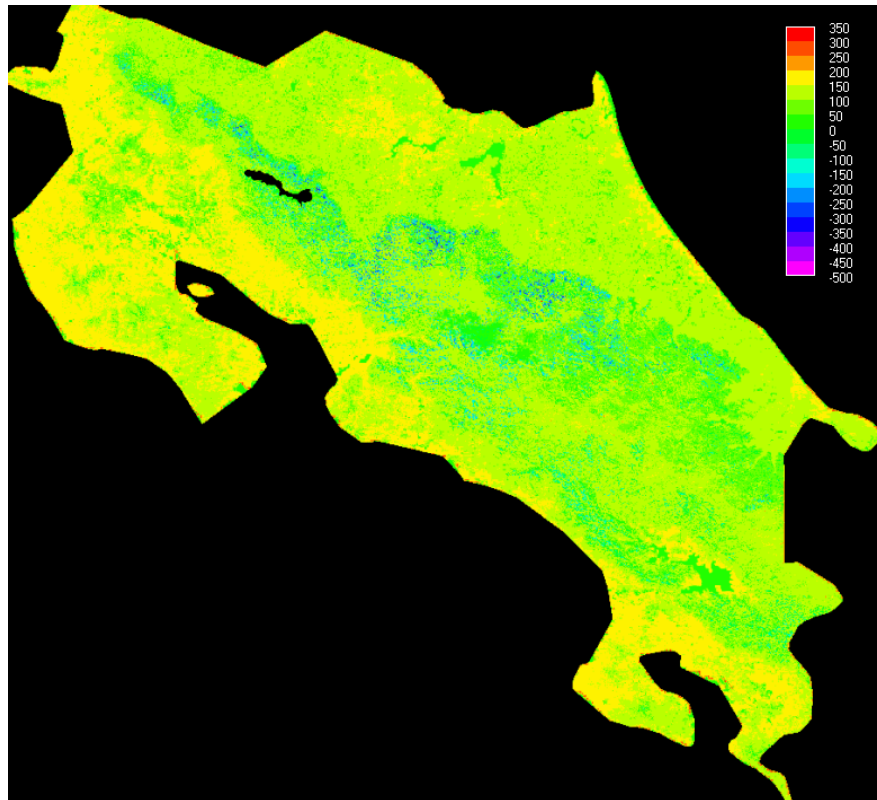


**Figure 162** Gain/loss in water income (USD/Ha./yr) between a PES conservation future and a NOPES (no conservation) future on a pixel basis.

#### 4.21 References

- Arazi, A. D. Sharon, A. Khain, A. Huss and Y. Mahrer (1996) The Windfield And Rainfall Distribution Induced Within A Small Valley: Field Observations and 2-D Numerical Modelling. *Boundary-Layer Meteorology* 83: 349–374, 1997.
- Arazi, A. D. Sharon, A. Khain, A. Huss and Y. Mahrer (1996) The Windfield And Rainfall Distribution Induced Within A Small Valley: Field Observations and 2-D Numerical Modelling. *Boundary-Layer Meteorology* 83: 349–374, 1997.
- Burrough, P.A. and McDonnell, R.A. (1998) Principles of Geographical Information Systems, 2nd Edition. Oxford: Oxford University Press.
- Castro Salazar, R. (2004) Water : moving from a free good to a tradeable one. [http://www.us.es/ciberico/archivos\\_word/ReneCastroagua.doc](http://www.us.es/ciberico/archivos_word/ReneCastroagua.doc)
- Hansen, M.; DeFries, R.; Townshend, J.R.; Carroll, M.; Dimiceli, C.; Sohlberg, R.. 2003. 500m MODIS Vegetation Continuous Fields. College Park, Maryland: The Global Land Cover Facility.
- Jeness, Jeff S. 2004. Calculating landscape surface area from digital elevation models *Wildltfe Society Bulletin* 32 (3) 829-839.
- Legates, David R. and Gregory J. McCabe (1999) Evaluating the use of "goodness of fit" measures in hydrologic and hydroclimatic model validation. *Water Resources Research*, 1999, 35:233-241
- Mitchell, P.L (1997) Misuse of regression for empirical validation of models. *Agricultural Systems*, Vol. 54 No 3 pp 313-326
- Mulligan, M. and Burke, S.M. (2005a) DFID FRP Project ZF0216 Global cloud forests and environmental change in a hydrological context. Final Report. December 2005.
- New, M., M. Hulme, and P. D. Jones. 2000. Global 30-Year Mean Monthly Climatology, 1901-1960 (New et al.). Data set. Available on-line [<http://www.daac.ornl.gov>] from Oak Ridge National Laboratory Distributed Active Archive Center, Oak Ridge, Tennessee, U.S.A.
- Ruel J-C.; Mitchell S.J.; Dornier M. (2002) A GIS Based Approach to Map Wind Exposure for Windthrow Hazard Rating. *Northern Journal of Applied Forestry*, Vol. 19, no. 4, pp. 183-187.
- Ruel J-C.; Mitchell S.J.; Dornier M. (2002) A GIS Based Approach to Map Wind Exposure for Windthrow Hazard Rating. *Northern Journal of Applied Forestry*, Vol. 19, no. 4, pp. 183-187.
- Zadroga, F. 1981. The hydrtological importance of a montane cloud forest area of Costa Rica In Lal R. and Russell K.W. (Eds.)*Tropical Agricultural Etydrology*. John Wiley & Sons Ltd. pp.59-73.

# **5 PART II MODEL DOCUMENTATION**

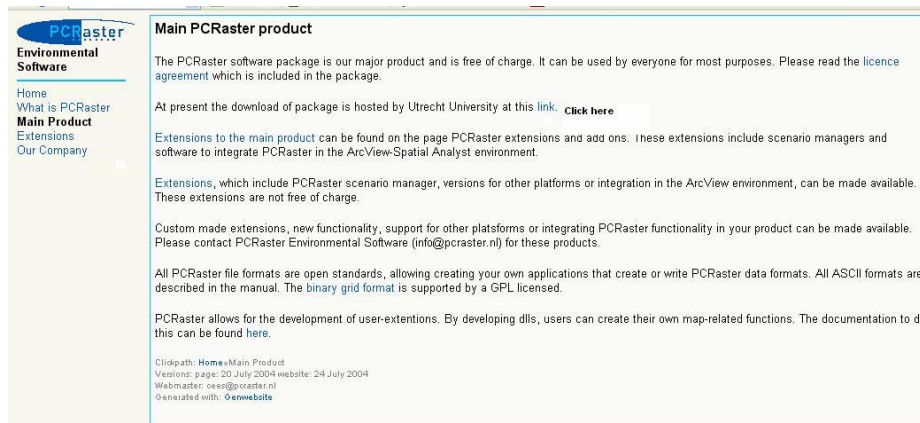
## 5.1 Installing the PCRASTER software<sup>23</sup>

With this document you will be able to download and install all of the components needed for a full installation of PCRASTER for windows.

### 5.1.1 Main product

First you must download the install file (around 13 MB)

1. PCRaster web page: <http://www.pcraster.nl/>
2. From the Home left side menu click: “Main Product”
3. then click on the word “link” (see below) to go to:  
<http://pcraster.geog.uu.nl/pcrwin32/index.html>



4. In the <http://pcraster.geog.uu.nl/pcrwin32/index.html> web page that appears scroll down to go to the “Download” section in the text and click: “PCRaster Setup, self installing file”.
5. Select “Save” and save the PCRasterSetup.exe file to your Desktop.

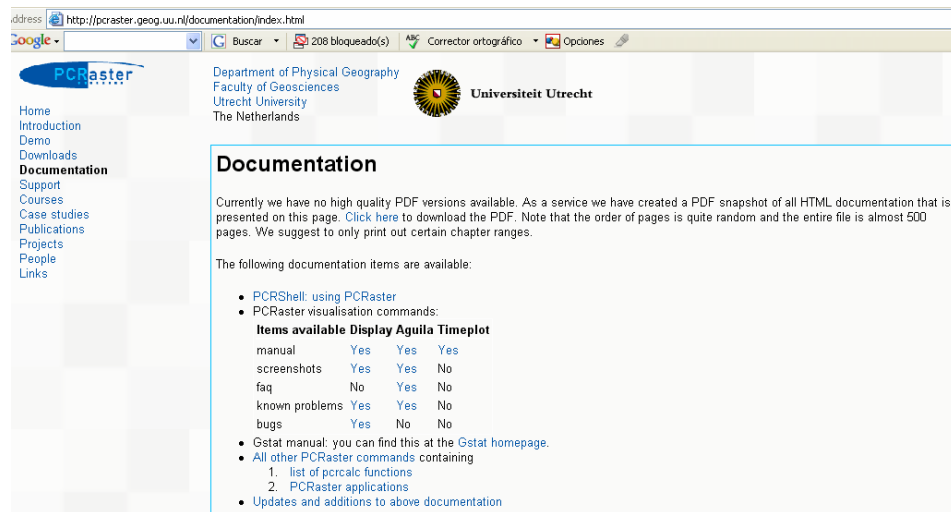


<sup>23</sup> Web page images copyright PCRASTER Environmental Software

6. Then go to the text again and click: “**Register here**”, fill the Registration form and submit it. You will be sent an “Installation Password key” by email.
7. Once you have received the email with the password, go to your Desktop and double click the file “PCRasterSetup.exe” you saved there, in order to proceed with the installation of the PCRaster software.
8. Select “Run” and then enter the Installation Password.
9. Click “Next”
10. Read the disclaimers etc and Click “I Agree” if you do.
11. Click “Next”
12. Leave the location destination as the default one: C:\PCRaster\ and click “Next” for the installation to be completed.
13. Click “Finish”

### 5.1.2 PCRaster Manual

1. The PCRASTER manual is installed with the software on your machine (but not as a printable PDF). If you want a printable version :
2. Go to: <http://pcraster.geog.uu.nl/>
3. Select “Documentation” from the left side menu
4. All the PCRaster documentation is available in PDF format (494 pages). Click “Click here” in the text and download the PDF file (see below).



5. Alternatively, you can check the manual on-line by clicking on “All other PCRaster commands” in the text. .
6. The on-line version of the manual is also available at: <http://pcraster.geog.uu.nl/index.html>. Select “Home” from the left menu and then click “PCRaster Version 2 Manual” in the text.

### 5.1.3 Pccalc update download

1. Every few months updates are made to the software which improve its functionality. You only need the latest update.
2. Go to: <http://pcraster.geog.uu.nl/index.html>
3. Select “Downloads” from the left side menu

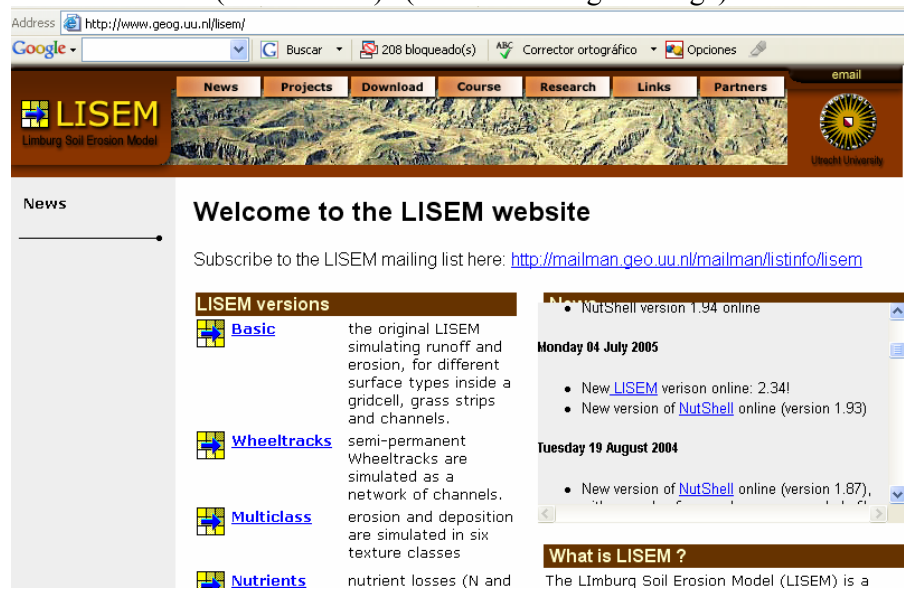
4. Select “Installation of PCRaster for Microsoft Windows” from the main page
5. Select “Pcrcalc update”
6. Click “Pcrcalc update.zip file”
7. Save the zip file in the PCRaster directory and unzip all of the the contents into the c:\PCEaster\apps folder (which was created when you installed PCRASTER) on your computer

#### 5.1.4 *Aguila update download*

8. Aguila is one of the main map visualisation packages that comes with PCRASTER. Updates are also made to this package so you need to download the latest version :
9. Go to: <http://pcraster.geog.uu.nl/index.html>
10. Select “Downloads” from the left side menu
11. Select “Installation of PCRaster for Microsoft Windows” from the main page
12. Select “Aguila update” and then “Updates of Aguila can be found at the Aguila project page”
13. Click “aguila-041208.zip” (the date in the filename may change)
14. Save the zip file in the PCRaster directory and unzip the content into the c:\PCRaster\apps folder

#### 5.1.5 *Nutshell and Mapedit downloads*

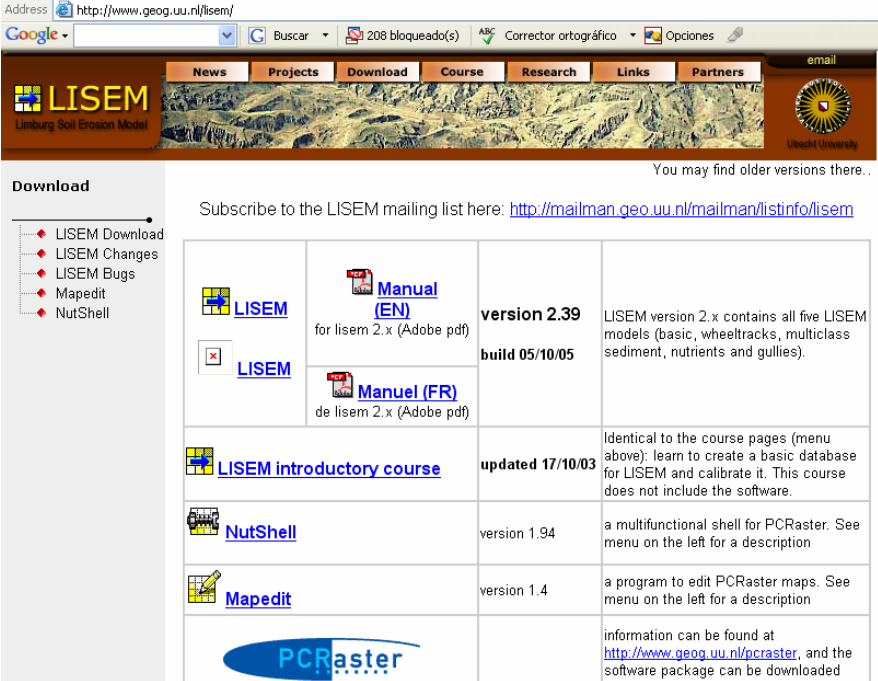
15. Nutshell is a windows interface for working with PCRASTER. It is useful for those not familiar with the DOS shell. To download and install it :
16. Go to: <http://pcraster.geog.uu.nl/index.html>
17. Select “Downloads” from the left side menu
18. Select “A mapedit program (link to litem home page)” from the main page
19. Scroll down the NEWS menu from the LISEM website until we find: “Nutshell online (version 1.93)” (the version might change)



The screenshot shows a web browser window displaying the LISEM website. The address bar shows <http://www.geog.uu.nl/litem/>. The website has a navigation menu with links for News, Projects, Download, Course, Research, Links, and Partners. The main content area is titled "Welcome to the LISEM website" and includes a subscription link for the LISEM mailing list. A "LISEM versions" section lists four categories: Basic, Wheeltracks, Multiclass, and Nutrients. A "News" sidebar on the right shows a list of updates, with the most recent being "NutShell version 1.94 online" dated Monday 04 July 2005. Below this, there are entries for "New LISEM version online: 2.34!" and "New version of NutShell online (version 1.93)" dated Tuesday 19 August 2004. A "What is LISEM?" section at the bottom explains that LISEM is the Limburg Soil Erosion Model.

20. Select “Nutshell”

## FIESTA Final Technical Report



The screenshot shows the LISEM website with a navigation menu (News, Projects, Download, Course, Research, Links, Partners) and a sidebar with a 'Download' section. The main content area contains a table of software and manuals. Below the table is the PCRaster logo.

 <a href="#">LISEM</a>	 <a href="#">Manual (EN)</a> for liseM 2.x (Adobe pdf)	<b>version 2.39</b> <b>build 05/10/05</b>	LISEM version 2.x contains all five LISEM models (basic, wheeltracks, multiclass sediment, nutrients and gullies).
 <a href="#">LISEM</a>	 <a href="#">Manuel (FR)</a> de liseM 2.x (Adobe pdf)		
 <a href="#">LISEM introductory course</a>		<b>updated 17/10/03</b>	Identical to the course pages (menu above). learn to create a basic database for LISEM and calibrate it. This course does not include the software.
 <a href="#">NutShell</a>		version 1.94	a multifunctional shell for PCRaster. See menu on the left for a description
 <a href="#">Mapedit</a>		version 1.4	a program to edit PCRaster maps. See menu on the left for a description
			information can be found at <a href="http://www.geog.uu.nl/pcraster">http://www.geog.uu.nl/pcraster</a> , and the software package can be downloaded

21. Click “Nutshell” and save “Nutshellsetup.exe” file in your Desktop
22. Double click “nutshellsetup.exe”
23. Click Run
24. Click Next
25. The application folder for installation has to be: C:\PCRaster\apps
26. Click Install
27. Click Next
28. Click Finish

### Mapedit

29. Mapedit is a program for making simple changes to PCRASTER maps
30. To install it go back to the webpage above and select “Mapedit” version 1.4 and save it in the PCRaster directory
31. Double click “Mapedit.zip” and unzip the content “mapedit.exe” into the C:\PCRaster\apps folder.

## 5.2 The FIESTA delivery model policy exercises

These are provided as a PDF powerpoint presentation (attached and available at [http://www.ambiotek.com/fiesta/user\\_documentation\\_fiesta\\_fog\\_delivery\\_model.pdf](http://www.ambiotek.com/fiesta/user_documentation_fiesta_fog_delivery_model.pdf))